Smart Innovation, Systems and Technologies 62

Xiaoqing Zeng
Xiongyao Xie
Jian Sun
Limin Ma
Yinong Chen *Editors*

International Symposium for Intelligent Transportation and Smart City (ITASC) 2017 Proceedings

Branch of ISADS (The International Symposium on Autonomous Decentralized Systems)

Springer

Smart Innovation, Systems and Technologies

Volume 62

About this Series

The Smart Innovation, Systems and Technologies book series encompasses the topics of knowledge, intelligence, innovation and sustainability. The aim of the series is to make available a platform for the publication of books on all aspects of single and multi-disciplinary research on these themes in order to make the latest results available in a readily-accessible form. Volumes on interdisciplinary research combining two or more of these areas is particularly sought.

The series covers systems and paradigms that employ knowledge and intelligence in a broad sense. Its scope is systems having embedded knowledge and intelligence, which may be applied to the solution of world problems in industry, the environment and the community. It also focusses on the knowledge-transfer methodologies and innovation strategies employed to make this happen effectively. The combination of intelligent systems tools and a broad range of applications introduces a need for a synergy of disciplines from science, technology, business and the humanities. The series will include conference proceedings, edited collections, monographs, handbooks, reference books, and other relevant types of book in areas of science and technology where smart systems and technologies can offer innovative solutions.

High quality content is an essential feature for all book proposals accepted for the series. It is expected that editors of all accepted volumes will ensure that contributions are subjected to an appropriate level of reviewing process and adhere to KES quality principles.

More information about this series at http://www.springer.com/series/8767

Xiaoqing Zeng · Xiongyao Xie
Jian Sun · Limin Ma · Yinong Chen
Editors

International Symposium for Intelligent Transportation and Smart City (ITASC) 2017 Proceedings

Branch of ISADS (The International Symposium on Autonomous Decentralized Systems)

Springer

Editors
Xiaoqing Zeng
Tongji University
Shanghai, Shanghai
China

Xiongyao Xie
Department of Geotechnical Engineering
Tongji University
Shanghai, Shanghai
China

Jian Sun
Shanghai Jiao Tong University
Shanghai, Shanghai
China

Limin Ma
School of Environmental Science and Engineering
Tongji University
Shanghai, Shanghai
China

Yinong Chen
Department of Computer Science and Engineering
Arizona State University
Tempe, AZ
USA

ISSN 2190-3018 ISSN 2190-3026 (electronic)
Smart Innovation, Systems and Technologies
ISBN 978-981-10-3574-6 ISBN 978-981-10-3575-3 (eBook)
DOI 10.1007/978-981-10-3575-3

Library of Congress Control Number: 2017935846

Printed on acid-free paper

This Springer imprint is published by Springer Nature
The registered company is Springer Nature Singapore Pte Ltd.
The registered company address is: 152 Beach Road, #21-01/04 Gateway East, Singapore 189721, Singapore

Preface

The conference of ITASC (International Symposium on Intelligent Transportation and Smart City) was originated from idea of Intelligent Transportations and Information Technology. The 1st ITASC conference started as branch of the International Symposium on Autonomous Decentralized System (ISADS) was held in March 2013 in Mexico City. In the inauguration event, researchers and practitioners from China, Japan, USA, Mexico, and other countries shared in research, technologies, and experience in metro construction and maintenance. Main technologies discussed in that conference have been built and operated in rail transit in China and Japan. The 2nd ITASC was successfully held in May of 2015 in Shanghai. Over 40 specialists, researchers, and practitioners presented latest work in the conference, including academicians from China and Austria, chief technology officer from central bank of Mexico, and authoritative entrepreneurs. More than 300 people from about 50 universities and corporations attended the conference.

ITASC 2017 carries on the success of the previous two meetings and is held in May 19–21 in Shanghai. The symposium focuses on green transportation and urban utility and offers a forum for researchers, practitioner, and entrepreneurs to discuss the latest research and developments in transportation, civil engineering, information technology, and environment engineering. The topics of the symposium include the theoretical foundation, modern technologies and their applications in intelligent transportation and smart city, aiming at building a harmony for our city life. During the symposium, we focus on discussing how to deploy new techniques and products into transportation, municipal construction, and information controlling, and thus, promote the progress of these related science and technology.

In this proceeding, we chose 31 articles from more than 60 submitted articles, which cover several professional fields, such as transportation and civil engineering, IT, environmental science, and quite a few of these articles chose a specific prospective to describe the new ideas of crossing different professional fields, which gave readers great inspiration of solving problems. As the prosperous development of technologies combined with IT growing in China, there are urgent needs and huge application prospects to keep more and more attention on the intelligent

transportation and smart city, which has already been successfully implemented in some developed areas.

Like the former ITASC symposiums, we again invited the top scholars from all over the world, including specialists of universities, entrepreneurs, and even the governments, to share their wonderful discoveries and experiences, and 200–300 people may attend the symposium in estimation. We hope all those who are interested in improving our urban living qualities could attend ITASC 2017 to communicate with us, and give our sincere thanks to all sponsors, press, print, and electronic media for their excellent coverage of this conference.

Shanghai Xiaoqing Zeng

Contents

Combined PCA and NB to Predict Traffic Incident Duration

Yechun Lao, Shuyan Chen(✉), and Ningning Song

School of Transportation, Southeast University, Nanjing, Jiangsu, China
{220142555,chenshuyan,220142528}@seu.edu.cn

Abstract. An accurate prediction of incident duration plays an important role in obtaining traffic information for travelers timely and making appropriate decisions for traffic managers. As the characteristics are significantly different from each other, models were established for each type of incident, i.e. stopped-vehicle incidents, lost-load incidents and accidents. After data pretreatment, Principal component analysis (PCA) was carried out for each type of incident. Afterward, Naive Bayes (NB) model was applied for the data processed after PCA to predict incident durations. The experimental results indicated that the model obtained high prediction accuracy for those incidents which lasted less than 60 min and the prediction performance of accidents worked best. Besides, the prediction accuracy was 77.46%, 82.08% and 86.34% for each type of incident within 20 min' error, respectively. In conclusion, the results showed that the combined model of PCA and NB is a promising application to predict incident duration.

Keywords: Incident duration · Prediction · Data pretreatment · Principal component analysis · Naive Bayes

1 Introduction

Traffic incident which is one of the major causes leading to non-recurring congestion, refers to the event that cause temporary reduction in traffic capacity, such as accident, breakdown, weather and construction. Both the traffic control measures to be taken as well as the information to be given to drivers depend on how long incidents are expected to influence traffic [1].

As a result of the difference of the data that researchers used, various methodologies have been employed to build models for incident duration forecast, which mainly include two aspects: one is the construction of the probability distribution of incident duration; the other is the analysis of the impact of external factors on incident duration. The former regards incident duration as a random variable, which satisfies a certain probability density function, such as: lognormal distribution [2], log-logistic distribution [3] and weibull distribution [4]. The latter can be divided into two categories: one is the parameter model and the other is semi-parametric or non-parametric model. The parameter model quantifies the relationship between incident duration and its influence factors, including the regression analysis and risk analysis, like log-based regression model [5],

X. Zeng et al. (eds.), *International Symposium for Intelligent Transportation and Smart City (ITASC) 2017 Proceedings*, Smart Innovation, Systems and Technologies 62, DOI 10.1007/978-981-10-3575-3_1

Support Vector Regression model [6], Partial Least Squares Regression model [7], hazard-based duration model [3] and competing risks mixture model [8]. The semi-parametric or non-parametric model mainly contains Decision Tree [9], Classification Tree [10], Fuzzy Logic Theory [11], Bayesian Neural Networks [12], Bayesian Decision Tree [13], Artificial Neural Network and Support Vector Machine [14].

Although a lot of methods have been proposed to predict incident duration, there remains some deficiencies among the existing methods. On the one hand, some algorithms are complicated and take a lot of time to train, e.g. ANN and decision trees. On the other hand, the prediction accuracy of them is not satisfied, and there is a great room for improvement. In addition, some methods only pay attention to the relationship between dependent variables and independent variables, whereas ignoring the relationship between different independent variables.

Naive Bayes model based on principal component analysis is a good way to build the relationship between dependent variables and independent variables, simultaneously considering the complex internal relationship among these factors. It not only has a simple structure and needs less complicated calculation, which makes it won't take long time to train, but also results in preferable prediction accuracy.

2 The Combined Model of PCA and NB

Define $\{X_1, L, X_n, C\}$ is the attribute set of the sample space E, among them: $X_i (i = 1, L, m)$ is a continuous attribute, $X_j (j = m + 1, L, n)$ is a discrete attribute, C is a class attribute. Their values are represented by the corresponding lower case letters of them. S_x is the covariance matrix for all samples of continuous attribute set $\{X_1, L, X_m\}$. $P(\cdot)$ represents a discrete probability value, $p(\cdot)$ represents the value of probability density function.

Assume the m eigenvalues and corresponding eigenvectors of S_x respectively as λ_1, L, λ_m and u_1, L, u_m, where the eigenvector u_1 is a column vector $u_i = (u_{i1}, L, u_{im})^T$. For the orthogonal matrix $U = (u_1, L, u_m)^T$, set new attribute sets as $Y^T = (Y_1, L, Y_M)^T = UX^T$. According to the definition of Jacobi determinant, we have: $|J| = |U| = 1$. In this way, we get the relationship of combined probability density distribution functions between Y and X, as follows:

$$p(y_1, L, y_m) = \frac{p(x_1, L, x_m)}{|J|} = p(x_1, L, x_m) \tag{1}$$

Suppose ∇X to be any subset of $\{X_{m+1}, L, X_n, C\}$. As there is no relationship between the fitting condition of $Y^T = UX^T$ and the value of ∇X, correspondingly we get:

$$p(y_1, L, y_m|\nabla x) = \frac{p(x_1, L, x_m|\nabla x)}{|J|} = p(x_1, L, x_m|\nabla x) \tag{2}$$

The following describes how to handle the situation that both continuous variables and discrete variables exist in sample space, combining Eq. (2). For the sake of clarity,

we firstly take into account a case of two attributes and set as X1 (continuous variable) and X2 (discrete variable) respectively. Suppose to discretize the range of X_1 as several sub-interval of continuous values, with each interval corresponding to a discrete value. For any interval $[x_1, x_1 + \Delta]$, we can obtain the following based on Bayes' theorem:

$$P(c|x_1 \le X_1 \le x_1 + \Delta, x_2) = \frac{P(x_1 \le X_1 \le x_1 + \Delta|x_2, c)P(x_2, c)}{P(x_1 \le X_1 \le x_1 + \Delta|x_2)P(x_2)} \tag{3}$$

On the basis of Mean-value Theorem:

$$\begin{cases} P(x_1 \le X_1 \le x_1 + \Delta|x_2, c) = P(\xi|x_2, c)\Delta \\ P(x_1 \le X_1 \le x_1 + \Delta|x_2) = P(\eta|x_2)\Delta \end{cases}$$

Where: $p(\xi|x_2, c)$ and $p(\eta|x_2)$, respectively, are the corresponding median of probability density function for the interval $[x_1, x_1 + \Delta]$. So the Eq. (3) can be transformed as:

$$P(c|x_1 \le X_1 \le x_1 + \Delta, x_2) = \frac{P(\xi|x_2, c)\Delta P(x_2, c)}{P(\eta|x_2)\Delta P(x_2)} = \frac{P(\xi|x_2, c)P(x_2, c)}{P(\eta|x_2)P(x_2)} \tag{4}$$

As $\Delta \to 0, P(c|x_1 \le X_1 \le x_1 + \Delta, x_2) \to P(c|x_1, x_2)$ and $\xi, \eta \to x_1$, consequently we gain:

$$\lim_{\Delta \to 0} P(c|x_1 \le X_1 \le x_1 + \Delta, x_2) = P(c|x_1, x_2) = \frac{P(x_1|x_2, c)P(x_2, c)}{P(x_1|x_2)P(x_2)} \tag{5}$$

Extend the above results to high dimension attribute space and set $\Delta X = (X_{m+1}, \Lambda, X_n)$, then:

$$P(c|x_1, \Lambda, x_m, \Delta x) = \frac{P(x_1, \Lambda, x_m|\Delta x, c)P(\Delta x, c)}{P(x_1, \Lambda, x_m|\Delta x)P(\Delta x)} \tag{6}$$

With regard to the attribute set $\{Y_1, \Lambda, Y_m, X_{m+1}, \Lambda, X_n, C\}$, the following equation is established:

$$P(c|y_1, \Lambda, y_m, \Delta x) = \frac{P(y_1, \Lambda, y_m|\Delta x, c)P(\Delta x, c)}{P(y_1, \Lambda, y_m|\Delta x)P(\Delta x)} \tag{7}$$

With a comparison between Eqs. (6) and (7), combining with Eq. (2), it can be inferred that: $P(c|x_1, \Lambda, x_n) = P(c|y_1, \Lambda, y_m, x_{m+1}, \Lambda, x_n)$. After linear transformation, multivariate Gaussian vectors still submit to Multivariate Gaussian distribution. In addition, the irrelevance of Gaussian distribution is equivalent to independence. Therefore, if X_1, Λ, X_n obey Multivariate Gaussian distribution, so it is with Y_1, Λ, Y_m and the variables are independent of each other.

On the premise of non-destructive information, the original feature set $\{X_1, \Lambda, X_n\}$ is mapped to $\{Y_1, \Lambda, Y_m, X_{m+1}, \Lambda, X_n\}$, through orthogonal rotation transform. And the new attributes have a certain degree of independence. Thus, the sample distribution is approximate to the conditional independence assumption of Naive Bayes, which provides a favorable condition for the application of Bayesian Theory.

In Bayesian theory, the posterior probability is used as the classification index, which means the category with the maximum conditional probability output will be marked as a target value.

$$c^* = \arg\max_{c \in C} P(c|x_1, L, x_n) = \arg\max_{c \in C} P(c|y_1, L, y_m, x_{m+1}, L, x_n) \tag{8}$$

Assume that the variance matrix of $Y = \{Y_1, L, Y_m\}$ is a diagonal matrix, with λ_1, L, λ_m as its major diagonal elements. The corresponding variance of each component for Y reflects the information contained in the original index and it's measured by variance contribution rate:

$$\Delta\lambda_j = \frac{\lambda_j}{\sum_{i=1}^{m} \lambda_j} (1 \le j \le m)$$

According to the variance contribution rate in descending order, rearrange the attributes. Generally, when the cumulative variance contribution rate is more than 85%, the corresponding attributes can represent most of the information offered by the original variables, simultaneously eliminating the noise. Classically, supposing there are k attributes (k principal components) meeting the requirements: Y_1, L, Y_k, respectively. Then Bayes decision rule changes into:

$$c^* = \arg\max_{c \in C} P(c|y_1, L, y_k, x_{m+1}, L, x_n) \tag{9}$$

3 Data Description

The data set contains 1,853 entries of traffic incident data collected from May 1, 2005 to September 13, 2005 in Utrecht, a central city in the Netherlands [1]. In this data set, incident duration is the time between the detection and the clearance of an incident on the road. The parameter information of each item is presented in Table 1. There are three basic types of traffic incidents: stopped vehicle, lost load and accident.

A preliminary statistical analysis for all incident data and each type of incident is presented in Table 2, which shows that the parametric characteristics for each type of incident have a great difference from each other. Therefore, we will model each type of incident later.

Table 1. Basic information of traffic incident parameters

Parameters		Value
Time	By the week	weekday = 1 or weekend = 0
	By the day	peak hour = 1 or off peak hour = 0
Physical	Incident type	stopped vehicle/lost load/accident
	Vehicle type	truck = 1 and passenger car = 0
	Number of vehicles	0/1/2/3 or more than 3
	Only damage or casualties	(Only for accident) casualties = 1
	Damage to road equipment	Yes = 1 or No = 0
Response	Fire brigade required	Yes = 1 or No = 0
	Ambulance required	Yes = 1 or No = 0
	Tow truck required	Yes = 1 or No = 0
	Police force required	Yes = 1 or No = 0
	Track research required	Yes = 1 or No = 0
	Repair service required	Yes = 1 or No = 0
	Fluid to be cleaned required	Yes = 1 or No = 0
Management	Traffic control required	Yes = 1 or No = 0
	Road management required	Yes = 1 or No = 0
	Road inspector required	Yes = 1 or No = 0

Table 2. Results of statistical analysis

Incident type	Stopped-vehicle	Lost-load	Accident	All
Entries number	571	379	903	1853
Mean (min)	43.73	26.64	42.74	39.75
Standard deviation	37.90	19.58	41.38	37.40
Minimum (min)	2	1	0	0
Lower quartile	19	14	23	20
Median (min)	31	23	33	30
Upper quartile	57	34	48	47
Maximum (min)	282	139	435	435
Skewness	2.14	2.20	5.32	4.43
Kurtosis	6.47	7.77	38.99	32.18

Besides, normal probability plots (95% confidence interval) for all incident data and each type of incident are shown as Fig. 1, which indicates that the data does not obey normal distribution.

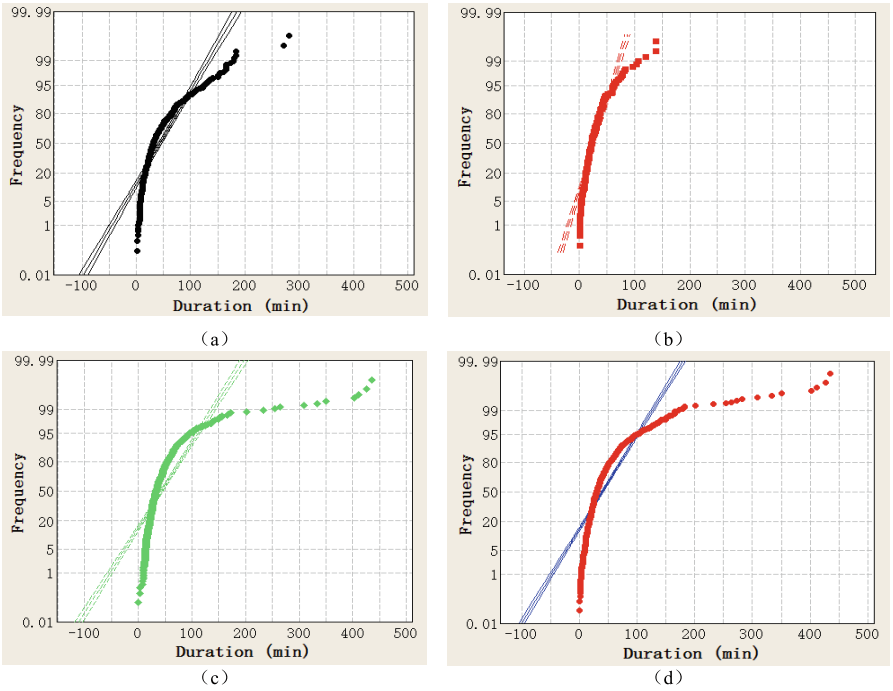

Fig. 1. Normal probability plot: (a) stopped-vehicle; (b) lost-load; (c) accident; (d) all accident

To figure out the distribution of incident duration, log-normal distribution, log-logistic distribution and weibull distribution are used to fit for all incident data and each type of incident, respectively.

As shown in Table 3, p-value of log-normal distribution and log-logistic distribution is smaller than 0.05, which means incident duration for all incident data and each type of incident is subject to log-normal distribution or log-logistic distribution. Moreover, the values of Anderson-Darling (AD) for log-logistic distribution is smaller than the ones for log-normal distribution, that is, log-logistic distribution is more suitable for incident duration of this data set. The fitting results of log-logistic distribution is presented in Fig. 2, which indicates that the incident duration between 10 min and 60 min have a great ratio. Some incidents that last from 90 min to 180 min have a great effect on the large standard deviation.

Table 3. Fitting results of four distribution functions

Distribution	Stopped vehicle		Lost load		Accident		All	
	AD	P	AD	P	AD	P	AD	P
Normal	31.043	<0.005	12.955	<0.005	87.956	<0.005	136.193	<0.005
Log-normal	0.456	>0.05	0.808	>0.05	4.313	>0.05	4.329	>0.05
Log-logistic	0.682	>0.05	0.481	>0.05	1.261	>0.05	0.766	>0.05
Weibull	3.682	<0.005	2.615	<0.005	35.221	<0.005	37.057	<0.005

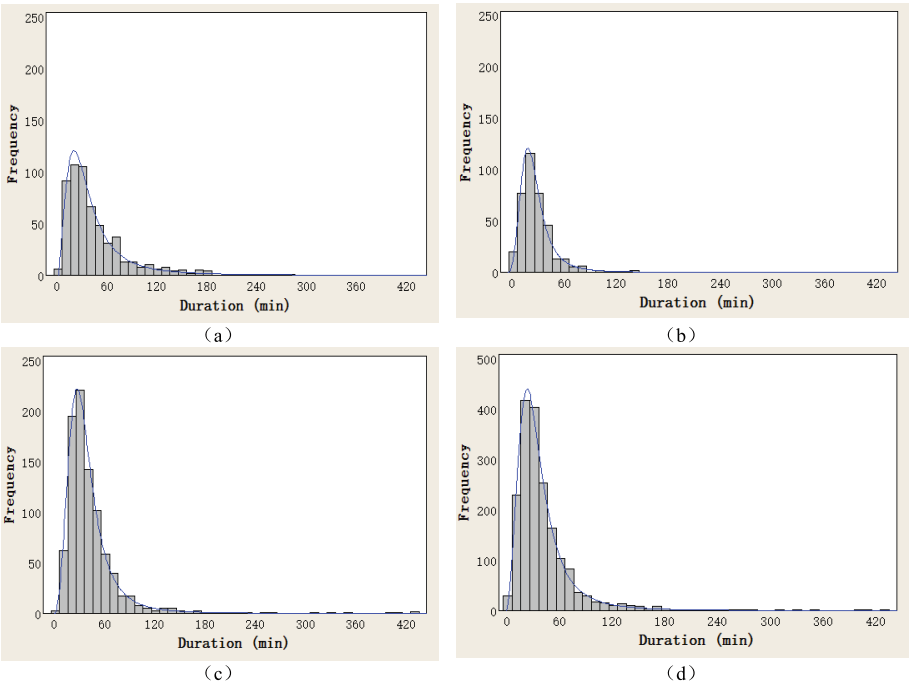

Fig. 2. Fitting results of log-logistic distribution: (a) stopped-vehicle; (b) lost-load; (c) accident; (d) all accident

4 Experiments Study

Firstly, according to the Chebyshev theorem, we set the incidents of small probability as outliers. We went through the detection of outliers based on Minitab. Secondly, on the basis of SPSS, principal component analysis was carried out. Before that, KMO and Bartlett's test should be satisfied. Thirdly, Naive Bayes classifier was processed on Weka, a free and open source software platform for data mining, to train and validate the data. By referring to related literature, we chose five evaluation indexes: prediction accuracy within 10 min' error, prediction accuracy within 15 min' error, prediction accuracy within 20' min error, prediction accuracy within 30' min error and mean absolute error, respectively. The basic steps of the experiment are as follows,

(1) Data pretreatment. Considering incident duration obeys a log-logistic distribution for each type of incident, at the 95% confidence level, we dropped the outliers on Minitab, leaving 559, 346 and 886 instances for each type of incident, respectively.
(2) KMO and Bartlett's test. Based on SPSS, P-values for each are small than 0.05, that is variables are relevant to each other. Meanwhile, the values of KMO for each type of incident are all more than 0.5, which means principal component analysis is suitable. Among them, the value of KMO for accidents is more than 0.7.

(3) Determining the number of principal components. We chose the number of principal components of which the cumulative variance contribution rate is more than 85%.
(4) Establishing the equations for every principal component. Data in the component matrix divided by the square root of corresponding eigenvalues gives out the corresponding coefficient to each index of the equations.
(5) Calculating the principal component scores. Bring the normalized data into the equations of principal components, to gain the corresponding principal component score for every instance.
(6) Applying discretization for continuous attributes. As the naive Bayesian toolbox of Weka assumes that all the variables of the data set are discrete and finite variables, first of all, the continuous variables are discretized. Incident durations were discretized as equal-width ones, at 5-min intervals.
(7) Dividing Data into the training set and the testing set. Every time, 25% instances were selected to test the prediction accuracy of Naive Bayesian Model established by the other 75% instances.
(8) Modelling based on Naive Bayes classifier by using the training set. For each type of incident, apply Naive Bayes classifier to deal with data obtained from the principal component analysis.
(9) Predicting and evaluating on the testing set. According to the evaluation indexes, sort out the predicting results.

Finally, we got three models for forecast. As summarized in Table 4 below, more than half of the instances of lost-load and accident are predicted within 10 min' error, but the percentage for stopped vehicle is inferior. The combined model of PCA and NB has a good performance, all exceeded 75%, on forecasting for each type of incident within 20 min' error. During the low and middle time periods (<30 min, 30–60 min), the combined model of PCA and NB has reached a relatively high prediction accuracy, of which there may be two reasons. In the first place, there was more instances during that time period, comparing with high time period, which was benefit for better learning of the data. In the second place, on the short time range, the error is relatively small, consequently resulting in high prediction accuracy. Furthermore, prediction accuracy within 15 min' error for each type of incident approached 80% during low time period (<30 min). Correspondingly, prediction accuracy of the instances among the long time range is not high. The reason may be that with great randomness, incident duration is related with many factors, thus large differences of data itself do exist. Moreover, it's acceptable with greater error for such instances. Last but not least, within the same error range, prediction accuracy of accidents is the highest, compared with that of stopped vehicle and lost-load incidents. It's probably that the value of KMO for accidents is 0.775, the highest, which indicates that principal component analysis is ideal for instances of accidents. In addition, among the three types, the instance of accidents is the most, which is conducive to data mining.

Table 4. Prediction results of the combination of PCA and NB model

Incident type		Stopped-vehicle	Lost-load	Accident
Mean absolute error		0.1556	0.1783	0.1260
Prediction accuracy within 10 min' error	<30 min	55.09%	61.11%	65.99%
	30–60 min	40.12%	46.39%	52.78%
	>60 min	18.11%	46.67%	31.01%
	Total	42.93%	56.36%	55.53%
Prediction accuracy within 15 min' error	<30 min	80.75%	79.49%	78.59%
	30–60 min	68.86%	55.67%	70.83%
	>60 min	33.07%	53.33%	56.59%
	Total	67.44%	71.68%	72.23%
Prediction accuracy within 20 min' error	<30 min	88.68%	88.03%	90.43%
	30–60 min	79.04%	70.10%	85.83%
	>60 min	46.46%	66.67%	75.19%
	Total	77.46%	82.08%	86.34%
Prediction accuracy within 30 min' error	<30 min	93.58%	93.59%	95.47%
	30–60 min	89.82%	79.38%	94.17%
	>60 min	67.72%	80.00%	88.37%
	Total	88.19%	89.02%	93.91%

Jiyang et al. [13] built a model based on Bayesian Decision Method-Based Tree, and she got a prediction accuracy of 79% for lost-load incident within 10 min' error and 65% for the accident within 20 min' error. Compared with their results, ours within 20 min' error is higher; while in the periods of short duration, our model's performance is inferior to theirs. Wu et al. [6] employed SVM to predict incident duration; Wang et al. [7] made use of Partial Least Squares Regression. Within 10 min' error, we got the best prediction accuracy for accidents and lost-load incidents, compared with the researches of Wang and Wu; within 15 min' error, prediction accuracy for accidents of ours is better than that of what Wu did; within 20 min' error, as to the prediction accuracy for accidents and stopped-vehicle incidents, ours is better than that of Wang's research. When it turns to mean absolute error, ours for stopped- vehicle incidents and accidents is lower, compared with the research of Wang.

Compared to their prediction results, the model we built based on a combined model of Principal Component Analysis and Naive Bayes made an improvement, especially for accidents, thus making it an alternative way to predict duration.

5 Conclusions

In this paper, we established a combined model of Principal Component Analysis and Naive Bayes to mine the potential relationship between incident duration and its influential factors. The prediction accuracy within 20 min' error for each type of incident is 77.46%, 82.08% and 86.34%, respectively. Compared with the previous research, the prediction accuracy is acceptable. However, it must be pointed out that the prediction

performance of accidents is better than the others. We summarize the reasons as follow: on one hand, the value of KMO for accidents is the highest, more than 0.7, indicating PCA is ideal for accidents; on the other hand, instance of accidents is the most, contributing to fully learning of data. With a wide variety of influential factors, strong random, it is of significance to improving data collection by replenishing data constantly and gathering as many factors as possible. What's more, prediction accuracy of incidents over 60 min didn't work well. There can be two chief causes. Firstly, sample imbalance, large incident duration instances is less than the small and the middle ones. Secondly, a large number of inconsistent records in the data set, that is, although some instances have same attributes, their durations are significantly different from each other. Hence, our further study will pay more attention to manipulating inconsistent records and making use of appropriate sampling techniques. Meanwhile, we will make the effort on more different methods to improve the predict performance of incident duration.

Acknowledgements. This work was supported by National Natural Science Foundation of China under Grant No. 61374195, the "Fundamental Research Funds for the Central Universities" and the "Research and Innovation Project for College Graduates of Jiangsu Province" No. SJLX15_0064.

References

1. Knibbe WJJ, Alkim TP, Otten JF, et al (2006) Automated estimation of incident duration on Dutch highways. In: 2006 IEEE intelligent transportation systems conference. IEEE
2. Giuliano G (1989) Incident characteristics, frequency, and duration on a high volume urban freeway. Transp Res Part A Gen 23(5):387–396
3. Lin L, Wang Q, Sadek AW (2016) A combined M5P tree and hazard-based duration model for predicting urban freeway traffic accident durations. Accid Anal Prev 91:114–126
4. Nam D, Mannering F (2000) An exploratory hazard-based analysis of highway incident duration. Transp Res Part A Policy Pract 34(2):85–102
5. Garib A, Radwan AE, Al-Deek H (1997) Estimating magnitude and duration of incident delays. J Transp Eng 123(6):459–466
6. Wu WW, Chen S, Zheng C (2011) Traffic incident duration prediction based on support vector regression. In: Proceedings of the ICCTP, pp 2412–2421
7. Wang X, Chen S, Zheng W (2013) Traffic incident duration prediction based on partial least squares regression. Procedia-Soc Behav Sci 96:425–432
8. Li R, Pereira FC, Ben-Akiva ME (2015) Competing risks mixture model for traffic incident duration prediction. Accid Anal Prev 75:192–201
9. Ozbay K, Kachroo P (1999) Incident management in intelligent transportation systems
10. Smith KW, Smith BL (2001) Forecasting the clearance time of freeway accidents. The Center
11. Wang W, Chen H, Bell MC (2002) A study of characteristics of motorway vehicle breakdown duration. In: Eleventh international conference on road transport information and control (Conf. Publ. No. 486). IET

12. Parka H, Haghania A, Zhangb X (2016) Interpretation of Bayesian neural networks for predicting the duration of detected incidents. J Intell Transp Syst Technol Plann Oper 20(4): 385–400
13. Jiyang B, Zhang X, Sun L (2008) Traffic incident duration prediction grounded on Bayesian decision method-based tree algorithm. J Tongji Univ (Nat Sci) 36(3):319 (in Chinese)
14. Yu B et al (2016) A comparison of the performance of ANN and SVM for the prediction of traffic accident duration. Neural Netw World 26(3):271

Improve the Urban Basic Construction of Facilities and Guarantee the Urban Traffic Flow

The Research of Traffic-Nodes After Completing the In-Plane Four-Palace Type Expressway Networks

Jianyong Fei(✉)

Urumqi Bureau of Municipal Construction, Urumqi, China
269365547@qq.com

Abstract. This paper shows new-arisen traffic-nodes problems and the economic and social benefits brought from the Urumqi in-plane four-palace type expressway networks. It analyzes the present state of traffic-nodes, digs out the reasons for this. Furthermore, it brings up feasible solutions and scheme. It draws summary and reflection of the integrated traffic networks construction, and notes them down as valuable experience for the subsequent engineering. At last, I come up with thought and future planning of traffic management and organization.

Keywords: The in-plane four-palace type expressway networks · Traffic-nodes · Present traffic state · Solutions and planning

By rebuilding and enlarging the capacity of Urumqi's main road networks, 3-year lasting construction of the in-plane four-palace type expressway from 2012 to 2014 has realized the networking and three dimensional network system of expressway frame in central area. The in-plane four-palace type expressway networks has greatly improved the urban traffic environment, and perfected the road networks of Urumqi. In view of the reality, since this project was finished, it has obviously benefited Urumqi's traffic. Moreover, it has promoted the development of Urumqi's traffic and communication industry, this project has achieved immense economic and social benefits as well. By enlarging and remolding the routes, uplifting and rebuilding the ground expressway, building and transforming the intersections and ramps, not only have they improved the holistic traffic capacity and the service of the outer ring roads, removed the traffic bottlenecks and the jamming point, and enhanced the links and transformation of expressway and backbone road networks, but also it has strengthen the function of urban ring expressway. In the progress of building the in-plane four-palace type expressway, it was supported by the Government of Urumqi; it got consistent high raise and recognition in the industry; it was supported by all the citizens. During the period when it was gradually put into practice, it achieved successfully in the society. In all, in-plane four-palace type expressway networks has laid solid foundation for Urumqi's development and planning pattern in the future!

X. Zeng et al. (eds.), *International Symposium for Intelligent Transportation and Smart City (ITASC) 2017 Proceedings*, Smart Innovation, Systems and Technologies 62, DOI 10.1007/978-981-10-3575-3_2

Meanwhile, because of the great change resulted from "Siphonic Effect", which is caused by the transformation of the expressway backbone, and some influence which is caused by the limits of building overhead roads in the central area, traffic-nodes problems have arisen since the in-plane four-palace type was finished. The in-plane four-palace type roads project acts as the most significant municipal road engineering, so how to evaluate its benefits of improving urban traffic situation roundly, systematically, and accurately? How to master the reconstruction of urban traffic flow distribution after it was finished? How to diagnose and analyze the newly emerging traffic-nodes problems to improve the situation? How to build a far better integrated traffic network in order to provide basis, facts of traffic analysis for the subsequent road networks in the central areas such as "three-line crisscross"? How to provide useful experience and lessons for the subsequent construction of expressway network in the peripheral cities? These matters call for great attention. For this reason, although the engineering was completed, the traffic is in good condition; we still should dig into these matters and take actions to perfect it (Fig. 1).

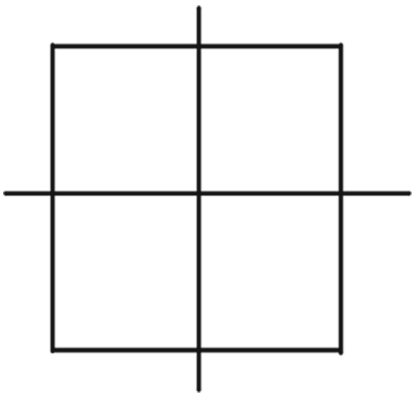

Fig. 1. The in-plane four-palace type expressway networks

1. Be serious about the investigation of the present situation, and evaluate the central road network traffic operation condition and effect reasonably.

The plan and construction of traffic system are supposed to be dynamic. For the reason that it must be advancing, though the reality may differs from the plan due to the changes in the development of social economy, we should take actions dynamic scrolling and always adjust measures.

The research of the in-plane four-palace type expressway networks analyzes its construction scale and adaptation to urban traffic demands, and the inner structure and function of the expressway networks in the aspect of level of construction and technical performance of road networks. It aims at revealing the use quality of the in-plane four-palace type expressway networks to optimize plans, offer information and gist for further decisions. With all sorts of quantitative index, we are able to analyze the urban traffic flow distribution and the differences from the previous traffic system. Also we can evaluate its effect that this engineering promotes traffic system running. The evaluation will

stands for "two combinations": Combination of the efficiency evaluation of expressway system and the effect of traffic organization to other kinds of roads; Combination of improvement of go through in sections of highway or important roads and changes of new-formed urban traffic flow distribution. With quantitative analysis in different aspects and from different views, we can evaluate the function and main effects of the in-plane four-palace type engineering in urban traffic system systematically and accurately.

2. Research and diagnose of traffic matters after in-plane four-palace type expressway was built, and the following plans, measures to perfect it.

On the basis of first-stage evaluation, aiming at the coming up problems of traffic-nodes, we can carry out specific survey to accurately evaluate the extent, peculiarity, and factors of traffic jam. As a result, it's possible to think of comprehensive actions, including regional engineering, traffic management, and traffic organization as well.

(1) According to the present situation after the first two phases were completed, we draw up conclusions about the main traffic-nodes.
   ① Liudaowan Overpass Ramps: south to the overpass is a north-to-south exit section where the traffic flow of north-to-south mainline of East Outer Ring Road, west-to-south turning ramp of Kenan Elevated Road and Liudaowan ground elevated ramp causes junction. Due to the seven up-down road streams change into three and the capacity of them differs vastly, it makes this point a prominent traffic-node in the whole road network.
   ② Back Street Off-ramp of East Outer Ring Road:It leads to serious jam because of the poor traffic capacity of the off-ramp roundabout and ground road junction.
   ③ Renmin Road Off-ramp: the traffic capacity of off-ramp entrance lane crossing is far from needs, which causes serious congestion.
   ④ Yuejing Street Overpass of East Outer Ring Road: As the planning and design for Yuejing Street Overpass haven't been put into practice, the old one being malformed overpass, huge traffic flow and complicated headings contribute to serious traffic jam.
   ⑤ West-to-north Off-ramp of Kenan Elevated Road: The fact that the traffic capacity of off-ramp entrance intersection is poor causes serious traffic jam and even influences the traffic stream in the artery.
   ⑥ Off-ramp of Kunming Road and ground road of Suzhou Road: the new-widen Suzhou elevated pier body has huge impact on ground traffic capacity and traffic flow capacity of transformation and organization. In this case, it's hard to satisfy vast ramps traffic demands of transforming on the ground. Different traffic flow directions disturb one another, which leads to frequent "Deadlock" phenomena and influences off-ramp traffic of Kunming Road evidently.
   ⑦ Off-ramp of Hetan Five Layers Overpass and Xinyi Road junction: The fact that the point of Hetan Five Layers Overpass off-ramp falling point is quite near Xinyi Road caused the result that the straight movement from Hetan relief road can't effectively interweave with right turn movement from off-road. Therefore, it results in a conflict point, and worse traffic jam.

(2) Through analysis and judgments, the factors of traffic-nodes are concluded as follows:

① Limited by the central land and other factors, several overpass ramps and up-down ramps don't reach the potential result. E.g. The impact of intersections.

The traffic capacity of intersection in much degree influences that of up-down ramps. In the crossing, vehicle is controlled by forbidden signal, so it is forced to slow down, stop, and then restart, accelerate. In addition, the outer ring road is located in the central area, the inner road networks running isn't that fluent. Traffic jam always happens during pick hours. The car waiting line being too long causes that traffic flow in the off-ramp is impossible to evacuate, which means ramp stream runs slowly, such as back street off-ramp of East Outer Ring Road, Yuejing street off-ramp of East Outer Ring Road, west-to-north off-ramp of Kennan Elevated Road and so on.

② in-plane four-palace type road engineering mainly widens the present elevated roads, so the new pier body inevitably will influence ground traffic capacity, especially in the ground roads' entry and exit:

Limited by elevated bridge pier body, new-built ramps take the place of separate belt or side pavement. Worse still, it has negative impact on some housing estates so that they must gather with new roads. Take Yuejing street off-ramp of East Outer Ring Road(two-lane road) for example, east to off-ramp, near News Building, traffic flow in the doorway collects and distributes through off-ramp, which leads to heavy jam in the right lane, also it influences the traffic capacity of ramps, slows the traffic stream and causes long waiting line.

③ After enlarging in-plane four-palace type roads' capacity and networking expressway, due to its apparent "Siphonic Effect", urban traffic flow distribution changes greatly, and it triggers new-arisen traffic jam matters.

④ Several traffic-nodes congestion also has something to do with other projects under construction that occupy land resource and the fact that the following engineering has not been operated.

At present, 1 line of Urumqi rail transit engineering is tense but orderly. It is principally underground construction of interval station, and it is completely closed. Occupying large construction field results in ground roads traffic organization changes so that it weakens present basic traffic capacity and then it intensifies partial road section's traffic pressure during peak hours.

(3) In my opinion, taking those issues as point cut, on the basis of thoroughly, deeply investigating present traffic running problem, we should make plans in terms of regional engineering transformation, traffic management, adjustment and perfection of traffic organization. Here is the analysis of overall perfection thought:

Given that we should guarantee expressway running benefits, as congestion may influence the whole road networks, it's a reasonable choice to weaken the traffic function of expressway sub-flow (If necessary, adopt the way of temporarily closing ramps), and link expressway traffic to ground roads. By doing so, we can avoid that several jamming points leads to "Cask Theory" in the whole expressway system.

Elevated off-ramp and ground road intersection's perfection is supposed to be priority. Research includes how to widen the entrance road of off-ramp and ground intersection, how to perfect ground intersection organization, and how to coordinate, response and control ground intersection signals when congestion elevated line is spreading.

As for ground road beneath the extended elevated road, we'd better enforce our research into traffic organization perfection plan when it's in complicated road environment, perfect turning-around position, traffic signal control and traffic flow direction organization. In particular, avoid congestion spreading in Suzhou Road due to different traffic flow directions, which reciprocally overlay and disturb and then contributes to "Deadlock" phenomenon.

Based on this analysis thought, I come up with some advice for current main traffic-nodes problems in in-plane four-palace type roads as follows:

① Liudaowan Overpass Ramp: On the basis of feasibility study report, it's possible to close Liudaowan north-to-south ramp and carry out East Outer Ring Road (Nanhu East Road-Renmin Road) green wave traffic management during the peak hours or when at the "7-3" converging point exists heavy traffic jam. In terms of long-dated traffic organization planning, I suggest that we should put Kelamayi east second-phase project and Second East Ring Road elevated project as soon as possible. If the two projects could be in use immediately they're finished, numerous vehicles could distribute through the two elevated roads. As a consequence, it will obviously ease present traffic pressure from East Outer Ring Road, and remove current traffic-nodes.

② Back Street Off-ramp of East Outer Ring Road: A study report shows that it's useful to strengthen the traffic capacity of off-ramp roundabout and ground road intersection part and make measures to perfect traffic organization.

   i. It's suggested that the exit at Back Street Off-ramp of East Outer Ring Road should cancel left-turn flow (to Dongfeng Road). This traffic flow could go through Dongfeng Road, Wuxing Road, turn right to Jianguo Road and turn left so that straight-left conflict points at the crossing of off-ramp exit and then increase off-ramp traffic flow speed;

   ii. It's suggested that the exit at Back Street Off-ramp of East Outer Ring Road should cancel the crossing links Wuxing South Road. This traffic flow could turn right continuously to join Wuxing South Road or via Renmin Road off-ramp of East Outer Ring Road. At the same time, transform off-ramp exit into two-lane two-way road.

③ Renmin Road Off-ramp: Investigate and draw up actions to coordinate ground intersection with elevated off-ramp traffic organization and control plans at super saturation state.

④ Yuejing Street Overpass of East Outer Ring Road: Study partial-widen engineering measures to improve Yuejing Street bridgehead traffic capacity and traffic organization perfection plans.

⑤ West-to-north Off-ramp of Kenan Elevated Road: Study engineering measures to widen ground road at West-to-north off-ramp falling point and measures to organize, manage, coordinate and perfect ground intersection and off-ramp traffic.

The reason for peak-hour congestion in West-to-north Off-ramp of Kenan Elevated Road is that we cut down the numbers of lanes of ground system. It used to be one-way lane. During peak hours, traffic flow change into two lanes, plus a ground relief road to integrate traffic flow at ground crossing signal lamps. Since right-turn traffic flow is too much, which leads to long waiting line, it weakens traffic capacity.

It's suggested that we'd widen ground road for one lane to north at off-ramp falling point, levy a bungalow at Hepingqu bridgehead, and widen Aletai Road by adding one speed-change lane to increase right turn vehicle speed. It's suggested that construct pedestrian overpass at the gate of Xinjiang University, the museum's signal lamps. Meanwhile, remove present ones to decrease congestion resulted from traffic flow's waiting line. In this way, the overall traffic capacity in current section could be improved, and traffic pressure of these three ramps could be relieved.

Combined with long-dated traffic organization plans and thoughts, we can consider building elevated road at Xihong Road-Wooden Factory grade separation. Lessen ground road traffic pressure by connecting oriented interconnected ramp with Kenan Elevated Road, and congestion during peak hours could be removed fundamentally.

⑥ Off-ramp of Kunming Road and ground road of Suzhou Road: Study partial-construction engineering measures to improve ground road traffic transformation capacity of traffic flow from ramps and traffic organization and management plans. Especially perfect different direction traffic flow's turn around position.

⑦ Off-ramp of Hetan Five Layers Overpass and Xinyi Road junction: Study ideal plans to adjust Hetan Road broken section in Xinyi Road Overpass field. Setting two individual collector-distributor lanes to avoid conflict between right-turn traffic flows from five layers overpass off-ramp and straight-on traffic from Hetan relief road. At present, we can widen Hetan eastern relief road which links northeastern ramp. Besides, it is wise to widen the old one-way lane into one-way two-lane, remove, move back and build new high retaining wall, improve traffic capacity of relief road to Hetan mainline, and shorten vehicle waiting line on the relief road.

In addition, we should pay attention to connections between traffic-nodes and system improvement. Take these measures as point cut, we should think further and perfect plans on the basis of in-plane four-palace type expressway networks system analysis. To guarantee the effect and compare all sorts of plans, it is better to carry out systematical, deep, intuitive test, adjustment and perfection through field investigation.

3. Conclusion and suggestion of integrated in-plane four-palace type expressway traffic network engineering experience.

After the in-plane four-palace type expressway networks were completed, it serves as the most significant project to extent to peripheral area and to carry out arterial road networks transformation. From my point of view, it's quite necessary to analyze traffic function and arisen problems after in-plane four-palace type roads was completed from the aspect of integrated traffic networks. Make it clear the traffic function connection and link point between central area expressway system and arterial road system, between central area expressway system and peripheral expressway networks. Come up with

specific conclusions and propose for sub subsequent central arterial road networks and peripheral expressway networks construction as follows:

(1) Construct peripheral through traffic to evacuate outer traffic, to distribute vehicle for foreign trade and freight vehicle.

Through traffic and freight transport has huge impact on urban traffic. Through traffic lacks peripheral main road, especially traffic flow in the east that it can't run smoothly. Most of it runs on north-southern roads such as Hetan Road, which occupies limited resources of north-southern roads. The future road networks should solve this problem firstly, perfect peripheral through and freight passageway, and reduce traffic pressure of central urban area road networks. Doing as follows:

① Enlarge eastern and western ring freeway construction in city peripheral field to shield regional traffic's interference to Urumqi's urban area;
② Tuwu huge freeway urban section is changed from Hetan Road far phase to eastern ring freeway, so it passes by urban massif. We can transform Wukui freeway into urban expressway (the Second Ring Road in the West), recover Midong-Ganquanbao section of Hetan Road to urban expressway, speed up to construct urban second ring expressway in the east to reduce in-plane four-palace type expressway system traffic pressure;

(2) Plan well-connected urban road networks which gives priority to expressway and arterial road, and adds secondary trunk road and feeder highway.

Expressway system offers vehicle continuous traffic service that isn't disturbed by crossing signal delay, which means the speed is faster than ground roads. It even takes advantage in speed when traffic flow approaches designed traffic capacity over ground system. Although in-plane four-palace type expressway system set ramps linking ground roads in many places, passageways are much farther than ground crossings. What it mainly serves is middle-long distance vehicle. If too many short distance vehicles gather on expressway, it will certainly reduce the efficiency of expressway system.

Combining Urumqi's traffic development goal, construct efficient road traffic system, which construct expressway and arterial road as road networks skeleton, and take secondary trunk road, feeder highway as road networks basis. It is functional and has clear aspects. What's more, it can develop with other means of transportation in a balanced way.

(3) Improve the traffic capacity of at-grade intersection, increase partial grade separation.

Traffic delay resulted from traffic saturation at crossings acts as the main reason for traffic jam. Improving the traffic capacity of at-grade intersection and increasing partial grade separation could improve the running state of elevated expressway. General crossings have poor traffic capacity because of straight-straight, straight-left and left-left conflict points. Traffic lamp control, channelization traffic and grade separation are able to decrease or remove the crossing conflict points.

In the central area where available land is limited, it's wise not to set huge overpass. When the traffic flow is not that huge, channelization, multi-phase signal control and

simple grade separation are ideal actions. Only when general measures can't solve the problem do we consider setting overpass. According to traffic demands forecast model, predict traffic flow in main road crossings and construct new overpass at the intersections of expressway's crossings or expressway-arterial road crossings.

(4) Strive to develop public transportation, and reduce the rate of personal transportation.

Faced with influence of urban traffic flow, doubled motor vehicle and "wasp waist" traffic bottleneck between new-old towns, depending on big-scale road construction will only put urban traffic problem into a vicious circle. To avoid urban traffic state worsening further, we must construct competitive urban public transportation system instead of personal cars. Give priority to recently constructed BRT in Urumqi's urban traffic planning and construction.

Public transportation could be ground, underground or overhead. Compared with cars, public transportation vehicle occupies less space but has bigger passenger traffic capacity. Complete integrated public transportation system which take rail transit as skeleton, including numerous means of transportation such as bus rapid transit, conventional public transit and taxis.

(5) Plan and construct external traffic hub facilities.

By setting traffic hub station, it improves urban transportation accessibility, and reduces the differences among stations so that it can balance popularity distribution. In this way, we can drive core cities' distribution, activate cities' peripheral land, induce new distribution of urban popularity and employment, and promote to perfect cities' space form. Setting traffic hub stations plays an important role in improving transportation (long-distance passenger traffic, conventional public transit, BRT, subway and so on) running efficiency, and is an significant aspect of improving urban transportation service level.

References

1. Dorigo M, Gambardella LM (1997) An ant system: a cooperative learning approach to the traveling salesman problem. IEEE Trans Evol Cooperation (S1089-778X) 1(1):53–66
2. 王川.车路协同环境下交通控制与诱导协同研究[D]. [硕士学位论文].兰州理工大学,2014
3. 王艳青.面向城市复杂道路的交通状态识别手段与算法研究[D].[硕士学位论文].同济大学,2015
4. 王奕曾,金立名,袁腾飞,城市道路交叉口车辆排队交通流状态理论研究,《城市建设理论研究》,第 6 卷第 1 期,72 页,2016 年 1 月

Speed Control of Pure Electric Vehicle Based on Adaptive Fuzzy PID Controller

Linghui Xu[1], Jia Lu[2], and Jian Zhang[1(✉)]

[1] Research Center for Internet of Mobility, Southeast University, Nanjing 210096, China
jianzhang@seu.edu.cn
[2] Southeast University, Nanjing 210096, China

Abstract. Adaptive speed control of pure electric vehicle (PEV) has been an answer to automotive automated control in a connected vehicle environment. In various traffic conditions, real-time speed adjustment is necessary. In this paper, an adaptive fuzzy proportional integral differential (PID) controller is set up and a relevant speed control system is modeled. The simulation results in MATLAB show a very good performance of the adaptive speed controller especially when PEV are required to accelerate or decelerate with a large range. It is indicated that this adaptive speed controller is adaptable to various speed requirements of traffic conditions.

Keywords: Automated speed control · Adaptive fuzzy PID controller · Separately excited DC motor · Simulink Toolbox

1 Introduction

In recent years, the increasing number of automobiles has given rise to traffic jams, road accidents, automobile exhaust pollution and excessive fuel consumption. As a result, traffic problems become an important limiting factor hampering safe and ecological development of transportation. Under such circumstances, electric vehicle has been regarded as an alternative of fuel vehicle for less pollution and consumption.

After about 60 years of stagnation since 1930, the outlook of electric vehicle shifted dramatically in 1990's [1]. Since then, electric vehicle has attracted wide attention and massive research investments. Consequently, a wide range of electric vehicles are created by different automakers, like Think City of Ford, EV1 of GM, and so forth [2, 3]. Among them, some have been put into practical use.

The objective of this paper is to present an adaptive speed controller of pure electric vehicle driven by separately excited DC motor. This adaptive fuzzy PID controller, combining the advantage of fuzzy logic and PID controller, satisfies self-adjustment of the controller parameters and improving the capability of eliminating the steady-state error [4]. For the adaptive controller, one input is the real-time speed error between target speed and real speed of vehicle, and the output is desired duty cycle of the PWM signal. The output signal is transmitted to control armature voltage of the electric motor. The driving process of separately excited DC motor is discussed in detail and its mathematical model is simplified as the foundation of the adaptive speed control system.

X. Zeng et al. (eds.), *International Symposium for Intelligent Transportation and Smart City (ITASC) 2017 Proceedings*, Smart Innovation, Systems and Technologies 62, DOI 10.1007/978-981-10-3575-3_3

The remainder of this paper is organized as follows. Section 2 provides an introduction on the driving process of the separately excited DC motor and the development of mathematical model. Section 3 analyzes the test results of the adaptive speed controller based on the speed control system model in Simulink surroundings. Section 4 closes the paper with conclusion.

2 Separately Excited DC Motor

Pure electric vehicle driven by separately excited DC motor is taken into consideration in this paper. With regard to this type of motor, the excitation current is taken no account of as it has nothing to do with the armature current. The meaning of each parameter involved in this section is listed in Table 1.

Table 1. Parameters definition of driving process

Notation	Description	Notation	Description	Notation	Description
U	External voltage of motor	T	Electromagnet torque of motor	F_t	Driving force of vehicle
E_a	Induced electromotive force of armatures	T_L	Load torque of motor	F_f	Rolling resistance of vehicle
I_a	Armature current of motor	m_a	Cross weight of vehicle	F_w	Air resistance of vehicle
R	Total resistance of armatures	δ	Converse factor of rotating mass	F_i	Slope drag of vehicle
R_a	Internal resistance of motor	r	Wheel radius of vehicle	F_j	Acceleration resistance of vehicle
C_e	Structure constant of motor	i_g	Transmission ratio of vehicle	α	Road slope
C_T	Torque constant of motor	i_o	Final reduction ratio of vehicle	C_D	Coefficient of air drag
n	Rotating speed of motor	η_t	Mechanical efficiency of transmission system	A	Frontal area of vehicle
Φ	Magnetic flux	f	Coefficient of rolling resistance	V	Vehicle speed

The variation of V and T is shown in Fig. 1, with armature voltage increasing from U_1 to U_2. Due to inertia effect, the initial speed V_1 has no change at the first time. Meanwhile, electromagnet torque has a sudden change from T_1 to T_2. Subsequently, vehicle speed increases and electromagnetic torque decreases by degrees with the growing n, as the trajectory from Point2 to Point1 in the picture. If the time internal τ between the former state (Point2) and the latter one (Point1) is assumed to be quite small, the average acceleration during it approximately equals to the instantaneous acceleration caused by T_2.

$$F_t = F_f + F_w + F_i + F_j = fm_a g\ \cos\alpha + \frac{C_D A V^2}{21.15} + m_a g\ \sin\alpha + \delta m_a \frac{\partial V}{3.6\partial t} \tag{1}$$

$$F_t = F_f + F_w + F_j = fm_a g + \frac{C_D A V^2}{21.15} + \delta m_a \frac{\partial V}{3.6\partial t} \tag{2}$$

$$F_j = \delta m_a \frac{\partial V}{3.6\partial t} = \frac{(T_2 - T_L) i_g i_o \eta_t}{r} \tag{3}$$

$$T_L = \left(fm_a g + \frac{C_D A V^2}{21.15} \right) \frac{\mathrm{r}}{i_g i_o \eta_t} \tag{4}$$

$$\begin{cases} n = \frac{V i_g i_o}{0.377 r} \\ T = \frac{C_T \Phi}{R_a} U - \frac{C_e C_T \Phi^2}{R_a} n \\ T_L = \left(fm_a g + \frac{C_D A V^2}{21.15} \right) \frac{\mathrm{r}}{i_g i_o \eta_t} \\ F_j = (T - T_L) \frac{i_g i_o \eta_t}{r} \\ \frac{\partial V}{\partial t} = \frac{3.6 F_j}{\delta m_a} \\ V' = V + \frac{\partial V}{\partial t} \tau \end{cases} \tag{5}$$

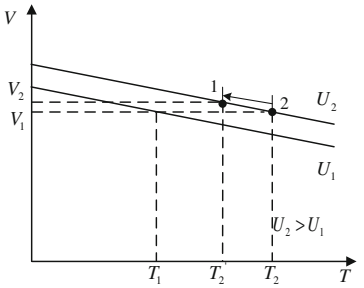

Fig. 1. Variation of vehicle speed and electromagnetic torque with increasing voltage

The kinetics of vehicle is generally expressed in Eq. (1). As the slope of flat roads is similar to zero, Eq. (1) is simplified into Eq. (2). In this case, T_L in Eq. (3) can be regarded as the equivalent resistance torque causes by F_f and F_w, as shown in Eq. (4).

Summing up the above, the mathematic model of separately excited DC motor in pure electric vehicle is built in Eq. (5).

3 Simulation and Results

In order to validate the performance of adaptive fuzzy PID control of pure electric vehicle, an adaptive speed control system is modeled in MATLAB with Simulink Toolbox [5]. This system in Fig. 2 consists mainly of an adaptive fuzzy PID controller module and a mathematical model module of separately excited DC motor. These two modules are connected by convertor subsystem (Table 2).

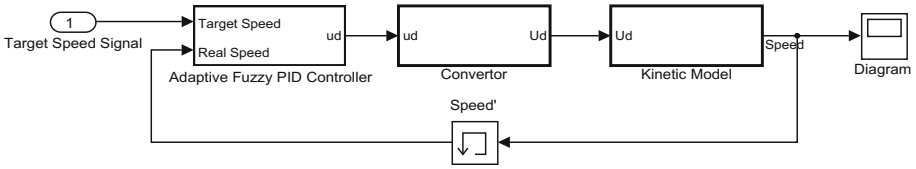

Fig. 2. Simulation model of the adaptive speed control system

Table 2. Parameters of adaptive speed control system

Notation	Value	Unit	Notation	Value	Unit	Notation	Value	Unit
K_e	0.2	-	U_{nom}	210	V	r	0.32	m
K_{ec}	0.22	-	I_{nom}	190	A	i_g	1.070	-
K_{u1}	0.8	-	n_{nom}	3000	$\mathrm{r{\cdot}min^{-1}}$	i_o	4.4	-
K_{u2}	2.2	-	R_a	0.0265	Ω	f	0.015	-
K_{u3}	0.01	-	$C_e\Phi$	$\frac{U_{nom}-I_{nom}R_a}{n_{nom}}$	$\mathrm{V{\cdot}(r{\cdot}min^{-1})^{-1}}$	C_D	0.35	-
k_{p0}	0.38	-	$C_T\Phi$	$9.55C_e\Phi$	$\mathrm{N{\cdot}m{\cdot}A^{-1}}$	A	1.8	$\mathrm{m^2}$
k_{i0}	0.48	-	m_a	1980	kg	δ	1.05	-
k_{d0}	0	-	τ	0.01	s	η_T	0.95	-

The maximum speed $V_{\max}$ is calculated as $V_{\max} = \frac{0.377 n_{nom} r}{i_g i_o} = 76.87$ km/h, then the maximum speed tested is chosen as 75 km/h. During each test, an acceleration (deceleration) process directly from one to another is regarded as a stage.

In Fig. 3, the increase of vehicle speed is made up of six accelerating stages. Desired accelerations of these stages are all around 2 $\mathrm{m/s^2}$. The subsequent decrease of speed from the maximum to 2 km/h is also of six stages, as shown in the latter part of the target speed signal. Desired deceleration of them are all around -2 $\mathrm{m/s^2}$. The corresponding variation of real speed is shown in black solid lines in this picture. It is found that the real speed lines remains broadly consistent with the target speed lines. As shown in Table 3, the variation of acceleration is acceptable in general. Small mean absolute error of acceleration in each stage means that real acceleration is broadly in line with the desired one. In addition, minor mean absolute derivation of acceleration shows a small rate of change of real acceleration. The smaller the rate of change is, the more comfortable environment will be given for passengers. The response time of each

stage approximately equals to the desired one, which means that the real speed controlled by the adaptive speed control method tends to stabilize within a period as expected. Besides, tiny values of maximum error, mean absolute error, and steady-state error of speed all denote that real speed are highly consistent with target one in each stage. Also, small mean absolute derivative of speed in each line means that real speed maintains stabilization during a certain period. That is to say, satisfactory vehicle speed is achieved by the adaptive speed control method within a predetermined time frame in a general comfortable way.

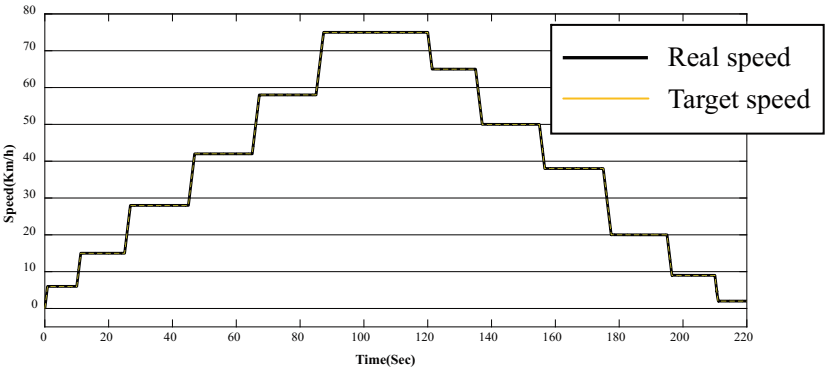

Fig. 3. Variation of vehicle speed with expected speed variation less than 20 km/h

Table 3. Differences in acceleration process with expected speed variation less than 20 km/h

V_{target} (km/h)	$a_{desired}$ (m/s^2)	$a_{\max}$ (m/s^2)	a_{MAE} (m/s^2)	a_{MAD} (m/s^2)	$t_{response}$ (s)	$Verror_{\max}$ (km/h)	V_{MAE} (km/h)	V_{MAD} (km/h)	$Verror_{ss}$ (km/h)
6	2.0080	2.0114	0.0425	0.0737	0.01	0.0003	0.0005	−0.0463	0.0001
15	2.0000	2.0006	0.0227	0.0382	0.01	0.0003	0.0001	−0.0308	0.0002
28	1.9951	1.9969	0.0081	0.0118	0.00	0.0004	0.0001	−0.0510	0.0003
42	2.0046	2.0911	0.0065	0.0076	0.00	0.0005	0.0003	−0.0335	0.0005
58	2.0020	2.1874	0.0070	0.0073	0.00	0.0007	0.0005	−0.0213	0.0006
75	2.0009	2.3608	0.0324	0.0470	0.03	0.0007	0.0001	0.0156	0.0006

The result of deceleration process is show in Table 4. Minimum decelerations are all much less than the desired ones, especially in the last stage. Nonetheless, the adaptive speed controller can be used for practical applications as the minimal value of minimum decelerations is −3.6331 m/s^2, acceptable for passengers at least. Apart from that, small mean absolute errors and mean absolute derivative of decelerations of first five stages also shows the ordinary compliance and stability of real decelerations. When in the last stage, mean absolute error and mean absolute derivative of deceleration are much more than others. It may be due to the constant adaptation of deceleration with a little bigger range, when vehicle accelerating from a small speed to a relatively smaller one. The response time of each stage tends to equal to the target one, which shows an ideal reaction of the adaptive speed controller. In addition, control effect on vehicle speed is

great. Tiny values of maximum error, mean absolute error, and steady-state error of speed and small mean absolute derivative of it show both accuracy of the speed control and stability of results in extensive time.

Table 4. Differences in deceleration process with expected speed variation less than 20 km/h

V_{target} (km/h)	$d_{desired}$ (m/s^2)	$d_{\max}$ (m/s^2)	d_{MAE} (m/s^2)	d_{MAD} (m/s^2)	$t_{response}$ (s)	$Verror_{\max}$ (km/h)	V_{MAE} (km/h)	V_{MAD} (km/h)	$Verror_{ss}$ (km/h)
65	−1.9984	−2.6675	0.0170	0.0170	0.00	0.0025	0.0024	0.0234	0.0006
50	−2.0032	−2.7582	0.0141	0.0141	0.00	0.0033	0.0037	0.0384	0.0005
38	−1.9960	−2.7542	0.0171	0.0184	0.00	0.0031	0.0033	0.0382	0.0004
20	−2.0000	−2.8513	0.0158	0.0157	0.00	0.0063	0.0065	0.0540	0.0003
9	−1.9971	−3.3064	0.0312	0.0326	0.00	0.0077	0.0064	0.0451	0.0007
2	−2.0046	−3.6331	0.2594	0.2893	0.11	0.0016	0.0009	0.0172	0.0004

Generally speaking, the adaptive speed controller plays a good role in acceleration process with expected speed variation more than 20 km/h. For six separate stages in Table 5, there is little differences between maximum accelerations and desired values. In addition, value of each mean absolute error and each mean absolute derivative are all quite small. Therefore, real accelerations of these separate stages are ideal with high stability. Besides, tiny maximum error, mean absolute error and steady-state error of speed as well as small mean absolute derivative in each line are obtained based within expected response times. It is illustrated that speed control based on the adaptive fuzzy PID controller is suitable for acceleration and deceleration requirements with great changes.

Table 5. Differences in acceleration process with expected speed variation more than 20 km/h

V_{target} (km/h)	$a_{desired}$ (m/s^2)	$a_{\max}$ (m/s^2)	a_{MAE} (m/s^2)	a_{MAD} (m/s^2)	$t_{response}$ (s)	$Verror_{\max}$ (km/h)	V_{MAE} (km/h)	V_{MAD} (km/h)	$Verror_{ss}$ (km/h)
0–25	2.0013	2.0047	0.0107	0.0191	0.01	0.0004	0.0001	−0.0415	0.0004
0–35	2.0005	2.0039	0.0076	0.0138	0.01	0.0006	0.0001	−0.0415	0.0005
0–45	2.0000	2.0034	0.0059	0.0108	0.01	0.0007	0.0002	−0.0415	0.0007
0–55	1.9997	2.0031	0.0049	0.0088	0.01	0.0009	0.0003	−0.0416	0.0008
0–65	1.9995	2.0029	0.0041	0.0075	0.01	0.0010	0.0004	−0.0417	0.0010
0–75	1.9994	2.0028	0.0075	0.0140	0.03	0.0022	0.0017	−0.0453	0.0011

In Table 6, it can be found that the adaptive speed control has a good performance in controlling both acceleration and speed. Minimum accelerations are similar to the desired ones. Moreover, mean absolute error and mean absolute derivative of acceleration in each line are small. On the other hand, error and derivative of speed in each line all have tiny values regardless of the little longer response time. Furthermore, it is a fact that different types of errors and derivative of deceleration in the previous lines are

almost all more than those in the latter lines, while the situation of vehicle speed is exactly the opposite. It may be caused by the reason that deceleration process with higher variation is more likely to remain a stable deceleration, while the one with smaller variation has to adjust the deceleration constantly with a relatively wider range.

Table 6. Differences in deceleration process with expected speed variation more than 20 km/h

V_{target} (km/h)	$d_{desired}$ (m/s^2)	$d_{\max}$ (m/s^2)	d_{MAE} (m/s^2)	d_{MAD} (m/s^2)	$t_{response}$ (s)	$Verror_{\max}$ (km/h)	V_{MAE} (km/h)	V_{MAD} (km/h)	$Verror_{ss}$ (km/h)
25–2	−2.0028	−2.0075	0.0701	0.1175	0.11	0.0006	0.0008	0.0398	0.00005
35–2	−2.0015	−2.0062	0.0497	0.0859	0.11	0.0010	0.0014	0.0427	0.00005
45–2	−2.0007	−2.0059	0.0393	0.0676	0.11	0.0021	0.0028	0.0452	0.00005
55–2	−2.0003	−2.0075	0.0329	0.0557	0.11	0.0026	0.0035	0.0478	0.0001
65–2	−2.0000	−2.0092	0.0287	0.0473	0.11	0.0040	0.0051	0.0501	0.0001
75–2	−1.9998	−2.0127	0.0258	0.0412	0.11	0.0056	0.0067	0.0523	0.0001

4 Conclusion

This paper presents a real-time adaptive speed control method for pure electric vehicle in a connected vehicle environment. This method applies fuzzy logic and PID controller to control the armature voltage of motor. An adaptive speed control system is modeled in MATLAB with Simulink Toolbox to test performance of the speed control method. It is mainly made up of an adaptive fuzzy PID controller module and a drive system module of separately excited DC motor. Results show that the adaptive speed controller plays a good role in adapting speeds of vehicle to targets within desired time frames. Especially when vehicle is expected to accelerate or decelerate with a huge change of speed, this controller has a great performance on both acceleration (deceleration) and speed control.

Acknowledgements. This study is partially supported by the National Key R&D Program in China (No. 2016YFB0100906) and the Science and Technology Demonstration Project of Ministry of Transport of China (No. 2015364X16030).

References

1. Chan CC (1993) An overview of electric vehicle technology. Proc IEEE 81(9):1202–1213
2. Chan CC (2002) The state of the art of electric and hybrid vehicles. Proc IEEE 90(2):247–275
3. Riezenman MJ (1998) Engineering the EV future. IEEE Spectr 35(11):18–20
4. Zheng J, Zhao S, Wei S (2009) Adaptive fuzzy PID control for switched reluctance motor direct drive servo hydraulic press. In: International Conference on Measuring Technology and Mechatronics Automation, pp 771–774
5. Åström KJ, Hägglund T (2001) The future of PID control. Control Eng Pract 9(11):1163–1175

Designing a Dynamic Control Platform of Electric Bus Vehicles

Gang Zhong(✉), Tingting Yin, Jian Zhang, and Linchao Li

School of Transportation, Southeast University, No. 2 Sipailou, Xuanwu District, Nanjing 210096, China
anhuizhonggang@126.com, yttwen@163.com, jianzhang@seu.edu.cn, lilinchao123@163.com

Abstract. The dynamic control of bus vehicles can reduce the emergencies during the running time of the buses, such as bunching. Electric bus vehicle is one category of new energy vehicles which are environmentally friendly transportation means. A dynamic control platform of electric bus vehicles can make up the disadvantages of control strategies based on human experience. In this paper, we put forward such a platform to deal with the problem. The overall structure of the platform is proposed first, and four sub-systems are designed to implement the functions of data collection, storage, processing and releasing. The ways of data communication between inside and outside environment are illustrated based on the description of different kinds of data. Moreover, we design control strategies of the platform which mainly combine holding and skipping, and an example is given to explain the implements of the control strategies and the data processing sub-system.

Keywords: Electric bus vehicles · Dynamic control · Data communication

1 Introduction

The development of public transit is an effective method to deal with problems of congestion, pollution and resources waste. Advanced Public Transportation Systems (APTS), which combines communication technologies with systems engineering, can make the public transit more appealing to passengers. Moreover, electric bus vehicles have been widely employed by the public transit systems in recent years to protect the environment. An efficient platform of electric bus vehicles is a support method for bus dynamic controlling and dispatching. It also can predict the travel time of bus vehicles and display the real-time information. Data collection and communication can be achieved by Vehicle-Infrastructure Cooperation Systems (VICS).

Some researches about bus control platforms were concentrated on communication technologies. Gao [1] designed an Information Release System (IRS) based on the wireless network. In this system, short-haul communication between vehicles and bus stations could be realized by ZigBee, while long-haul communication between different bus stations or between stations and the control center could be realized by Wi-Fi.

X. Zeng et al. (eds.), *International Symposium for Intelligent Transportation and Smart City (ITASC) 2017 Proceedings*, Smart Innovation, Systems and Technologies 62, DOI 10.1007/978-981-10-3575-3_4

Zhang and Ran [2] proposed an analytical method of communication connectedness aimed for the dynamic dispatching, which mainly focused on the distances between vehicles and the communication mode. Sumcad et al. [3] invented a communication method which used the multimedia messaging service to realize the real-time communication between vehicles and the control center.

Meanwhile, other researchers focused on structures of bus control platforms. Cao [4] put forward an intelligent bus system which was divided into five modules: data communication module, data receiving module, data processing module, data display module and data storage module. However, this system just aimed to realize the function of monitoring vehicles. Zou [5] designed an overall bus system structure which stipulated the contents of information interaction including vehicle-to-vehicle and vehicle-to-infrastructure. Brata et al. [6] designed a data collection system for the planning of bus lines, and the system contained three functions which were data collection, data updating and data management.

Previous researches on bus control platforms only designed part of the bus system, which were lack of systematisms. Moreover, electric bus vehicles have different features from the normal ones. One is the process of charge-discharge, and the other is energy recovery design which happens at the braking moment.

A systematic dynamic control platform of electric bus vehicles is put forward in this paper. Section 2 is the overall structure of the platform and the function design of each sub-system. Section 3 is the design of data agreement, communication and interaction. Dynamic control strategies and a simple example are given in Sect. 4. Section 5 is the conclusion.

2 Overall Structure

The proposed dynamic control platform of electric bus vehicles contains four sub-systems which are respectively Data Collection Sub-system (DCS), Integrated Database (ID), Data Processing Sub-system (DPS) and Data Releasing Sub-system (DRS). The overall structure of the platform is showed in Fig. 1.

A. *Data Collection Sub-system.* Data Collection Sub-system is the foundation of the dynamic control platform of electric bus vehicles. APC data, IC Card data, GPS data, sensors data and station passengers' data should be collected in this sub-system. Collection technologies and contents are listed in Table 1 as follow. One of the most remarkable features is the sensors data which show the special features about electric bus vehicles. For example, pedal position can reflect the energy recovery phenomenon.
B. *Integrated Database.* Integrated Database can store and manage all static, dynamic and historic data about electric bus vehicles. It can be divided into four sub-databases which are collection database, static database, historic database and thematic database. Data description will be explained in details in Sect. 3.

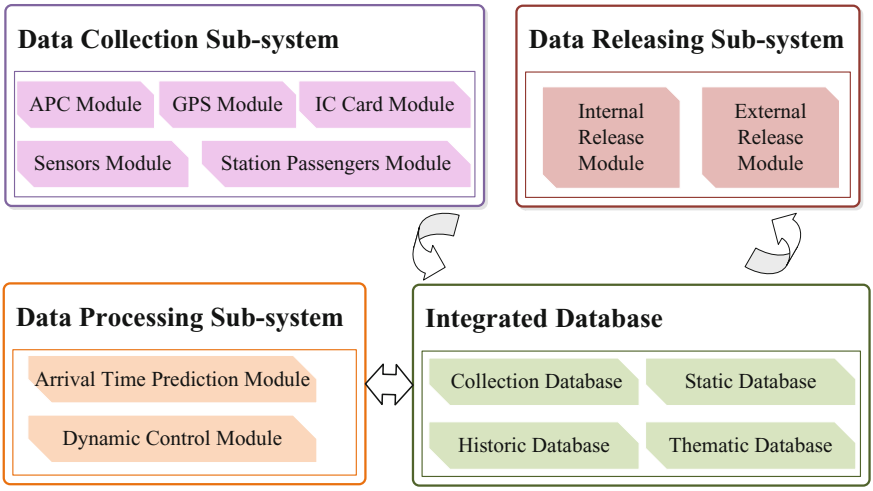

Fig. 1. The overall structure of the platform

Table 1. Collection technologies and contents of every module

Module	Technologies	Contents
APC	Initiative infrared detectors: set at the front and back doors	Passenger boarding/alighting data
IC card	Integrated circuit card: hold by passengers	Only passenger boarding data (including individual information)
GPS	Global positioning system: a technology of automatic vehicle location	Longitude, latitude, height, speed and time at a high frequency
Sensors	Magnetic sensor, Voltage sensor, Displacement sensor	Speed, The quantity of electricity, Pedal position
Station passengers	Video signal detection counter	Passengers flow at every bus station

C. *Data Processing Sub-system.* There are two functions in Data Processing Sub-system. The former is used for bus arrival time prediction and the latter is for dynamic control of vehicles. Arrival time prediction is the main demand of passengers as well as the criterion of when, where and how to control bus vehicles. Control strategies will be introduced in Sect. 4.

D. *Data Releasing Sub-system.* Data Releasing Sub-system has two functions served for two different groups which are passengers and managers. Internal Release Module is designed to release control orders to managers while External Release Module is designed to release predicted arrival time to passengers. The release methods and contents of different modules are showed in Fig. 2.

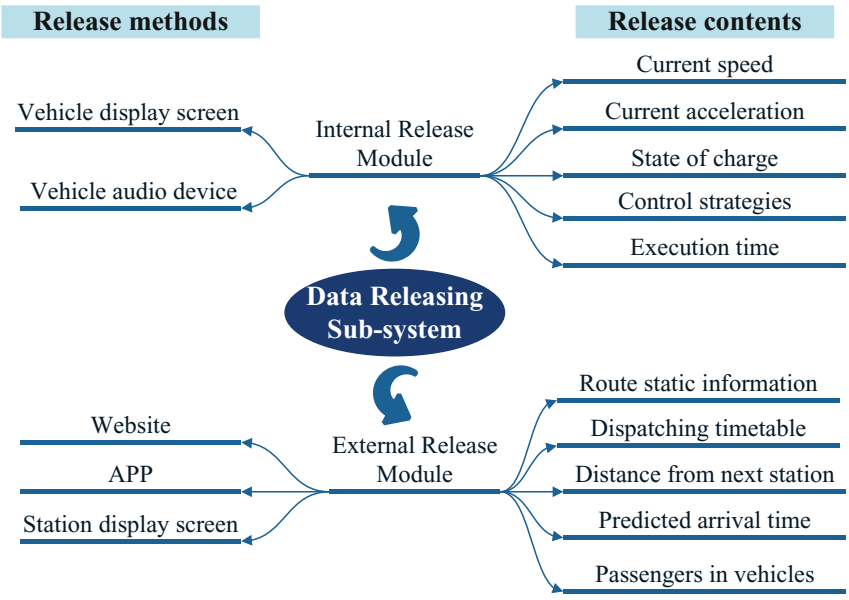

Fig. 2. The methods and contents of data releasing sub-system

3 Data and Communication

A. *Data Description.* The proposed platform contains kinds of data which are collection data, static basic data, historic data and some processed data. All the data should be stored, processed and analyzed in the Integrated Database. The details are listed in Table 2.

Table 2. Data categories in different sub-databases

Sub-database	Contents
Collection database	APC data, IC data, GPS data, station passengers' data and vehicle sensors data
Static database	Information of routes, vehicles, stations and vehicle shift
Thematic database	Vehicle in and out data, dynamic control data and weather
Historic database	Historic contents of center collection database, static database and thematic database

Entity Relational Diagram (E-R Diagram) can describe the entities, relations and attributes of data. In this section, E-R Diagram of the proposed Integrated Database is drawn in Fig. 3. Only some key attributes of each entity which are marked by the term

"PK", are listed as examples. Relationships between every two entities are dependency and relevance. The dashed line means the former and the solid line means the latter.

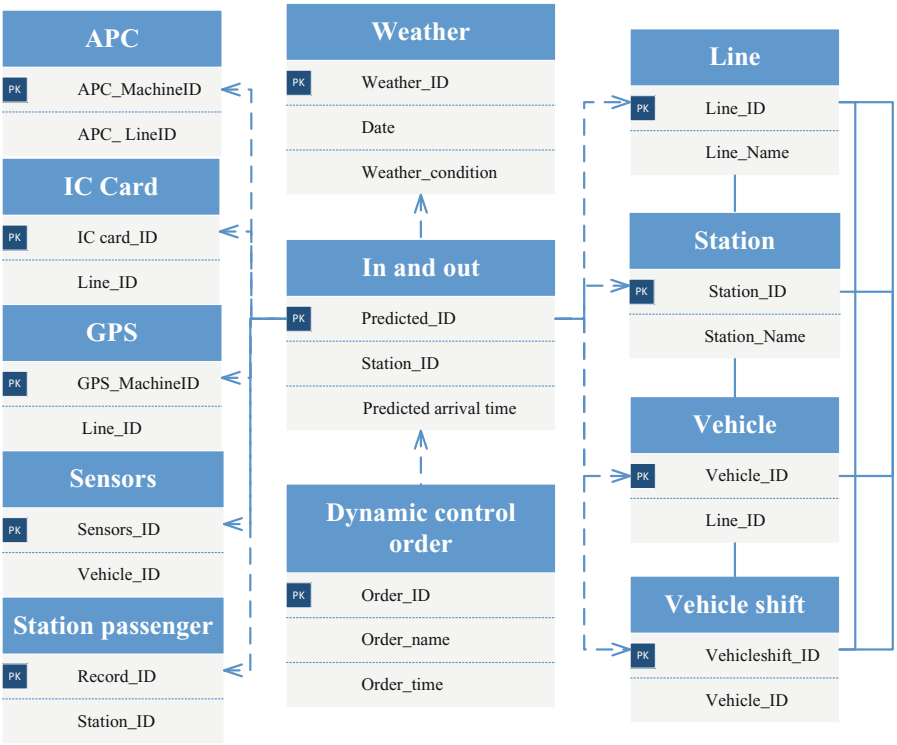

Fig. 3. E-R diagram of the proposed integrated database

B. *Data Communication.* There are four steps during the data communication process. They are data access, data storage, data processing and data releasing respectively. The process is listed below and showed in Fig. 4.

- APC data, IC Card data and Sensors data are obtained during the travel in real-time, and they can be transferred from vehicles to station temporary storage devices by Dedicated Short Range Communications (DSRC) when vehicles arrive at stations.
- All the three kinds of data and GPS data, station passengers' data are transferred to the collection database in the integrated database by General Packet Radio Service (GPRS).
- Data in Collection Database, Static Database and Historic Database are adopted to data processing, and processing results are sent back to Thematic Database.
- Thematic data can be released by kinds of devices: external devices such as websites, APPs, and station display screens, and internal devices such as vehicle display screens and vehicle audio screens.

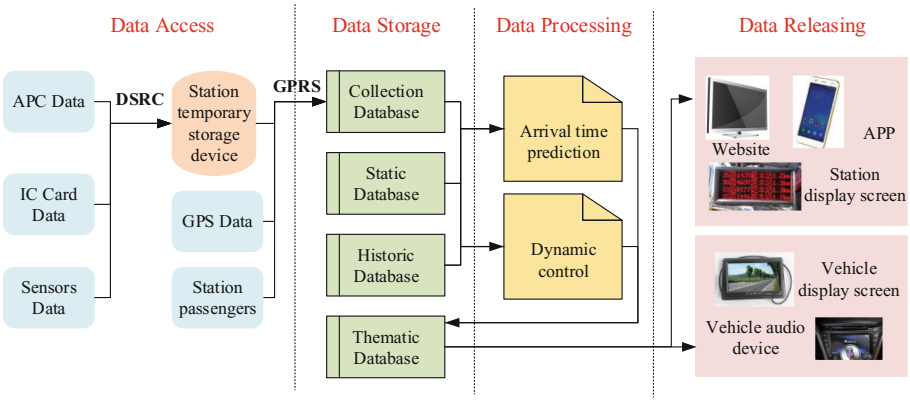

Fig. 4. Data communication process

4 Dynamic Control

A. *Dynamic Control Strategies.* Bus control can be classified into two types which are planning control and dynamic control. Dynamic control strategies are station control strategies such as holding, skipping and boarding limits, and inter-station control strategies such as speed regulation, traffic signal priority [7].

A previous study [8] showed the relationship between the variance of bus headways and the waiting time of passengers at stops, which revealed that there was a positive correlativity between the average waiting time of passengers at stops and the variance of bus headways.

$$E(W) = \frac{E(H)}{2} + \frac{\text{var}(H)}{2E(H)} \tag{1}$$

Where *E(W)* is the average waiting time of passengers at stops; *E(H)* is the average headway of buses; *var(H)* is the variance of bus headways.

Data Processing Sub-system is the hardcore of the proposed dynamic control platform. In this paper, two strategies which are holding and skipping are recommended in the data processing sub-system. "Holding" means that vehicles delay for a short time at stations after passengers' alighting and boarding, while "skipping" means that vehicles skip some stations for catching the schedule. The two control strategies have no effects on the traffic flow on the road segments. The dynamic control strategies in this platform refer to previous research [9] and a few changes are given. The flow chart is showed in Fig. 5.

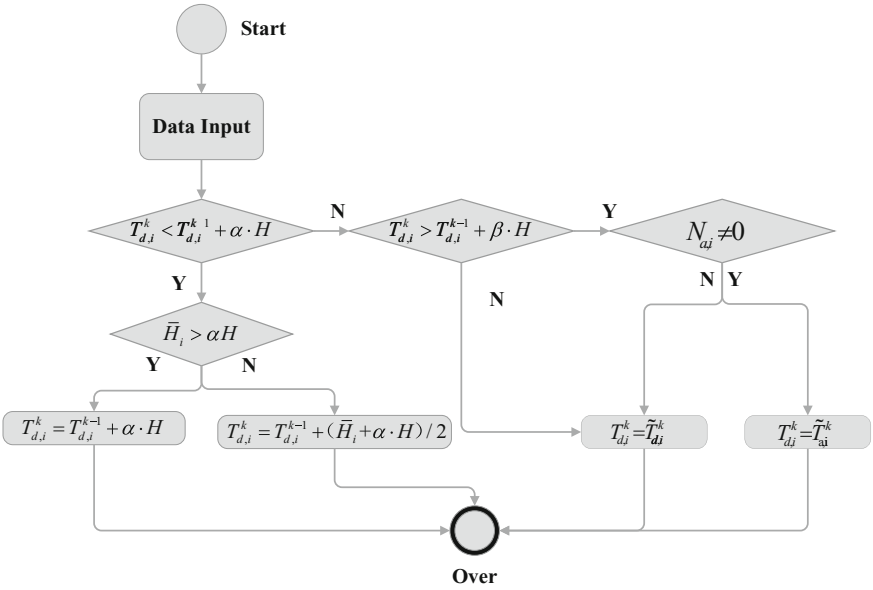

Fig. 5. The flow chart of dynamic control strategies

Arrival time prediction module is the foundation of a dynamic control module which needs the prediction results as the basis for making decisions. Some indexes and parameters are presented below:

k: Index of the bus vehicles, $k = 1,2,3\ldots,K$;
i: Index of the bus stations, $i = 1,2,3\ldots,I$;
$T_{d,i}^{k}$: The actual departure time from station i of bus k;
$T_{a,i}^{k}$: The actual arrival time at station i of bus k;
$\tilde{T}_{d,i}^{k}$: The predicted departure time from station i of bus k;
$\tilde{T}_{a,i}^{k}$: The predicted arrival time at station i of bus k;
α: The key parameter of bus holding;
β: The key parameter of bus skipping;
H: The dispatch headway;
$\tilde{H}_i$: $\tilde{H}_i = (\tilde{T}_{d,i}^{k+1} - T_{d,i}^{k-1})/2$;
λ_1: Time period of alighting per person;
λ_2: Time period of boarding per person;
$N_{a,i}$: Alighting passengers at station i;
$N_{b,i}$: Boarding passengers at station i;

B. *Dynamic Control Example.* To make the control strategies easier to understand, a simple example of dynamic control is given below. The diagram of bus vehicles travel is showed in Fig. 6. Five inconsecutive stations of the same bus route and

three consecutive bus vehicles are included in the example. The actual departure time of the preceding vehicle, the predicted departure time of the target vehicle and the behind one, and the numbers of alighting and boarding passengers are listed in Table 3.

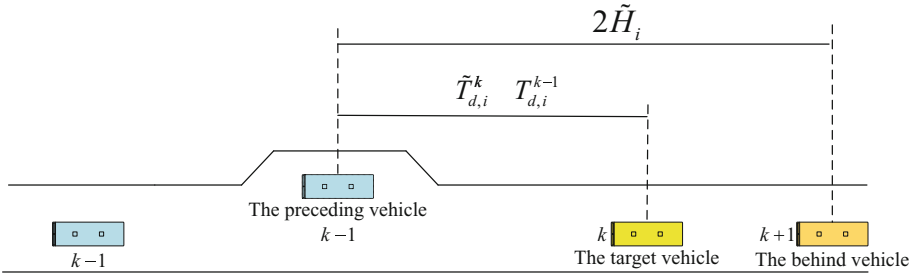

Fig. 6. The diagram of bus vehicles travel

Table 3. Information of bus running in the example

No.	Objects	Station 1	Station 2	Station 3	Station 4	Station 5
1	The preceding vehicle	07:25:12	07:28:24	07:31:46	07:35:32	07:39:33
2	The target vehicle	07:28:03	07:30:17	07:34:54	07:40:01	07:46:03
3	The behind vehicle	07:34:50	07:38:01	07:40:07	07:44:57	07:48:33
4	Alighting passengers	2	3	6	5	10
5	Boarding passengers	5	8	10	2	0

Note: 1. The actual arrival time of the preceding vehicle; 2. The predicted arrival time of the target vehicle; 3. The predicted arrival time of the behind vehicle; 4. Number of alighting passengers of the target vehicle; 5. Number of boarding passengers of the target vehicle.

In order to simplify the calculation, make the key parameter of bus holding $\alpha = 0.7$ and the key parameter of bus holding $\beta = 2.0$ [10]. Suppose that the arrival time and the departure time meet with the formula (2), and $\lambda_1 = 1$ s/person, $\lambda_2 = 2$ s/person, $H = 3$ min.

$$T_{d,i}^{k} = T_{a,i}^{k} + \max(\lambda_1 \cdot N_a, \lambda_2 \cdot N_b) + \text{holding time} \tag{2}$$

The results of dynamic control on the target bus vehicle are showed in Table 4.

Table 4. Results of dynamic controls

Objects	Station 1	Station 2	Station 3	Station 4	Station 5
The original departure time	07:28:03	07:30:17	07:34:54	07:40:01	07:46:03
Control strategies	/	Holding	/	/	Skipping
Duration/s	/	13	/	/	/
The adjusted departure time	07:28:03	07:30:30	7:35:07	7:40:14	07:45:56

5 Conclusion

A dynamic control platform of electric bus vehicles is proposed in this paper. Four sub-systems are Data Collection Sub-system, Integrated Database, Data Processing Sub-system and Data Releasing Sub-system. The design of data communication and the integrated database are based on the combing of data sources and contents. Data processing is a key function of the platform to realize the real-time dynamic control of bus vehicles. Holding and skipping control strategies are adopted in the data processing sub-system. An explanatory example is given to introduce the concrete implementation steps.

Electric bus vehicles' characteristics are considered in the data collection sub-system, such as charge-discharge process and pedal position whose data can reflect the energy recover phenomenon. How to apply the characteristics to the data processing sub-system need more consideration. What's more, control strategies should be selected more carefully, and the suitability of the dynamic control model also should be testified in the future studies.

Acknowledgment. This study is supported by the National Basic Research Program of China (973 Program-No. 2012CB725405), the Science and Technology Demonstration Project of Ministry of Transport of China (No. 2015364X16030 and No. 2014364223150), and the National Natural Science Foundation of China (Grant No. 51308115).

References

1. Gao LC (2010) Public traffic information distribution system design and implement based on wireless network. MS thesis, Dalian University of Technology, Dalian, China
2. Zhang J, Ran B (2014) An analysis method on communication connectivity of bus dynamic dispatching under the connect vehicles environment. CN Patent 102737503A, 29 Aug 2014
3. Sumcad AJ, Sidhu N, Krause KR (2014) System and method for processing vehicle communications. US Patent 12059938, 28 Jan 2014
4. Cao M (2012) Research and implementation on intelligent bus system based on ZigBee technology. MS thesis, Xi'an Technology University, Xi'an, China
5. Zou F (2014) Design and verification of the CVIS data exchange standards. MS thesis, Beijing Jiaotong University, Beijing, China
6. Brata AH, Liang D, Pramono SH (2015) Software development of automatic data collector for bus route planning system. Int J Electr Comput Eng (IJECE) 5(1):150–157

7. Ibarra-Rojas OJ, Delgado F, Giesen R et al (2015) Planning, operation, and control of bus transport systems: a literature review. Transp Res Part B Methodol 77:38–75
8. Osuna EE, Newell GF (1972) Control strategies for an idealized public transportation system. Transp Sci 6:52–72
9. Fu L, Yang X (2002) Design and implementation of bus-holding control strategies with real-time information. Transp Res Rec: J Transp Res Board 1971:6–12
10. Yin T, Zhong G, Zhang J et al (2016) A hybrid real-time bus control strategy with multi-criterion evaluation. In: 16th COTA International Conference of Transportation Professionals (CICTP 2016), Shanghai, China (to be published)

Research on Modern Tram Auxiliary Safety Protection Technology Based on Obstacles Detection

Gang Wang(✉), Xiaoqing Zeng, Dong Bian, and Weiyang Wang

Key Laboratory of Road and Traffic Engineering of Ministry of Education, Tongji University, No. 4800 Cao'an Road, Shanghai 201804, China
zbwg77@163.com

Abstract. Due to the special running environment, modern tram has the certain safety hazard in the running process, so this research proposed an auxiliary safety protection technology based on obstacle detection for the modern tram. By the detector obtaining information of anterior obstacles and coordinate matching to identify the location of obstacles and relative location of tram rail. For the obstacles in the range of tram rail, this research can calculate the distance between tram and obstacles, as well as compute train protection curve dynamically, therefore it can provide the warning information to the driver. Finally, the results of simulation experiments proved the validity of this research, and it can provide the dynamic protection information based on the detective data.

Keywords: Tram · Obstacle detection · Auxiliary safety protection · Train protection algorithm

As a means of rail transit, modern tram enjoys high popularity in recent years for it is green, proper-cost and has ideal capacity. As a result, many cities in China has planned and built it. Compared with other means of rail transit, tram has more safety hazard as it is not completely closed. The driver should be responsible for the safety when operating the tram system. Based on the safe driving model of finding obstacles—service braking (or emergency braking), driver's view distance limit the maximum speed of tram in certain sectors. Meanwhile, in the night or under extreme weather like rain, snow and fog, driver's field of view will be so greatly limited and weakened that driver is hardly to find the potential obstacles. Once the driver cannot brake in time, tram will rush into collision or even derail. Therefore, it means a lot to develop an auxiliary safety protection system to enhance visual effect for modern tram.

This article provides a modern tram auxiliary safety protection technology based on obstacle detection. It equips tram with suitable detector to obtain the dynamic information of anterior obstacle and then it can identify the location of obstacles and relative location of tram rail by train location technology. As to obstacles invading tram rail, it identifies the relative distance from tram and takes the obstacles as the end of movement authority to calculate the dynamic tram protection curve. If obstacles don't appear in that detection cycle, the auxiliary safety protection system will take the fixed stopping location (such as station) as the end of movement authority to calculate protection curve.

X. Zeng et al. (eds.), *International Symposium for Intelligent Transportation and Smart City (ITASC) 2017 Proceedings*, Smart Innovation, Systems and Technologies 62, DOI 10.1007/978-981-10-3575-3_5

1 Research on Obstacle Detection Technology

Obstacle detection technology uses sensors to obtain aim's information in the environment. The obstacle detection technology in tram is an in-vehicle detection technology. Presently in-vehicle detection technology is widely applied to smart car field and it is divided into active detection and passive detection [1]. Active detection emits electromagnetic waves with certain power and frequency band towards target field and detects obstacles with echo analysis and sorts of radar technology stand for it; Passive detection is almost visual detection technology [2] which uses equipment as CCD camera to obtain information direct from the environment and calculate data of interest. Passive detection is noninvasive because it is low-power and doesn't increase noise but obtains a large amount of information. However, it fails under extreme weather for its information sources completely depends on the outside [3].

Tram runs almost in the cities and shares right of way in certain sectors with urban road traffic so the obstacles that invade into tram rail include general vehicle, pedestrians and other objects falling into and remaining in rail. Detector can detect anterior obstacles. According to the standard of EN13452-1, modern tram runs at the speed of 50 km/h. As to tram with steel wheel on steel rail, service braking deceleration is 1.2 m/s^2 and emergency braking deceleration needs 2.8 m/s^2 at least(pneumatic-tired tram on guide rail requires higher one) [4]. If tram runs at the speed of 50 km/h, braking distance is within

Table 1. Comparison among sorts of obstacle detection technology

Alternative obstacle identifying technology	Ultrasonic radar	Infrared radar	Laser radar	Millimeter wave radar	Visual detection
Long-distance detection ability	Poor	Average	Average	Strong	Average
Target identifying ability	Poor	Poor	Average	Average	Strong
Excluding false-alarm ability	Poor	Average	Strong	Strong	Average
Stability of temperature	Bad	Average	Good	Good	Good
Penetrating power in dark	Strong	Strong	Strong	Strong	Poor
Penetrating power all day	Poor	Average	Average	Strong	Poor
Low hardware cost possibility	Average	Average	Poor	High	Average
Low information processing cost possibility	Average	Average	High	High	Average
Performance in dusty/smoky environment	Average	Average	Average	Good	Bad

100 m and emergency distance is about 50 m, so the detector must detect 200 m anterior rail. At the same time, detector requires certain horizontal angle and pitching angle to detect obstacle within tram height.

According to the requirements above, Table 1 analyzes and compares several mature detectors' features.

After study, millimeter wave radar takes some advantages in all-day using, detection distance, detection stability, low cost. So this article takes millimeter wave radar as the detector of tram.

2 Design of Auxiliary Safety Protection Function

2.1 Analysis of Function Demands

The tram auxiliary safety protection mainly provides collision warning. Unlike cars that can yield by changing lanes, tram is limited to the rail, so it's necessary to identify the location of detected anterior obstacles and relative location of tram rail. In this way, we can estimate the threat to tram. This research will make the relative matching calculations with tram location information.

To guarantee the function of collision warning, relative equipment and algorithm should meet the following requirements:

- The radar detector chosen in Sect. 1 is supposed to offer accurate relative position of tram and target.
- Train location technology should provide tram location and speed information with small errors.
- Relative algorithm can calculate in-rail distance between invader and tram, and can offer tram protection curve.

2.2 Design of Auxiliary Safety Protection Framework

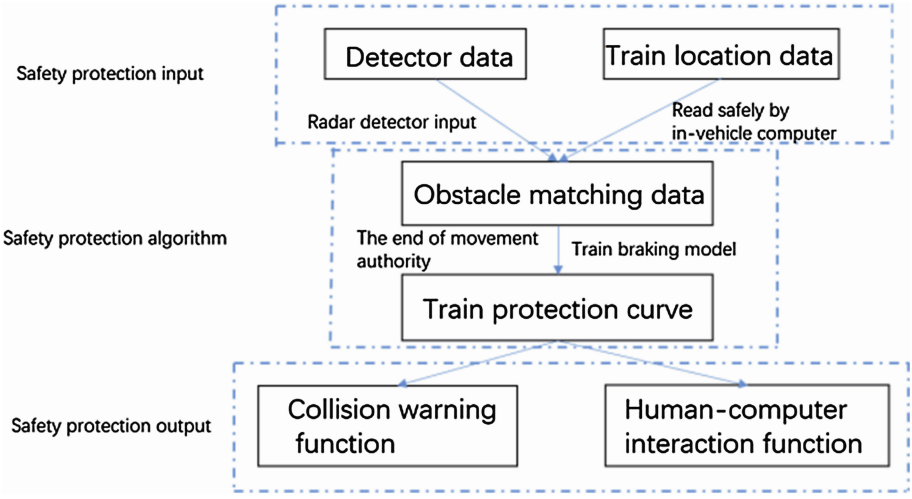

2.3 Design of Collision Warning Function

Achieve the function of collision warning relies on computing train protection curve dynamically. Train protection curve is the direct expression of train braking model, it shows the relation between drop-in speed and distance in braking process. Auxiliary driving system needs to work out the end of movement authority dynamically and then draws train protection curve. This research builds a cluster of protection curves referring to ETCS's train protection method [5].

EBD (The Emergency Brake Deceleration Curve): In the running process, every end of movement authority correspond one EBD curve. EBD curve is the outermost curve in a cluster of protection curves, and it won't be triggered in normal situation. Once EBD curve is exceeded, train's stopping location will exceed the end of movement authority, which means collision happens.

Therefore, train braking forming, driver's response time, the error of train location and speed and other factors should be taken into consideration when calculating EBI (The Emergency Brake Intervention Curve). When train running state exceeds EBI curve, system needs to operate emergency braking automatically.

With the same theory, train also has maximum service braking curve SBD (The Service Brake Deceleration Curve) and maximum service braking trigger curve SBI (The Service Brake Intervention Curve). When train's running state triggers this curve, system needs to operate maximum service braking.

Meanwhile, to remind and warn driver, we set up reminding point I and warning point W. By computing SBI backward, Fig. 1 shows the relation among several curves. Calculation formula of a cluster of curves is explained in detail in Sect. 3.3

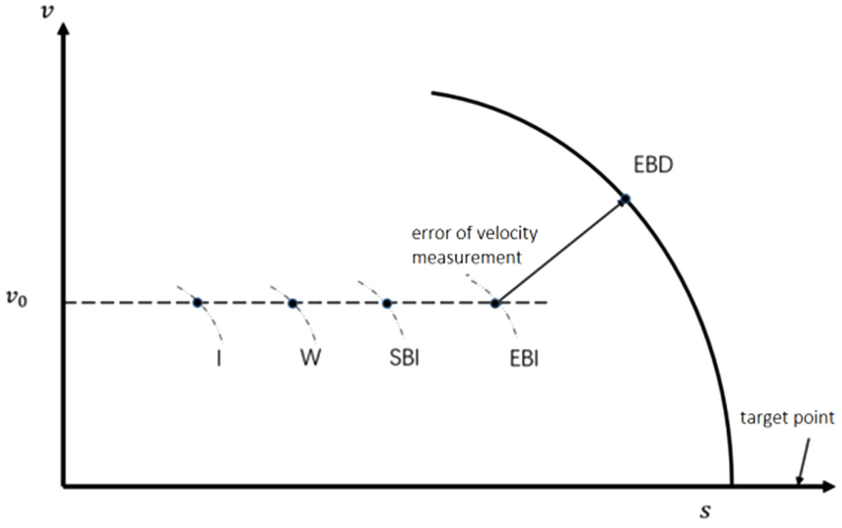

Fig. 1. Relation between EBD and other curves

When tram is approaching the end of movement authority, auxiliary driving system will remind the driver of safe guide speed. This strategy includes reminding point I and warning point W. I is to remind driver that tram is about to exceed speed limit, and provides driver with adequate time to operate. Once tram surpass I point, system will remind driver to slow down by sound and light; Exceeding W point means it is to trigger maximum service braking curve, and if no operation is carried out, tram will trigger maximum service braking automatically over SBI supervision. Under this circumstance, if the speed is still above safety line and exceed EBI supervision point, system will perform emergency braking to guarantee safety.

Human-computer interaction in the braking process is designed as "remind—ask—brake" three steps: When tram triggers I point, system reminds driver with sound and light. When tram triggers W point and driver doesn't slam on brake, system will give explanation interface. If driver doesn't choose in the interface until tram triggers SBI supervision curve, tram will operate maximum service braking automatically. According to the combination of human engineering and driver's response time, it's proper to set 5 s as trigger time among I point, W point and SBI curve.

Because tram rail is not completely closed in some sectors, it's possible that obstacles that suddenly invade the rail may be close. Taking this obstacle as the end of movement authority will make the present situation exceed I point envelope. Given that this happens mostly when pedestrians rush into rail, and the walking period lasts about 2 s. So on this occasion, braking strategy can be operated with driver's help. Detailed process is as Fig. 2.

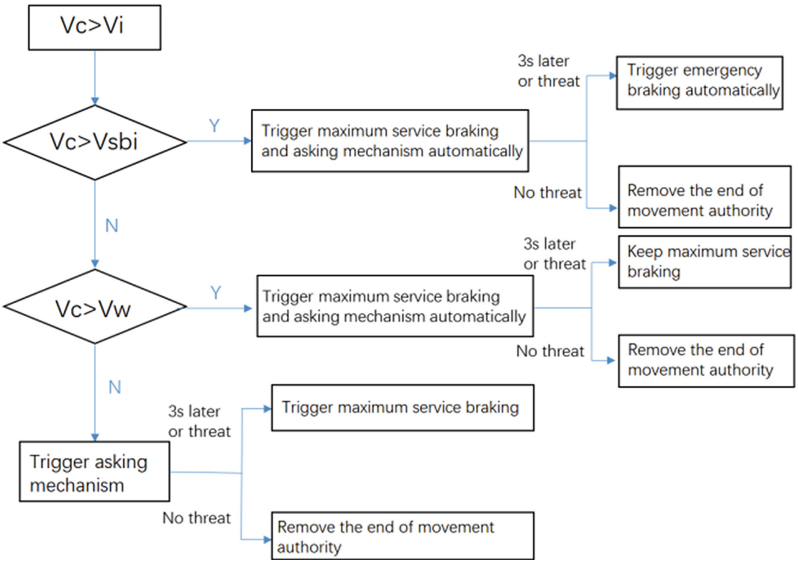

Fig. 2. Braking strategy when the invader is too close

If the invading obstacle threatens and $v_c > v_{EBI}$ (v_c means present speed), which equals that tram is over EBI curve. In this case, even emergency braking will arrive at

the end of movement authority and tram can't avoid this collision. But this seldom happens.

If pedestrians walk into the rail, driver can make the all-clear sound by pressing the button and get it back to normal. Meanwhile, the system will remove that end of movement authority after pedestrians are out of rail.

The human-computer interaction process require driver to make choices to inform the system if the threat reached by algorithm is true. Since driver is given little time to react, equipment for surface choice is suggested to be physical button that is more stable.

3 Design of Auxiliary Safety Protection Algorithm

3.1 Algorithm Input

3.1.1 Radar Data Input

This research assume that, by the method of analyzing waveform and filtering background noise, raw data detected by chosen radar could at least provide auxiliary safety protection system with data input of reasonable sampling frequency as follows:

$$[\alpha, \theta, \rho] \tag{1}$$

In this: α means obstacle's pitching angle; θ means obstacle's horizontal course angle; ρ means obstacle's distance from tram.

According to polar coordinate conversion formula, eliminating targets higher than vehicle, we can work out two-dimensional coordinate:

$$\begin{bmatrix} x_{ob} \\ y_{ob} \end{bmatrix} = \begin{bmatrix} \rho \cos \alpha \cos \theta \\ \rho \cos \alpha \sin \theta \end{bmatrix} \tag{2}$$

3.1.2 Train Location Data Input

(1) Building running line coordinate system
This research uses in-vehicle radar as detector. Radar coordinate system will make relative movement to ground in train's speed. To conveniently study the absolute position relation between ground and rail line, applying local coordinate system data to running line coordinate system could meet the accuracy demand.
Besides, local coordinate system is relatively independent system build in part areas to help with building, urban planning and science research.

(2) Modeling train's running line
Based on local coordinate system, we can model running line according to the assumptions below: a. Analyze running line form abstractly, and divide it into straight line, curve line and intersection line; b. Ignore the influence of transition curve and assume that straight line is connected direct with curve line of fixed curvature radius. So we can indicate every sector in this way:

$$\left[n, x_1, y_1, s_1, x_2, y_2, s_2, r, x_o, y_o, d, i, c, s, m,\right] \tag{3}$$

In this: n is sector number; (x_1, y_1) (x_2, y_2) is origin-destination coordinate; s_1, s_2 is mileage between O-D; r is curvature radius in sector; (x_o, y_o) is center coordinate of curve sector; d is the running direction of train in this curve sector. If it's clockwise, d = 0; If it's counter-clockwise, d = 1; i is the value of slope in sector; s is the mileage of this sector; m is the number of balise in this sector. Moreover, define rail limit range W = maximum width of train $w + 2\delta$, δ is safety margin.

(3) The way of train's location data input
Input data as follows:

$$\left[n, n_1, n_2, x, y, s_d, s, v_{cur},\right] \tag{4}$$

In this: n is the number of last balise; n_1 is the sector number of last balise; n_2 is the sector number of train; (x, y), is the ground coordinate of last balise; s_d is the relative mileage from line beginning seen as 0 point to last balise; s is the accumulated mileage from last balise to train's real-time position; v_{cur} is train's dynamic speed.

3.2 Algorithm of Obstacle's Absolute Location

3.2.1 Determine Train's Coordinate

In the model algorithm, train need obtain its dynamic location information. Assume that train lies in sector-n_2, and then we can obtain the sector information as follows:

$$\begin{bmatrix} n_2, x_1^{n_2}, y_1^{n_2}, s_1^{n_2}, x_2^{n_2}, y_2^{n_2}, s_2^{n_2}, r^{n_2}, \\ x_o^{n_2}, y_o^{n_2}, d^{n_2}, i^{n_2}, c^{n_2}, s^{n_2}, m^{n_2} \end{bmatrix} \tag{5}$$

Based on the situation of straight sector and curve sector, computing train's dynamic coordinate $\left(x_{tr}, y_{tr}\right)$ and running direction β.

Straight sector: Compute dynamic location by (6) and (7).

$$\begin{bmatrix} x_{tr} \\ y_{tr} \end{bmatrix} = \begin{bmatrix} \dfrac{x_1^{n_2} + \lambda x_2^{n_2}}{1+\lambda} \\ \dfrac{y_1^{n_2} + \lambda y_2^{n_2}}{1+\lambda} \end{bmatrix}, \lambda \frac{s_d + s - s_1^{n_2}}{s_2^{n_2} - s_d - s} \tag{6}$$

$$\beta = \begin{cases} \tan^{-1}\dfrac{y_2^{n_2} - y_1^{n_2}}{x_2^{n_2} - x_1^{n_2}}, & x_2^{n_2} - x_1^{n_2} > 0 \\ \tan^{-1}\dfrac{y_2^{n_2} - y_1^{n_2}}{x_2^{n_2} - x_1^{n_2}} + \pi, & x_2^{n_2} - x_1^{n_2} < 0 \text{ and } y_2^{n_2} - y_1^{n_2} \geq 0 \\ \tan^{-1}\dfrac{y_2^{n_2} - y_1^{n_2}}{x_2^{n_2} - x_1^{n_2}} - \pi, & x_2^{n_2} - x_1^{n_2} < 0 \text{ and } y_2^{n_2} - y_1^{n_2} < 0 \\ \pi/2, & x_2^{n_2} - x_1^{n_2} = 0 \text{ and } y_2^{n_2} - y_1^{n_2} > 0 \\ -\pi/2, & x_2^{n_2} - x_1^{n_2} = 0 \text{ and } y_2^{n_2} - y_1^{n_2} < 0 \end{cases} \tag{7}$$

Curve sector: Compute dynamic location by (8) and (9). In this, σ is calculated by relative location between (x_{tr}, y_{tr}) and sector beginning.

$$\begin{bmatrix} x_{tr} \\ y_{tr} \end{bmatrix} = \begin{bmatrix} x_o^{n_2} + r^{n_2} \cdot \cos\sigma \\ y_o^{n_2} + r^{n_2} \cdot \sin\sigma \end{bmatrix} \tag{8}$$

$$\beta = \begin{cases} \sigma + \dfrac{\pi}{2}, & d^{n_2} = 1 \\ \sigma - \dfrac{\pi}{2}, & d^{n_2} = 0 \end{cases} \tag{9}$$

3.2.2 Obstacle Equals the End of Movement Authority in Calculation

Formula of convert obstacle's radar coordinate system to line coordinate system as follows:

$$\begin{bmatrix} x_{OB} \\ y_{OB} \end{bmatrix} = \begin{bmatrix} x_{tr} + x_{ob} \cdot \cos\beta - y_{ob} \cdot \sin\beta \\ y_{tr} + x_{ob} \cdot \sin\beta + y_{ob} \cdot \cos\beta \end{bmatrix} \tag{10}$$

With analytic geometry formula, we can calculate the distance from (x_{ob}, y_{ob}) to the nearest rail sector's center line. If it is less than $\dfrac{w + 2\delta}{2}$, then consider obstacle is within rail limit and calculate its in-rail distance from train by formula. Formula (11) is used in straight sector, while formula (12) is used in curve sector.

$$S_{ob} = \sqrt{\left(x_{ob} - x_o^{n_2+j+1}\right)^2 + \left(y_{ob} - y_o^{n_2+j+1}\right)^2 - \left(\frac{\left|nx_{ob} + my_{ob} + c\right|}{\sqrt{n^2 + m^2}}\right)^2} \tag{11}$$

$$S_{ob} = \alpha r^{n_2+j+1} + s^{n_2+j} \tag{12}$$

3.3 Supervision Curve Algorithm

(1) Emergency braking curve EBD
Emergency braking curve EBD describes braking distance that train stops completely or reaches the upper speed limit of speed-limit sector. The target of braking curve is generally divided into two kinds: The first is the end of movement authority, which means train must brake completely before reaching the end of movement authority. The second is the change of speed limit curve, which means train should always be under the speed limit. We see in-rail obstacle as the end of movement authority to compute dynamic protection curve. Then we can compute EBD backward from the end of movement authority according to kinemics braking model, and it will intersect with speed limit

$$S_{eb} = \frac{(v_{end}^2 - v_{org}^2)}{2a_{eb\gamma}} \tag{13}$$

In this:
v_{org} is train's initial velocity;
v_{end} is train's targeted braking velocity. As for situation when obstacle equals the end of movement authority, $v_{end} = 0$;
$a_{eb\gamma}$ is train's maximum braking deceleration(take rotary mass coefficient and slope influence into consideration);
S_{eb} is emergency braking state distance

(2) The emergency brake intervention curve EBI
The emergency brake intervention curve EBI calculates it lacks train cutting off traction and starting braking between EBI and EBD. It includes driver's reaction delay, cutting off traction delay and inertia until starting braking three phases. Fig-n describes how EBD changed into the other supervision curves, and EBI is calculated by formula (14)–(16)

$$\Delta v = a_{tr\gamma} t_{tr} \left(1 + r_V\right) \tag{14}$$

$$\Delta s = \Delta v t_{tr} + S_{lo} \tag{15}$$

$$S_{EBI}\left(v_0\right) = S_{EBD}\left(v_0 + \Delta v\right) + \Delta s \tag{16}$$

In this:
$a_{tr\gamma}$ is train's maximum traction acceleration(take rotary mass coefficient and slope influence into consideration);
t_{tr} is the total of starting braking delay and driver's response time;
r_V is the error coefficient of velocity measurement;
Δs is the distance increment in the worst condition.

(3) Maximum service braking curve SBD and intervention curve EBI
Same with (1) and (2), we can work out SBD curve solution formula (17)

$$S_{sb} = \frac{(v_{end}^2 - v_{org}^2)}{2a_{sb\gamma}} \tag{17}$$

And SBI curve solution formula (18), the conversion from SBD to SBI is direct translation.

$$S_{SBI1}(v_0) = S_{SBD}(v_0) + v_0 t'_{tr} \tag{18}$$

(4) Alarm warning curve
This model has two reminder points: reminding point I and warning point W. They get time interval from SBI curve and they are calculated by formula (19) and (20).

$$S_W(v_0) = S_{SBI}(v_0) + v_0 t_W \tag{19}$$

$$S_I(v_0) = S_{SBI}(v_0) + v_0 t_I \tag{20}$$

4 Algorithm Simulation Verification

This research apply simulation verification to strategy algorithm by using Python programming languages and lays primary construction of modern tram's running environment. Most importantly, it designs experiments for the analysis of obstacle influence and train protection curve and basically shows the validity of strategy algorithm.

4.1 Construct Simulation Environment

Compared with traditional transit simulation program that only concerns about one-dimensional running environment, due to in this research tram needs to detect obstacles along the rail, we are supposed to construct two-dimensional lines. Figure 3 is one tram line abstractly extracted from a certain real line.

(1) Program Design
Program main progress is vehicle-control program, and other subfunctions include coordinate conversion module, obstacle generation module, coordinate inverse transform module and protection curve generation module.

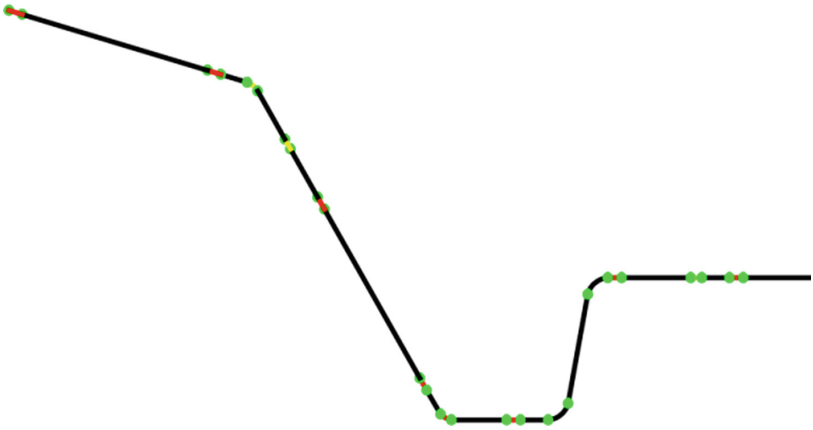

Fig. 3. The sketch of simulation line

4.2 The Result of Simulation Experiment

(1) Verification of train protection curve generation module
As it shows in Fig. 4, they are four protection curves of the end of movement authority beyond 2200 m. Algorithm can output protection in terms of obstacle position and train's location input.

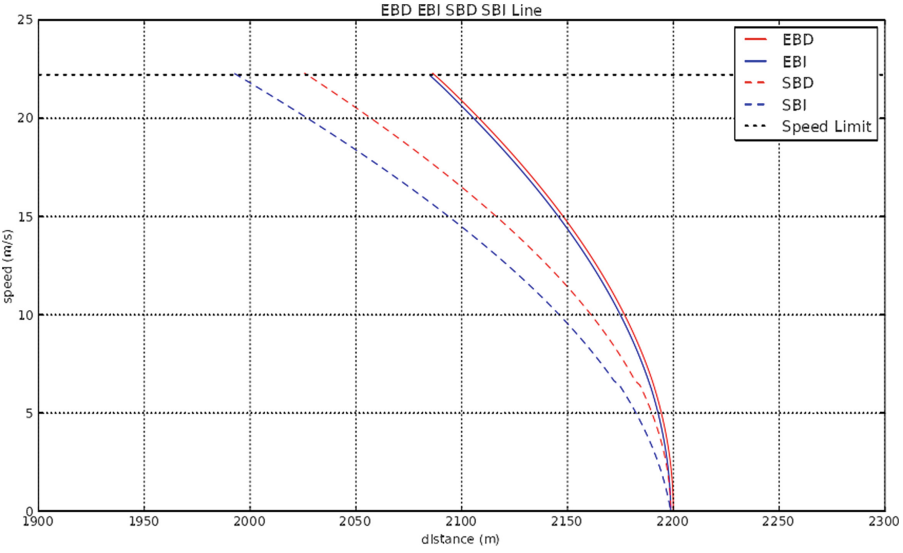

Fig. 4. A certain protection

(2) Verification of instantaneity in protection curve generation
In Fig. 5, simulation experiment assumes that train detector stops somewhere inside the rail. It randomly generates a target that moves in a fixed direction and with a constant velocity. The target could be detected when it invades the rail. In this case, it will influence the train protection curve of this detection cycle for a period. This time, the simulated obstacle stays 14 s in rail, and it influences the mileage from 3143 m to 3156 m. So it leads to an abrupt change in a cluster of train protection curves. It's obvious in the picture that a length of protection curve gets close train, which indicates obstacle's invasion makes a change to the end of movement authority. Besides, the surface formed by this cluster of protection curves is not entirely parallel to t-axis, which means obstacle crosses rail limit sideways.

The result of simulation experiment confirms that auxiliary safety protection algorithm can dynamically detect the obstacle detected by radar and then generate train protection curve.

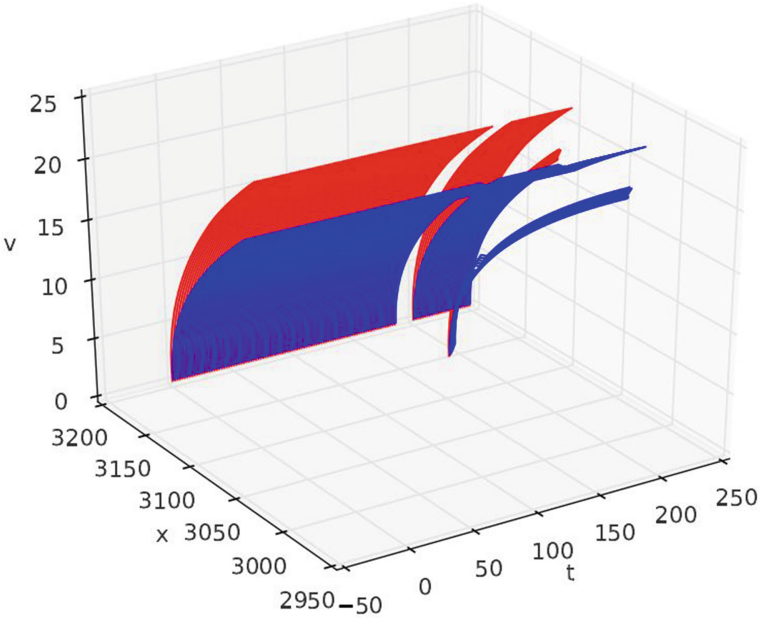

Fig. 5. Variation trend of protection curve

(3) Verification of train's running
Fig. 6 is speed record line generated by simulation experiment which simulates the situation of pedestrians crossing the rail limit. In the simulation experiment, driver drives the tram with obstacle and braking information offered by auxiliary safety protection system. By choosing a sector of simulated line, we assume that obstacle

appears when tram reach certain speed and driver triggers maximum service braking. 4 s later, obstacle disappears and train reaccelerates until stops in the station.

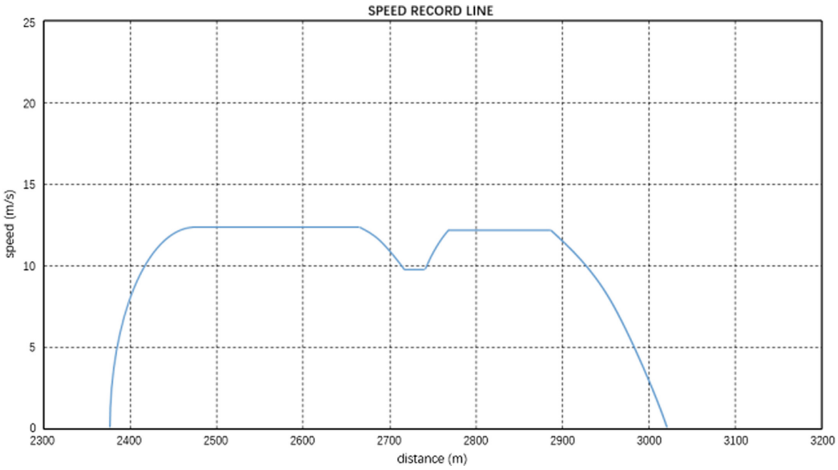

Fig. 6. Speed record line

The result of simulation shows, when obstacle could be accurately detected, auxiliary safety protection algorithm is able to dynamically calculate train protection curve and put forward decelerate braking strategy.

In the simulation process, we suppose that driver follows relative control strategy.

Based on accurate radar detection data and train location data, the present auxiliary driving strategy algorithm design could dynamically ensure the relative location of obstacle and rail limit and convert threatening obstacle into the end of movement authority in train protection curve. In this way, system can mark all the braking supervision points based on protection curve to make collision warning.

5 Conclusion

Aiming at the problem that tram running environment has potential threat, this article put up with an auxiliary safety protection method based on obstacle detection, it analyzes the method of locating the dynamic end of movement authority and train protection curve based on detector's data and train location data. Finally, we confirm the instantaneity and validity of algorithm by programming simulation experiment.

References

1. Ruowang C (2012) Research on image detection algorithm of train's anterior obstacle. Southwest Jiaotong University
2. Rui Z (2010) Design and realization of millimeter automotive anti-collision radar. Jiangsu University, June 2010
3. Xu Y, Li K, Lian X (2003) Recent development of smart car's machine vision. Autom Eng 25(5):438–443
4. STRMTG, Ref.4 《GT3-DTW-Obstacles Fixers V2》 [S]
5. ERA.ERTMS_040026, Introduction To ETCS Braking Curves [S]

Research on the Queue Length Prediction Model with Consideration for Stochastic Fluid

Xiaoqing Zeng, Jifei Zhan(✉), Linxiang Yang, Qipeng Xiong, and Yujia Chen

Tongji University, Shanghai, China
seairlove@tongji.edu.cn

Abstract. Research on queue length model lacks the consideration for stochastic fluid. This paper makes equivalent queue length prediction models from two-fluid theory, considering that traffic flow is composed of road traffic and congested traffic. With the simulation in VISSIM, it proves the equivalent queue length prediction models in paper can quantitatively describe the existence of stochastic traffic fluid in road.

Keywords: Traffic flow · Road traffic · Congested traffic · Queue length · Stochastic fluid

1 Research Status at Home and Abroad

Research on queue length model at home and abroad can be divided into two parts: micro level and macro level and the basis of the research are phenomenon and laws of queuing in traffic flow theory. At the micro level, scholars studied car following behavior and lane-changing behavior are characteristics of queuing in single lane. At the macro level, the considering characteristics of traffic flow, they assumed that traffic flow is continuous and has existence of some laws. So far, research findings by scholars at home and abroad in theory of queuing can be summarized as waiting line theory, probability theory shock wave theory and accumulative curve technique.

Here are some theories of queuing in traffic flow:

(1) If any distribution cannot describe the traffic flow, we cannot calculate the queuing length in probability theory because probability theory can only provide the average and the maximum length.
(2) Waiting line theory is based on the point queue that cannot describe the situation of large vehicular traffic.
(3) Accumulative curve technique can solve the calculation of queue length in a steady state. But it's hard to use the graphic method to work out the traffic queue.
(4) Upon the shock wave theory, a branch of fluid dynamics, we can supply clarity to describe the phenomenon that excluding the traffic flow is unstable.

The equivalent queue length worked out on the basis of the two-fluid theory is longer than the real queue length, so this two-fluid theory is suitable for congested traffic flow.

X. Zeng et al. (eds.), *International Symposium for Intelligent Transportation and Smart City (ITASC) 2017 Proceedings*, Smart Innovation, Systems and Technologies 62, DOI 10.1007/978-981-10-3575-3_6

2 Queue Length Prediction Model with Consideration for Stochastic Fluid

2.1 Analysis of Three Vehicle Detectors

We all know that there are differences between the traditional traffic flow theory and the real facts. The stochastic fluid caused by traffic queue is not considered into traditional traffic flow theory [1–3].

Based on two-fluid theory, we assume that all vehicles run on the single lane and form a queue when the light turns to red. There are three vehicles running states: (1) traffic density is equal to the blocking density when the speed is 0 km/h in area A; (2) influenced by blockage ahead, the speed is down to 0 km/h in area B; (3) traffic flow remains a steady state in area C. the traffic states is steady in area A and area C while unsteady in area B (Fig. 1).

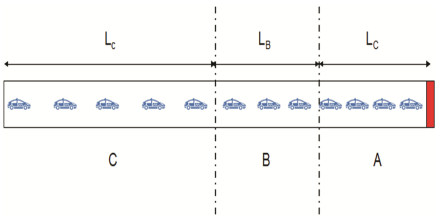

Fig. 1. State transform map of traffic flow

According to traffic two-fluid theory, the states can be divided into the congestion flow caused by queuing ahead and free flow whose density is the best one k_m. The flow in area B is defined as weighted sum of flow in area C and area A. Then the real traffic flow state is approximately equal to two-fluid state.

As shown in Fig. 2, in realities of situation, two-fluid theory can give the solutions to calculations of queue length. Apart from real queue length and the queue length based on two-fluid theory, we call the latter the equivalent queue length L'_q and the equivalent queue length including the real queue length in area A and area B that is part of queue length of stochastic fluid. So we can get the inequality: $L'_q > L_q$.

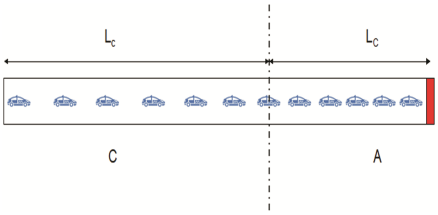

Fig. 2. State transform map of traffic flow based on two-fluid theory

2.2 Equivalent Queue Length Model of Congested Traffic Flow

According to the two-fluid theory, it exists a bias in the results that real queue length is composed of optimal traffic flow k_m and congested traffic flow k_j, especially when real density is larger than optimal density. Therefore, we define the traffic jams flow as the combination of congested traffic flow and stochastic flow and the two-fluid states are that of traffic jams flow and real traffic flow. Here is the state transform map of traffic jams flow (Fig. 3).

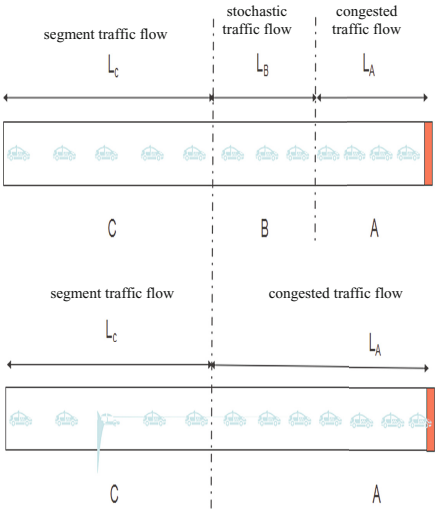

Fig. 3. State transform map of two-fluid considering to the traffic jams flow

The value of the equivalent queue length can be collected by the two pairs of detectors. The detectors are thought as the parking line detector and the route detector due to their location. The number of vehicles collected by the parking line detector is $N_D(t)$ and the route detector is $N_u(t)$ when the average speed is $V_c(t)$. The location of the parking line detector is on the parking line while that of the route detector is undefined, and usually the route detector's layout is at a place where traffic fluid is steady (Fig. 4).

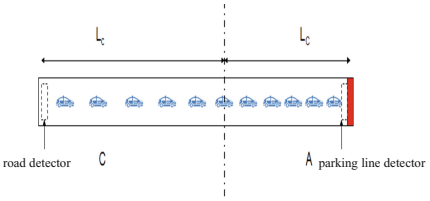

Fig. 4. The location of detectors

According to the principle of conservation in traffic, we give the formula below.

$$N(t) = N_0 + N_U(t) - N_D(t)$$

In the formula, N_0 represents the amount of vehicles between two detectors at the moment $t = 0$, and $N_u(t)$ represents the amount of vehicles passing by the route detector at the moment t. $N_D(t)$ indicates the amount of vehicles passing by the parking line detector at the moment t. $N(t)$ represents the amount of vehicles between two detectors at the moment t.

In accordance with the traffic flow theory, we know that $N = KL$. So we conclude that:

$$N = L_D * k_z + (L - L_D) * k_c$$

In the formula, L_D represents the equivalent queue length between two detectors at the moment t, and k_z indicates the density of traffic jams flow while k_c indicates the density of traffic flow in real route. L is the length of the route. As a result, we obtain the queue length prediction model as follows

$$L_D = \frac{N_0 + N_U(t) - N_D(t) - k_c L}{k_z - k_c}$$

In the realities of infact, it happens that many vehicles change lanes and for the multiple lanes, we take them as many of the single lanes in which overtaking situations are not existed. So we obtain the formula for the average equivalent queue length in multiple lanes.

$$\overline{L_D} = \frac{\sum_{i=1}^{M} N_U(i, \mathrm{t}) + N_0 - \sum_{i=1}^{M} N_D(i, t) - \overline{k_c} LM}{M(\overline{k_z} - \overline{k_c})}$$

In the formula, $\overline{L_D}$ represents the average equivalent queue length in signal intersection entrance lanes at the moment t and $N_U(i, t)$ represents the accumulated amount of vehicles arriving at the route detector of lane i at the moment t. $N_D(i, t)$ indicates the amount of vehicles arriving at the parking line detector of lane i at the moment t. The average traffic flow density in each lane can be expressed by $\overline{k_c}$. L is the amount of lanes in route. In this model, all traffic parameters excluding k_z can be collected by the detector or traffic surveying.

2.3 Analysis of the Spatial and Temporal Properties of Density of Traffic Jams Flow

Based on the analysis above, we know that the value of equivalent queue length is certain if we get the value of density of traffic jams flow k_z and it's necessary to make an analysis of the spatial and temporal properties of density of traffic jams flow. Because of the

existence of stochastic fluid in real traffic, it's hard to get the value of stochastic fluid density and we assume that stochastic fluid density is positively correlated with the distance of the vehicle from the parking line, that is, the traffic density uniformly increases from k_c to k_j.

(1) Model of density of traffic jams flow
According to the two-fluid theory, we know that traffic jams flow is the combination of congested traffic flow and the traffic flow whose average density value is $0.5(k_c + k_j)$. So the expression for the model of traffic jams flow is defined below.

$$k_z = \frac{(k_j + k_c)(\Delta N - k_c L) - L_A k_c (k_j - k_c)}{2(\Delta N - k_c L) - L_A (k_j - k_c)}$$

In the expression, L_A represents the real queue length within the stop line before the red light time is over. The real queue length can be received from the measure or simulation.

(2) Relationship between density of traffic jams flow and the amount of stuck vehicles
The road distance of simulation is 700 m, and the distance between the location of the detector and the source of traffic is 150 m. The location of parking line detector is on the parking line in signal intersection entrance. Lane width is 3.5 m, and signal interval is 60 s. The time for red light is 35 s to ensure that the traffic flow length is not too short. The speed of car is 50 km/h (48,58) and the average traffic density is 20 veh/km (Fig. 5).

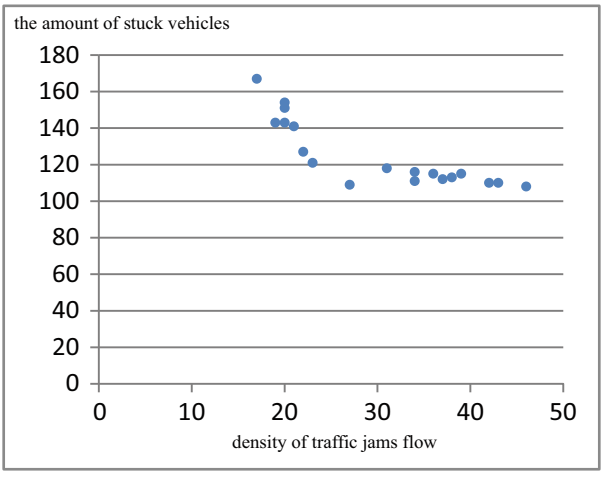

Fig. 5. The relationship diagram of density of traffic jams flow and the amount of stuck vehicles

In the graph, considering that the length of route L is a fixed value and there are few stuck vehicles, we conclude that there is a close inverse correlation between

density of traffic jams flow and the amount of stuck vehicles. If the amount of stuck vehicles is large, that is, the road is busy, density of traffic jams flow remains a fixed value. The fewer the number of stuck vehicles, the density of traffic jams flow is closer to stop density k_j, in other words, the stochastic fluid is ignored.

For analysis of the critical point, it is calculated that when the number of stuck vehicles is less than 15, the density of traffic jams flow is close to the congested traffic flow, that is, there isn't the situation of stochastic fluid and the evanesce time of queue is about 0.6 cycle time. When the number of stuck vehicles is more than 28, the congested traffic flow is close to the fixed value, about 110 veh/km, with the increasing of the amount of stuck vehicles. In this situation, the evanescing time of queue is about 1.8 signal cycle time.

(3) Relationship between road length and density of traffic jams flow

Under the situation, that number of stuck vehicles and road density are fixed values, it is clear that the longer road length, the smaller density of traffic jams flow. However, with the increasing of road length, the amount of stuck vehicles is increasing. The paper uses the method of simulation to study the spatial properties of density of traffic jams flow. In the simulation, we set three routes with lengths of 700 m, 1000 m, 1300 m. The distance between the location of the detector and the source of traffic is 150 m. The location of parking line detector is on the parking line in signal intersection entrance. Lane width is 3.5 m, and signal interval is 60 s. The time for red light is 35 s to make sure that the traffic flow length is not too short. The type of vehicle is cars whose speed is 50 km/h (48,58) and the average traffic density is 20 veh/km (Fig. 6).

According to the analysis of the relationship of density of traffic jams flow and the number of stuck vehicles in different road length, we conclude that density of traffic jams flow is close to a fixed value that is irrelevant to road length.

For analysis of the critical point, it is calculated that when the number of stuck vehicles is less than 18 and L = 550 m, the density of traffic jams flow is close to the congested traffic flow, and the evanescing time of queue is about 0.6 cycle time. When the number of stuck vehicles is more than 28, the congested traffic flow is close to the fixed value. In this situation, the evanescing time of queue is about 1.8 signal cycle time.

When the number of stuck vehicles is less than 32 and L = 850 m, the density of traffic jams flow is close to the congested traffic flow, that is, there isn't the situation of stochastic fluid and the evanescing time of queue is about 0.5 cycle time. When the number of stuck vehicles is more than 48, the congested traffic flow is close to the fixed value. In this situation, the evanescing time of queue is about 1.8 signal cycle time. When the number of stuck vehicles is less than 38 and L = 1150 m, the density of traffic jams flow is close to the congested traffic flow, that is, there isn't the situation of stochastic fluid and the evanescing time of queue is about 0.6 cycle time. When the number of stuck vehicles is more than 50, the congested traffic flow is close to the fixed value. In this situation, the evanescing time of queue is about 1.8 signal cycle time.

(4) Relationship between road density and density of traffic jams flow

The road distance of simulation is 700 m, and the distance between the location of the detector and the source of traffic is 150 m. The location of parking line detector

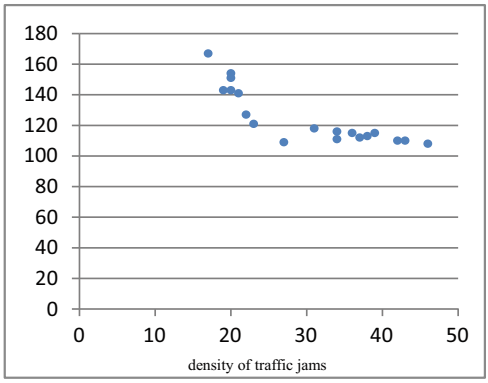

（1）L=550m

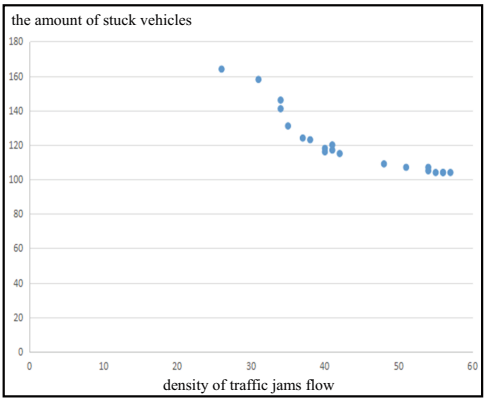

（2）L=850m

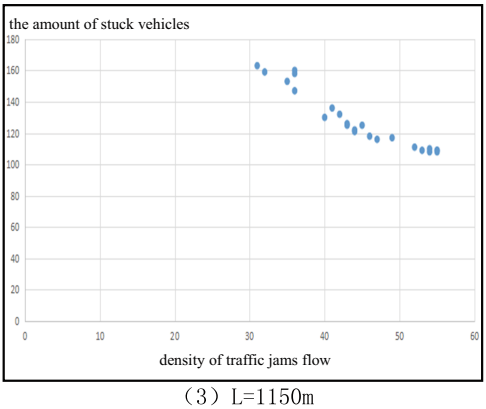

（3）L=1150m

Fig. 6. The relationship diagram of density of traffic jams flow and the amount of stuck vehicles in different road length

is on the parking line in signal intersection entrance. Lane width is 3.5 m, and signal period is 60 s. The effective green time is 25 s (Fig. 7).

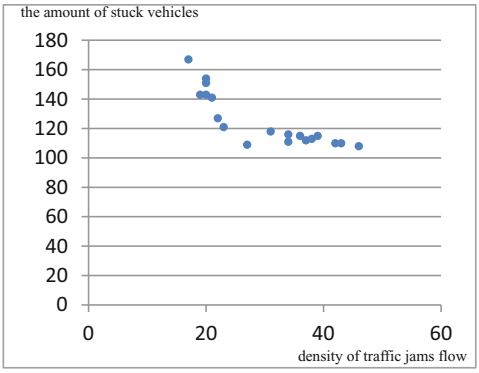

（1）k_c=20veh/km

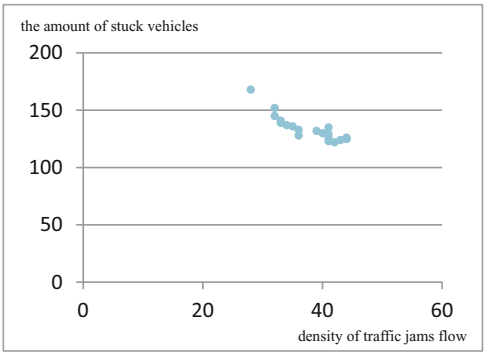

(2) k_c=40veh/km

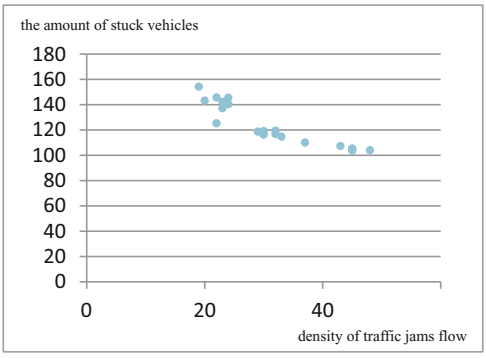

(3) k_c=13. 75veh/km

Fig. 7. The relationship diagram of density of traffic jams flow and the amount of stuck vehicles in different road density

Under the circumstance of congestion and condition that road length is fixed value, we know that the larger road density is, the more density of traffic jams flow is and the value is close to $0.44(0.5k_c + 1.5k_j)$.

For analysis of the critical point, it is calculated that when the number of stuck vehicles is less than 18 and it meets $k_c = 20$ veh/km, the density of traffic jams flow is close to the congested traffic flow, and the evanescing time of queue is about 0.6 cycle time. When the number of stuck vehicles is more than 28, the congested traffic flow is close to a fixed value. In this situation, the evanescing time of queue is about 1.8 signal cycle time. When the number of stuck vehicles is less than 28 and it meets $k_c = 40$ veh/km, the density of traffic jams flow is close to the congested traffic flow, and the evanescing time of queue is about 0.6 cycle time. When the number of stuck vehicles is more than 40, the density of traffic jams flow is close to a fixed value, and the evanescing time of queue is about 1.8 cycle time. When the number of stuck vehicles is less than 16 and it meets $k_c = 13.75$ veh/km, the density of traffic jams flow is close to the congested traffic flow, and the evanescing time of queue is about 0.7 cycle time. When the number of stuck vehicles is more than 48, the density of traffic jams flow is close to a fixed value, and the evanescing time of queue is about 1.8 cycle time.

As what mentioned before, we first have some measured data to give the value of k_j and k_z. According to some descriptions in traffic flow theory, we learn that density of traffic congestion reaches the maximum when the speed of traffic fluid is 0 km/h. The values of k_j and k_z are influenced by some factors, such as canalization and driving habits, etc. Usually, the value of k_j is defined as 160 veh/km. In practical application, the values of k_j and k_z are certain after the traffic survey and analysis to data. The range of density of traffic jams flow is between $0.5(k_c + k_j)$ and k_j in the condition of strong traffic jam. Considering the traffic fluid parameters and analysis of the spatial and temporal properties of density of traffic jams flow in VISSIM, we proposed that density of traffic jams flow reduces linearly from k_j when the evanescing time of real queue is about α cycle time. And when the evanescing time of real queue is about β cycle time, it is the critical point for the congestion condition, at this time, density of traffic jams flow is close to a fixed value labeled as $0.44(0.5k_c + 1.5k_j)$ according to analysis of the spatial and temporal properties of density of traffic jams flow.

We can give the relationship expression of density of traffic jams flow.

$$k_z = \begin{cases} k_j, \Delta N < k_c L + \dfrac{\alpha(k_j - k_c)s_r f_1 g_e L_c}{3600 m_1} \\ k_j - \dfrac{3600 m_1 (0.34k_j - 0.22k_c)}{2(k_j - k_c)s_r f_1 g_e L_c}\Delta N, k_c L + \dfrac{0.5(k_j - k_c)s_r f_1 g_e L_c}{3600 m_1} \le \Delta N \le k_c L + \dfrac{2(k_j - k_c)s_r f_1 g_e L_c}{3600 m_1} \\ 0.44(0.5\mathrm{kc} + 1.5\mathrm{kj}), \Delta N > k_c L + \dfrac{\beta(k_j - k_c)s_r f_1 g_e L_c}{3600 m_1} \end{cases}$$

In the expression, S_1 indicates the road saturation flow and g_e indicates the effective green light time whose units are seconds. f_1 represents reduction factors of the traffic going straight ahead influenced by the steering vehicles in this intersection. L_c represents the average space headway of queue traffic whose units are kilometers and m_1 indicates the number of the toll lanes (Fig. 8).

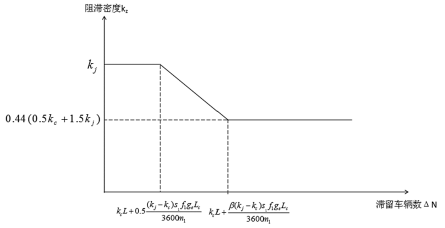

Fig. 8. The relationship diagram of density of traffic jams flow and the amount of stuck vehicles

In practical application, the values of α and β are affected by a number of factors. According to analysis above, the range of α is limited between 0.5 and 1 while the range of β is limited between 1.5 and 2. For convenience, the values of α and β are respectively calibrated to 0.8 and 1.8.

3 Taking the Number of Accumulated Vehicles

Based on the analysis, we need to learn the value of two parameters $N_U(t)$ and $N_D(t)$. The progress is that first we choose a closed highway and set the detectors on the both upstream and downstream of the highway. The distance between two detectors that are used to collect the number of vehicles passing away is L and sampling period is T.

If the moment is corresponds to the moment at the end of cycle j, it has an expression of the number of accumulated vehicles passing by the upstream detector at the moment t.

$$N_U(j) = N_U(j-1) + N'_U(j)$$

In the expression, $N_U(j)$ indicates the number of accumulated vehicles passing by the upstream detector at the end of cycle j while $N_U(j-1)$ indicates the number of accumulated vehicles passing by the upstream detector at the end of cycle $j-1$. $N'_U(j)$ represents the amount of accumulated vehicles passing by the upstream detector in cycle j. The value of j is an integer starting from 1. As for the setting of initial values, when the value of j is 0, the number of accumulated vehicles are 0.

The expression of downstream detector almost equals to that of upstream detector.

$$N_D(j) = N_D(j-1) + N'_D(j)$$

Similarly, $N_D(j)$ indicates the number of accumulated vehicles passing by the downstream detector at the end of cycle j while $N_D(j-1)$ indicates the number of accumulated vehicles passing by the upstream detector at the end of cycle $j-1$. $N'_D(j)$ represents the amount of accumulated vehicles passing by the upstream detector in cycle j. The value of j is an integer starting from 1. As for the setting of initial values, when the value of j is 0, the number of accumulated vehicles are 0.

4 Simulation Verification for the Queue Length Model

(1) Build the simulation
The road distance of simulation is 800 m, and the distance between the location of the detector and the source of traffic is 150 m. The location of parking line detector is on the parking line in signal intersection entrance. Lane width is 3.5 m, and signal period is 70 s. The effective green time is 25 s. The time for red light is 40 s to make sure that the traffic flow length is not too short. The type of vehicle is cars whose driving expectation speed is 80 km/h (75,110). The source of traffic performs the fluid by the flow of 900 veh/h. Furthermore, it's necessary to set the queue length detector at the location of parking line to collect the parameters of real traffic queue.

(2) Data acquiring and analyzing
Before the simulation, the value of k_j needs to be defined through traffic survey and when vehicle speed is 0, that is, the vehicle is added to a queuing, the density of traffic flow remains k_j. For simplicity to simulation, the value of k_j is labored as 160 veh/km. To reduce errors, the density of traffic jams flow is a fixed value labeled as $0.44(0.5k_c + 1.5k_j)$ according to analysis and traffic survey. In the progress of error analysis, we choose the difference of queue length and the relative error these two parameters to prove the validity of equivalent queue length model of congested traffic flow (Tables 1 and 2).

(3) Simulation for the model of equal queue length in multilane
The road and the signal timing is the same as the model in single lane. We set two lanes in the simulation. Compared with the non-congestion traffic flow in model of equal queue length in single lane, we use congestion traffic flow to simulate traffic condition and collect the data from the 11th signal cycle. Car's driving expectation speed distribution is 50 km/h (48,58). The source of traffic performs the fluid by the flow of 2000 pcu/h (Tables 3 and 4).

Table 1. The figure of the simulation in single lane

Cycle	Number of vehicles collected by route detector (pcu)	Number of vehicles collected by parking line detector (pcu)	Density of vehicles at the route detector (pcu/km)	Density of traffic jams flow k_z(pcu/km)	Equivalent queue length (m)	Practical queue length (m)
3	56	37	11	153	82	69
4	69	55	8	160	78	62
5	90	70	13	152	89	77
6	106	87	10	153	108	72
7	126	105	12	150	102	88
8	146	122	12	146	132	108
9	176	140	19	121	152	113
10	189	157	8	116	148	110
11	208	174	12	117	128	108
12	224	191	19	116	130	104

Table 2. The figure of error analysis to the model of queue length in single lane

Cycle	Real queue length (m)	Difference between the lengths (m)	Relative error	Equivalent queue length (m)	Difference between equivalent lengths (m)	Relative error of equivalent lengths
3	69	7	10.1%	82	13	18.8%
4	62	4	6.5%	78	16	25.8%
5	77	3	3.9%	89	12	15.6%
6	72	7	9.7%	98	36	36.1%
7	88	5	5.7%	102	14	15.9%
8	108	10	9.3%	132	24	22.2%
9	113	9	8%	152	39	34.5%
10	110	6	5.5%	148	38	34.5%
11	108	3	2.8%	128	20	18.5%
12	104	10	9.6%	130	26	25%
Average	91.1	6.4	7.1%	113.9	22.8	24.7%

Table 3. The figure of the simulation in multilane

Cycle	Number of vehicles collected by route detector (pcu)	Number of vehicles collected by parking line detector (pcu)	Density of vehicles at the route detector (pcu/km)	Density of traffic jams flow k_z(pcu/km)	Equivalent queue length (m)	Practical queue length (m)
11	343	283	20	153	132	94
12	376	315	17	160	128	96
13	413	347	17	152	130	92
14	450	378	26	153	141	98
15	475	409	19	150	138	100
16	511	440	17	146	136	97
17	556	471	23	121	148	113
18	589	502	23	116	171	121
19	622	533	18	117	156	119
20	660	564	22	116	172	122

Table 4. The figure of error analysis to the model of queue length in multilane

Cycle	Real queue length (m)	Difference between the lengths (m)	Relative error	Equivalent queue length (m)	Difference between equivalent lengths (m)	Relative error of equivalent lengths
3	94	13	14%	132	38	40.4%
4	96	12	13%	128	32	33.3%
5	92	2	2%	130	38	41.3%
6	98	9	9%	141	43	43.9%
7	100	6	6%	138	38	38%
8	97	8	8%	136	39	40.2%
9	113	12	11%	148	35	31%
10	121	8	7%	171	50	41.3%
11	119	15	13%	156	37	31.1%
12	122	16	13%	172	50	41%
Average	105.2	10.1	9.6%	145.2	40	38.2%

5 Summary

Based on the simulation results above, we know that the average equivalent queue length in single lane is 113.9 m and its relative error is 24.7% when the values in multilane are 145.2 m and 38.2%. It reflects the existence of stochastic fluid in practical traffic flow due to the situation that all the equivalent queue lengths are longer than the practical queue lengths [4–6].

The reason why all the errors of equivalent queue lengths in multilane are longer than that in single lane is that there are overtaking behaviors among different lanes which results in complex conditions.

Some stochastic factors that cause the error make the traffic flow complex during the period of transition. In practical application, the value of the density of traffic jams flow must be verified by simulation or obtained through actual observations.

Analysis in paper shows that the model of equal queue length can quantitatively describe the practical queue length, and the equivalent queue length model can quantitatively reflect transition stage of stochastic fluid in traffic flow.

References

1. 王殿海 (2002) 交通流理论[M].北京:人民交通出版社
2. 王川久,杨兆升 (2003) 城市交通流诱导系统的框架研究[J].吉林大学学报(工学版)
3. 杨兆升 (1997) 姜桂艳.城市交通流诱导系统结构框架研究[J].公路交通科技 9,14(3):6–10
4. Marcotte P (1983) Network optimization with continuous control parameters. Transp Sci 17:181–197
5. Smitll MJ (1979) Traffic control and route choice: a simple example. Transp Res 13(4):289–294
6. Chen Y (2001) Integrating heterogeneous autonomous control systems. Elektron J-South Afr Inst Electr Eng 18(1):36–37

Research on the Model of Traffic Signal Control and Signal Coordinated Control

Xiaoqing Zeng, Chaoyang Wu(✉), Yujia Chen, Qipeng Xiong, and Cong Wei

Tongji University, Shanghai, China
wcy@tongji.edu.cn

Abstract. This paper points to the shortfalls of the research on the traffic and signal coordinated control, and makes a model of traffic signal control and signal coordinated control. In the model, we use the minimum driving time as optimized object to adjust green signal ratio and pause rate in various intersections in real time, the green signal ratio is set as signal control strategy and the pause rate is taken as vehicle navigation strategy. The model is aim at coordinated control of the vehicles and signal. Also, this paper solves the model with the methods based on genetic algorithm (GA).

Keywords: Signal coordinated control · Traffic signal control · Minimum driving time · Green signal ratio · VISSIM4.30

1 Research Status at Home and Abroad

The foreign scholars first led the studies on the coordinated control of the vehicles and signal in the early nineteen seventies. However, since the technology of traffic information publishing is not yet mature, then they carried out the study mainly on the relationship between signal timing strategy and traffic flow assignment in network.

Since the 1990s, many scholars in China found and focus on the problem of coordinated control of the vehicles and signal. They have yielded many results. Scholars like Yang Zhaosheng in 2005 analysis the operation principle of out-door guidance system and fixing timing control system, set a control model and use the dynamic speed model to improve the information distribute strategy [1]. Scholars like Dai Hong in 2006 carried out a flow distribution model of the integration with signal control system and traffic guiding and the model based on the genetic algorithm has good simulation effect in the little network of roads without the aid of OD of urban road network. Scholars like Bao Lixia in 2007 set up a model of integration with traffic control and guidance, which takes total travel time minimum as the optimization goal and is based on real-time traffic flow parameters instead of OD matrix estimation. The model searches the optimal solution in the small layout and adjusts frequently the signal timing and flow distribution [2]. Scholars like Gu Yuanli in 2008 made a model in what the minimum cost per unit time is taken as the optimized object. The model is restricted by the network traffic flow equilibrium and solves the model of coordination between traffic guidance and signal control with the methods based on ant colony algorithm [3, 4]. Scholars like Wang Chuan

X. Zeng et al. (eds.), *International Symposium for Intelligent Transportation and Smart City (ITASC) 2017 Proceedings*, Smart Innovation, Systems and Technologies 62, DOI 10.1007/978-981-10-3575-3_7

in 2014 proposed a model of coordination between traffic guidance and signal control with the methods based on the idea of cooperative vehicle-infrastructure. This model also takes total travel time minimum as the optimization goal and the green signal ratio is set as signal control strategy and the optimal pause rate is taken as vehicle navigation strategy in framework of cooperative vehicle-infrastructure system. This model received great result of optimizing in the miniature road network but benefit less on the applicability because of the cooperative vehicle-infrastructure technology [4].

From the research status at home and abroad above, there are some shortcomings in cooperative vehicle-signal: (1) most research focus on the framework of cooperative control while least research on the model itself of cooperative control; (2) now the research on the signal control and traffic guidance is based on the traffic control, or based on the traffic guidance; (3) the research on the cooperative control and guidance today has lack of research on the system structure which results of bad applicability; (4) the weak real-time performance is found on the research on the cooperative control and guidance that means some models indirectly calculate the total travel time based on correlative theory of the traffic flow and historical traffic data. The main reasons are two: one is that it is hard to get the real time data of vehicle queue length in traveling and the other is these models lack the calculations of real time vehicle queue length.

2 Model of Traffic Signal Control and Signal Coordinated Control

2.1 Modeling Idea

The study proposed a model of integration with traffic control and guidance to balance traffic over space and time according to optimal coordinated control strategy. The model is based on data gathering and transmission that includes speed data collected by the detector in each signal cycle and signal timing data transmitted by the traffic signal control system, when assumed that all vehicles in road network are subjected to control strategy. Through consulting literature materials, we know that the common traffic evaluation indicators now mainly include total driveling time, vehicle delay time and accessibility of network. Since the total driveling time is the indicator drivers prefer to pay attention to, the paper takes that as the evaluation indicator and makes a model of calculating the total driveling time in network based on the studies in queue length prediction model. The constraints of this model are saturation degree, saturation variance and traffic balance methods, etc. In the model, the green signal ratio is set as signal control strategy and the pause rate is taken as vehicle navigation strategy to improve the cooperative control of vehicles and signal, making the traffic equilibrium and saving driveling time.

2.2 Model Used for Computing Travel Time

Most of models used for computing travel time like Green shield's Model are based on the relationship of speed and flow in the traffic flow theory. These models computed travel time by historical traffic data, lack of real time and perform bad impact on those networks of road where traffic changes are small. While they are used in the networks of road where traffic changes are big, calculation accuracy will become a serious

problem. Some scholars obtained the traffic parameters collected by car embedded devices and roadside equipment. This method can improve the accuracy but the realizability of the model is unsatisfied.

1. Distance. According to our study, traffic volumes in a road are made up of free traffic volumes and congested traffic volumes. The length of traffic flow is equal to free travel distance. Because it exists the disturbing flow (random flow) in the reality traffic flow, the accuracy in the calculations of vehicles travel length that counts as the difference between length of the road and practical queuing length is bad. Introduced the concepts of queuing length equivalents, we take the situation of the random flow in consideration and deduce the model used for computing total travel time in strong traffic congestion performs well in accuracy.

$$L'(t) = L - L_D$$
$$L_D = \frac{N_0 + N_U(t) - N_D(t) - k_c L}{k_z - k_c}$$

   $L'(t)$ represents the free travel distance at t moment, L_D represents the equivalent of queuing length when N_0 expresses the amount of vehicles between two detectors when $t = 0$, $N_U(t)$ represents how many vehicles pass the detector which is set roadside and $N_D(t)$ is the amount of vehicles pass the detector which is set at the stop sign.
2. Average speed. The average speed of one road is defined as the average speed of free traffic flow which is collected by the detectors. And the formula for calculating the average speed is below.

$$\overline{V} = \frac{\sum_{n=1}^{N_U(t)} v_n}{N_U(t)}$$

   In the formula, $\overline{v}$ represents the average travel speed and v_n represents in a specific period of time t the average travel speed of vehicles which pass the detector.
3. Model used for computing travel time. The travel time is equal to the traffic distance divided by the average speed and the formula is below. T_{a1} means the travel time.

$$T_{a1} = \frac{L - L_D}{\overline{V}}$$

$$T_{a1} = (L - \frac{N_0 + N_U(t) - N_D(t) - k_c L}{k_z - k_c}) \frac{N_U(t)}{\sum_{n=1}^{N_U(t)} v_n}$$

2.3 Intersection Delay Model

The model of intersection delay used in the paper is from HCM 1985 that is widely used in China, and the formula is below.

$$d = 0.38C\frac{(1-\lambda)^2}{1-\lambda x} + 173x^2\left[(x-1) + \sqrt{(x-1)^2 + \frac{16x}{S}}\right]$$

In the formula, C, λ, x, S respectively indicate signal cycle length, green split, and saturation degree and flow.

The delay model in HCM includes the average delay caused by the uniform arrival and random delay caused by the random arrival, and the model is fit to calculation of delay time whose saturation degree is around 1. In summary, the paper defined the real-time total travel time as the sum of travel time and delay time in intersection. The math expressions are below.

$$\mathrm{T} = T_{a1} + T_{a2} = T_{a1} + d$$

2.4 Coordination Model and Constraints

The model of traffic signal control and signal coordinated control in the paper takes minimum driving time, which drivers focus on, as the objective function. Assumed that cycle length in intersection is fixed, green signal ratio is set as signal control strategy and the pause rate is taken as vehicle navigation strategy. The model can express below.

$$F = \min \sum_{a=1}^{n} (T_{a1} + T_{a2})$$

$$s.t.\begin{cases} \bar{x} = \dfrac{1}{n}\sum\limits_{i=1}^{n} x_i < \psi \\ S^2 = \dfrac{1}{n}\sum\limits_{i=1}^{n} (x_i - \bar{x})^2 < \sigma \\ \sum\limits_{a\in A(k)} u_a^n(t) = OD_k^n + \sum\limits_{a\in A(k)} v_a^n(t) \\ v_a^n(t) = q_a^n(t)/T_{a1} \\ 0 < \lambda < 1 \\ 0 \le u, q \le \tau \end{cases}$$

Constraints of the model include saturation, traffic volumes, pause rate and diverging rate, and split. Here are explains for each constraint.

1. Saturation constraint. Saturation degree is an important evaluating indicator in traffic status distinguishing. If the average saturation degree is too high, it means traffic volume is too large. If the variance of saturation degree is too big, it means imbalances in traffic flows. Therefore, it's necessary to restrict the mean and variance of the saturation degree. Here gives the formula of the average saturation degree.

$$\bar{x} = \frac{1}{n}\sum_{i=1}^{n} x_i$$

In the formula, x_i represents saturation degree in each road. ψ is the maximum in the saturation degree, so the mean of saturation degree has a range of values:

$$0 < \bar{x} < \psi$$

The formula of the variance of saturation degree is below.

$$S^2 = \frac{1}{n}\sum_{i=1}^{n} (x_i - \bar{x})^2$$

σ is maximum in the variance of saturation degree and variance of saturation degree has a range of values below.

$$S^2 < \sigma$$

2. Traffic volumes constraint. In the network, parking rate of the road whose terminal point is k is equal to sum of OD demands from k to n and diverging rate of the road whose terminal point is n.

$$\sum_{a \in A(k)} u_a^n(t) = OD_k^n + \sum_{a \in A(k)} v_a^n(t)$$

In the formula, OD_k^n indicates OD demands from k to n and $A(k)$ refers to the routes start from k when $B(k)$ refers to the routes whose terminal point is n.

3. Formula of diverging rate. Formula of diverging rate is below.

$$q_a^n(t) = \int_t^{t+T_{a1}} v_a^n(w)dw$$

When the diverging rate of the route a changes very little, the formula can be simplified.

$$q_a^n(t) = v_a^n(t)(t + T_{a1} - t)$$
$$v_a^n(t) = \frac{q_a^n(t)}{T_{a1}}$$

In this formula, $v_a^n(t)$ represents the diverging rate of the route a whose terminal point is n at the moment t while $q_a^n(t)$ means the traffic volume of the route a.

4. Constraint of diverging rate, pause rate and green split. If model is solved, it may happen that the value of diverging rate or pause rate is too large which is impossible in real situation. So restricting them is important.

$$0 \leq u, q \leq \tau$$

The constraint of green split is based on the definition of itself.

$$0 < \lambda < 1$$

The maximum of the green split is limited to 1 and the value range is related to the intersection signal timing.

3 Solution Based on Genetic Algorithms in Coordination Model

3.1 Code Design

Code can regard as the process turns data into the chromosome genes. Relatively we call decode, the process turns chromosome genes back to the data. The main ways you code are binary encoding, float encoding and gray-code method, etc. Binary encoding is widely used in genetic algorithms to change data into the string 0/1. This method is much effective, convenient to crossover and mutation. So we use binary encoding and turn the parameters like green split and pause rate into the k-character string 0/1.

$$u_i = a_{ik}a_{ik-1}a_{ik-2} \ldots a_{i1}$$
$$\lambda_i = b_{ik}b_{ik-1}b_{ik-2} \ldots b_{i1}$$

There are n_1 parameters of green split that called λ_i and n_2 parameters of pause rate called u_i, so the total length of individuals chromosome in group is equal to $k * (n_1 + n_2)$.

The formula of decoding is below.

$$\lambda_i = \sum_{j=1}^{k} \frac{b_{ij}2^{j-1}}{2^k - 1}$$
$$u_i = u_{i\max} \sum_{j=1}^{k} \frac{a_{ij}2^{j-1}}{2^k - 1}$$

In the formula, $u_{i\max}$ represents the maximum pause rate in the route i.

3.2 Fitness Function Design

In the genetic algorithm, chromosome fitness only depends on fitness function. The design of fitness function relates directly to optimal solutions. The design principles

include non-negative result, maximization problem, smaller amount of computation, etc. In order to solve the minimum problem, the fitness function can be designed below.

$$Fit(f(x)) = C_{\max} - f(x)$$

$c_{\max}$ represents the maximum estimator of the function $f(x)$.

The model of vehicle-signal coordinated control paper proposed is kind of the minimum problem. And the fitness function is designed below so that it meets the requirement of maximization and non-negativity.

$$Fit(f(x)) = \max(C - f(x)) = C_{\max} - \min \sum_{a \in A(k)} (Ta1 + Ta2)$$

3.3 Penalty Function Design

Fitness function with constraint can change to that without constraint by penalty function in genetic algorithms. The way to build the penalty function is the way to solve the problem that is fitness function with constraint. There are two ways to build penalty function: conjunctive form and disjunctive form, and which one is chosen depends on the actual conditions. Another advantage in building penalty function is that this function punishes the unfeasible solutions and ensures chromosome in every generation keeps amount of unfeasible solutions so that we can find the optimal solution between feasible and unfeasible solutions in genetic algorithm.

Considering to the penalty function, the fitness function can be designed below.

$$fit(f(x)) = f(x) + p(x)$$

$$fit(f(x)) = f(x) * p(x)$$

In the function expression, $f(x)$ represents the objective function while $p(x)$ penalty function. The way used in the paper is disjunctive form.

3.4 Genetic Operator Design

According to the genetic algorithms and genetic operators selected, we can keep the chromosome in last generation down to next generation. The selection method we use is Monte Carlo Method. This method's formula is below.

$$p_i = \frac{f_i}{\sum_{i=1}^{M} f_i}$$

In the expression, p_i represents the possibility for genes of the individual i passed on to the progeny. And f_i means the corresponding result of the fitness function.

3.5 Crossover Operator Design

According to genetic algorithms, we change part of a gene between individuals who are selected in the species on the last generation and the new individual appears. Crossover operator plays most important role in genetic algorithms and it is the main way to get new individual and to make a progress of global optimization, also it's the key feature compared to other optimization algorithms. Common crossover operators include single-point cross-operation, double-point cross-operation, multi-point cross-operation, uniform crossover operator and shuffle crossover operator. The design in paper is single-point cross-operation and the probability is 0.6.

3.6 Mutation Operators Design

According to mutation operators in genetic algorithms, we reverse some genes of individuals and make them a new one. Similarly in crossover operator which reflects global convergence in algorithms, as a method to complement during new individuals generation, mutation operators is also important in genetic algorithms and demonstrates local convergence that ensures individual varieties. Common mutation operators include basic bit uniform mutation, uniform mutation, and non-uniform mutation, etc. The design in paper is basic bit uniform mutation and the probability of mutation is 0.09.

4 Simulation

To accord with the actual traffic status in road networks, the paper takes a simulation experiment to testify the validity of the model. The simulation objects are Tianlin Road and its affiliated network including Yishan Road, Gumei Road, Guiping Road and the tunnel of Tianlin Road. The simulation has a background that is the transportation node improvement project of Central Link and Tianlin Road. We build a network with four intersections and perform a simulation (Figs. 1 and 2).

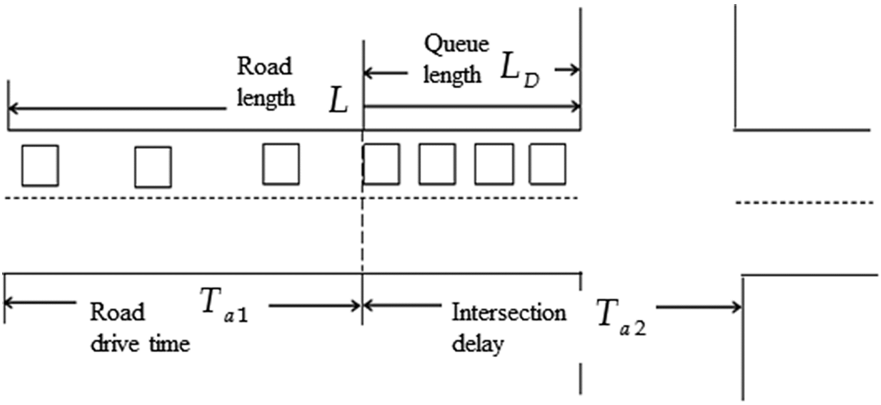

Fig. 1. Road network sketch

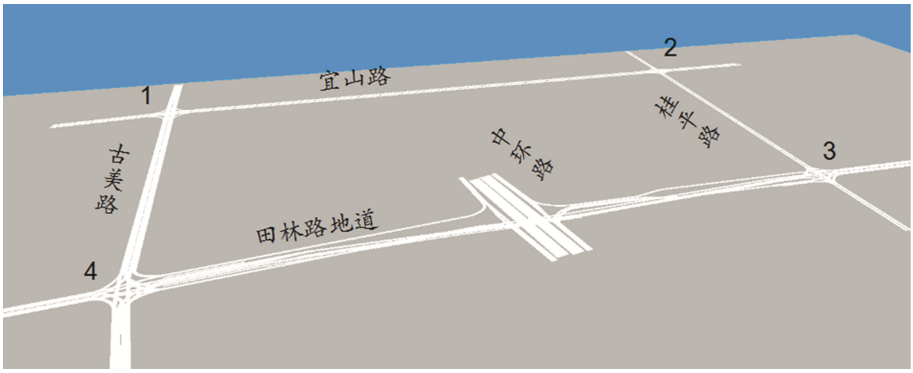

Fig. 2. 3D rendering of the network in VISSIM

The assumptions in the simulation are below:

(1) OD demands are given fixed values
(2) Maximum of pause rate and diverging rate is 3pcu/s.

The rendering below shows the network and each node number.

Four intersections with each two pairs of traffic lights are two signal phases and cycle length is 60s. The values of signal timing are in Fig. 3.

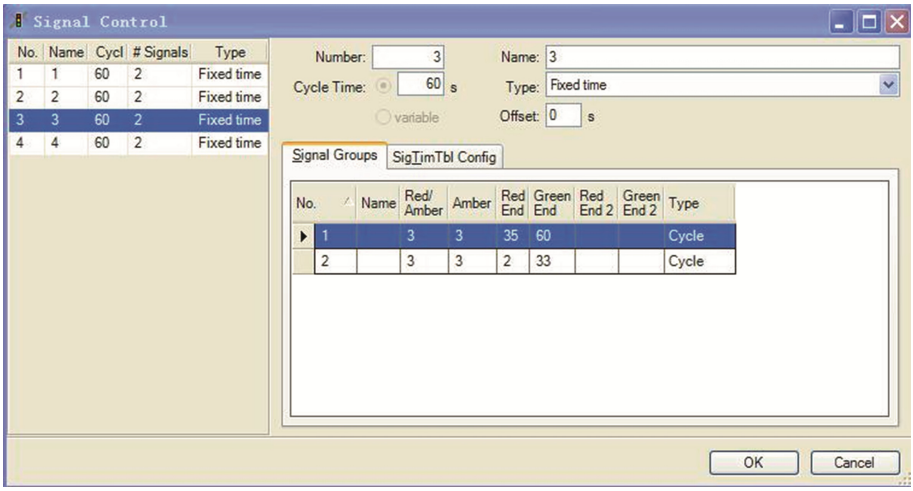

Fig. 3. The settings of signal timing in VISSIM

According to the OD demands written in *Traffic volume forecasting of the tunnel of Tianlin Road*, we assume that there are four trip OD: node 1-node 3, node 3-node 1,

node 2-node 4, node 4-node 1 and the OD demand in each node is 800pcu/h, 700pcu/h, 700pcu/h, 600pcu/h. The demands are fixed values and solved by setting the route.

The coordination model can be solved by Genetic Algorithm Direct Search Toolbox in MATLAB. And the value of parameter x has a upper and lower bound which can be expressed by two matrix.

$$L = [0, 0, 0, 0, 0, \ldots 0, 0, 0, 0]$$

$$U = [3, 3, 3, \ldots 0.97, 0.97, 0.97 \ldots 3, 3, 3, 3,]$$

In the genetic algorithm, the number of population size is 30, and fitness scaling function is set as proportional. Selection function is set as Roulette while mutation function is Uniform. The probability of mutation is 0.09. Crossover function is set as single point. Cross-operation probability is 0.6. The maximum of iteration algebra is 5600 and other parameter values are default. After 5600 iterations, it makes out the excellent which is in Fig. 4.

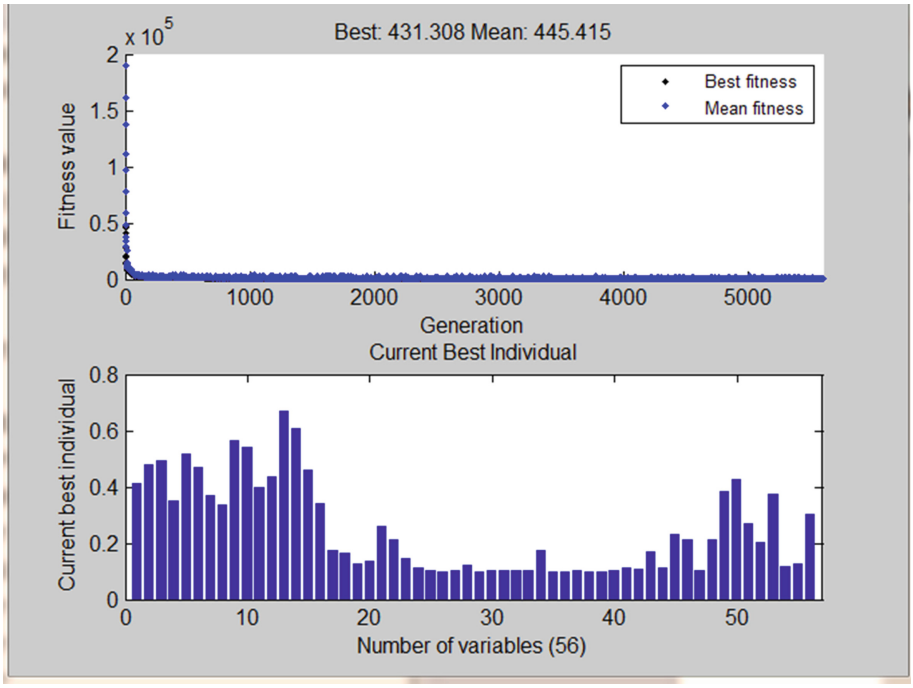

Fig. 4. The valued graphs of final solution

Table 1. The figure of the network after optimization

Route	Volume of traffic	Pause rate	Split
1–2	0.41	0.17	0.56
2–1	0.48	0.17	0.54
2–3	0.49	0.13	0.4
3–2	0.35	0.14	0.44
3–4	0.52	0.26	0.67
4–3	0.47	0.21	0.6
1–4	0.37	0.14	0.33
4–1	0.33	0.11	0.46

The optimum for the main parameters in network was shown in the table above (Table 1).

We enter the pause rate and split optimized into VISSIM by setting the route. By contrasting driving time in each route and total travel time in network and setting the time to simulate as 15 min, we can solve the best timing plans in four intersections below (Fig. 5).

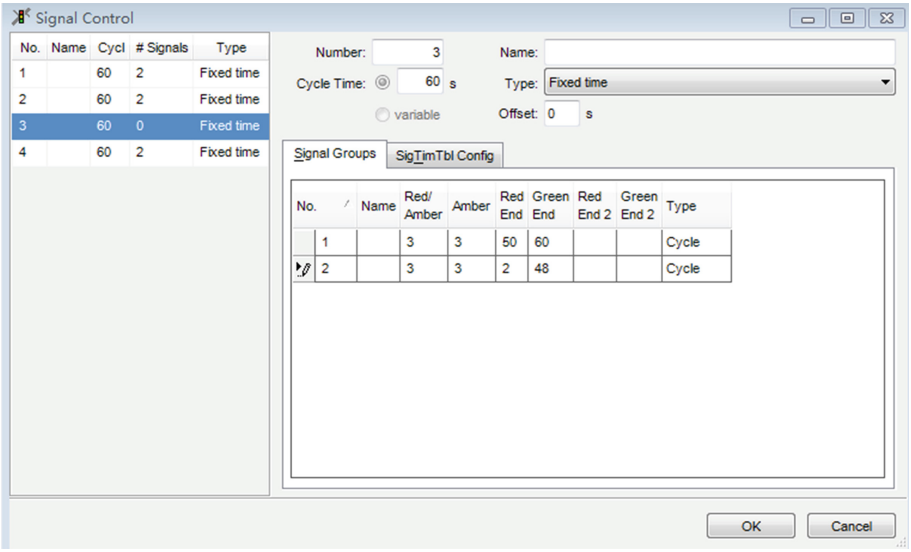

Fig. 5. The timing plans of optimization

1. Differences in total travel time in network. Without the optimization, the total travel time was 634.78s. After the optimization, it changed to 431.3s. Due to the model of traffic signal control and signal coordinated control, the total travel time in network was reduced to 1/3 the time that is 254.93s which means the model performs well in saving travel time (Figs. 6 and 7).

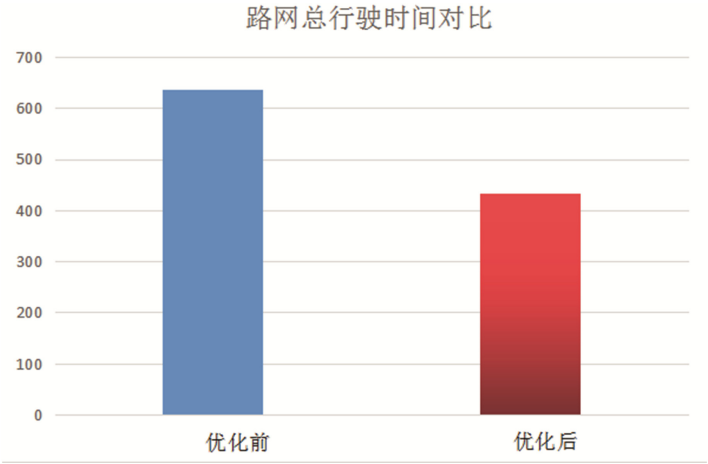

Fig. 6. The comparison for the total travel time in network

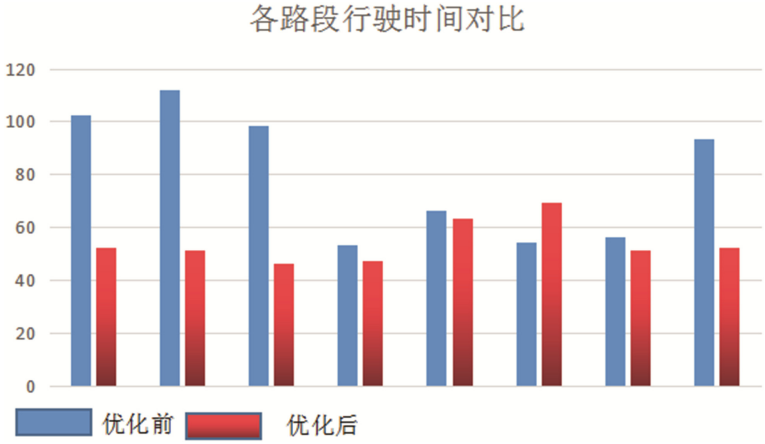

Fig. 7. The comparison for the travel time in each route before and after optimization

2. Differences in travel time in each route. On the basis of the table, we learn that there is an obvious gap in travel time in each route before the optimization. And the situation is improved after the optimization. So the model paper proposed can balance the travel time in each route and distribute flow reasonably (Table 2).

Table 2. The travel time in each route before and after optimization

Route	Travel time before optimization	Travel time after optimization
1–2	102	52
2–1	112	51
2–3	98	46
3–2	53	47
3–4	66	63
4–3	54	69
1–4	56	51
4–1	93	52

5 Summary

The paper builds a model of traffic signal control and signal coordinated control. We use the minimum driving time as optimized object to adjust green signal ratio and pause rate in various intersections in real time, the green signal ratio is set as signal control strategy and the pause rate is taken as vehicle navigation strategy. Based on the traffic simulation software VISSIM4.30, we build a small network. With the help of initial data of some roads and the GUI tool in MATLAB, this paper tested the model's good performance in coordinated control. We also give the solutions based on genetic algorithms and the key formula. Furthermore, we take the before-and-after comparisons at the length of travel time to validate the effectiveness of model.

References

1. 杨兆升,刘新杰,保丽霞 (2005) 城市交通控制与交通流诱导系统协同的模式与策略研究. 第一届中国智能交通年会论文集, 505–511
2. 保丽霞,杨兆升等.交通流诱导与控制协同的双目标优化模型及准最优求解算法.吉林大学学报 37(2):319–324 (2007)
3. 乐群星,魏法杰.蚂蚁算法的基本原理及其研究发展现状.北京航空航天大学学报(社会科学版) 8(4):5–8 (2005)
4. Dorigo M, Gambardellal M (1997) An ant system: a cooperative learning approach to the traveling salesman problem. IEEE Trans Evol Cooper (S1089-778X) 1(1):53–66
5. 王川.车路协同环境下交通控制与诱导协同研究. [硕士学位论文]. 兰州理工大学 (2014)
6. 王艳青. 面向城市复杂道路的交通状态识别手段与算法研究. [硕士学位论文]. 同济大学 (2015)
7. 王奕曾,金立名,袁腾飞,城市道路交叉口车辆排队交通流状态理论研究,《城市建设理论研究》,第 6 卷第 1 期, 72 页, 2016 年 1 月

Research on the Behavior of Routes Choice Under the Information Availability

Xiaofang Shan[1(✉)], Zheng Wang[2], and Yingchang Zho[2]

[1] School of Economics and Management, Tongji University, Shanghai, China
2669926067@qq.com
[2] College of Transport and Communications, Shanghai Maritime University, Shanghai, China
1648687822@qq.com, czyc502@163.com

Abstract. This paper is to study the routes choice under the influence of information and discuss the influence of information on the routes choice of travelers. It is based on the Logit model to construct the routes choice model under the influence of information and simulate after that. The simulation results show that the information has a great influence on the routes choice of travelers and prove that the model meet the requirement of accuracy.

Keywords: Information · Routes choice · Logit model · Simulation

1 Introduction

With the rapid urban growth and sprawl in China, the scale of cities is more and more big, and has caused more and more traffic demands. The existing traffic facilities can no longer meet the needs of the travelers in China. With the Intelligent Transportation System (ITS), especially the Advanced Traveler Information System (ATIS) appears and provides accurate, real-time information on subway, light rail transit and buses, which provides effective basis for traveler's decision-making when he makes route choices, the traffic conditions improved. However, as the ATIS provides too much information and adds serious interference to traveler's decision, the traffic problems engender again. For example many people choose the same path according to the real-time information by ATIS provide. The best way to solve the above problem is to simplify the information that ATIS provides, and improve the real utility of information, which makes the travelers get real-time, accurate and efficient information. It is necessary to research on the routes choices under the effect of information, which improves the efficiency of ATIS and traffic management.

X. Zeng et al. (eds.), *International Symposium for Intelligent Transportation and Smart City (ITASC) 2017 Proceedings*, Smart Innovation, Systems and Technologies 62, DOI 10.1007/978-981-10-3575-3_8

2 Establishment of the Model

2.1 The Fundamental Routes Choice Model Based on MNL Model

In order to establish the fundamental routes choice model based on MNL model, this paper makes the following assumptions:

(1) The travelers have n alternatives to choose from origin to destination at any time;
(2) C_i delegates the generalized travel resistance of alternative i;
(3) M_i delegates the generalized, implicit utility of alternative i;

Then the probability that travelers choose the alternative i is as follows:

$$P_i = \frac{\exp[-\theta C_i + \gamma M_i]}{\sum_{k=1}^{n} \exp[-\theta C_k + \gamma M_k]} \tag{1.1}$$

In this formula, θ, γ are the distribution parameters. θ ∈ [0,1], θ delegates the traveler's reaction to the travel resistance; ∈ [0,1]; γ is the variable from which travelers could benefit to make decision; Hence, γ indicates the degree that decision makers rely on or use the information.

2.2 Routes Choice Model Under Information Availability

In this paper, routes choice model under information availability is efficacious only under certain assumptions and hypothesis as follows:

(1) Assuming that traveler depends entirely on the information when choose the routes and the information can provide different level description of routes.
(2) Relative to the negative effect of noisy and redundant information, we only consider the positive impact of information on travel routes choice in this paper. Therefore, the coefficient of information efficiency α must be in a certain range, and this model assumes that α ∈ [0,1]; When α = 0, the value of information is zero, which means that information cannot describe the road conditions; Travelers can only according to their instinct to judge which route is best for themselves; When α = 1, the information can completely describe real road conditions without information redundancy; The travelers can make scientific decision if they know the routes condition clearly.
(3) Travelers must depends on the relevant information completely when they make decisions, and the decision-makers do not use the recessive utility to make decisions.

According to formula 1.1, the probability that travelers choose route i based on information cost is:

$$P_i = \frac{\exp[-C_{Ii}]}{\sum_{k=1}^{n} \exp[-C_{Ik}]} \tag{1.2}$$

$$C_{Ii} = \alpha C_{0i} \tag{1.3}$$

Set C_{Ii} to be the travel cost of route i in the lead of the information; C_{0i}: the objective cost of route i, and shows with travel time;

$$P_i = \frac{\exp[-\alpha C_{oi}]}{\sum_{k=1}^{n} \exp[-\alpha C_{ok}]} \tag{1.4}$$

The formula above is the routes choice model under the information availability. It shows that we can calculate the probability of each route when α and C_{0i} have been known, and the travelers can choose the reasonable route following the probability.

2.3 The Empirical Calculation of Model

In order to verify the influence of information availability on travelers routes choice; this paper will give α and C_{0i} values respectively. There are two cases, one has only two routes between the OD, another has four paths between OD, as shown in Fig. 1(a) and (b). Then we calculate the probability according to Formula 1.4, and the calculation results as shown in Fig. 1(c) and (d).

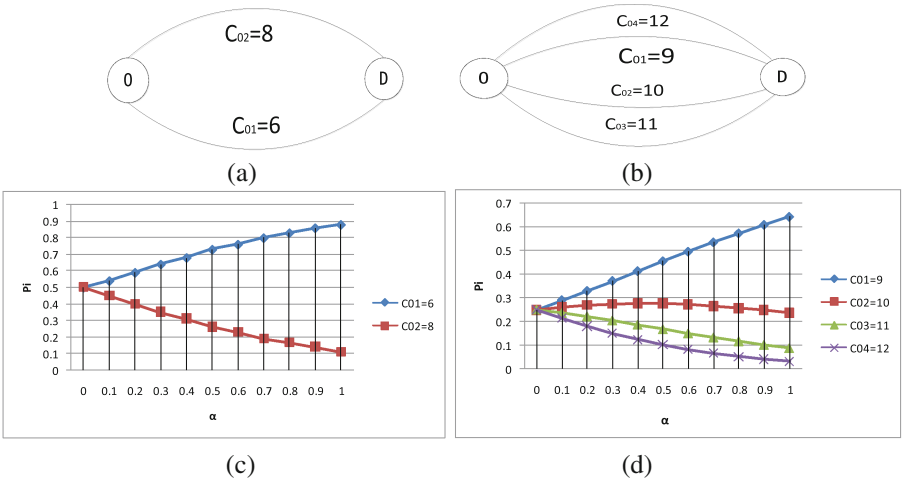

Fig. 1. (a) Two routes, (b) four routes (c) two routes choice probability, (d) four routes choice probability

Figure 1(c) and (d) show that when α = 0, the information is completely unable to describe the actual condition of roads, so the probability that travelers choose each routes is equal. With the value of α increased gradually, the information can describe the roads better and better to travelers, and the probability to choose route 1 becomes bigger; however the probability to choose other routes becomes smaller.

To sum up, when $\alpha = 0$, information can provide none value, and the information can't reflect the traffic conditions between O and D; Travelers make decisions only rely on their own feelings, and choose one of the alternative paths to travel. With the increase of α, the information can provide more much value, and travelers can calculate the travel cost according to the information they received, thereby they can choose the route which favours their travel. So the information availability has a great influence on travelers' decision making.

3 The Simulation System Design and Analysis

3.1 Simulation Modeling of Travel Choice Under the Influence of Information

In order to estimate the probability that travelers choose certain route under the information availability, and observe directly the effects of α on P_i, this paper will use Netlogo simulation on it. Lastly, It will be judged whether the calculation results is approximate to the objective reality according to the simulation results.

Under the condition of the objective travel cost that the routes can be chosen, the travel of 100 vehicles is simulated according to the different value of α in this paper. vehicle select two routes randomly under the influence of information, and two data monitors which separately represent "yellow_car" and "black_car" are set in the system. The monitor's function is to count the total number of vehicles to choose two routes which travel cost is respectively 6 and 8. Finally set up a plotter called Toyal_car. The abscissa and ordinate stand for simulation time and total number of vehicle respectively. According to the real-time simulation process, the system will draw the total number of vehicles in the coordinate system at the time until the end of the simulation. The probability to choose two routes can be intuitively seen under a certain value of α as the number of vehicles into the system is 100.

3.2 The Simulation Parameters Setting

(1) α: set to be the slider, can be value 0, 0.1, 0.2, 0.3,…, 1;

(2) C_{0i}: set to be the objective travel costs of two optional route, be value 6 and 8 respectively;

(3) T: the simulation time, Set to be 2s, all vehicles can run within 2s from point O to D as the simulation interface is limited and the coordinate difference between the O and D is small.

(4) N_{vel}: the number of vehicles in the system, set to be 100 and all vehicles are in the origin O.

3.3 The Analysis of Simulation Results

The simulation results are shown in Fig. 2(a)–(k) when α is equal to 0, 0.1, 0.2,…, 0.9, 1:

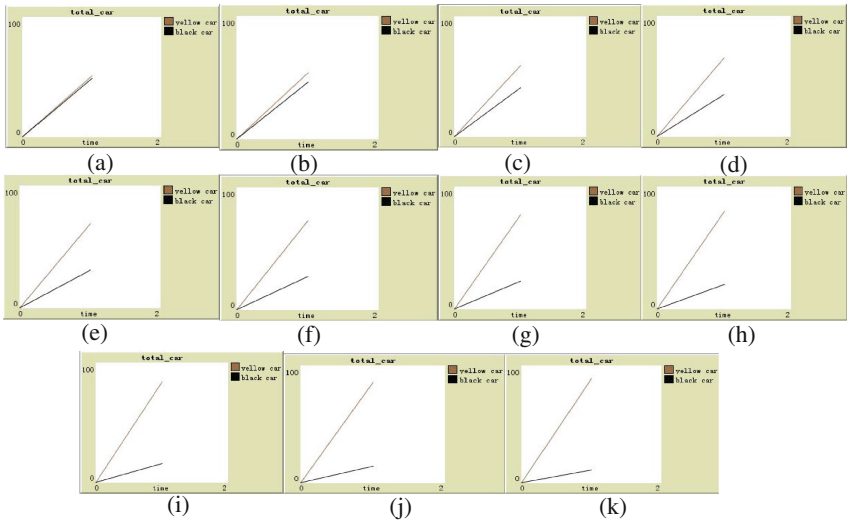

Fig. 2. (a) (α = 0) Toyal_car, (b) (α = 0.1) Toyal_car, (c) (α = 0.2) Toyal_car, (d) (α = 0.3) Toyal_car, (e) (α = 0.4) Toyal_car, (f) (α = 0.5) Toyal_car, (g) (α = 0.6) Toyal_car, (h) (α = 0.7) Toyal_car, (i) (α = 0.8) Toyal_car, (j) (α = 0.9) Toyal_car, (k) (α = 1) Toyal_car

From Fig. 2(a)–(k), with the value of α increasing from 0 to 1, the slope of the straight line on behalf of the yellow car becomes bigger, on the contrary, the slope of the straight line on behalf of the blue car declines gradually, and the angle of two lines is bigger and bigger; namely more travelers choose the route which objective travel cost is lower. Setting N_y, N_b separately represent the number of vehicle of yellow_car and black_car after simulation; when $\alpha = 0$, $N_y = 51$, $N_b = 49$; When $\alpha = 0.1$, $N_y = 54$, $N_b = 46$; When $\alpha = 0.2$, $N_y = 59$, $N_b = 41$; When $\alpha = 0.3$, $N_y = 65$, $N_b = 35$; When $\alpha = 0.4$, $N_y = 69$, $N_b = 31$; When $\alpha = 0.5$, $N_y = 73$, $N_b = 27$; When $\alpha = 0.6$, $N_y = 77$, $N_b = 23$; When $\alpha = 0.7$, $N_y = 80$, $N_b = 20$; When $\alpha = 0.8$, $N_y = 84$, $N_b = 16$; When $\alpha = 0.9$, $N_y = 86$, $N_b = 14$; When $\alpha = 1$,$N_y = 89$, $N_b = 11$. The probability to choose two routes can be seen directly, such as when $\alpha = 0.7$, the probability to choose the route of $C_{0i} = 6$ is 0.8, and the another is 0.2; these are very close to the results of 0.802184, 0.197816 calculated above.

With the increase of information availability, the description of the current road condition in traffic information is more and more detailed and real; the travelers always choose the route which travel cost is lower. That means information is vitally important to travelers decision making.

4 The Conclusion

This paper analyzes the effect of information availability on routes choice, and establishes the model under information availability based on the multivariate Logit model, then values the relevant data and calculates, so the correctness and applicability can be

verified. Finally the paper simulates through the Netlogo simulation software and analyses according to the simulation results. Comprehensive of the empirical calculation and the simulation results shows that the model is feasible and applicable in this paper; what's more, this illustrates that information has a great influence on the routes choice. With the wide use of ATIS system, information is gradually being apply to people's travel decisions.

References

1. Fan W-B, Li Z-C, Jiang G-F (2009) Modeling of commuters' day to day route choice behaviors based on reference-dependent approach. J Traffic Transp Eng 1:96–108
2. Zhou W, Zhao S-C (2012) Quantitative analysis of travelers' route choice behavior based on mixed logit model. J Jilin Univ 43(2):304–309
3. Li, Z-C, Huang, H-J: The study of advanced traveler information system's influence on the traveler choice behavior. Highw Traffic Technol (2005)
4. Katsikopoulos KV, Fisher DL, Duse Anthony Y, Duffy SA (2002) Risk attitude reversals in diver's route choice when range of travel time is provided. Hum Factors 44(3):466–473
5. Tawfik, AM, Rakha, HA, Miller, SD: An experimental exploration of route choice: identifying drivers choices and choice patterns, and capturing network evolution. IEEE (2010)
6. Zhou, Y, Wu, J: The research on drivers' route choice behavior in the presence of dynamic traffic information. IEEE (2006)

Research on Lateral Stability of Double Semitrailer Road Train

Hao Zhang[1,2(✉)], Ze-kai Ren[3], Hong-wei Zhang[1,2], and Chuan-jin Ou[1,2]

[1] Research Institute of Highway Ministry of Transport, Beijing 100088, China
zhang.hou@rioh.cn
[2] Key Laboratory of Operation Safety Technology on Transport Vehicles Ministry of Transport, Beijing 100088, China
[3] School of Automotive Engineering, Harbin Institute of Technology, Weihai 264209, China

Abstract. Double semitrailer road train simulation model was established based on TruckSim in order to research the driving stability and improve combination vehicles performance. Tractor semitrailer simulation model was established as comparing model. Simulation of steady static circular test was carried out to research steering characteristic. Single lane change tests on double semitrailer road train and tractor semitrailer were also carried out to research lateral stability and the yaw rate, lateral acceleration and their rearward amplification (RA) was selected as evaluation index. The results shown that double semitrailer road train have appropriate deficiency steering characteristic and good driving stability. Apparently, it's not as good as tractor semitrailer. The results serve as a useful reference for accelerating the popularization and application and promoting the development of vehicle industry technology .

Keywords: Double semitrailer road train · Vehicle dynamics · Driving stability · TruckSim

1 Introduction

Road train is widely used in EU, the USA and Australia, which can greatly improve the efficiency of logistics and transport and ensuring driving safety [1]. In China, the infrastructures of road have excellent conditions compared with the developed countries. But road train is not allowed to drive on highway according to the law on road traffic safety, which limiting its application and development.

In order to speed up transport development and promote road transport industry upgrading, guiding opinions on transportation to promote healthy development of the logistics industry was promulgated by the Ministry of Transport (MOT) in May, 2013. It plays an important role to improving transportation and logistics industry development and promoting the technical level of transport equipment through developing vehicle equipment. The aim for truck upgrade is becoming more specialization, more clean and standardization.

X. Zeng et al. (eds.), *International Symposium for Intelligent Transportation and Smart City (ITASC) 2017 Proceedings*, Smart Innovation, Systems and Technologies 62, DOI 10.1007/978-981-10-3575-3_9

Double semitrailer road train is made up of a tractor which tracts two semi-trailers, and it is coupling by a fifth wheel or dolly. It's the development direction of road train. This structure is usually called B-double or B Train, and it's selected as the main simulation object. The fifth wheel coupling can be found at the end of the first semi-trailer and provides more stability to the unit than a road train can. The lead semitrailer has a turntable at the end, so it can connect to another semitrailer without a converter dolly [2].

Lateral stability is one important and significant indicator of the drive stability for road train [3–5]. The driving stability of vehicle is one of the key problems in the current research, which involves the safety of human life and property [6–8]. Lateral stability of double semitrailer road train would have a different characteristic compared with tractor semitrailer. So, it is necessary and significate to research the driving stability of double semitrailer road train and provide reference for the development of road train in China.

2 Simulation Model Established

B-double simulation model was established by TruckSim with the references of dimensions used commonly in abroad, which is 25.25 m long and 60 t weight. As a reference, the standard tractor and semitrailer simulation model was also established, which is 18.10 meters long and 49 t weight. Simulation parameters of B-double tractor semitrailer are shown in Table 1 and simulation models are shown in Figs. 1 and 2.

Table 1. Simulation parameters of B-double and tractor semitrailer

Parameters	B-double			Tractor semitrailer	
	Tractor	1st trailer	2nd trailer	Tractor	Trailer
Dimension (mm)	7160 × 2495 × 3560	8690 × 2550 × 3980	11200 × 2550 × 3980	7160 × 2495 × 3560	14600 × 2550 × 4000
Mass (kg)	8800	7800	7800	8800	8100
Wheelbase (mm)	3315 + 1370	8020 + 1310 + 1310	7820 + 1310 + 1310	3215 + 1370	7460 + 1310 + 1310
Wheel center spacing (mm)	2030/1860/1860	1820/1820/1820	1820/1820/1820	2030/1860/1860	1820/1820/1820

Fig. 1. B-double simulation model

Fig. 2. Tractor semitrailer simulation model

3 Driving Stability Analysis

1. Steady Static Circular Analysis

The steady static circular test was carried out according to the related rules in Controllability and stability test procedure for automobile (GB/T 6323-2014).

There are three important parameters that could reflect the characteristics of the train according to the vehicle dynamics, yaw rate, lateral acceleration and roll angle. Figure 3 shows the trajectory of double semitrailer road train. The specific results are shown form Figs. 4, 5 and 6.

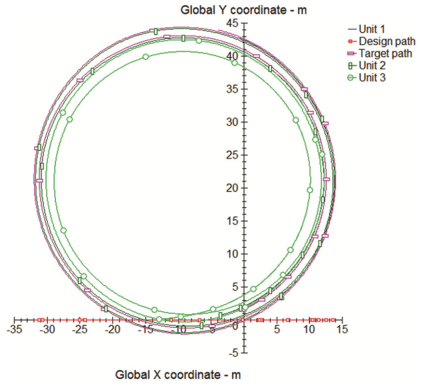

Fig. 3. Trajectory

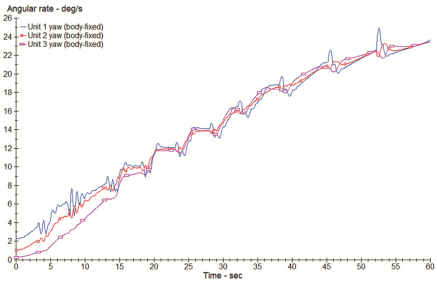

Fig. 4. Time response of yaw rate

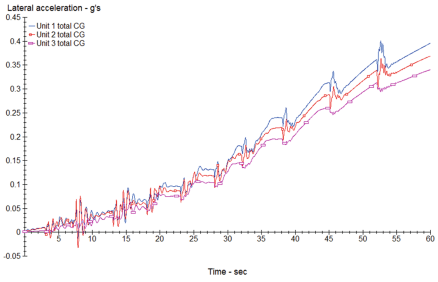

Fig. 5. Time response of lateral acceleration

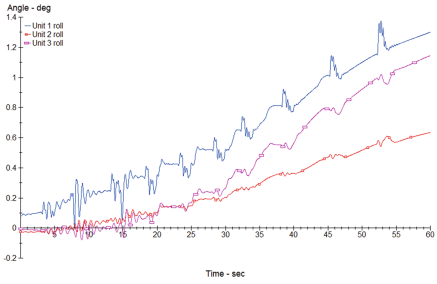

Fig. 6. Time response of roll angle

Test results show that the lateral acceleration of train increases continuously with the increasing speed, and the max acceleration value exceed 0.35 g. The steady static circular test mainly used to evaluate the steering characteristics. Deficiency steering characteristic should appear in normal vehicles to ensure the driving safety. Simulation results show a significant deficiency steering characteristic as the turning radius increases with the increasing speed.

2. Single Lane Change Analysis

Single lane change test simulation on double semitrailer road train and semitrailer were carried out according to Road vehicles-Heavy commercial vehicle combinations and articulated buses-Lateral stability test methods (GB/T 25979-2010) [9]. Input signal was the designed trajectory in the rearward amplification part of TruckSim, as shown in Fig. 7. In the standard requirements, the train will travel at the speed of 80 km/h, 90 km/h and 100 km/h, and dynamic characteristics of the vehicle system is analyzed under different speed conditions. In fact, the change and trend of performance parameters is basically the same in different speed, and now simulation results with the vehicle speed 100 km/h is used as an example of dynamic characteristics, as shown from Figs. 8, 9, 10, 11, 12 and 13. Simulation results for other vehicle speed conditions were shown in Tables 2 and 3.

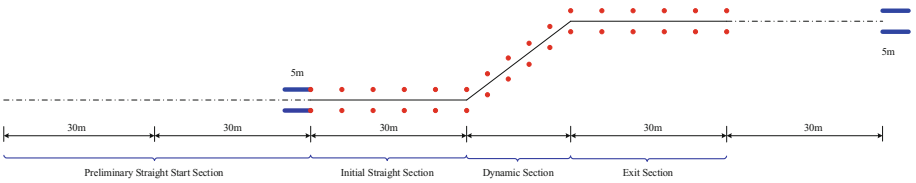

Fig. 7. Trajectory of single lane change test

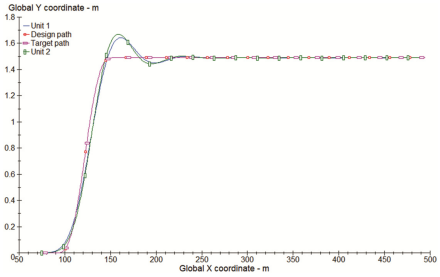

Fig. 8. Trajectory of tractor semitrailer at 100 km/h

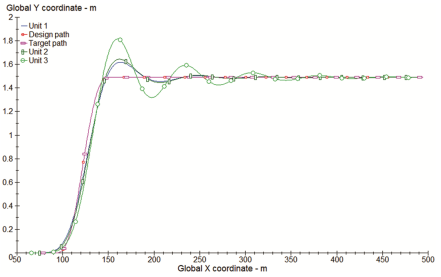

Fig. 9. Trajectory of B-double at 100 km/h

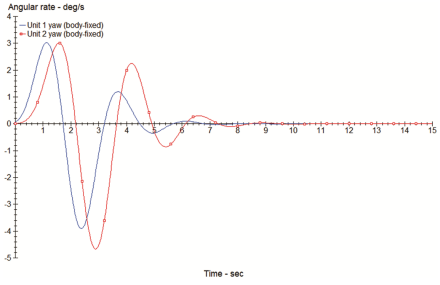

Fig. 10. Yaw rate of tractor semitrailer at 100 km/h

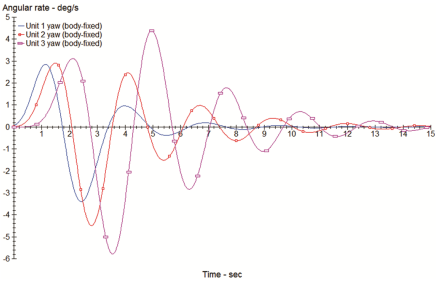

Fig. 11. Yaw rate of B-double at 100 km/h

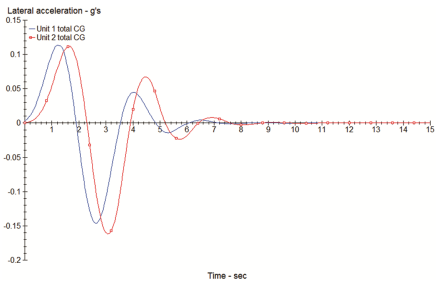

Fig. 12. Lateral acceleration of tractor semitrailer at 100 km/h

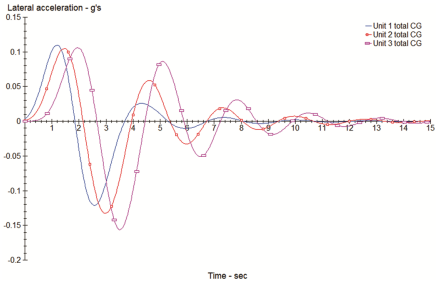

Fig. 13. Lateral acceleration of B-double at 100 km/h

Table 2. Single lane change simulation results

Value				
Subjects		Speed		
		80 km/h	90 km/h	100 km/h
Tractor semitrailer	Yaw rate of tractor (°/s)	3.2242	3.5896	3.9076
	Yaw rate of trailer (°/s)	3.3858	4.0446	4.6672
	Lateral acceleration of tractor (g)	0.1084	0.1284	0.1458
	Lateral acceleration of trailer (g)	0.1088	0.1356	0.1619
B-double	Yaw rate of tractor (°/s)	2.9840	3.2235	3.4009
	Yaw rate of 2nd trailer (°/s)	3.8657	4.8331	5.7770
	Lateral acceleration of tractor (g)	0.0949	0.1091	0.1213
	Lateral acceleration of 2nd trailer (g)	0.0979	0.1264	0.1564

Table 3. Rearward amplification results

Value				
Subjects		Speed		
		80 km/h	90 km/h	100 km/h
Rearward amplification for yaw rate	Tractor semitrailer	1.0501	1.1268	1.1944
	B-double	1.2955	1.4993	1.6987
Increasing proportion		23.4%	33.1%	42.2%
Rearward amplification for lateral acceleration	Tractor semitrailer	1.0037	1.0559	1.1107
	B-double	1.0313	1.1582	1.2897
Increasing proportion		2.7%	9.3%	16.1%

Simulation results in Tables 2 and 3 show that the yaw rate, lateral acceleration and their rearward amplification would increase with the increasing simulation speed in the single lane change test. Rearward amplification for lateral acceleration of double semitrailer road train and tractor semitrailer are both less than 2.0 which suggested by A Test for Evaluating the Rearward Amplification of Multi-Articulated Vehicles (SAE J2179-2000). The results shown that double semitrailer road train have good driving stability.

4 Conclusion

Double semitrailer road train simulation model was established based on TruckSim and tractor semitrailer simulation model was established as comparing model. Simulation of steady static circular test was carried out to research steering characteristic. Single lane change tests on double semitrailer road train and tractor semitrailer were also carried out to research lateral stability and the yaw rate, lateral acceleration and their rearward amplification (RA) was selected as evaluation index. The results shown that rearward amplification for yaw rate of double semitrailer road train increases by 23.4% at 80 km/h, 33.1% at 90 km/h, and 42.2% at 100 km/h and rearward amplification for lateral acceleration increases by 2.7% at 80 km/h, 9.3% at 90 km/h, and 16.1% at 100 km/h. Apparently, it's not as good as tractor semitrailer, but the simulation results meet the requirements of the standard. Double semitrailer road train have appropriate deficiency steering characteristic and good driving stability. The results serve as a useful reference for accelerating the popularization and application and promoting the development of vehicle industry technology.

Acknowledgements. This work is supported by Ministry of Transport project of basic research for application No. 2014 319 223 020 and the central public welfare research institutes for basic research funds No. 2015-9031.

References

1. Aurell J, Wadman T, Trucks V (2007) Vehicle combinations based on modular concept. Volvo Trucks, Sweden, NVF reports
2. What is a Road Train?. http://www.vintageroadhaulage.com.au/faq/what-is-a-road-train/
3. Xu H, Liu H, Yu Z (2006) Overview of tractor-trailer stability study. J Highway Transp Res Develop 23(2):141–150
4. Zhang Y, Xu H, Liu H (2016) Transient rollover state of tractor and double trailer combination based on TruckSim. J Jilin Univ (Eng Technol Edn) 46(4):1065–1069
5. Ou CJ, Liu XD, Zhang HW, et al (2012) Parameters match and optimization on controllability and stability of tractor-semitrailers. In: The twelfth COTA international conference of transportation professionals, pp 2368–2378
6. Liu H, Xu H, Cao X et al (2010) Lateral stability of tractor-semitrailer under non-typical lane-change. J Jiangsu Univ 31:150–154
7. Zong C, Zhu T, Wang C, Liu H (2012) Multi-objective stability control algorithm of heavy tractor semi-trailer based on differential braking. Chin J Mech Eng 25(01):88–97

8. Tang B (2015) Research on simulation analysis on lateral stability of tractor-semitrailer and comprehensive evaluation model. Research Institute of Highway, M.O.T.
9. GB/T 25979-2010 (2011) Road vehicles-heavy commercial vehicle combinations and articulated buses-lateral stability test methods. Standards Press of China

Research on Lateral Stability of Center Axle Trailer Train

Hao Zhang[1,2(✉)], Ze-kai Ren[3], and Hong-wei Zhang[1,2]

[1] Research Institute of Highway Ministry of Transport, Beijing 100088, China
zhang.hou@rioh.cn
[2] Key Laboratory of Operation Safety Technology
on Transport Vehicles Ministry of Transport, Beijing 100088, China
[3] School of Automotive Engineering,
Harbin Institute of Technology, Weihai 264209, China

Abstract. Center axle trailer train simulation model was established by using TruckSim, in order to promote vehicle standardization and application. Simulation of single lane change test were carried out to research its driving stability. Driving stability test system of center axle trailer train has been set up for handling stability and lateral stability test. The correction and reliability of vehicle simulation model was verified by comparing the simulation and test results. Simulation model could reflect the behaviors of the center axle trailer train. The results can provide a model for the centre axle trailer train driving stability simulation and can provide technical guidance for vehicle performance research.

Keywords: Center axle trailer train · Driving stability · Steady static circular · Single lane change

1 Introduction

Guiding opinions promoting healthy development of the logistics industry was promulgated by Ministry of Transport in May 2013, in order to speed up the transformation of transport development mode and promote the upgrading of road transport industry, exerting the important role of transportation in the development of logistics industry. Improving technical level of transport equipment through developing the standard truck is one of the important tasks to upgrade the profession, clean and standardization of transport equipment's.

The trial operation on super long train of Long Yun Group was replied and proposed by MOT in June 2015, to improve the efficiency of transport organization and reduce logistics costs. Making combination of truck, semitrailer and center axle trailer is approved to form the long train and run on the specified roads, exploring and carrying out a demonstration on the improvement of truck equipment's. There are five center axle trailer train running on the highway between Harbin and Qiqihar so far.

X. Zeng et al. (eds.), *International Symposium for Intelligent Transportation and Smart City (ITASC) 2017 Proceedings*, Smart Innovation, Systems and Technologies 62, DOI 10.1007/978-981-10-3575-3_10

GB 1589-2016 (Limits of dimensions, axle load and masses for motor vehicles, trailers and combination vehicles) was promulgated and implemented on July 26, 2016. GB 1589-2016 defines center axle trailer and limits the dimensions and masses [1]. The related standards, regulations and policies mentioned above built the development foundations of center axle trailer train in China.

In China, the produce of truck and trailer is produced by different manufacturing enterprises and the related standards are also proposed just for truck or trailer. There are less test method that for train to ensure the quality and security. Testing for lateral stability from the view of train is one significant and necessary issue to ensure driving safety.

2 Vehicle Model Established

TruckSim delivers the most accurate, detailed, and efficient methods for simulating the performance of multi-axle commercial and military vehicles. TruckSim is universally the preferred tool for analyzing vehicle dynamics, developing active controllers, calculating a truck's performance characteristics, and engineering next-generation active safety systems.

The center axle trailer train simulation model was established by TruckSim as shown in Fig. 1. Simulation parameters is shown in Table 1.

Fig. 1. Simulation model

3 Road Test

The center axle trailer train simulation model was established by TruckSim to effectively carry out the driving stability simulation. In order to determine the effectiveness of the simulation model, vehicle road test program was developed to carry out the road test. By comparing the test results with the simulation results, the validity of the simulation model is verified. Steady state circular run test and single lane change test are chosen as the main test content. The test is carried out according to the requirements of the standards GB/T 25979-2010.

Table 1. Parameters of center axle trailer train

Parameters	Value	Parameters	Value
Mass of truck (kg)	16865	Mass of trailer (kg)	18020
Truck wheelbase (mm)	5595	Trailer wheelbase (mm)	1310
Axle 1 wheel center spacing of truck (mm)	1995	Trailer mass center hight (mm)	1480
Axle 2 wheel center spacing of truck (mm)	1892	Distance between mass center and hitch of trailer(mm)	6285
Truck mass center height (mm)	1454	Axle 1 spring rate of truck (N/mm)	2000
Distance between mass center and axle 1 of truck (mm)	4338	Axle 2 spring rate of truck (N/mm)	2500
Wheel center spacing of trailer (mm)	1896	Spring rate of trailer (N/mm)	3500
Hitch height (mm)	400	Distance between hitch and axle 1 of truck (mm)	7000

3.1 Test Vehicle

Centre axle trailer train which is manufactured by SINOTRUK was selected as test vehicle, as shown in Fig. 2. The length of the train is 18.75 m and contains two 7.82 m carriages.

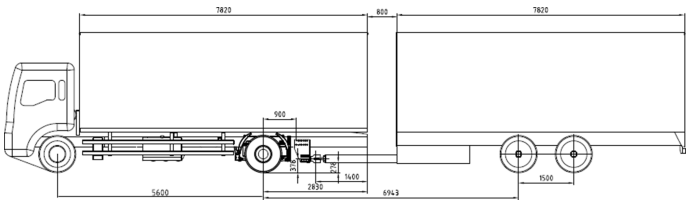

Fig. 2. Test vehicle

3.2 Test Methods

Single lane change test was carried at the speed of 80 km/h according to GB/T 25979-2010 (Road vehicles-Heavy commercial vehicle combinations and articulated buses-Lateral stability test methods) and the input signal to the steering wheel is one complete sin wave which frequency is 4 Hz. Hold the steering wheel in the middle position 5 s and record the speed, steering wheel angle, yaw rate, lateral acceleration [2].

3.3 Test System

Centre axle trailer train driving stability test system was designed, mainly used for vehicle handling stability and lateral stability test based on Real - time kinematic testing

technique and inertial measurement technology. It is mainly composed of VBOX 3i, RT3002 gyroscope, steering wheel measuring instrument, data logging system and so on. Its main structure and working principle of the system are shown in Fig. 3.

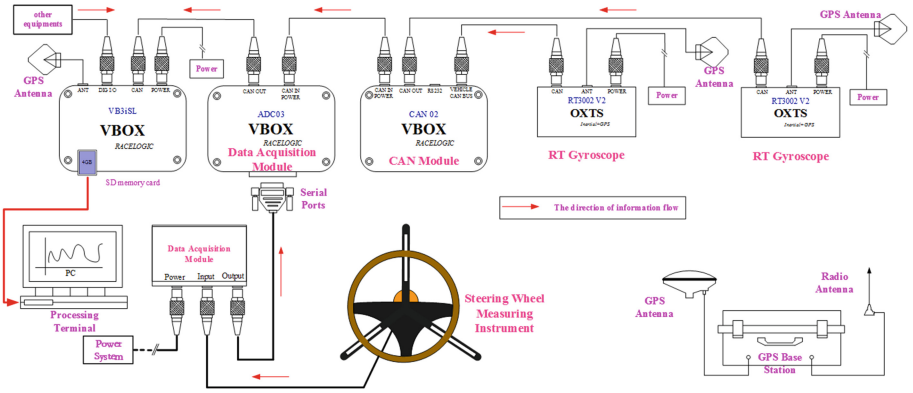

Fig. 3. Test system

In addition to a RT 3002 gyroscope and GPS antenna, its power supply system installed in the center axle trailer, GPS base station placed in the empty space, the rest of the devices are installed on the truck tractor.

4 Results Analysis

The correction and reliability of vehicle simulation model was verified by comparing the simulation and test results.

Rearward Amplification of center axle trailer train, which refers to ratio of the maximum value of the motion variable of interest of a following vehicle unit to that of the first vehicle unit during a specified maneuver. It is one critical parameter to judge the lateral stability of center axle trailer train [3–5]. As a result, RA of the center axle trailer train should be taken into account when it comes to the lateral stability test.

The yaw-articulation angle rate is another important parameter to measure the stable state performance of center axle trailer train except some metrics mentioned above, means the time derivative of longitude angle between truck and trailer and it equals to the difference between truck yaw rate and trailer yaw rate [6, 7].

The single lane change test was carried out according to GB/T 25979-2010, shown in Fig. 4. And the results of simulation and road test were analyzed comparatively to prove the effectiveness of simulation model, shown form Figs. 5, 6, 7, 8, 9, 10, 11 and 12.

Results of single lane change test at the speed of 80 km/h show that rearward amplification for lateral acceleration is about 1.14 and conform the recommended value according to SAE J2179-2000 (A Test for Evaluating the Rearward Amplification of Multi-Articulated Vehicles) which suggests that should not exceed 2.0. The result shown that center axle trailer train has a good lateral stability performance.

Fig. 4. Test vehicle

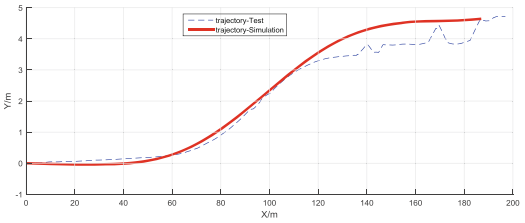

Fig. 5. Trajectory comparison

The curve change and trend is consistent and the numerical value consistency is good by simulation result and vehicle road test result comparison. The correction and reliability of vehicle simulation model was verified by comparing the simulation and test results.

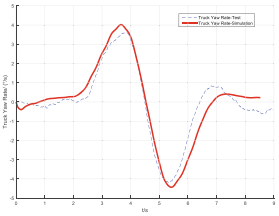

Fig. 6. Truck yaw rate

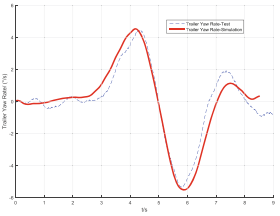

Fig. 7. Trailer yaw rate

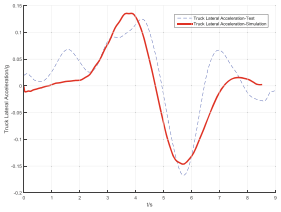

Fig. 8. Truck lateral acceleration

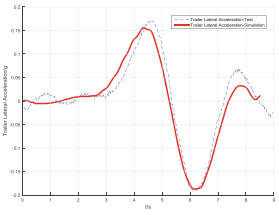

Fig. 9. Trailer lateral acceleration

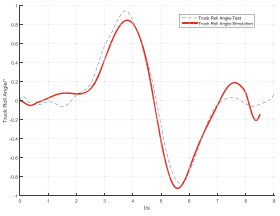

Fig. 10. Truck roll angle

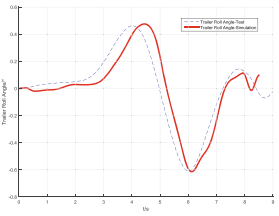

Fig. 11. Trailer roll angle

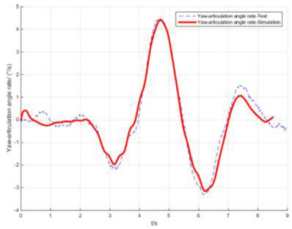

Fig. 12. Yaw-articulation angle rate comparison

5 Conclusions

Center axle trailer train simulation model was established by using TruckSim, in order to promote vehicle standardization and application. Simulation of steady static circular test and single lane change test were carried out to research its driving stability. Centre axle trailer train driving stability test system was designed, mainly used for vehicle handling stability and lateral stability test based on Real - time kinematic testing technique and inertial measurement technology. Centre axle trailer train which is manufactured by SINOTRUK was selected as test vehicle. Driving stability test system of center axle trailer train has been set up for handling stability and lateral stability test. The curve change and trend is consistent and the numerical value consistency is good by simulation result and vehicle road test result comparison. The correction and reliability of vehicle simulation model was verified by comparing the simulation and test results. Simulation model could reflect the behaviors of the center axle trailer train. The results can provide a model for the centre axle trailer train driving stability simulation and can provide technical guidance for vehicle performance research.

Acknowledgements. This work is supported by Ministry of Transport project of basic research for application No. 2014 319 223 020 and the central public welfare research institutes for basic research funds No. 2015-9031.

References

1. GB/T 1589-2016 (2016) Limits of dimensions, axle load and masses for motor vehicles, trailers and combination vehicles. Standards Press of China
2. GB/T 25979-2010 (2010) Heavy commercial vehicle combinations and articulated buses-lateral stability test methods. Standards Press of China
3. Tang B (2015) Research on simulation analysis on lateral stability of tractor-semitrailer and comprehensive evaluation model. Research Institue of Highway M.O.T, Beijing
4. Xu H, Liu H, Yu ZL (2006) Overview of tractor-trailer stability study. J Highway Transp Res Dev 23(2):141–150

5. Zhang Y, Xu H, Liu H (2016) Transient rollover state of tractor and double trailer combination based on TruckSim. J Jilin Univ (Eng Technol Edn) 46(4):1065–1069
6. Wei C (2008) Study on handing stability of caravan. Jiangsu University, Zhenjiang
7. Yang X, Li Y, Xiong J (2011) Analysis on the lateral stability and instability mechanism of tractor-semitrailer combination. Automot Eng 33(6):486–492

Research on Road Adaptability of Center Axle Trailer Train

Hao Zhang[1,2(✉)], Ze-kai Ren[3], Hong-wei Zhang[1,2], and Chao-zhi Huang[1]

[1] Research Institute of Highway Ministry of Transport, Beijing 100088, China
zhang.hou@rioh.cn
[2] Key Laboratory of Operation Safety Technology on Transport Vehicles Ministry of Transport, Beijing 100088, China
[3] School of Automotive Engineering, Harbin Institute of Technology, Weihai 264209, China

Abstract. Three different simulation models of center axle trailer train were established by using Auto TURN software, in order to research the passing stability and road adoptability. Highway ramp, first class highway and second class highway intersection models were established according to the requirement of JTG D20-2006. Research on road adaptability simulation of one 18.75 m long center axle trailer train and two 20.00 m long center axle trailer trains was carried out through the simulation models. The results show that three types of center axle trailer train have good adaptability in the highway ramp. At the intersection of first class highway, three vehicles can barely pass through, but in second class highway intersection, the swept path width of three vehicles is too wide, it is not recommended vehicle driving in this intersection. It found that the longer the vehicle, the worse the road passing ability. Simulation results serve as preferences for accelerating the deploying and optimizing the passing ability of center axle trailer train.

Keywords: Center axle trailer train · Passing ability · Road adaptability · Auto TURN

1 Introduction

The Ministry of Transport issued 'guidance of the Ministry of Transport on promoting the healthy development of the logistics industry of transportation' in May 2013 to accelerate transformation of development mode of transportation, promote the upgrading of road transport industry. It plays an important role of transport in the logistics industry development [1]. It takes effectively enhancing the level of transport equipment and technology as one of the important tasks and aims to vigorously develop the standardization of the lorry [2]. It also enhance the professionalization, clean and standardization of transport equipment level.

Center axle trailer train is one important form of road train [3, 4], which is the direction of future development of China's freight vehicles. It is necessary to research passing ability and road adaptability of the center axle trailer train to provide reference

X. Zeng et al. (eds.), *International Symposium for Intelligent Transportation and Smart City (ITASC) 2017 Proceedings*, Smart Innovation, Systems and Technologies 62, DOI 10.1007/978-981-10-3575-3_11

for whose development in our country. So, center axle trailer train is used as a research object and simulation model is established by the software Auto TURN to conduct the simulation analysis of turning clearance circle, swept path width. Channel circle test of actual vehicle was carried out to verify the reliability of simulation model.

2 Vehicle Model Established and Simulation Condition

A length of 18,75 m center axle trailer train was used as simulation models, hereinafter referred to as A Train as shown in Fig. 1. According to current standard GB 1589-2016, the maximum length of center axle trailer train is 20 m. There are two different kinds of 20.00 m center trailer train models, as shown in Figs. 2 and 3.

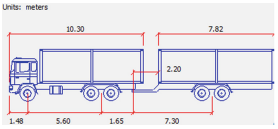

Fig. 1. A Train

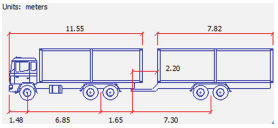

Fig. 2. B Train

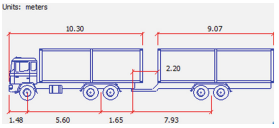

Fig. 3. C Train

Centre axle trailer train road adaptability is the study of traffic in highway ramp, first class road intersection and second class road intersection. According to the requirement of standard JTG D20-2006 'Design Specification for Highway Alignment', their simulation models were established by Auto TURN.

3 Research on Road Adaptability

3.1 Highway Ramp

As shown in Figs. 4 and 5, it can be seen that the 18.75 m center axle trailer train and the 20.00 m center axle trailer train hardly occupy all the road, but it can be passed

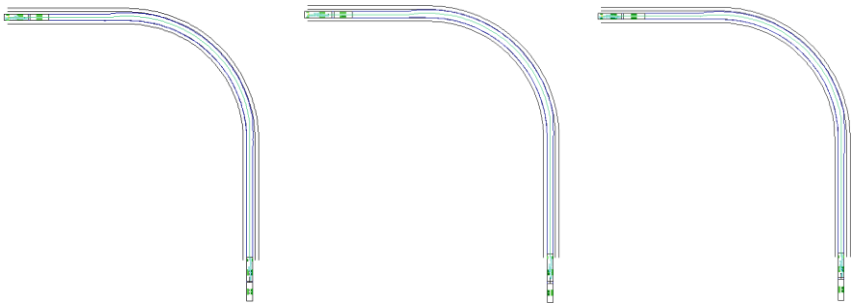

Fig. 4. Turn left simulation on highway ramp

smoothly when turning left and right. The center axle trailer train and highway ramp adaptability is good.

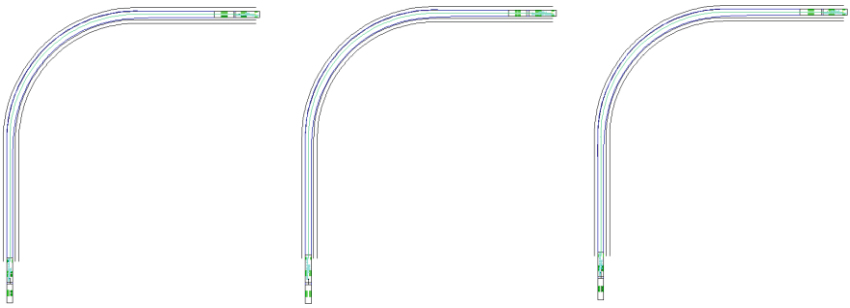

Fig. 5. Turn right simulation on highway ramp

3.2 First Class Road Intersection

First class road intersection simulation model is established by Auto TURN. First class road is a two way with four lane road. The lane width is 3.75 m and right side hard shoulder width is 2.5 m, the inner radius of pavement edge is 15 m, the width of semi-circular intermediate zone of road is 2.0 m [7]. Result of center axle trailer train turns left on first class road intersection simulation is shown in Fig. 6.

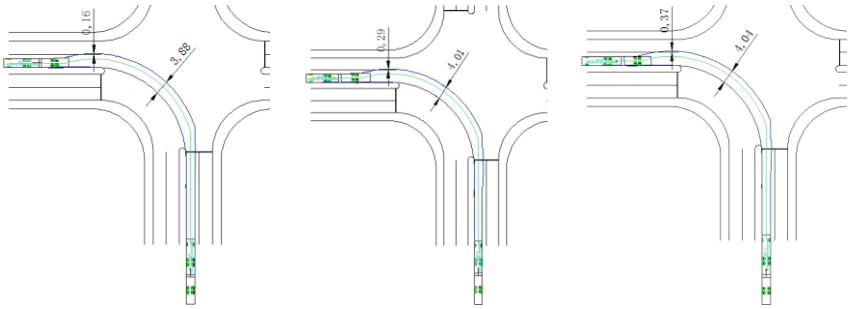

Fig. 6. Turn left simulation on first class road intersection

When center axle trailer train turns left on first class road intersection, the maximum swept path width of A Train, B Train and C Train is 3.88 m, 4.01 m and 4.04 m. The maximum swept path width of A Train is smaller than B Train and C train. Outermost right side of the train exceed adjacent lane 0.16 m, 0.29 m and 0.37 m respectively. The shorter the length of the train, the better the performance of the vehicle. Comparing train with the same length, B Train is better than C Train. So the structure is different, the performance is also different. Center axle trailer train can turn left on first class highway intersection and it may affect the other vehicles driving.

Result of center axle trailer train turns right on first class road intersection simulation is shown in Fig. 7.

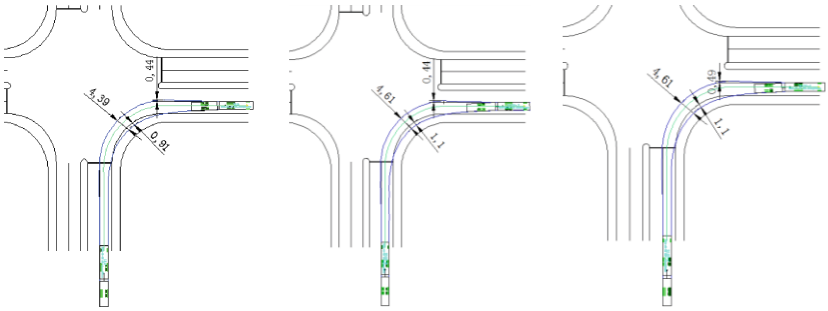

Fig. 7. Turn right simulation on first class road intersection

When center axle trailer train turns right on first class road intersection, the maximum swept path width of A Train, B Train and C Train is 4.39 m, 4.61 m and 4.61 m. Outermost left side of the train exceed adjacent lane 0.44 m, 0.44 m and 0.49 m respectively. Outermost right side of the train exceed adjacent lane 0.91 m, 1.10 m and 1.10 m respectively. The road adoptability of A Train is better than B Train and C train. Comparing train with the same length, B Train is better than C Train. Center axle trailer train can turn right on first class highway intersection and it may affect the other vehicles driving.

Result of center axle trailer train turns around on first class road intersection simulation is shown in Fig. 8.

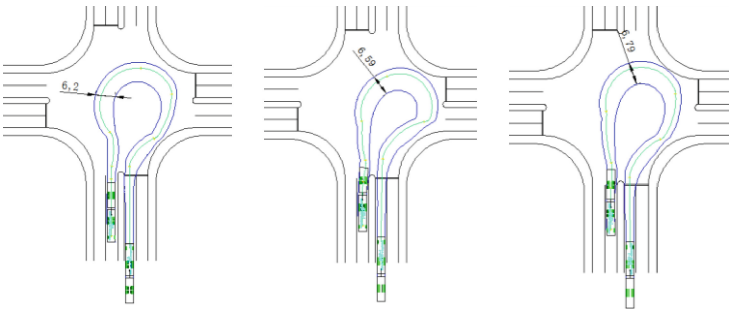

Fig. 8. Turn around simulation on first class road intersection

When center axle trailer train turns around on first class road intersection, the maximum swept path width of A Train, B Train and C Train is 6.20 m, 6.59 m and 6.79 m. The road adoptability of A Train is better than B Train and C train. Comparing train with the same length, B Train is better than C Train. Center axle trailer train can turn around on first class highway intersection.

3.3 Second Class Road Intersection

Second class road intersection simulation model is established by Auto TURN. Second class road is a two way road. Lane width is 3.75 m and right side hard shoulder width is 0.75 m, the inner radius of pavement edge is 15 m. Result of center axle trailer train turns left on second class road intersection simulation is shown in Fig. 9.

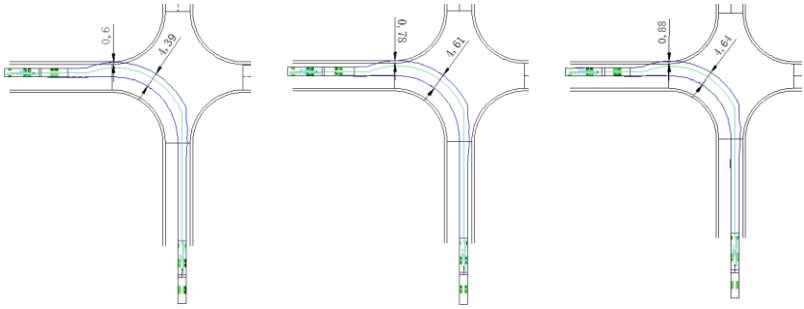

Fig. 9. Turn left simulation on second class road intersection

When center axle trailer train turns left on second class road intersection, the maximum swept path width of A Train, B Train and C Train is 4.39 m, 4.61 m and 4.64 m. The maximum swept path width of A Train is smaller than B Train and C train. Outermost right side of the train exceed adjacent road shoulder 0.60 m, 0.78 m and 0.88 m respectively. Comparing train with the same length, B Train is better than C Train. Center axle trailer train can turn left on second class highway intersection, but it may go off the road boundary.

Result of center axle trailer train turns right on second class road intersection simulation is shown in Fig. 10.

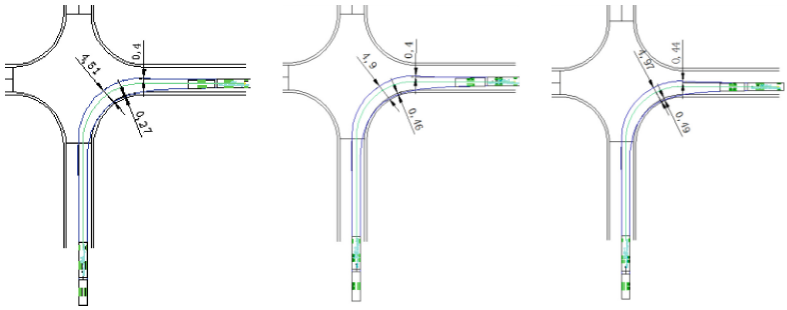

Fig. 10. Turn right simulation on second class road intersection

When center axle trailer train turns right on second class road intersection, the maximum swept path width of A Train, B Train and C Train is 4.51 m, 4.90 m and 4.97 m. Outermost right side of the train exceed adjacent road shoulder 0.20 m, 0.46 m and 0.49 m respectively. The maximum swept path width of A Train is smaller than B Train and C train. Outermost left side of the train exceed adjacent lane 0.40 m, 0.40 m and 0.44 m respectively. Comparing train with the same length, B Train is better than C Train. Center axle trailer train can turn left on second class highway intersection, but it may affect the other vehicles driving.

Result of center axle trailer train turns around on second class road intersection simulation is shown in Fig. 11.

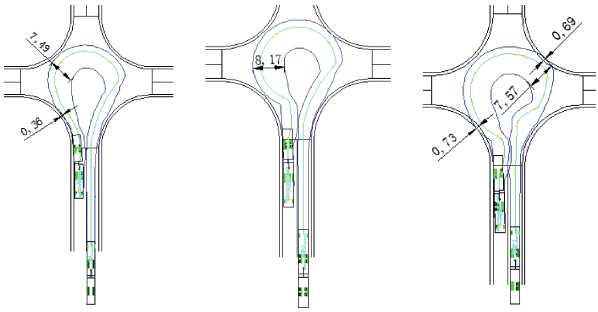

Fig. 11. Turn around simulation on second class road intersection

When center axle trailer train turns around on second class road intersection, the maximum swept path width of A Train, B Train and C Train is 7.49 m, 8.17 m and 7.57 m. Outermost right side of the train exceed adjacent road shoulder 0.36 m, 0 m and 0.73 m respectively. In the process of turning, swept path width is closely related path choice. The choice of the path directly determines the final trajectory. Center axle trailer train can turn around on second class highway intersection, but it may affect the other vehicles driving.

4 Conclusions

Three different simulation models of center axle trailer train were established by using Auto TURN software, and highway ramp, first class highway and second class highway intersection models were established according to JTG D20-2006. Research on road adaptability simulation of one 18.75 m long center axle trailer train and two 20.00 m long center axle trailer trains was carried out through the simulation models. The results show that three types of center axle trailer train have good adaptability in the highway ramp. At the intersection of first class highway, three vehicles can barely pass through, but in second class highway intersection, the swept path width of three vehicles is too wide, it is not recommended vehicle driving in second class road intersection. It found that the longer the vehicle, the worse the road passing ability.

The choice of the path directly determines the final trajectory. Simulation results serve as preferences for accelerating the deploying and optimizing the passing ability of center axle trailer train.

Acknowledgements. This work is supported by Ministry of Transport project of basic research for application No. 2014 319 223 020 and the central public welfare research institutes for basic research funds No. 2015-9031.

References

1. Ni Y (2011) Longer combination vehicles, the new force in the long-distance road transport on definition and application of longer combination vehicles. In: Commercial vehicle, pp 75–80
2. Ni Y (2011) Longer combination vehicles, the new force in the long-distance road transport on European Modular longer combination vehicles. In: Commercial vehicle, p 86–91
3. Akerman I, Jonsson R (2007) European modular system for road fright transport experiences and possibilities. TFK Report 2007:2 E
4. Eurlings C (2010) Longer and heavier vehicles in the Netherlands–facts, figures and experiences in the period 1995–2010. Directorate general for public works and water management (Rijkswaterstaat)
5. GB 1589-2016 Limits of dimensions, axle load and masses for motor vehicles, trailers and combination vehicles. Standardization administration of The People's Republic of China
6. QC/T 912-2013 Technical requirements for matching of towing vehicle and semi-trailer. Standardization administration of The People's Republic of China
7. JTG D20-2006 Design specification for highway alignment. Standardization administration of The People's Republic of China

Nonlinear Modeling and Analyzing of Tractor-Semitrailer Driving Stability Based on Simulink

Chuan-jin Ou(✉), Hong-wei Zhang, and Hao Zhang

Key Laboratory of Operation Safety Technology on Transport Vehicles, Research Institute of Highway, Ministry of Transport, Beijing 100088, China
cj.ou@rioh.cn

Abstract. In order to study how the nonlinear relationship between tire cornering force and sideslip angle affect the driving stability of tractor- semitrailer, mathematical model of tractor- semitrailer is established by using dynamics theory, and Simulink software is used to simulated analysis. Yaw velocity amplitude of tractor, lateral acceleration amplitude of tractor, yaw velocity amplitude of semitrailer and lateral acceleration amplitude of semitrailer are selected as evaluation indexes to analyze how the mass of semitrailer, fifth wheel lead and track width affect the driving stability of tractor- semitrailer. Simulation results show that it can improve the driving stability of tractor- semitrailer to reduce the mass of semitrailer and to increase fifth wheel lead and track width.

Keywords: Driving stability · Nonlinear modeling · Tractor-semitrailer · Simulink

1 Introduction

Tractor- semitrailer will swap under the combined action of steering wheel and external disturbance. Vehicles' sway characteristics will increase traffic channel width, driving resistance and tire wear, making the driving stability worse. Serious yaw will cause sideslip or rollover, and even traffic accidents. Therefore, the stability of semitrailer trains determines the safety of high-speed driving and curve driving. In the 1920s, researchers had been studied on the stability of vehicle combinations. In 1938, H. Ziegler of the University of Stuttgart carried out the theoretical analysis on the motion characteristics of Tractor- semitrailer under two conditions of uniform road running and transverse braking. Results showed that self-oscillation phenomenon occurred when vehicle speed exceeded a critical value, but the defect of assumption of the characteristics of pneumatic tires made the value of the results of little value. In 1951, D. Williams conducted a simplified analysis of a tractor-semitrailer to research the lateral motion characteristics of single-axle trailer and two-axle trailer. He assumed that the tire lateral force is a linear function of the lateral deformation of the tire [1]. Due to the lack of understanding of tire technology, its conclusions had great limitations. At present, computer modeling and simulation software have been used to build the tractor- semitrailer model, and some research achievements have been obtained. The linear dynamics

X. Zeng et al. (eds.), *International Symposium for Intelligent Transportation and Smart City (ITASC) 2017 Proceedings*, Smart Innovation, Systems and Technologies 62, DOI 10.1007/978-981-10-3575-3_12

model is mainly used for low speed and small steering wheel angle input, but it is not suitable in the case of high-speed and large-angle. In this paper, we consider the influence of the nonlinear characteristics of tires on the stability of the tractor- semitrailer.

2 Nonlinear Modeling of Handling Stability of Tractor-Semitrailer

In nonlinear model of handling stability of tractor-semitrailer, the nonlinear relationship between cornering force and sideslip angle of tire is considered, as well as the changes of vertical load on both sides of axles. The model is established with the following simplifications:

(1) The tractor-semitrailer is treated as a combination of two rigid bodies, which have relative movement between traction pin and fifth wheel.
(2) Roll degree of freedom and pitch degree of freedom are neglected.
(3) Rolling resistance of tires and air resistance are neglected.

Finally, the model is established, as shown in Fig. 1. Parameters of the model are shown in Table 1.

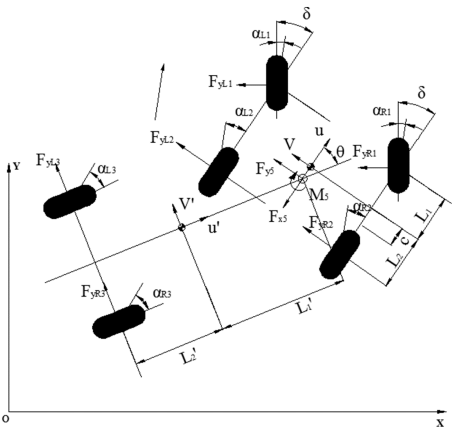

Fig. 1. Nonlinear model of tractor-semitrailer driving stability

Table 1. Parameters of tractor-semitrailer driving stability model

Symbols	Physical meanings	Symbols	Physical meanings
m	Mass of tractor	L_2'	Distance between semitrailer centroid and semitrailer rear axle
m'	Mass of semitrailer	c	Distance between tractor centroid and hitch point
I_z	Moment of inertia around tractor centroid	L	Wheelbase of tractor
I_z'	Moment of inertia around semitrailer centroid	L'	Wheelbase of semitrailer
u	Longitudinal velocity of tractor	h	Centroid height of tractor
u'	Longitudinal velocity of semitrailer	h'	Centroid height of semitrailer
v	Lateral velocity of tractor	F_{yL1}	Cornering force of left front wheel of tractor
v'	Lateral velocity of semitrailer	F_{yR1}	Cornering force of right front wheel of tractor
ω	Yaw velocity of tractor	F_{yL2}	Cornering force of left rear wheel of tractor
ω'	Yaw velocity of semitrailer	F_{yR2}	Cornering force of right rear wheel of tractor
δ	Front wheel angle	F_{yL3}	Cornering force of left wheel of semitrailer
θ	Articulated angle	F_{yR3}	Cornering force of right wheel of semitrailer
β	Sideslip angle of tractor	F_{x5}	Longitudinal component of hitch point force in tractor coordinate system
β'	Sideslip angle of semitrailer	F_{y5}	Lateral component of hitch point force in tractor coordinate system
α_{L1}	Sideslip angle of left front wheel of tractor	F_{zL1}	Vertical force of left front wheel of tractor
α_{R1}	Sideslip angle of right front wheel of tractor	F_{zR1}	Vertical force of right front wheel of tractor
α_{L2}	Sideslip angle of left rear wheel of tractor	F_{zL2}	Vertical force of left rear wheel of tractor
α_{R2}	Sideslip angle of right rear wheel of tractor	F_{zR2}	Vertical force of right rear wheel of tractor
α_{L3}	Sideslip angle of left front wheel of semitrailer	F_{zL3}	Vertical force of left wheel of semitrailer
α_{R3}	Sideslip angle of right front wheel of semitrailer	F_{zR3}	Vertical force of right wheel of semitrailer
L_1	Distance between tractor centroid and tractor front axle	M_5	Damping moment of fifth wheel
L_2	Distance between tractor centroid and tractor front axle	F_c	Centripetal force of tractor
L_1'	Distance between semitrailer centroid and hitch point	F_c'	Centripetal force of semitrailer

Equilibrium equation of tractor:

$$m(\dot{v} + u\omega) = \sum F_y \tag{1}$$

$$I\dot{\omega} = \sum M \tag{2}$$

Equilibrium equation of semitrailer:

$$m'(\dot{v}' + u'\omega') = \sum F_y{}' \tag{3}$$

$$I'\dot{\omega}' = \sum M' \tag{4}$$

in which,

$$\begin{aligned}
\sum F_y &= (F_{yR1} + F_{yL1})\cos\delta + F_{yR2} + F_{yL2} + F_{y5} \\
\sum M &= (F_{yR1} + F_{yL1})L_1\cos\delta + \frac{1}{2}(F_{yR1} + F_{yL1})L\sin\delta \\
&\quad - (F_{yR2} + F_{yL2})L_2 - F_{y5} - M_5 \\
\sum F'_y &= F_{yR3} + F_{yL3} - F'_{y5}\cos\theta + F'_{x5}\sin\theta \\
\sum M' &= -(F_{yR3} + F_{yL3})L'_2 \\
&\quad - (F'_{y5}\cos\theta - F'_{x5}\sin\theta)L'_1 + M'_5
\end{aligned}$$

Articulation speed relationship:

$$u' = u\cos\theta - (v - c\omega)\sin\theta \tag{5}$$

$$v' + L'_1\omega' = u\sin\theta + (v - c\omega)\cos\theta \tag{6}$$

Each sideslip angle:

$$\alpha_{L1} = \arctan\frac{v + L_1\omega}{u - L\omega/2} - \delta \tag{7}$$

$$\alpha_{R1} = \arctan\frac{v + L_1\omega}{u + L\omega/2} - \delta \tag{8}$$

$$\alpha_{L2} = \arctan\frac{v - L_2\omega}{u - L\omega/2} \tag{9}$$

$$\alpha_{R2} = \arctan\frac{v - L_2\omega}{u + L\omega/2} \tag{10}$$

$$\alpha_{L3} = \arctan\frac{v' - L'_2\omega'}{u' - L'\omega'/2} \tag{11}$$

$$\alpha_{R3} = \arctan\frac{v' - L'_2\omega'}{u' + L'\omega'/2} \tag{12}$$

According to vertical force equilibrium, the vertical force of the same axle is computed:

$$F_{z1} + F_{z2} + F_{z3} = (m + m')g \tag{13}$$

$$F_{z1}(L_1 + L_2 - c) - mg(L_2 - c) - F_{z2}c = 0 \tag{14}$$

$$F_{z3}(L_1' + L_2') - m'gL_1 = 0 \tag{15}$$

Ignoring suspension characteristics and body roll, vertical load of each side is:

$$F_R = \frac{1}{2}F_z + \frac{L_2 h}{(L_1 + L_2)L}F_c \tag{16}$$

$$F_L = \frac{1}{2}F_z - \frac{L_2 h}{(L_1 + L_2)L}F_c \tag{17}$$

in which,

$$F_c = m(\dot{v} + u\omega)$$

So

$$\begin{aligned} F_{zR1} = \frac{1}{2}[&\frac{L_2}{L_1 + L_2}(mg + \frac{2h}{L}F_c) \\ &+ \frac{L_2' c}{(L_1 + L_2)(L_1' + L_2')}(m'g + \frac{2h'}{L'}F_c')] \end{aligned} \tag{18}$$

$$\begin{aligned} F_{zL1} = \frac{1}{2}[&\frac{L_2}{L_1 + L_2}(mg - \frac{2h}{L}F_c) \\ &+ \frac{L_2' c}{(L_1 + L_2)(L_1' + L_2')}(m'g - \frac{2h'}{L'}F_c')] \end{aligned} \tag{19}$$

$$\begin{aligned} F_{zR2} = \frac{1}{2}[&\frac{L_1}{L_1 + L_2}(mg + \frac{2h}{L}F_c) \\ &+ \frac{L_2'(L_1 + L_2 - c)}{(L_1 + L_2)(L_1' + L_2')}(m'g + \frac{2h'}{L'}F_c')] \end{aligned} \tag{20}$$

$$\begin{aligned} F_{zL2} = \frac{1}{2}[&\frac{L_1}{L_1 + L_2}(mg - \frac{2h}{L}F_c) \\ &+ \frac{L_2'(L_1 + L_2 - c)}{(L_1 + L_2)(L_1' + L_2')}(m'g - \frac{2h'}{L'}F_c')] \end{aligned} \tag{21}$$

$$F_{zR3} = \frac{1}{2}[\frac{L_1'}{L_1' + L_2'}(m'g + \frac{2h'}{L'}F_c')] \tag{22}$$

$$F_{zL3} = \frac{1}{2}[\frac{L_1'}{L_1' + L_2'}(m'g - \frac{2h'}{L'}F_c')] \tag{23}$$

According to the tire magic formula, expression of lateral force is

$$F_{yi} = \mu F_{zi}[C \arctan[B\alpha_i - E(B\alpha_i - \arctan B\alpha_i)]] \tag{24}$$

The above equations can be used to obtain equations of motion of the tractor-semitrailer. As above formula contains nonlinear parameters, it is difficult to obtain analytical solutions of the equation set. Simulink software is used to build nonlinear dynamics model of tractor-semitrailer shown in Fig. 2.

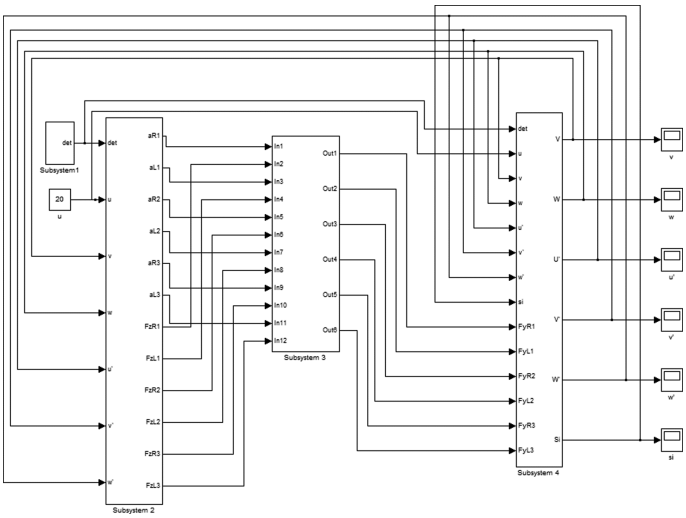

Fig. 2. Nonlinear dynamics Simulink model of tractor-semitrailer

3 Model Analysis

Parameters of the vehicle are inputted in the Simulink model as follows, $L_1 = 2.200$(m), $L_2 = 2.600$(m), $L = 2.050$(m), $L_1^{'} = 4.670$(m), $L_2^{'} = 4.670$(m), $L' = 1.830$(m), $m = 8800$(kg), $m' = 40000$(kg), $h = 1.2$(m), $h' = 1.8$(m), c $= 2.100$(m). The vehicle longitudinal velocity is 20 m/s. Front wheel angle input is a cycle of sinusoidal signal, which frequency is 0.2 Hz, and amplitude is 0.3 rad, as shown in Fig. 3. The nonlinear characteristic of tire cornering force is shown in Fig. 4. The transient response of the system is calculated by computer. Results are shown in Figs. 5 and 6.

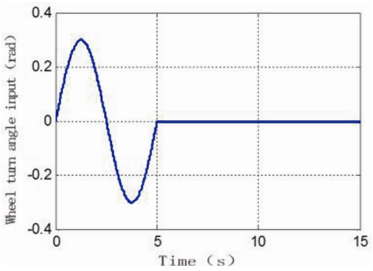

Fig. 3. Wheel turn angle input

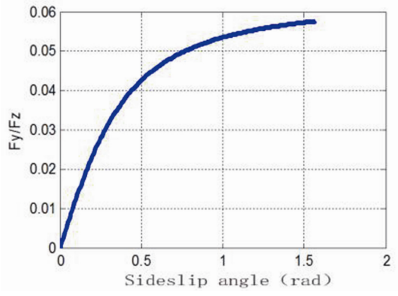

Fig. 4. Variation of tire cornering force

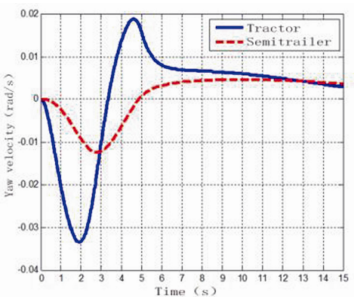

Fig. 5. Variation of yaw velocity

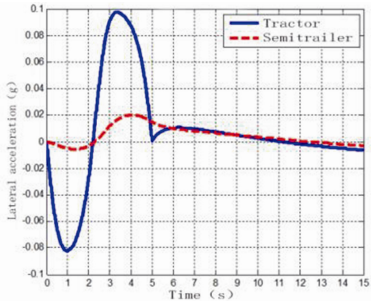

Fig. 6. Variation of lateral acceleration

It can be seen from Figs. 5 and 6 that the time when yaw velocity and lateral acceleration of the semitrailer reach the peak are delayed by 1 s relative to the tractor. The motion of semitrailer is lagged behind that of the tractor, because the semitrailer is connected with the tractor through traction pin. The lateral movement of the tractor transmits back to the front suspension part of the semitrailer through \ traction pin, and through trailer axle or stringer to the rear axle of the semitrailer, therefore, there is hysteresis. It can also be seen from Figs. 5 and 6 that both yaw velocity peak and lateral acceleration peak of the semitrailer are smaller than those of the tractor, and a number of studies [2–8] also show the same phenomenon, indicating that the articulated train has a good lateral stability. The system tends to be stable after 7 s.

Mass of semitrailer, fifth wheel lead and wheelbase of tractor are selected as main factors to analyze the effect of parameter changes on maximum yaw velocity of tractor, maximum lateral acceleration of tractor, maximum yaw velocity of semitrailer and maximum lateral acceleration of semitrailer.

(1) The mass of semitrailer is 10000 kg, 20000 kg, 30000 kg and 40000 kg, respectively, and the other parameters keep unchanged. The model is calculated by Simulink software, and the changes of tractor-semitrailer driving stability are obtained, as shown in Table 2. As can be seen from Table 2, with the increase of the mass of semitrailer, yaw velocity and lateral acceleration of vehicles increase, reducing the

stability of the vehicle combination. Therefore, vehicles should be properly loaded to prevent overloading.

Table 2. Changes of tractor-semitrailer driving stability parameters caused by semitrailer mass

m' (kg)	10 000	20 000	30 000	40 000
ω_{max} (rad/s)	0.0076	0.0110	0.0147	0.0188
ω'_{max} (rad/s)	0.0010	0.0021	0.0033	0.0047
Ay_{max} (g)	0.0519	0.0657	0.0813	0.0975
Ay'_{max} (g)	0.0201	0.0187	0.0192	0.0201

(2) Fifth wheel lead (L_2-c) is 0 m, 0.5 m, 1 m and 1.5 m, respectively, and the other parameters keep unchanged. The results shown in Table 3 indicate that with the increase of fifth wheel lead, yaw velocity and lateral acceleration of vehicles decrease, improving the stability of the vehicle combination.

Table 3. Changes of tractor-semitrailer driving stability parameters caused by fifth wheel lead

L_2-c (m)	0	0.5	1	1.5
ω_{max} (rad/s)	0.0238	0.0188	0.0135	0.0099
ω'_{max} (rad/s)	0.0047	0.0047	0.0070	0.0107
Ay_{max} (g)	0.1232	0.0975	0.0748	0.0555
Ay'_{max} (g)	0.0208	0.0201	0.0190	0.0174

(3) The wheelbase of tractor is 1.850 m, 1.950 m, 2.050 m and 2.150 m, respectively, and the other parameters keep unchanged. The results shown in Table 4 indicate that with the increase of the wheelbase of tractor, the stability of the system tend to be better slightly. Because the increase in wheelbase will increase the roll stability of tractor, but due to regulatory restrictions, the change in the wheel track is generally not large, so the wheelbase has little effect on the lateral stability.

Table 4. Changes of tractor-semitrailer driving stability parameters caused by front track of tractor

L (m)	1.850	1.950	2.050	2.150
ω_{max} (rad/s)	0.0190	0.0189	0.0188	0.0187
ω'_{max} (rad/s)	0.0046	0.0046	0.0047	0.0048
Ay_{max} (g)	0.0978	0.0977	0.0975	0.0974
Ay'_{max} (g)	0.0200	0.0200	0.0201	0.0202

4 Conclusion

The nonlinear dynamic model of tractor-semitrailer driving stability was established, considering nonlinear characteristics of tire lateral force and changes of vertical wheel load, and Simulink was used to simulate the model. Maximum yaw velocity of tractor, maximum lateral acceleration of tractor, maximum yaw velocity of semitrailer and maximum lateral acceleration of semitrailer were used as evaluation indexes to analyze the influence of mass of semitrailer, fifth wheel lead and wheelbase of tractor on tractor-semitrailer driving stability. The result shows that it is helpful to improve the stability of the system by reducing payload of semitrailer and increasing fifth wheel lead and wheelbase of tractor.

Acknowledgements. This work is supported by Ministry of Transport project of basic research for application (No. 2014 319 223 020) and Research on Modular System of Heavy Freight Vehicles (No. N-24504-20163).

References

1. Williams D (1951) The mathematical theory of the snaking of two-wheeled trailers. Proc Inst Mech Eng Automobile Div 5:175–190
2. Li X, Zhang J, Wang M (2009) Simulative analysis of tractor-semi trailer closed loop lateral stability. J Syst Simul 23(03):647–650
3. Zhang L, Zhang X, Ma B (2011) Direct intersection simulation and handling stability analysis of semitrailer. J Liaoning Univ Technol (Nat Sci Ed) 31(01):33–36
4. Wu X, Jiang J, Chen Y (1996) Computer simulation study on roll stability of tractor-semitrailer. Acta Armamentarii (Archies of armoured vehicles with engines), (03):1–13
5. Guan, Z (2006) Stability analysis about steering wheel angle step input controllability based on simulation tractor-semitrailer. Chin Agric Mechanization (01):88–91
6. Li X, Luo X, Ma J et al (2008) Computer simulation analysis of semitrailer turning characteristic. Tractor Farm Transporter 35(03):28–30
7. Zhang J-G (2010) Research on Driving Stability of Tractor-semitrailer Based on Closed Loop Control. Jilin University, Changchun (2010)
8. Song S-B (2007) Simulation Research of Roll Control System of Tractor Semitrailer Study. Jilin University, Changchun

Optimal Location of Charging Station of Electric Bus in Battery Replacement Mode

Yi Xiang and Yong Zhang(✉)

School of Transportation, Southeast University, Nanjing 210096, Jiangsu, China
491838528@qq.com, zhangyong@seu.edu.cn

Abstract. Electric vehicle charging mode determines the efficiency of electric vehicle charging, there are three charging modes-slow charging mode, fast charging mode and battery replacement mode. Electric bus (e-bus) is widely used in battery replacement mode. However, it is lack of theoretical guidance for the optimal locations of charging facilities for e-bus in battery replacement mode. In this paper, given the regional charging demand and considering the battery replacement mode, a mathematical model has been developed. Particle swarm optimization algorithm is proposed for solving this model. A case study on planning the locations of e-bus charging stations in Nanjing, China is presented. The results suggest that model can be used to locate e-bus charging station in battery replacement mode and provide reference for the optimal locations of charging facilities for e-bus.

Keywords: Battery replacement mode · Particle swarm optimization algorithm · e-bus · Optimal location

1 Introduction

Promoting the usage of electric vehicles (EVs) is a important measure to reduce vehicle exhaust emissions because of 40% of carbon dioxide emissions and 70% of other greenhouse gas emissions resulting from motorized transportation [1], China government is putting a great deal of effort into developing EVs. With the growth of usage of EVS electric buses (e-buses) emerged of advantages that facilitate the development of environmentally friendly public transportation [2]. E-bus have the capability to reduce energy consumption and tailpipe emissions [3]. Therefore, the use of e-buses can not only improve environmental but can also increase renewable energy use.

E-bus have been developed as a promising solution for reducing vehicle emissions and petroleum dependence. However, without sufficient and convenient charging infrastructure, e-bus will not be used by the broader public. Unlike EVs there are widely studied on the issue of Optimal location of charging facilities. There is less research on location selection for e-bus.

Charging mode is an important issue in Optimal locations selection for e-bus. Several types of e-bus fuel consumption technology are available, for instance hybrid electric vehicles (HEVs), battery electric vehicles (BEVs), and plug-in hybrid electric vehicles

X. Zeng et al. (eds.), *International Symposium for Intelligent Transportation and Smart City (ITASC) 2017 Proceedings*, Smart Innovation, Systems and Technologies 62, DOI 10.1007/978-981-10-3575-3_13

(PHEVs) [4], because BEVs have high cost-effectiveness, a set of e-bus use BEVS that with different charging mode In this study, the charging modes are investigated to find a number of advantages over different charging mode, for instance slow charging mode, fast charging mode and battery replacement mode.

Thus, an important and effective solution is to study the charging characteristics of e-bus and deploy public charging infrastructure. This requires careful planning for the optimal location of e-bus charging stations in order to provide a good charging service and to reduce the social cost.

This paper has two objectives. The first objective is to study the charging characteristics of e-bus. The second objective is to study the optimal location of charging facilities for e-bus. the first objective is to investigate the charging mode and charging level. By comparing the models, the most effective charging mode is selected. Then, regarding the second objective is to develop a model based on the p-median model. And solve this a mixed integer linear program by a heuristic based on Particle swarm optimization algorithm (PSO). The objective of the model is to locate a given number of charging facilities for e-bus.

1.1 Literature Review

An extensive literature exists on the optimal location of facilities problem. Research can be divided into three types. In the first set of these studies, the maximal covering location problem (MCLP) locating a number of facilities on a network to maximize the number of demand coverage introduced by Church et al. (1974) [5]. Farahani et al. (2012) review the covering problems in facility location [6]. Daskin et al. (2008) explain a taxonomy of location by discussing space discrete location problems [7].

In the second category of studies, flow-capturing location model (FCLM) aims to determine the optimal location of charging facilities. Hodgson et al. (1990) proposed the flow-capturing location model (FCLM) to capture location relative to flows and location-allocation problems [8]. Kim et al. (2012) proposed a mixed-integer linear deviation-flow refueling programming model to consider the limited capacity of charging facilities [9]. Huang et al. (2015) present a a novel Alternative Fueling Station (AFS) location mode by allowing for users who accept the incorporation of deviations from the shortest paths [10].

In the last group of studies, the p-median problem (PMP) locate facilities location to minimise the total demand-weighted distances in order to serve for the majority of the population was introduced by Hakimi et al. (1964) [11]. Sittipong et al. (2014) study the facility location model and used greedy algorithm. p-median algorithm and p-center algorithm to minimize the sum of the setup cost and transportation cost [12].

In recent years, due to rapid technological advances in EV, facility location models have been applied to study the location-planning problem of EV charging facilities.

In literature, there is less research on the optimal location of e-bus charging facilities, however, In recent years, with rapid technological advances in EV the problems related to the optimal location of EVs charging facilities have received much attention. Raffaela et al. (2015) develop a mathematical model based on stochastic user equilibrium

principle that wireless charging facilities for EVs stations be located on a network with maximum traffic flow [13].

Sylvia Y. He et al. (2016) presented an approach to locate public EV charging stations by incorporating the local constraints of supply and demand and comparing the optimal locations from three different location models based on a case study on EV charging stations location in Beijing [14]. Zhi-Hong Zhu et al. (2016) proposed a model of plug-in electric vehicles to solve the problem of charging station location and used a genetic algorithm-based method for solving this model [15]. Shengyin Li et al. (2016) developed a multi-period optimization model to capture the dynamics in the topological structure of network [16]. Jung et al. (2014) used a bi-level simulation-optimisation framework that mixed an upper level multiple-server allocation model and a lower level dispatch simulation approach to determine the EV charging locations [17]. He et al. (2015) also proposed a bi-level mathematical program based on equilibrium framework that aimed to minimise the sum of total travel and recharging time [18].

2 Problem Analysis

2.1 Selection of Charging Mode

There are three different charging modes: slow charging mode, fast charging mode and battery replacement stations. Each charging mode is compared as follows in Table 1.

Table 1. Comparison of charging mode

	Comparison of charging mode	Characteristics
Slow charging mode	After the vehicle battery is dead, the electric bus use a slow way to charge without unloading the battery	It has the advantages of long driving distance. it can be to meet the needs of the vehicle all day and charge only in the evening
Fast charging mode	Charging is completed in one hour(the real time depending on the battery's ability to accept), using a larger charging current to provide short-term services for electric vehicles	It is suitable for that The average daily range travel distance is greater than the battery and the vehicle can fast charges in the gap
Battery replacement mode	the battery out of power was removed and was replaced a set of fully charged battery, then bus leave	The time of electric vehicle battery replacement can be compressed within ten minutes

As charging mode discussed above, to choose the most suitable charging mode of electric bus is very important. Currently, the number of bus parking site is a large number and some sites are very close in distance, it is expensive to build charging facilities at each site, so it is not suitable for slow charging mode. As more bus lines and much car

battery capacity and charging not timely will result in departure delays, the use of fast charging is not suitable for fast charge mode charging. The replaced battery is proper, which is centralized battery to the nearest charging stations and centralized charging. This mode not only improves the efficiency of electrical equipment, reduce the charging equipment investment, but also prolong battery life through centralized management and unified maintenance of the battery.

Using battery replacement mode, the bus charge processes as follows: The bus arrived at first or last stop, then replace the bus battery. After change the battery, bus drive away at once. When empty battery is accumulated to a certain number can be filled with a vehicle. Then they will be transported to the battery charging station by vehicles. Empty batteries will be charged on the charging station, and then transport back to the bus parking site by the full delivery of the vehicle.

2.2 Demand Point and the Candidate Sites

We consider each bus stop departure station as charging demand point.

Firstly, buses run very regularly, because that buses depart daily according to a fixed frequency and fixed routes and from between the first and last bus parking site. one charge last for at least the whole route, to ensure the normal operation of the bus.

Secondly, urban construction land cost is high and electric bus will need to charge after bus generally arrive at the station. Therefore, a candidate sites in bus stop departure stations can avoid the construction of dedicated bus charging station.

There are too many bus stop departure stations, so we need to analyze the bus stop departure stations, according to the characteristics for power mode, the scale of public transit line, transportation convenience, covers an area of grid layout and other factors, in order to determine the typical bus stop departure stations as candidate sites. It follow the following principles: selecting a large-scale candidate sites ensure adequate charging time, accommodate most convenient bus line in the charging station and reduce distribution costs for battery; selecting candidate sites near the substation provide electricity to ensure that the substation or transformer rated capacity meet the demand of power load, in order to prevent unnecessary expansion and capacity increase; selecting candidate sites with convenient transportation is convenient for electricity vehicle distribution and avoid traffic congestion.

2.3 The Size of the Charging Station

According to 《specification of electric power supply and protection electric vehicles technical》, power battery charging station is divided into four levels. The different storage capacity, the level of charging stations, one-way distribution capacity and daily service capacity varies is shown in Table 2. The size of the charging station can be determined based on each charging station level.

Table 2. Charging station classification

Ratings of charging station	Distribution capacity (kVA)	The maximum number of bus	Land area (m^2)	Construction costs (Ten thousand yuan)
One rate	>5000	>500	>3400	1000
Two rate	3000–5000	200–500	2500–3400	800
Three rate	1000–3000	100–200	1500–2500	610
Four rate	<1000	<100	<900	460

2.4 Problem Description

In this paper, the problem of bus charging station location may be described that selecting *m* bus stop departure stations as the candidate sites of the charging station sever for the *n* demand points (all the bus stop departure stations need to be provided charging service), and each demand points gets service by only one charge stations. the main problem to be solved is to choose charging stations from candidate locations and to make a plan to arrange the charge that can meet the needs of the charging demand point and ensure the level of service. The aim is to achieve the minimum total cost of charging station.

2.5 Modeling Thought

Planning network of charging stations should consider the total cost and service. If we only to emphasize the cost of the charging station, it can not be guaranteed level of service. If only to emphasize service may cause loss profit of the bus company, which is not conducive to long-term development of bus operation. Therefore, construction costs, operating costs, and transportation costs are as three parts of the total cost in this paper. The service radius and charging station capacity (it usually represented by the number of batteries, in order to facilitate the calculation instead by the number of service buses) is a key index as a measure of the level of service. In actual operation, we must fully consider the impact of site selection for power mode and suitable service radius. It can guarantee the timely delivery of the battery to the charging station that the battery charging can be done within a fixed period of time to guaranteed service level. Location schematic is shown in Fig. 1. The cost can be represented as objective function, service is expressed into the maximum service capacity and he maximum service radius, represented by constraints. In order to meet the actual operation of the charging station, this paper based on the idea of 0–1 integer programming establish a cost-service model, reduce the total cost to achieve the basic level of service.

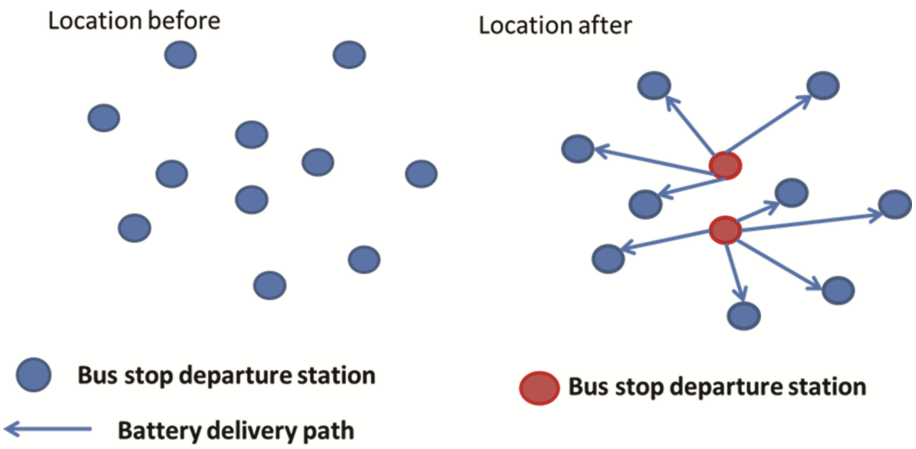

Fig. 1. Location model schematic

2.6 Model Formulation

Basic Assumptions. In order to solve the model and ensure the model is not too complicated, we make the following assumptions:

(1) Selecting charging station only within a certain range of candidate points, the number of charging station is variable;
(2) Only considering the transportation from the charging station to demand points;
(3) Completing the distribution of the rechargeable battery by only one time;
(4) Charge station provide services for the battery every day only one time;
(5) Transport cost is proportional to the distance of traffic and transport volumes of batteries;
(6) The unit freight rates is constant between the charging station and demand point;
(7) The capacity of each candidate site is a known constant;
(8) Investment cost of the establishment and operation of the charging station is known;
(9) Charging station service radius is known;
(10) Rechargeable battery capacity of charging station per day is known.

Symbol Definition. Model Symbol Description as follows:

r_j: whether Candidate site j was selected as decision variables, it is 1, and 0 otherwise;
X_{ij}: whether demand point i was provided charging services by the selected candidate points j as decision variables, it is 1, and 0 otherwise;
φ: distribution vehicle cost of unit demand and unit transportation distance;
q_i: the number of electricity buses need to be served at the point i;
d_{ij}: the distance between demand point i and j;
Q_j: charging station capacity limits of candidate sites j, expressed as the number of service buses;

i: a collection of sites that buses need to be provided battery replacement service;
j: a collection of candidate sites of charging station;
k: rate of return on investment;
α: payback period of investment;
E: the costs of infrastructure construction of charging stations, according to the charging station level;
θ: the reduction factor of the variable costs to the reduction coefficient of the initial investment costs;

2.7 Mathematical Model

Objective:

$$\min F = 365 \cdot \varphi \sum_i \sum_j X_{ij} q_i d_{ij} + \sum_{j=1}^{m} E_j \left[\frac{k(1+k)^{\alpha}}{(1+k)^{\alpha} - 1} \right] + \sum_{j=1}^{m} E_j \cdot \theta \tag{1}$$

Subject to:

$$\sum_{j=1} X_{ij} = 1, \quad \forall i \in I \tag{2}$$

$$\sum_i q_i X_{ij} r_j \le Q_j, \quad \forall j \in J \tag{3}$$

$$\sum_i r_j \le j, \quad \forall j \in J \tag{4}$$

$$d_{ij} r_j X_{ij} \le R, \quad \forall_i \in I, \quad \forall_j \in J \tag{5}$$

$$X_{ij} \in \{0, 1\} \tag{6}$$

$$r_j \in \{0, 1\} \tag{7}$$

The objective function (1) is the total of the transport costs, construction costs and operating costs. Transport cost mainly include batteries distribution costs in the process of replace battery. Construction costs include charging station initial investment. Operating expenses include the annual maintenance costs, material costs and staff salary costs, investment costs can be can be calculated by the reduction factor. The aim is to find the minimum value of the sum of the three types of cost; Formula (2) represents each point is only served by a charging station for services; Formula (3) indicates the capacity constraints of charging station; Formula (4) represents the highest number of charging stations; Formula (5) represents the distance of each demand point to the charging station meet service radius; Formulas (6) and (7) represents the decision variables.

2.8 Algorithm Principle

PSO (particle swarm optimization) is a computational method to simulate the behavior of birds flock's looking for food based on swarm intelligence. In PSO, a certain number of particles are set in the D-dimensional space of the position of the objective function. the i particle can be represented by D-dimensional vector $x_i = (x_{i1}, x_{i2}, \ldots x_{iD})^T$,which represents a feasible solution, the velocity of the particles represents with $v_i = (v_{i1}, v_{i2}, \ldots, v_{iD})^T$. The quality of solutions primarily is determined by the merits of the fitness of each particle. In general, the objective function is used as the fitness function. In the search space, each particle has a certain memory capacity and remember the locations searched with the best fitness: Individual extremum $pbest_i = (p_{i1}, p_{i2}, \ldots, p_{iD})^T$, whole population retain the current search of optimal fitness location: global extremum $gbest$. Particles in space achieve the position updates by tracking $pbest_i$ and gbest, the update of velocity and location according to Eqs. (8) and (9).

$$v_i^{t+1} = \omega \cdot v_{i1} + c_1 \cdot rand() \cdot \left(pbest_i^{t+1} - x_i^{t+1}\right) + c_2 \cdot rand() \cdot (gbest_i^{t+1} - x_i^{t+1}) \tag{8}$$

$$x_i^{t+1} = x_i^t + v_i^{t+1} \tag{9}$$

Where: v_i^{t+1} is the particle velocity, x_i^{t+1} is the current position of particle, $gbest_i^{t+1}$is global extremum of particle, $pbest_i^{t+1}$ is the individual extremum of particle, t is the iteration number; ω is a factor for the inertia weight; *rand ()* is a random number uniformly distributed in (0,1); c_1 and c_2 are learning factors, generally $c_1 + c_2 < 4$

2.9 Particle Code Design

In coding of particles, the particle dimension is the number of demand points, $i = (W_1, W_2, \ldots, W_n)^T$, the value of each dimension is the order of number of demand points, namely I-dimensional representation i demand points; each dimension of the particles were evaluated, its value is a candidate number for any charging stations, for example, m = 6, n = 10, then $dos\ [i] = m$ (m =1,2,3,4,5). In this paper, Since each demand point will have a charging station for service, so each particle on each dimension is corresponds to an integer value, the value is equal to the number of charging sites selected. Coding schematic is shown in Table 3.

Table 3. Illustrates the coding

i	1	2	3	4	5	6	7	8	9	10
	1	3	3	2	6	3	6	1	2	3

The above coding means that the charging station 1 serve demand point 1; the charging station 3 serve demand points 2 and 3; the charging station 2 serve demand points 4; ···. The task allocation in the algorithm is realized by a two dimensional array, the two-dimensional array will select the number of charging stations in order to be

stored in the row, each column in the row is stored in all demand points. A two-dimensional array of codes is available from the above example. Table 4 indicates the selected charging station 1 to provide charging services for demand point 1 and 8; ···.

Table 4. Dimensional array corresponding to the coding

Selected charging station	Demand points
1	1 8
2	4 9
3	2 3 6 10
6	5 7

2.10 Algorithm Implementation Process

In solving the problem of particle swarm algorithm, the number of particles is m in PSO; Let *x[i]* is the position of particles *i* in the population; *V[i]* is adaptive speed of the particle *i*; *fitness* is the fitness value of particles; *Pbest* is the best position for the particles themselves searched; *Pbest_fitness* is the best value for the particles themselves searched, which is adapted function values at *Pbest*; *Gbest* is the best location of the population in particle; *Gbest-fitness* is the fitness function value at *Gbest*. The step of algorithm is as follows:

(1) initializing the every particle *i* position *X[i]* and the velocity *V[i], i* = 1,2, …, *m* of particle swarm *i*;
(2) initializing particle historical best fitness value *Pbest_fitness* and the best fitness *Gbest-fitness* which is a great value, and calculates each particle's current *fitness*;
(3) initializing *Pbest and Gbest* by *X[i]*;
(4) Comparing current adaptive value and historical best fitness value, if the current value of particle is less than the historical best value, then the value is saved to *Pbest-fitness* and save the smallest value to the optimal value of *Pbest-fitness* in the population, and the position of the particle is saved to *Pbest*;
(5) Comparing the best fitness value *Pbest-fitness* of all the particles, and save a minimum value to the optimal value *Gbest-fitness* in the population, and record the particles;
(6) the position of the particle is saved to *Gbest*;
(7) For each particle, updating formula *X [i], V [i]* by the speed;
(8) loop iteration until the termination condition is satisfied.

3 Case Study

3.1 Preliminary Preparation

Nanjing main urban area (include Gulou, Xuanwu, Qinhuai, Jianye, Yuhuatai five section) has area of 400.57 km^2, the resident population of 388.3 million. According to the survey, there are total 208 routes and 3183 buses in Nanjing. This case is planning bus charging station site in Nanjing, the bus stop departure station of 57 are selected as

demand points, according to the number of bus routes of bus stop departure station, we select the largest demand stations of Nanbao Park, long-distance East station, silver City Dongyuan, Olympic New city, west gate of mochou lake park, Nanjing station-South Square East, Nanjing station-north Square East, Nanjing South station, Yangzhuang, Baima Park, Xiaohang community, Qixia, Sheshan Star City, south gate of Yuhuatai as candidate sites for the charging station, each preferred point data in Table 5.

Table 5. Candidate sites related datas

No.	Candidate bus stop departure stations	Latitude	Longitude	Charging station level	Capacity constraints (vehicle)	Construction costs
1	Nanbao Park	32.11378	118.7610	4	100	460
2	Long-distance East station	32.08364	118.8218	2	500	800
3	Silver City Dongyuan	32.02416	118.8447	3	200	610
4	Olympic New City	32.02793	118.7254	3	200	610
5	West gate of Mochou Lake Park	32.03832	118.7632	2	500	800
6	Nanjing station-South Square East	32.09101	118.7980	1	800	1000
7	Nanjing South station	32.04704	118.7644	1	800	1000
8	Nanjing station-North Square East	32.09489	118.7997	2	500	800
9	Yangzhuang	32.16635	118.7103	1	800	1000
10	Baima Park	32.06447	118.8146	4	100	460
11	Xiaohang community	31.98815	118.7446	3	200	610
12	Qixia	32.10188	118.9092	3	200	610
13	Sheshan Star City	32.14448	119.0101	3	200	610
14	South gate of Yuhuatai	31.99703	118.7790	2	500	800

According to research, relevant data were known as shown in Table 6.

Table 6. Parameter settings

Name	Parameter	Name	Parameter
Capital payback period/year	10	Each battery average distribution costs	0.4 yuan/km
Discount rate	0.1	The total number of public buses	3183
The construction costs account for percentage of annual operating expenses	10%	Charging service radius	20 km

3.2 Optimization Results

According to the optimal location of charging station model, the particle swarm algorithm were applied to this model, and then solved according to the operation steps mentioned above. Algorithm specific parameters are set as follows: Learning factor $c_1 = c_2 = 2$; inertia weight ω linearly reduced from 0.9 to 0.4; error is set to 0.01; population size N = 100; dimension 57; the iteration number is 200 times. Optimization results in Table 7, it get best result when iteration to the 60 time.

Table 7. Optimization results

Selected charging station	Corresponding to demand points
Nanbao Park	1 12 13 20 24 25 38
Long-distance East Station	17 34 55
West gate of Mochou Lake Park	4 11 15 33 44 52
Nanjing station-North Square East	14 26 28 36 54
Nanjing South station	31 32 46 48
Yangzhuang	5 6 10 19 22 27 29 46
Qixia	7 9 23 35 41 42 43 51 57
South gate of Yuhuatai	2 47 49 56 8

As we can seen from Table 7, considering the economy and service requirements, the charging station 1, 3, 16, 18, 21, 30, 50, 53 can been selected. In this assignment, the optimal total cost of charging stations network is 3.09 million yuan, the map depicts a optimal location of charging station was plotted in map, shown in Fig. 2.

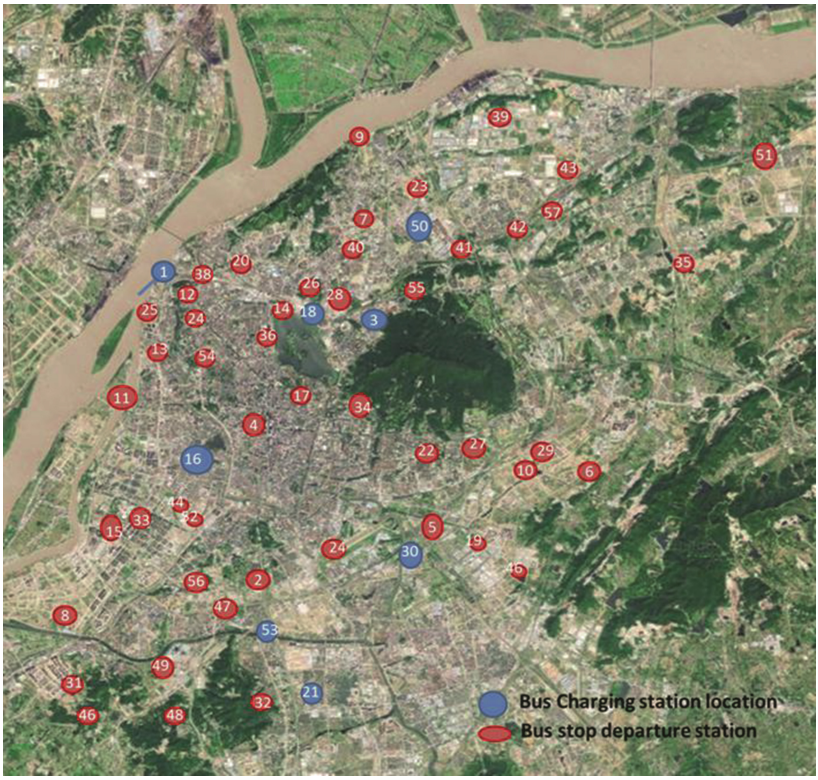

Fig. 2. Optimization result of E-bus charging station locations

4 Conclusion

With the continuous development of new energy vehicle, E-bus is the future development trend of public transportation. This paper aim is to solve the optimal location of e-bus charging station. We consider the charging station characteristics in battery replacement mode and built optimal location model. Based on particle swarm algorithm method, we solve the Nanjing e-bus optimal location of charging station, which reals that the method has wide applicability.

However, this model only consider that charge station provide services for the battery every day only one time, if the bus operating mileage is too long, one time replacement battery can not meet the needs of bus operators. In the case of large demand for replacement battery, it involves more complex conditions, such as the number of distribution times, the number of charging and the charging capacity, further research is needed.

Acknowledgments. This work was supported by the key technology of charging station network construction and operation in Nanjing No. Ks1513, the "Fundamental Research Funds for the Central Universities" and the "Research and Innovation Project for College Graduates of Jiangsu Province" No. SJLX15_0063.

References

1. Frade I, Ribeiro A, Gonçalves G, Antunes A (2011) Optimal location of charging stations for electric vehicles in a neighborhood in Lisbon, Portugal. Transp Res Rec: J Transp Res Board 2252. Transportation research record of the National Academies, Washington, DC, pp 91–98
2. Ke BR, Chung CK, Chen YC (2016) Minimizing the costs of constructing an all plug-in electric bus transportation system: a case study in Penghu. Appl. Energy 177:649–660
3. Lajunen A (2014) Energy consumption and cost-benefit analysis of hybrid and electric city buses. Transp. Res. Part C: Emerg. Technol. 38:1–15
4. Dong J, Liu C, Lin Z (2014) Charging infrastructure planning for promoting battery electric vehicles: an activity-based approach using multiday travel data. Transp. Res. Part C: Emerg. Technol. 38:44–55
5. Church R, ReVelle C (1974) The maximal covering location problem. Pap. Reg. Sci. 32:101–118
6. Farahani RZ, Asgari N, Heidari N, Hosseininia M, Goh M (2012) Covering problems in facility location: a review. Comput. Ind. Eng. 62:368–407
7. Daskin MS (2008) What you should know about location modeling. Naval Res. Logist. (NRL) 55:283–294
8. Hodgson MJ (1990) A flow-capturing location-allocation model. Geogr Anal 22:270–279
9. Kim JG, Kuby M (2012) The deviation-flow refueling location model for optimizing a network of refueling stations. Int J Hydrogen Energy 37:5406–5420
10. Huang Y, Li S, Qian Z (2015) Optimal deployment of alternative fueling stations on transportation networks considering deviation paths. Netw Spat Econ 15:183–204
11. Hakimi SL (1964) Optimum locations of switching centers and the absolute centers and medians of a graph. Oper Res 12:450–459
12. Dantrakul S, Likasiri C, Pongvuthithum R (2014) Applied p-median and p-center algorithms for facility location problems. Expert Syst Appl 41:3596–3604
13. Riemann R, Wang D, Busch F (2015) Optimal location of wireless charging facilities for electric vehicles: flow-capturing location model with stochastic user equilibrium. Transp Res Part C: Emerg Technol 58:1–12
14. He SY, Kuo YH, Wu D (2016) Incorporating institutional and spatial factors in the selection of the optimal locations of public electric vehicle charging facilities: a case study of Beijing, China. Transp Res Part C: Emerg Technol 67:131–148
15. Zhu Z, Gao Z, Zheng J, Du H (2016) Charging station location problem of plug-in electric vehicles. J Transp Geogr 52:11–22
16. Li S, Huang Y, Mason S (2016) A multi-period optimization model for the deployment of public electric vehicle charging stations on network. Transp Res Part C: Emerg Technol 65:128–143
17. Jung J, Chow J, Jayakrishnan R, Park J (2014) Stochastic dynamic itinerary interception refueling location problem with queue delay for electric taxi charging stations. Transp Res Part C: Emerg Technol 40:123–142
18. He F, Yin Y, Zhou J (2015) Deploying public charging stations for electric vehicles on urban road networks. Transp Res Part C: Emerg Technol 60:227–240

Design and Development of Earthquake Emergency Rescue Command System Based on GIS and GPS

Yujia Chen, Xiaoqing Zeng, and Tengfei Yuan(✉)

The Key Laboratory of Road and Traffic Engineering, School of Transportation Engineering, Ministry of Education, Tongji University, 4800 Cao'an Road, Shanghai, China
825674685@qq.com, zengxq@tongji.edu.cn, yuantengfei2010@126.com

Abstract. The Earthquake is one of the worst natural disasters, emergency rescue command is playing an essential role in the process of rescue. And with the rapid development of GPS and GIS, the paper introduces GPS as the location technique and GIS to realize the visualization. Based on this, the system contains three structural layers and several basic functions, which can achieve the optimal path planning and real-time location through the heuristic algorithm and improved genetic algorithm. So this system can collect the information of earthquake emergency accurately and rapidly and provide effective service for earthquake emergency rescue command.

Keywords: GIS and GPS · Global location system · Earthquake emergency rescue · The improved genetic algorithm

1 Introduction

Cites around the world have been centering on earthquake emergency rescue and the development of Global Position System (GPS) and Geographic Information System (GIS) to support earthquake emergency rescue command system. Currently, various techniques available for location and command system development. Location technique, such as base station, Wi-Fi, Bluetooth and RFID, can realize the precise position, but only limited to normal scenario with high infrastructure expenses. GPS-based position has been applied worldwide, and have high advantages over other location techniques in less infrastructure expenses. Meanwhile, there are a lot of techniques to develop the earthquake emergency rescue command system, but the Geographic Information System (GIS) has the particular advantages in the state of acceptance and popularity. In order to develop the earthquake emergency rescue command system which is high-efficiency and large volume, GPS and GIS have been proposed as a promising technique, due to deep market penetration and cost-effective performance.

Currently, fewer studies have been carefully conducted on development of the earthquake emergency rescue command system which is high-efficiency and large volume based on GPS and GIS. The main objective of this paper is to develop the earthquake emergency rescue command system which can realize electronic map display, precise

X. Zeng et al. (eds.), *International Symposium for Intelligent Transportation and Smart City (ITASC) 2017 Proceedings*, Smart Innovation, Systems and Technologies 62, DOI 10.1007/978-981-10-3575-3_14

real-time location and optimal path planning. The system is developed by the MapInfo's components MapX and MapXtreme installed on .NET platform.

This paper is organized as follows. Firstly, the paper reviews related works on studies of system functional framework design, real-time position data collection and optimal path planning algorithms. Secondly, the paper introduces the system functional framework design supported by the topological network. Thirdly, the paper describes the key skill of real-time position data collection and improved genetic algorithm for optimal path planning. Finally, the paper carries out the simulation experiment and evaluate the performance of this system due to rapid calculation speed and optional results.

2 Related Works

The Earthquake is one of the worst natural disasters that human face, so earthquake emergency rescue which is the key to reduce the damage of disaster reduction [1]. Earthquake emergency rescue command system is so important that many researchers have made a lot of work. During the 1994 Los Angeles earthquake, the emergency command and response system of the earthquake of US Federal Emergency Management Agency (FEMA) played an important role in the decision-making of the government emergency response and provided the important information technology support for emergency rescue decision [2]. Liu Xuemei proposed a set of fast thematic maps system applied to emergency rescue by studying the specific contents [3]. Shi Yunlong analyzed the complex adaptation of the earthquake rescue system from four features—aggregation, nonlinearity, flow, and diversity, and made an analog emulation based on Swarm, and performed a case study comparing the emulation results with practical rescue condition in Wenchuan earthquake [4].

For the real-time position data collection and accurate positioning, it is the data support of the earthquake emergency rescue command system. Wang Jun analyzed various errors the relative positioning and discussed the principle of real-time relative positioning with track RT to determine epicenter from track RT results [5]. Zhang Zhengfeng summarized and analyzed the current seismic exploration in GPS technology and cost issues, pointed out that the future of 3D seismic exploration based on OEMSTAR has good performance of positioning [6].

Optimal path planning is essential to dispatch the sources of rescue, so the efficient algorithms is so critical to calculate optimal solutions. Yuan proposed a single objective model which takes the shortest path travel time as the goal and considers the influence of road traffic and disaster diffusion, then designed an improved D algorithm to solve this problem [7]. Jotshi considered the impact of the disaster on the traffic conditions, setting the medical vehicles as the object, the shortest path travel time as the target to build the model [8]. Xie Hongwei proposed improved genetic algorithm and evolving algorithm to solve the best path problem of emergency decision support system [9]. Liu Fan built mathematics models for VRP of Emergency Logistic, and to apply GA to solve the model [10].

3 System Structure Design

3.1 Topology Network Structure Design

Earthquake emergency rescue command system which is centralized and intelligent, is developed by Global Position System, Global System for Mobile Communications and Geography electronic map, and it can schedule, monitor and manage in real time (seen in Fig. 1).

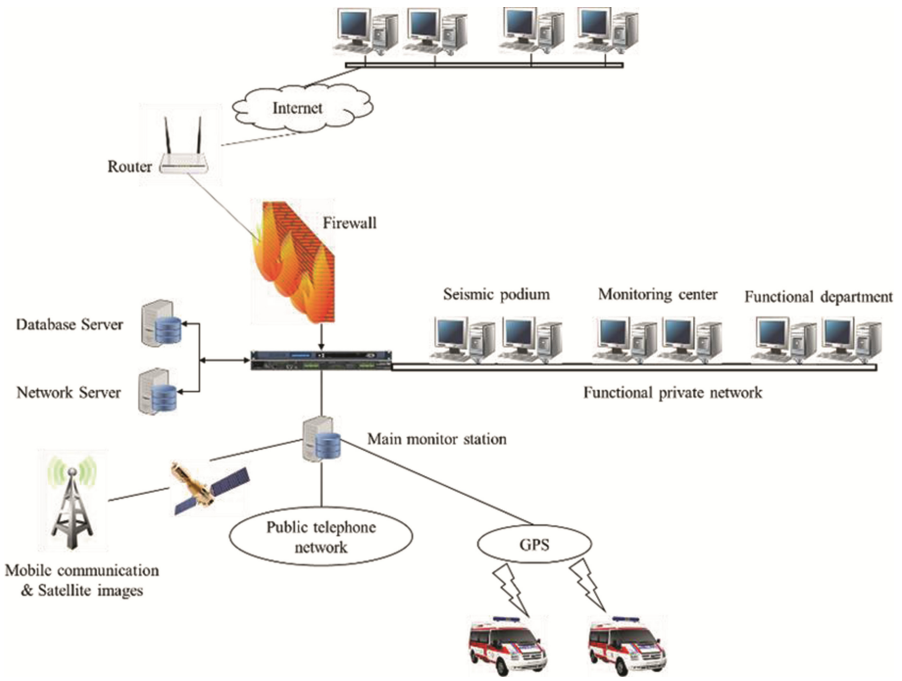

Fig. 1. System topology network structure

3.2 Functional Framework Design

The structure of earthquake emergency rescue command system adopts Client/Server (C/S) and Browser/Server (B/S). Client/Server (C/S) is applied to the private network, due to it has the characteristic of high security. Browser/Server (B/S) is applied to the public network, due to it is simple and it can remote access data. The system includes three layers (seen in Fig. 2).

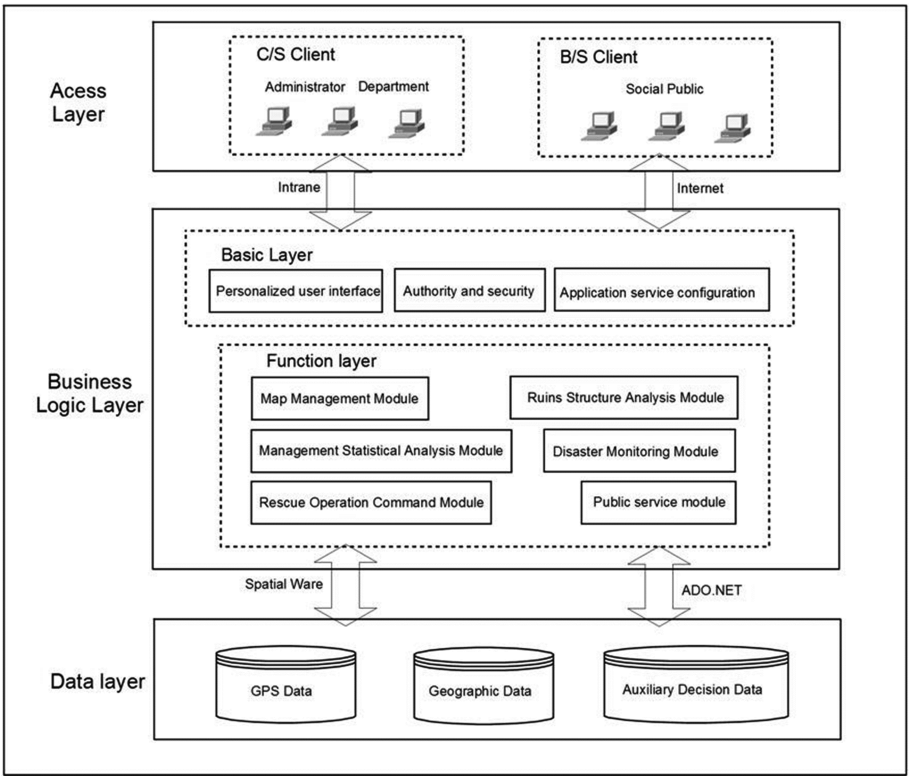

Fig. 2. System structure diagram

3.3 Access Layer

For the system administrators, the monitoring center staffs, command center staffs and other related functional department personnel, they have different permissions to access the corresponding function modules in private network; For the public, they can access some certain system function modules by the way of register or anonymity in the web service window.

3.4 Business Logic Layer

Business logic layer is the core of the entire system, which contains basic layer and functional layer. The functional layer is made up of the map management module, disaster monitoring module, ruins structure analysis module, management statistics module, rescue dispatch command module and public service module and other modules. The specific function are as follows:

(1) Map management module: display, scale, roam, label, distance, area, eagle eye, layer control, projection select, annotation style select and label style select etc.

(2) Disaster monitoring module: Real-time monitor the location, speed, direction, moving state of the vehicles and personnel, then understand the marching state of investigators, feedback the disaster information (degree and location of disaster) timely and form the disaster distribution map quickly.
(3) Ruins structure analysis module: predict the earthquake damage degree of buildings and analyze their vulnerability. According to the material type and structure to select suitable model to estimate the type of ruins.
(4) Management statistics module: manage and compute the relief supplies, count the number of casualties, calculate the speed curve rescue and collect the information of relief road etc.
(5) Rescue dispatch command module: according to the location and state of investigators, vehicles and relief routes and the feedback disaster information, commanders can implement the optimal path planning, dispatch supplies reasonably and distribute vehicles and personnel in real-time.
(6) Public service module: inquire information which includes attribute, location and request help etc.

In addition, basic layer is composed of personalized user interface, permission and safety, and application server etc.

3.5 Data Layer

The data layer is a place which stores the fundamental geographic data, GPS data and auxiliary decision data, it can be divided into the vector graphics data, map spatial data and attribute data according to the storage. Considering the characteristics of large amount of information data and high security requirement, this paper chooses Oracle9i relational database as the physical database. Through the spatial data engine Spatial Ware and ADO.NET, guarantee spatial data and attribute data are stored in the same and system can remote access them, so make sure the data are accessible, integrated, reliable and secure.

4 Key Tecnology

4.1 Location Data Collection

According to the recent research of earthquake disaster rescue, we learn that the critical period of relief is 1 to 5 days, especially 2 days. Because it is the golden age of rescue and the trapped person have high survival rate during the period. Based on the accurate location, we can confirm the position of trapped person quickly, so it can save the rescue time.

Real-time location data collection is the key of realizing precise location. Meanwhile it also plays an important role in earthquake emergency rescue, which can help us realize rapid response, decision, command, search and operation throughout the rescue process.

Real-time location data collection is received and decoded according to the real-time signal transfer (GPS receiver) [11]. At present, several GPS manufacturers follow

NMEA0183 protocol and computer communication, and the parameters of serial communication are as follows:

< CODE > Baud Rate = 4800 Data Bits = 8 Bits Stop Bit = 1 Bit no Barity < /CODE > .

Here, the GPS output data format adopts RMC and pattern of sentence is as follows:

… $GPRMC, 204148, A,3043.4531, N,12436.2514, E,57.12, 150904, ∗ 5D<CR><LF> …

The GP is the source of information, and RMC is the sentence pattern identifier, and the following are UTC (the format is hour, minute, second), GPS state (A is location state, V is navigation state), latitude (the first two are degree, the latter seven are point, and accurate to four decimal places), latitude symbols (N or S), longitude (the first three are degree, the latter seven are point, and accurate to four decimal places), longitude symbol (E or W), speed (unit is kilometer, even the total decimal point is five), UTC date (the

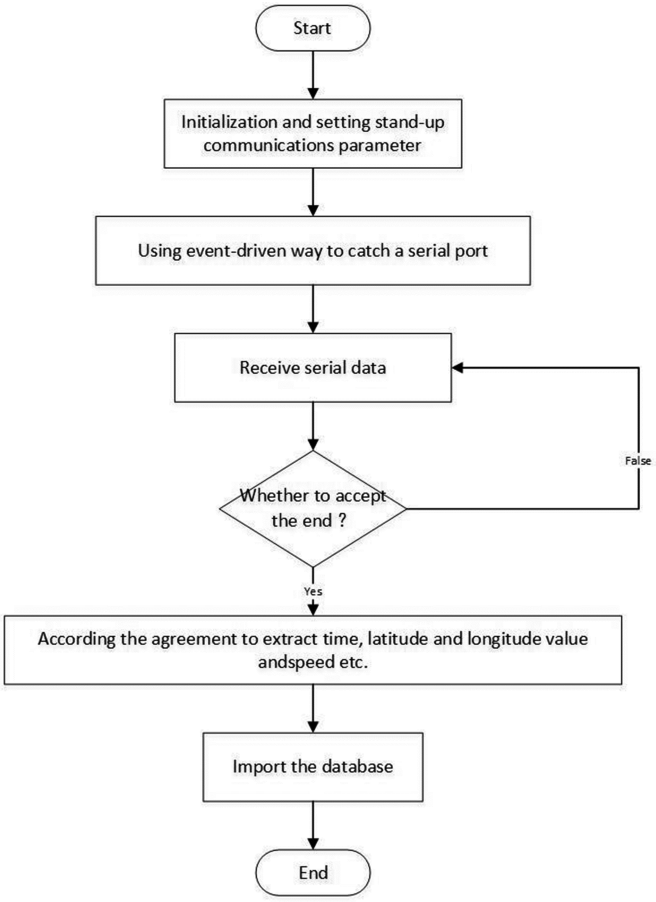

Fig. 3. Flow chart of GPS data collection and processing

format is day, month, year) and check code. <CR> is enter control character and <LF> is newline control character.

By means of serial communication interface MSComm controls to decode and extract the corresponding location information. MSComm (Microsoft Communications Control, MSComm for short) is ActiveX controls which can provide the simplified approach to send and receive data, then conduct serial communication programming under the Windows. Due to MSComm controls is not in the common tool window of Visual Studio.NET, firstly we must add and register before use it. The flow diagram of GPS data collection and processing is seen in Fig. 3.

In Fig. 3, the operations of setting the serial communication parameters include: set the communication port number, set the communication protocol, set the input mode, setting up the size of input buffer and transmission rate. The system adopts the Event-driven mode which is equivalent to the general process of the interrupt mode. When the serial port occurs event, MSComm will produce OnComm event. Event-driven mode is a very effective way to deal with the interactions of serial port, so it has the advantages of high efficiency, accuracy and simple programming etc.

Adding the real-time location data to the new temporary layer and set it to be editable state, then add mark which size, color, shape can be defined according to the requirements. Finally, it can highlight on the map and the real-time location implement interface is seen in Fig. 4 (Star is the locating position).

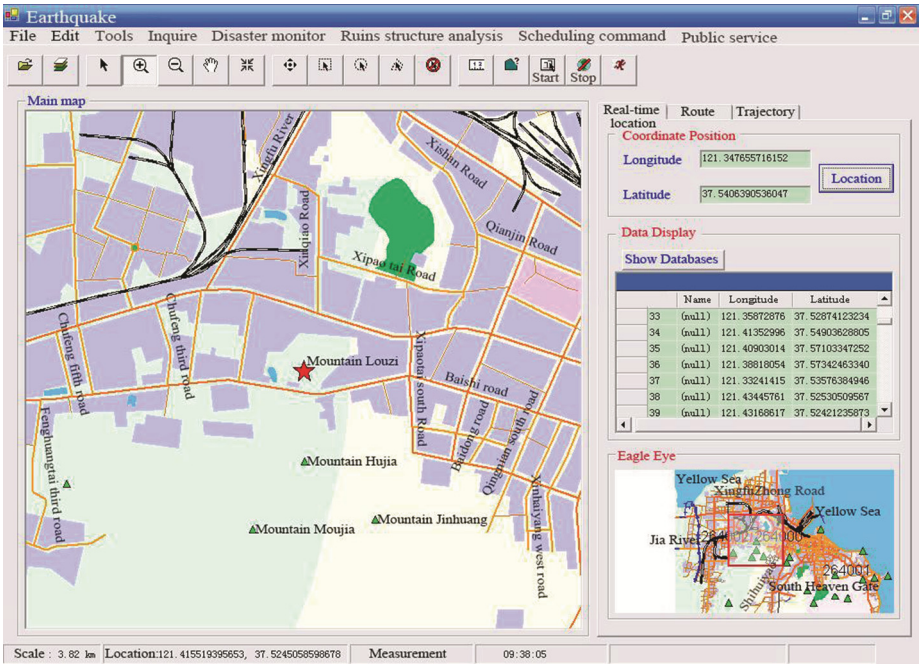

Fig. 4. Real-time location implement interface

4.2 Optimal Rescue Path Planning

In the earthquake relief, the vehicle scheduling is one of the most common and effective methods [12]. Due to rescue dispatch have some decision objectives, so we can't directly calculate the optimal by the shortest route model. Firstly, time is one of the most valuable resources, so it can't be ignored under the emergency rescue conditions; Secondly, due to the different road environment, different topography and different degree of the gravity of the situation, so the dangerous degree of every roads is different, so we calculate the probability to describe the possibility that vehicles pass the road safely, and put it as safety decision attribute of rescue dispatching. Therefore, put time and safety as the decision goal is the key to solute the optimal path. As we know, the genetic algorithm has the advantages of global optimization and potential parallel, and has certain advantages of solving the optimal path [9]. But the traditional genetic algorithm will produce a large number of invalid paths, in order to improve the efficiency of solving the optimal path and avoid the "premature" phenomenon, the paper adopts the improved genetic algorithm to solve the problem [13].

4.3 Mathematical Model of Optimal Path

The data model of the optimal path is described by graph theory: $G = (V, \{E\})$, where V is the set of nodes (i.e., the intersection), E is the set of sides. On each side E there is a t_{ij}, indicating the cost time pass by the road, which value can be calculated that the length of road divided by the average speed that earthquake doesn't occur.

In order to choose the best path which costs time least and safest, it also need to process data by calculating the probability. Assume that V_i and V_j are the ends of road and P_{ij} is the probability of passing safely from V_i to V_j. Due to the road is composed of several sections, so the total probability is equal to the product of the probability of each section. For example, suppose that $V_1 \rightarrow V_4 \rightarrow V_5 \rightarrow V_7$ this line is remarked as x, then there is:

$$P_x = P_{14}P_{45}P_{57} \tag{1}$$

For the probability of safety, we need transfer the indicators for it, and make it obey the basic calculation law. On both sides of formulation (1) take the logarithm and add negative sign.

$$-\lg P_x = -\lg P_{14} - \lg P_{45} - \lg P_{57} \tag{2}$$

Due to $0 < P_{ij} \leq 1$, so $-\lg P_{ij} \geq 0$. The probability of passing road safely is greater the value of $-\lg P_{ij}$ is smaller. Therefore, taking $-\lg P_{ij}$ as an index parameter of each section, the objective function of the optimal path can be obtained as follows:

$$minZ = min\left(\alpha_1 \sum t_{ij} + \alpha_2 \sum \left(-lgP_{ij}\right)\right) \tag{3}$$

Where $0 \leq i, j \leq n$, n is the number of vertex; α_1 and α_2 are weighting coefficients and indicate the importance of the two different indicators which are time and safety respectively.

4.4 The Improved Genetic Algorithm

(1) Chromosome Coding Presentation. A path is equivalent to a chromosome. Chromosome coding can't adopt the pattern of numerical encoding of traditional genetic algorithm, instead of the node sequence of the path. In this way, can express the practical significance of path directly and specifically, and it is helpful for selecting the fitness function and calculating the adaptive value. The number of node is gene. Due to the optimal path shouldn't include the loop, so there is no repeated genetic code in the chromosome. The first gene is the origin of path, and the last gene is destination of path, so the length of chromosome is varied, but maximum length can't be greater than N (N is total number of nodes). Chromosome gene in the first place always the path of the source node, the last node location gene is purpose, dyeing Is changing the length of the body, but may not exceed the maximum length N (N nodes of undirected graph). The storage structure of chromosome adopts linked list which advantages is that it can be insert and delete nodes dynamically.

(2) The generation of initial population. The traditional genetic algorithm generates the initial population randomly, but it will produce a large number of invalid path. The individual of initial population can't be broken circuit or loop, otherwise the evolution will be meaningless. In order to solve this problem, the specific process is as follows: start from the origin, and select the near point as the next node randomly and repeatedly, until find the destination, so it will not occur the broken circuit. Meanwhile in order to prevent the loop appearing, stipulate that the selected node of path will be marked, only the no marked node can be chosen for the node of new path, then the mark will refresh after the selection of every path.

(3) Fitness function. According to the formula (3), calculate the objective function value *Min Z*, The fitness function is as follows:

$$f(x) = \frac{1}{Min\ Z} \tag{4}$$

Min Z value is smaller indicates that $f(x)$ is better, and the corresponding solution is closer to the optimal solution. It can be seen from the fitness function that the optimal path will have the largest fitness function value.

(4) Selection. The function of selection is to choose good individuals to participate in breeding. Firstly, calculate the fitness function value; secondly, sort them from large to small. Select the individual in the form of roulette, the selection probability of an individual is proportional to its fitness function value, so the fitness function value is greater, the probability of being selected is higher [14]. If the same chromosome is produced, only one remained, the rest are deleted, and repeat the process until complete individual selection.

(5) Crossover. Recombining the partial genes of two individuals are to find better individuals. Traditional genetic algorithm recombines at one or more points randomly, and it is easy to appear the broken circuit or loop. For the specific needs of path, this paper adopts the mode that crossover once at the first repeated point except the start and end points. For example, a pair of parent individuals from the start node 1 to the end node are G_1 and G_2, imply as follows respectively:

$$G_1(1, 3, 5, 6, 7, 8, 9)$$

$$G_2(1, 2, 4, 5, 8, 9)$$

It can be seen that the crossover of two individuals is node 5, and this will generate the new individuals $G_1^{'}$ and $G_2^{'}$:

$$G_1^{'}(1, 3, 5, 8, 9)$$

$$G_2^{'}(1, 2, 4, 5, 6, 7, 8, 9)$$

After crossover, it will generate repeated gene in the chromosome and indicate that appear the loop which must be deleted. This paper adopts the mode that delete the gene before from the front to last repeated gene to remove the loop. For example, when the gene G, $G(1, 2, 3, 4, 2, 6, 8, 9)$ occurs the loop, deletes $(2, 3, 4)$, then gains $G^{'}(1, 2, 6, 8, 9)$.

(6) Mutation. In order to increase the variety of population and prevent them premature, population adopt the mutation operators to change one or more genes of selected individuals. But it can't mutate randomly like the traditional genetic algorithm which can produce the broken circuit and loop phenomena easily. Due to the heuristic search algorithm has the characteristics that it can calculate the local optimal solution rapidly and exactly, this paper introduces it to mutation, the procedures of path mutation are as follows:

1. Setting the size of the mutation individual is M, and select the node i $(i = 2, 3, \ldots, M - 1)$ randomly from parent generation;
2. Search all nodes that they are near the node i $(i = 2, 3, \ldots, M - 1)$, except the start and end, remarked as N_m.
3. Apply the heuristic search algorithm to produce the optimal path r_1 from start node i to the end node j.
4. Apply the heuristic search algorithm again to produce the optimal path r_2 from the end node j to the start node i.
5. If the path r_1 and r_2 don't exit the repeated nodes (except node j), the paths will be given up and don't mutate. Otherwise, the two paths will be the new individuals of mutation, and it can prevent the broken circuit appearing.

4.5 The Implementation of Algorithm

Step 1: Import the topological road network from the topology file.
Step 2: Determine the algorithm parameters, including size of population, number of heredity, genetic algebra, crossover rate, crossover rate, and mutation rate etc.
Step 3: Initial population.
Step 4: Evaluate the fitness of individuals in the population.
Step 5: Judge whether the algorithm rule is satisfied. If it is satisfied, the output will be matched according to the node number of optimal path, and generate in the electronic map, then exit. Otherwise, continue to the next step.
Step 6: Select according to the fitness value.
Step 7: Crossover according to the crossover rate.
Step 8: Mutate according to the mutation rate.
Step 9: Return to step 4.

5 System Simulation Application

According to the simulation application, this system is accurate in earthquake emergency rescue and complete the test in the Yantai city electronic map, the accuracy of location is less than 5 m. In the experiment, there are selected 67 nodes and 89 paths (except the loops) in the road network, and the Euclidean distance between origin and destination

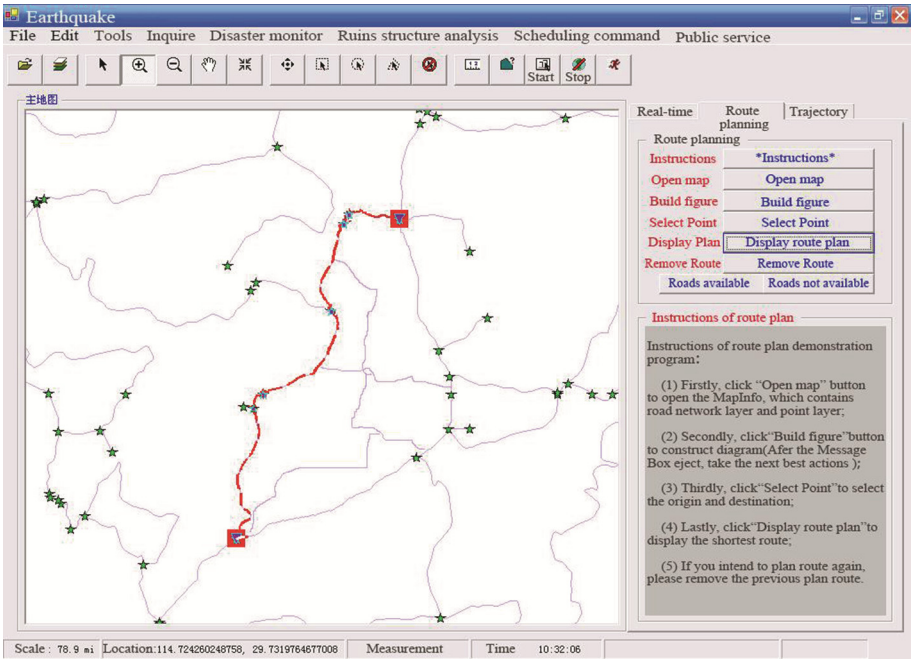

Fig. 5. The optimal path output results

is 41 km. The initial population of the experiment is 100, and the maximum number evolution is 50, the probability crossover is 0.7, the probability of mutation was 0.01, α_1 and α_2 adjustment coefficients are 0.73 and 0.27. The optimal path of improved genetic algorithm is seen in Fig. 5, the distance of optimal path is 46.3 km, the consumption time of this algorithm is 0.81 s, and the number of node in path is 34.

The adaptive values and convergence curves of traditional genetic algorithm and improved genetic algorithm are seen in Fig. 6. The adaptive value of improved genetic algorithm is 0.117, number of convergence is 21, but the adaptive value of traditional genetic algorithm is 0.115, number of convergence is 30. The results show that by using the improved genetic algorithm to plan the optimal path can search the global optimal solution rapidly and effectively.

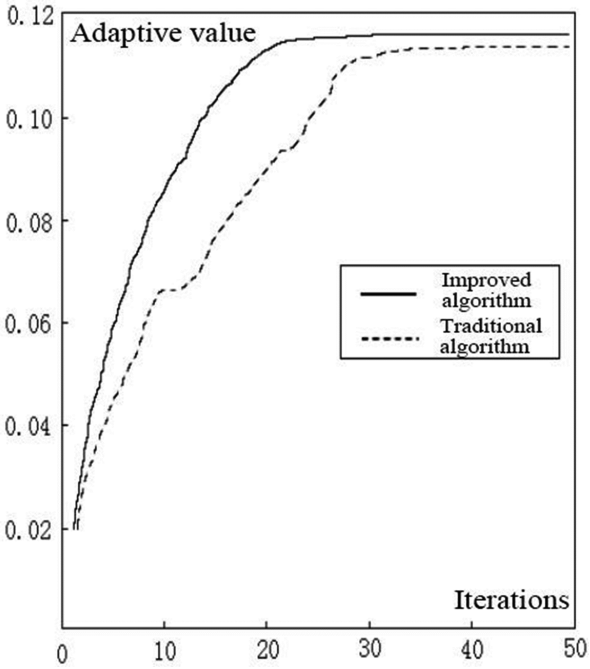

Fig. 6. Traditional genetic algorithm and improved genetic algorithm contrast

6 Conclusion

This paper proposes GIS and GPS based design and implementation of earthquake emergency rescue system, and studies the key technologies deeply, and the system is applied to the earthquake emergency command process. The system is developed to implement GPS data collection, and it realize the accurate real-time location. The paper adopts the improved genetic algorithm to eliminate the invalid paths and realize the rescue optimal path planning rapidly and accurately, so it improves the performance of system which can schedule real-time and dynamically. Therefore, the system is universal

which can be applied to the emergency rescue monitoring, scheduling and management of natural disasters and public health emergencies.

Acknowledgement. This work is supported by College of Surveying and Geo-Informatics of ShandongJianzhu University. The authors are grateful for the reviewer of initial drafts for their helpful comments and suggestions.

References

1. Deshi X, Xiong S, Hong C, Chonggang M, Jiansheng H (2004) Summarization of earthquake emergency and rescue in China. Recent Dev World Seismolog 6:1–7
2. Chonggang M, Hongsheng H, Xiaofeng X, Zengjie F, Fanluan S (2009) The recent development of the emergency management system. Overview Disaster Prev 04:20–31
3. Liu X (2010) Design and realization of thematic map quick mapping for rescue work of earthquakes based on ArcGIS engine. Southwest Jiaotong University
4. Shi Y (2010) Model design and analog modulation of emergent earthquake recue system based on CAS theory. China University of Geosciences, Beijing
5. Wang J (2013) GPS real-time relative positioning and its application in earthquake early warning. Institute of Seismology, China Earthquake Administration
6. Zhang Z (2013) The research on integrated seismic acquisition and processing based on high precision positioning. Jilin University
7. Yuan Y, Wang D (2008) Path selection and algorithm for emergency logistics management. Comput Ind Eng 56(3):1081–1094
8. Jotshi A, Gong Q, Batta R (2009) Dispatching and routing of emergency vehicle in disaster mitigation using data fusion. Soc Econ Plan Sci 43(1):1–24
9. Xie H, Zhang X, Yuan Z, Yu X (2005) Best path analysis of emergency decision system based on improved genetic algorithm. Comput Appl 25(04):737–738+789
10. Fan L (2012) Research on vehicle routing problem of emergency logistics based on genetic algorithm. Xi'an University of science and Tecnology
11. Shubi Z, Liu ZC (2002) Design and implementation of vehicle monitoring system based on GIS. Bull Surv Map (6):31–33
12. Jin X, Zhang G, Li J, Chen H (2004) Research and realization of emergent scheduler technologies based on GIS. Comput Eng 30(20):180–182
13. Wang XP., Cao LP (2002) Genetic algorithm—theory, application and software realization. Xi'an Jiaotong University Press
14. Ahn CW, Ramakrishna RS (2002) A genetic algorithm for shortest path routing problem and the sizing of populations. IEEE Trans Evol Comput 6(6):566–579

Analysis on the Role of Transport Equipment Standardization in the Development of Multimodal Transport

Xue-li Zhang[1,2], Chen Li[1,2(✉)], Chao-zhi Huang[1,2], and Yi Xu[3]

[1] Key Laboratory of Communication of Transport Vehicle Operation Safely Technology, Beijing 100088, China
c.li@rioh.cn
[2] Research Institute of Highway, Ministry of Transport, Beijing 100088, China
[3] School of Transportation and Vehicle Engineering, Shandong University of Technology, Zibo 255049, China

Abstract. As an intensive and efficient mode of transport organization, multimodal transport embodies the results of the comprehensive transport system and the overall level of the development of the logistics industry. Compared with the international advanced level, the development of multimodal transport in China is still in its initial stage, so that the standardization of transport equipment is more significant for the development of multimodal transport.

1 Introduction

Multimodal transport was first found in the Warsaw Convention of 1929 (the Uniform Convention of Certain Provisions about international air transport) [1]. China's transport industry standard "multimodal transport of goods terminology" (draft) defines the multimodal transport as a mode of transport which goods are loaded by an unmodified carrier unit, are transported in two or more modes one after another, and are not operated in the rapid transit process of transport modes. Multimodal transport combines the advantages of a variety of modes of transport and has unparalleled advantages than other transportation organization forms. Such as: reducing the turnover time of cargo freight, improving transport efficiency and reducing the risk of damage and loss of goods; reducing the complexity of documents and procedures; reducing the full cost of transport related; reducing the total cost of logistics [2]. The quickly built multimodal transport system with smoothly infrastructure interlinks, efficient transport organization, advanced transport equipment widely used, internet sharing of information resources, perfect regulations and standards, can speed up the development of multimodal transport, and is not only important measure of the expansion of effective supply in the current field of transport and the developing reform of the supply side, but also important to promote the long-term stable and rapid development of China's economy and to build a well off society in an all-round way. Transport equipment is the carrier and tool of goods transport, the standard is the technical support of economic activities and social

X. Zeng et al. (eds.), *International Symposium for Intelligent Transportation and Smart City (ITASC) 2017 Proceedings*, Smart Innovation, Systems and Technologies 62, DOI 10.1007/978-981-10-3575-3_15

development, from the current stage, the transport equipment standardization is the basis of multimodal transport development.

2 The Equipment of Multimodal Transport

The multimodal transport equipment is the main carrier, tool and material basis of multimodal transport [3]. According to the usual classification method, the multimodal transport equipment mainly includes the following categories:

(a) Logistics unit: transportation pallet, container bag, cage container etc.
(b) Loading unit mainly refers to three classes of units: the container (ISO international standard container; inland container; special container such as refrigeration container and filling container), semi-trailer (highway freight trailer; semi-trailer both used in highway and railway, etc.), swap-body (Europe swap-body).
(c) Delivery unit: special equipment with standard delivery unit, including railway car, semi-trailer special rolling ship etc.
(d) Transport equipment: special equipment which can conveniently replace standard carrier units between different modes of transport, including semi-trailer, hoisting equipment (top and bottom hanging crane), rolling equipment (roll on/roll off of highway-railway, highway-waterway, railway-waterway).

3 Standardization of Multimodal Transport Equipment at Home and Abroad

3.1 Abroad Research Status of Multimodal Transport Equipment Standardization

In the United States and Europe, a more perfect standard system of multimodal transport equipment has been established after more than half a century of development [4]. Van semi-trailer and inland container multimodal transport has become the main equipment both in the standard system of Europe and in the United States. Based on the standard of the United States and Europe limits about the value of vehicles size and quality, a rail transport semi-trailer and inland container standard has been established. Swap-body is included in the multimodal transport equipment series and standards in Europe. Important multimodal transport equipment like the hoisting and transport equipment of semi-trailer and inland container, the pallet and the railway car is included in multimodal transport system.

3.1.1 The United States Standard System of Multimodal Transportation Equipment

The limit of the size of the United States road vehicles is based on the United States Federal road vehicle standards, and quality limits meet the American bridge method on the trailer axle load requirements.

The size limit of the semi-trailer in United States is based on the United States vehicle standard, and the quality limit is based on the trailer axle load requirements for bridge regulation of the United States. The record system and product quality self certification system was implemented for the United States road vehicle products, and the implementation of compulsory certification system for railway vehicles [5]. Vehicle companies need to register in the United States Department of transportation information and record the production information, road vehicle enterprises in accordance with federal standards and industry standards for testing and self-certification. Railway products need AAR compulsory certification. If the products have quality problems or cause a traffic accident, the company should follow the recall system and recall the vehicles for maintenance or replacement. The related equipment standards to the carrying unit and standard pallet, sling and railway flatcar is shown in Table 1.

Table 1. Multimodal transport equipment and standard requirements of the United States

Equipment specifications		Standard	Outline Dimensions (mm)	Maximum Mass (Kg)
Class	Size			
Inland container	20, 28, 40, 45, 48, 53 feet	AAR M-930	maximum (53 feet) 16154 × 2600 × 2896	30,480
Semi-trailer	28, 45, 48, 53 feet	AAR M-931	maximum (53 feet) 16154 × 2600 × 4115	29,485
ISOcontainer	20, 30, 40, 45 feet	ISO 668 ISO 1496	maximum (54 feet) 13716 × 2438 × 2896	30,480
Standard tray	48” × 40” 40” × 40”	ISO 6780	1219 × 1016 1016 × 1016	
Spreader	40/60 t			40/60 t

(1) Van semi-trailer and inland container

In the multimodal transport equipment and technology system of USA, the American Association of Railroads (AAR) had made the rail transport semi-trailer van standard (AAR M-931) and inland container standard (M-930). AAR M-931 standard provides that the size limits of van trailer should comply with the United States standards for road vehicles, the quality limits should comply with the United States bridge method. AAR M-930 provides that the inland container standard is based on ISO 668, made a full range of ISO container in inland container standard, but according to the agreement between the States, some states add two kinds of standards such as container standard for 48 feet and 53 feet, and made the external dimensions of inland container for 2600 mm as the road vehicle standards. The standard of van semi-trailer and inland container of the United States was included in the ISO standard series, the size of mainstream pallet was

specified as 1219 × 1016 mm. The internal width of van semi-trailer and inland container can accommodate two long pallets of 1219 mm. 30 standard pallets can be placed in both semi-trailer and inland container of 53 feet.

(2) Hoisting and transport equipment

The hoisting position of inland container for rail and waterway in the United States is same as the ISO container, because of 45, 48 and 53 feet container set angle casting at 40 feet position that can be lifted and stacked. Except for the quay-crane, the gantry crane of container crane and semi-trailer, and the walking type crane can be used for container lifting. The maximum total weight of the container in USA is less than 30480 kg regardless of length, therefore, lifting capacity, the lifting coverage and the spreader parameters are provided in the AAR standard. The wrap-around crane and self-propelled crane of the van semi-trailer is shown in Fig. 1.

Fig. 1. The wrap-around crane and self-propelled crane of the van semi-trailer

(3) Railway flatcar

The railway flatcars of the United States are used for transporting van semi-trailer and container. Generally, the railway flatcars for transporting van semi-trailer have telescopic traction seat (for fixing king pin) which can be used for container double deck transportation when be packed up. At the beginning, as shown in Fig. 2, the horizontal loading system with a walking mechanism of the railway semi-trailer is fixed on the

Fig. 2. Railway semi-trailer in USA

special van semi-trailer, thus the van semi-trailer can move on the tracks. Container railway flatcar with ship structure and for double-deck container transportation, as shown in Fig. 3, can be divided into triple form flat and five form flat.

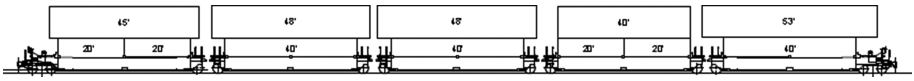

Fig. 3. Five form railway flatcar

3.1.2 European Multimodal Transport Equipment Standard System

European rail transport equipment standards include the European Union road vehicle standard 96/53 EEC, inland container standards, swap-body standard EN283, EN284 and the international railway union UIC standard [6].

European highway semi-trailers, containers and other products such as the swap-bodies should be mandatory certificated. Semi-trailers are in compliance with the EU vehicle certification and parts certification standards and need to do certification tests of several parts and vehicle system. The container and the swap-body also need to be certified and tested according to the relevant standards of the European inland container, the international standard container and the swap-body. Semi-trailer for rail transport and the swap-body should be certificated according to the EN12642, UIC596-5 testing standards, through third party certification test or witness test, be issued relevant certification and products label in line with the standard requirements, then these products can be placed on the railway for hoisting, fixing and transportation.

The railway transportation of the carrying unit should meet the requirements of 596-5 UIC and 571-4 UIC in the position of the semi-trailer, the container and the swap-body, the identification of fixing and hoisting. The European multimodal transport equipment standard is shown in Table 2.

(1) Van semi-trailer, inland container and swap-body

The three freight carrier unit as van semi-trailer, inland container and swap-body has formed a sound standard system with the development of technology for decades. The highway-railway transport semi-trailer is designed on the basis of the European standard EEC 96/53 for road vehicles, the length and width of inland container also need to comply with the size limit requirements of EU standards for road vehicles, namely the maximum width 2550 mm (refrigerator width: 2600 mm). The design for highway-railway transport van semi-trailer and swap-body should meet the test standards of EN12642 and EN283, thus maintaining the consistency of the requirements of the railway freight carriage. Put forward specific requirements of inland container A1371 strength standard requirements for container size, quality limits, FCL and components and testing, to ensure the coordination of size and quality standards of the vehicle and highway.

(2) Railway flatcar

The railway flatcar for semi-trailer, container and swap-body should comply with the International Union of Railways UIC 596-5 and UIC 571-4 on the requirements of the position and the identification of fixing and hoisting for the semi-trailer and the container swap body. The standard limits railway flatcar structure, size and fixed seat height series etc.

Table 2. European multimodal transport equipment standard

Equipment specifications		Standard	Outline Dimensions (mm)	Maximum Mass (Kg)
Class	Size			
Inland container	45 feet	A1371(draft)	13716 × 2550(2600) × 2896	34,000
ISO container	20, 30, 40, 45 feet	ISO 668 ISO 1496	13716 × 2438 × 2896	30,480
Swap-body	7150 mm, 7450 mm, 7820 mm	EN 283, EN 284	7150 × 2500 × 2670 7450 × 2500 × 2670 7820 × 2500 × 2670	16,000
Semi-trailer	Front turning radius 2040 mm, traction pin to the last 12000 mm	EEC-96-53 EN12641 EN12642 UIC 596-5	13720 × 2550(2600) × 4000	34,000(Total mass of semi-trailer train 40,000)
Standard tray		ISO 6780	1200 × 800 1200 × 1000	

3.2 Domestic Multimodal Transport Equipment Standardization

The current inland container contains three different size such as 20 feet, 40 feet and 45 feet, railway container special flatcars have two kinds of X6B and X70 with the development of shipping container [7]. The size and total quality of all kinds of transport equipment is shown in Table 3 [8].

China's logistics unit, loading unit and a carrying tool standards were made by the relevant departments themselves, the standard was unreasonable, poor economic benefit, and had not formed open intermodal equipment society coordinated environment, mainly existed the following problems [9].

(1) Pallet size can not match the container

At present, China's logistics unit, loading unit and a carrying tool standards were made by the relevant departments themselves, thus did not match each other. The interior size of the container is conflict with international standard pallet loading module. Such as series 1 container, the internal width is 2330 mm, if the standard size pallet of 1200 mm × 1000 mm is used, two parallel pallets will not be put in the container, and as shown in Fig. 4, only one vertical pallet and one horizontal pallet can be put in the container.

Table 3. Dimensions and total quality of transport equipment in China

Name	Specification	Length (mm)	Height (mm)	Width(mm)	Total Mass (Kg)
Container	20 feet	6058	2438	2591	30,480
	40 feet	12192	2438	2896	30,480
	45 feet	13716	2438	2896	30,480
Railway container special flatcar	X6B	16338	3220	1166	60,000
	X70	13466	3220	1169	70,000
Van semi-trailer		13750	2550	4000	40,000
Tray		1200	1000		

Fig. 4. Current situation of container and pallet matching

Thus, the container loading pallet will not be fully loaded, the interior space will not be effectively used, mechanical work will not carried out, the logistics efficiency will not effectively improved, and the logistics cost will not significantly reduced.

(2) Loading unit can not coordinate railway flatcar

Loading units and vehicle standards in our country are not coordinated [10]. Railway container special flatcar, container and semi-trailer and truck are not coordinated in size and load, this caused lose tons and low space utilization efficiency in multimodal transport. Such as the X70 special railway container vehicle, lose tons and space utilization deficiency will appear if two standard 20 foot container or one 40 foot containers are put in the vehicle. This is the reason of current China's railway proposing manufacturing and using wide containers.

(3) Lack of study on railway piggyback vehicle and its freight unit's standardization

Piggyback transportation has been developed in Europe and the United States and other countries for decades, and has a mature technology and standard. Because of the management system of our country, piggyback has just started. The standards of semi-trailers, inland containers and other industry standards are being developed because of the release and implementation of the national mandatory standard GB1589-2016 [11].

There's only two railway piggyback transport flatcars were trial-produced and test run, and it requires accumulating related experimental research and experience. Although there are foreign standards can be used for reference, but also should be adapted to the truth of China's railway, highway and water transport.

4 Thinking and Suggestion for the Standardization of Multimodal Transport Equipment in China

China's development of multimodal transport, transport equipment integration, standardization should be the basis and focus of recent development. China should establish coordinated multimodal transport standard systems, should make and revise a number of related transportation equipment standards, should increase the strength of the research, development, testing, certification and application of international container, inland container, semi-trailer and exchangeable container, should strengthen the research and use of large and efficient handling equipment and fast transport equipment, should develop special railway flatcars, highway-railway dual purpose semi-trailer and other specialized transport equipment and transport units, should develop piggyback highway-railway drop and pull transport technology and equipment, land and sea transport trailer roll-on technology and equipment, and should achieve seamless connection between drop and pull transport equipment and transfer equipment. Specific recommendations are as follows:

(1) The groups researching roads, waterways, railways, aviation sector related technology and standardization should be set up. Standard systems which can improve multimodal transport equipment and standards to be made and revised should be researched. Series of related standards should be made and revised in order of priority to support the development of multimodal transport.
(2) The national mandatory standards GB1589-2016 "cars, trailers and train the external dimensions, axle load and quality limit" were issued in July 26, 2016.

Table 4. Recommended values of the standard for inland container and swap-body

	The length (mm)	Width (mm)	Height (mm)	Weight (Kg)	Strength test
Wide inland container	13720	2550	2896	34000	Reference AAR930
Swap-body	7820	2550	2670	16000	Reference EN283

Note: cold storage box width is 2600

The technical requirements of the relevant semi-trailer, the standard of the inland container and the swap-body should be researched, made and revised in accordance with requirements of the national mandatory standards GB1589-2016. Recommended values of the standard for inland container and the swap bodies proposed as shown in Table 4.

(3) Special requirements of semi-trailer and related vehicle on the railway piggyback including the overall size, total quality, tight fixation and related strength requirements and tests should be researched and analyzed. And humpback trailer technical standards according with GB1589-2016 should be made.

(4) Related standards and requirements for semi-trailers, containers and other main freight units should be researched by railway transportation related research departments. Standards and requirements for multi function railway flatcar technology should be researched and made to meet the needs of the development of multimodal transport equipment.

(5) The adaptability of standard semi-trailers on rolling ships should be researched by related waterway transportation research departments. Requirements for rolling transport semi-trailer, special requirements and related bolt fixing requirements should be made to develop make the road transport semi-trailer can adapt to water transport as soon as possible, and to promote the development of multimodal transport.

(6) Freight unit total quality should be specified, the multimodal transport of goods transport station with tools such as tractor, hoisting equipment should be standardized to realize fast and safe transport.

References

1. Zhou G (2007) Analysis of development of the multi- modal transport. Logistics Sci-Tech 30:99–100
2. Li G (2014) Design of a hybrid hub and spoke network with capacity constraints. Chanan University
3. Chen F, Choi E, Epps J, Lichman S, Ruiz N (2005) A study of manual gesture-based selection for the PEMMI multimodal transport management interface. In: International conference on multimodal interfaces, pp 274–281
4. Janelle DG, Beuthe M (1997) Globalization and research issues in transportation. J Transp Geogr 5(3):199–206

5. Beresford A, Pettit S, Wang CC (2000) An analysis of multimodal transport routes for construction equipment in Vietnam. 《Aluminium》, September 2000
6. Gaillet J (1996) Towards realizing integrated European system architecture. Intell Transp Realizing Future Abstr Third World Congr Inteligente Transp Syst 13:156–178
7. GB/T 1413-2008, Series 1 freight containers-Classification, dimensions and ratings. China Standard Press, 20, Beijing
8. Yuan J (2010) Standardization of container multimodal transport and analysis of its economic motivation. Beijing Jiaotong University, Beijing
9. Li J, Zhao J, Wang J (2014) The problems of the standardization of container multimodal transport in our country. Traffic Stand 24:107–110
10. Ling S (2005) Current situation and Development Countermeasures of railway participation in international container multimodal transport in China. Transp Stand 1:75–77
11. GB1589-2006 (2016) Limits of dimensions, axle load and masses for road vehicles. China Standard Press, Beijing

Analysis of Urban Resident Bus Travel Decision with Physical Expenditure

Tengfei Yuan(✉), Xiaoqing Zeng, and Yujia Chen

The Key Laboratory of Road and Traffic Engineering, School of Transportation Engineering, Ministry of Education, Tongji University, 4800 Cao'an Road, Shanghai, China
yuantengfei2010@126.com, zengxq@tongji.edu.cn, 825674685@qq.com

Abstract. With the improvement of living standard of urban residents recently, people are more and more attention to the comfortableness, convenience and environmental quality of travel. Therefore, the study of the variation of physiology and psychology during trip has become a hot topic in the traffic domain, while bus travel is more sensitive to them. Based on the above description, this study uses the heart rate test and SP survey to obtain the subjective and objective data of physical expenditure during the bus trip, and get the main factors of physical expenditure by analyzing the survey data. Then, by establishing the logistic regression model to analyze the relationship whether the relevant factors of physical expenditure are considered and the result show that the factors of physical expenditure can reduce the probability of bus travel choice.

Keywords: Physical expenditure · Heart rate test · SP survey · Bus travel decision · Logistic regression model

1 Introduction

Public traffic is vital to the urban transport system, but the low service quality of public transport and low bus sharing rate have been widely accepted [1]. Therefore, while focus on developing public traffic, we should pay close attention to the quality of bus service, in order to meet the demand of public traffic travelers. Especially the quality of regular bus service, which directly impacts on the choice of bus travel, because it can describe the process of bus service and bus travel decision reasonably, as well as grasp the disadvantages of bus and factors of bus travel decision [2]. Only in this way, can improve the quality of bus service and attraction of bus.

On the perspective of public traffic service, we should explore the factors of bus travel choice and mechanism that affect bus travel decision to meet the demand of the contemporary tendency. In the process of travel, travelers not only have the time consumption and cost consumption, but also need physical expenditure to maintain basic physiological activities [2]. Hill defined the physiological cost that the travelers need to pay for travel as "physical consumption of travel behavior" [3]. With the improvement of economic, the sensitivity of economic factors have weakened gradually. According to analyzing the 20 consecutive years' statistical data, Robert Kull and Dirk Helbing

X. Zeng et al. (eds.), *International Symposium for Intelligent Transportation and Smart City (ITASC) 2017 Proceedings*, Smart Innovation, Systems and Technologies 62, DOI 10.1007/978-981-10-3575-3_16

found that physical expenditure is relatively constant compared with the time and cost factors [4]. Meanwhile the physical expenditure during bus travel is more sensitive than other travel modes, so we should give enough attention.

Based on the above background, this paper investigates and analyzes the data of physical expenditure during bus travel in Jinan City, and acquires the main factors of physical expenditure, then uses logistic regression model to quantitatively analyze the relationship whether the relevant factors of physical expenditure are considered. This paper expects that by studying the physical expenditure of bus travel to improve the bus choice rate and the quality of bus service, as well as have a certain significance for the future research.

2 Related Works

Physical expenditure e is the necessary energy that the body maintain normal temperature and various activities, and it is throughout the entire process of travel. So the relevant researches gradually pay attention to the physical expenditure of travel [16].

According to study the correlation between the travel decision behavior and the state of physiology and psychology, Van Ouwerkerk pointed out that travelers' physiological and psychological state have a certain affect the choice of the travel modes in some traffic situation [5]. Robert Kull and Dirk Helbing statistically analyzed the data of travel time, cost and consumption, and made a conclusion that the physical expenditure remains at a relatively stable state during the travel decision process, while the time and cost have declined a lot [4]. Li Congying put the physical expenditure as the impedance of accessibility to accurately assess the urban planning and transportation planning, and established non-motorized transportation accessibility model [6]. Guo Hanying established the urban passenger travel mode choice model based on the study of the passengers' physiological and psychological characteristics [7]. An Jian pointed that physical expenditure has an important role in process of travel decision by studying the objective physical expenditure and subjective fatigue perception in travel link [8].

Therefore, the physical expenditure has a significant impact on the travel decision, especial the more sensitive bus travel. The study refers to the bus (including regular bus and BRT), which service level is low and has the more obvious characteristics.

Bus the trip link usually contains many sub processes, which are going to bus station, waiting for the bus, on the bus and leaving the bus station. Particularly in the process of the bus ride, in order to maintain the body balance, travelers grasp the handrail to overcome the bump, which is caused by vehicles' acceleration, deceleration, turning and driving in the poor condition. Therefore, it is easy to increase travelers' physical expenditure and make body local tissue feel fatigue [9]. So when study the bus travel decision, we should consider not only the economic factors but also the physiological factors, such as physical expenditure. Economic factors mainly include personal income, time value, which determine the travel money budget (TMB) and travel time budget (TTB); physiological characteristics mainly perform energy expenditure (EE) and it mainly have a decisively impact on the travelers' energy budget (TEB) [2].

According to the above analysis, we conclude that the traveler's travel decision is not in accordance with a certain order, but integrates the travel mode, travel time, route, and many other factors [2]. Thus, estimating the travel time, costs, together with the physical expenditure can be more accurately defined as a real travel decision process. Simultaneously, physical expenditure of bus is more sensitive than other travel modes, it is key to consider physical expenditure for making bus travel decision.

3 Data Collection and Analysis

3.1 Data Collection Methods

In order to assess the physical expenditure scientifically during human activities, a lot of scholars have used a variety of methods for decades, and specific methods can be divided into six categories: (1) behavioral observation; (2) questionnaire, including diet records, recalls and interviews; (3) heart rate monitoring method; (4) indirect calorimeter calories count or breathing assays; (5) double-labeled water method; (6) mechanical or electronic motion sensor method (such as three-dimensional accelerometer) [10]. Among them, the first two methods are too subjective and poorly objective, so we should combine these methods to research the bus choice behavior.

In order to study the bus decision behavior under physical expenditure systemically, this study combined the subjective and objective methods, which are heart rate detection method and SP survey. Since previous studies have found that the heart rate has a good linear relationship with the physical expenditure [11]. Hence, this research monitors heart rate of the bus traveler as a way to collect the objective data, and the SP survey is selected as a way to collect the subjective data.

3.2 SP and RP Survey

The purpose of the survey is to collect the subjective and objective data of physical expenditure and explore the characteristics of travel behavior under physical expenditure. This study selects Mio Alpha wrist to measure heart rate, which is easy to operate and it need not wear the chest strap, and it can measure heart rate accurately and frequently. At the same time, the respondents are required to be independent, normal and 11 years old or older.

As we all know, setting the options is vital to the survey. Many factors affect the bus travel behavior and some are difficult to acquire, so this research sets the survey options carefully and systematically (Fig. 1).

(1) Setting the objective survey options. The scope of the investigation includes personal attributes and bus travel behavior characteristics. Personal attributes are composed of gender, age, occupation, personal income and whether own private vehicles [12]. Due to actual bus travel behavior contains many sub processes, so the investigation should include the average heart rate of each process, trip purpose, start time, the time of arriving at bus station, the time of waiting for bus, the numbers

of transfer, the load condition, the seat status, the time of bus ride and private traffic condition, etc. (Figs. 2, 3 and 4)

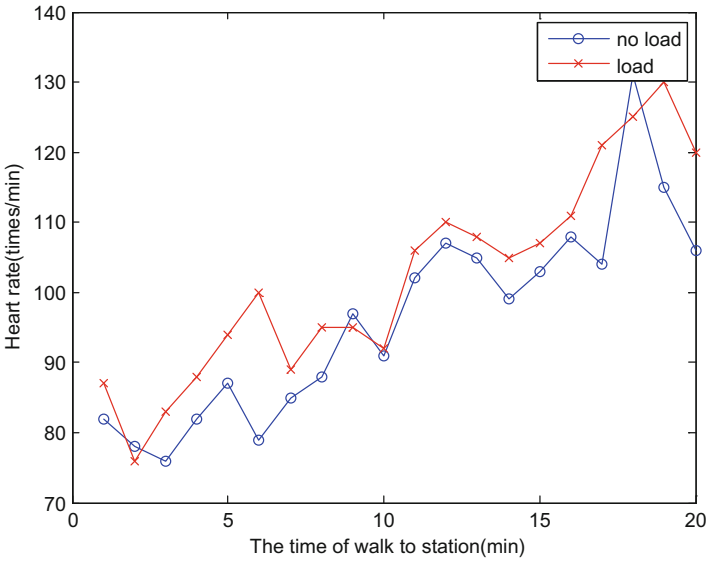

Fig. 1 The relationship between heart rate and time of walk to station

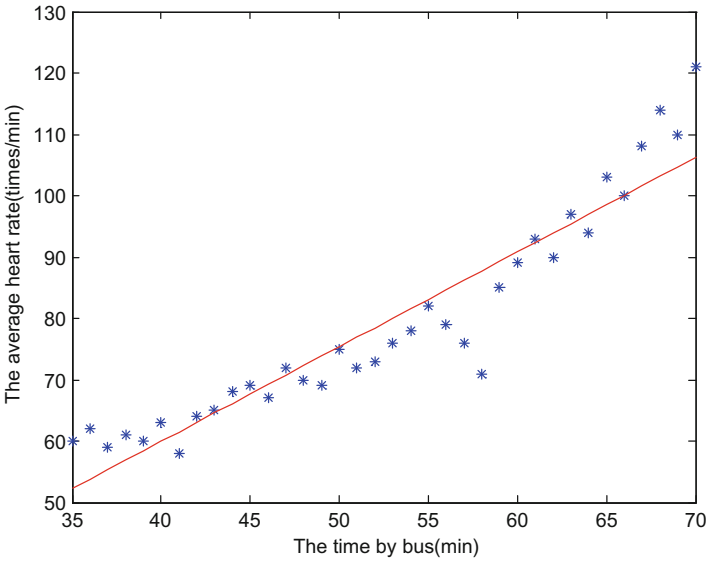

Fig. 2 The relationship between average heart rate and time by bus

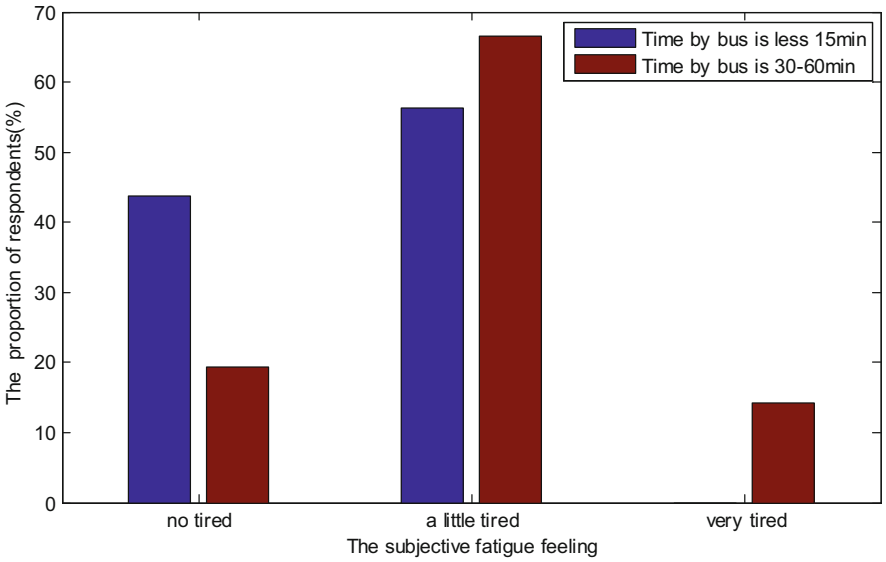

Fig. 3 The relationship between the subjective fatigue feeling and time by bus

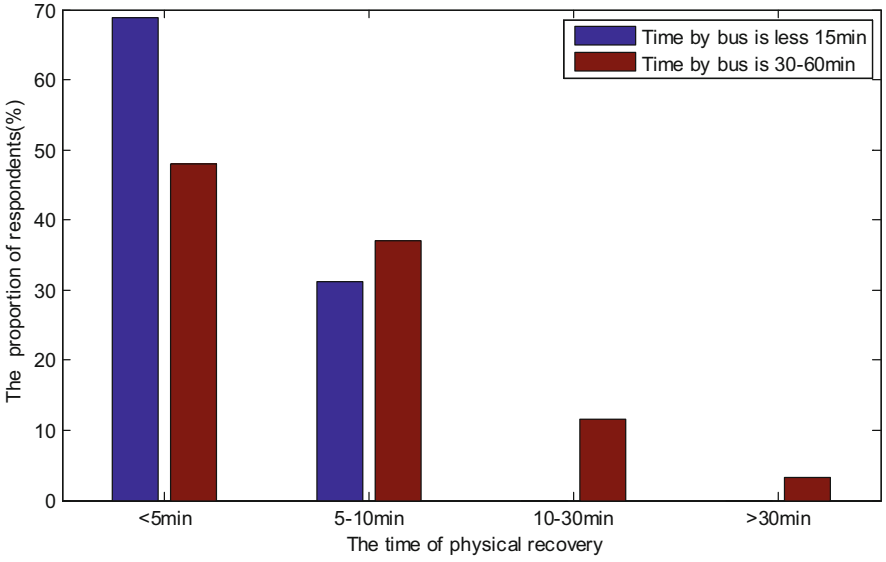

Fig. 4 The relationship between the time of physical recovery and time by bus

(2) Setting the subjective survey options. If the subjective options were set too many, the respondents are difficult to answer [11], so this survey put results of bus choice

as the most direct solution under many factors, especially the physic expenditure (Figs. 5, 6 and 7).

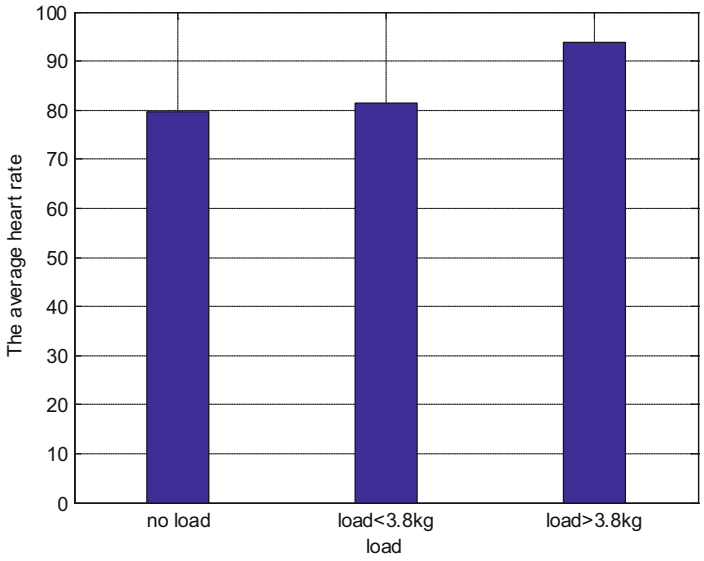

Fig. 5 The relationship between the average heart rate and load

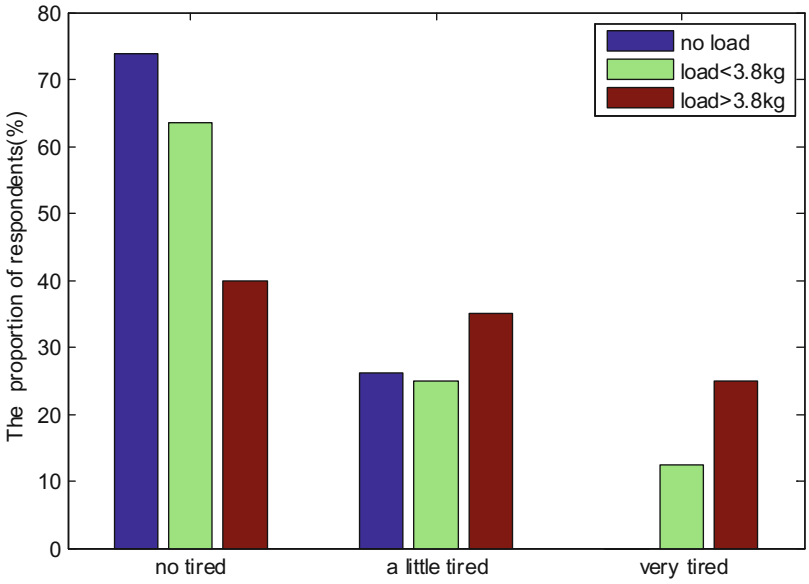

Fig. 6 The relationship between the subjective fatigue feeling and load

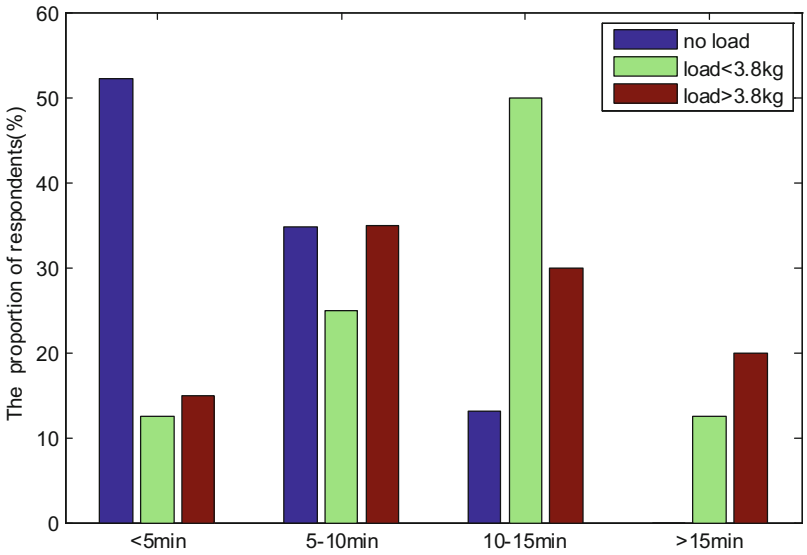

Fig. 7 The relationship between the time of physical recovery and load

In order to better reflect the impact of physical expenditure on bus travel decision, this research set the related options, which are the subjective fatigue feeling and physical recovery time. Due to the definition of fatigue feeling is rather vague, we classified the

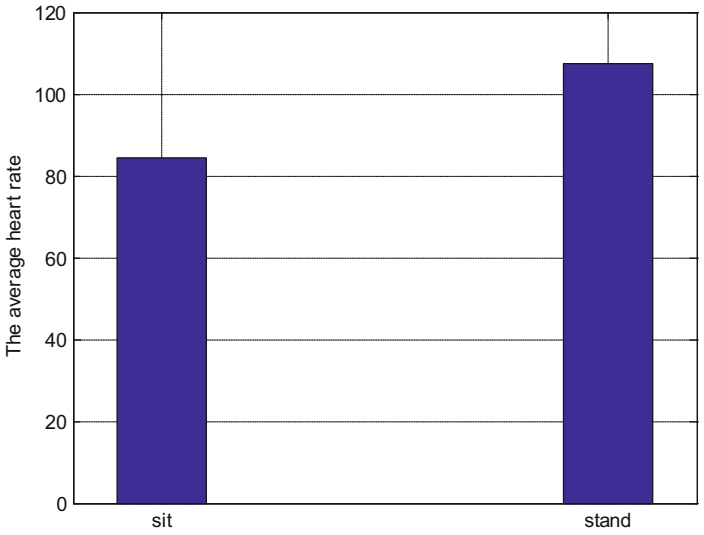

Fig. 8 The relationship between the average heart rate and seat

level of fatigue by no tired, a little tired and very tired and classified the recovery time by less than 5 min, 5 ~ 10 min, 10 ~ 30 min and more than 30 min. Lastly, design the questionnaire by specifying the above setup options (Figs. 8, 9 and 10).

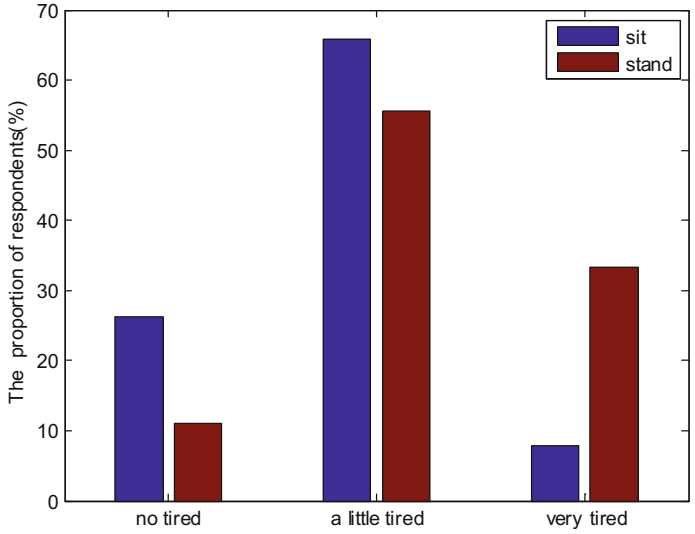

Fig. 9 The relationship between the subjective fatigue feeling and seat

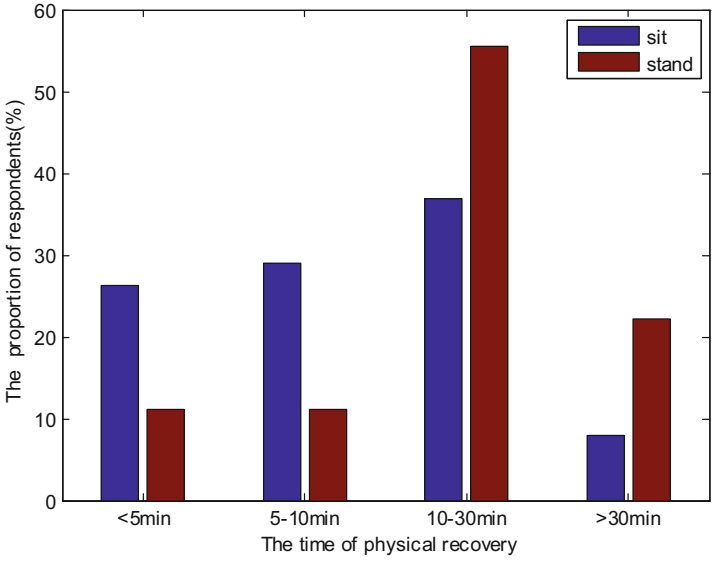

Fig. 10 The relationship between the time of physical recovery and seat

(3) Implement the investigation of physical expenditure. This survey selects some typical bus lines in Jinan city as respondents, and the passengers are in different ages, and requested to fill out this questionnaire. In this way, the survey obtains 600 valid questionnaires (Fig. 11).

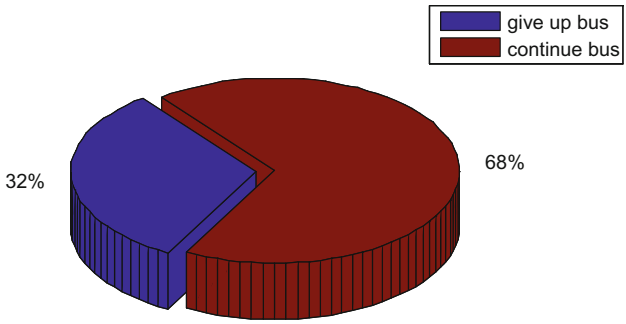

Fig. 11 The bus travel decision under the subjective fatigue feeling

3.3 Survey Data Processing and Analysis

After processing the survey data found that the coverage of this study covers relatively average, and consistent with the distribution of trip indicators in Jinan City. Through the analysis of survey data, this study acquired the following conclusions.

(1) Regardless of age and sex, under the same load condition, people walk to bus station for longer, the average heart rate is greater.
(2) When take bus longer, the average heart rate is higher, as well as more and more people feel very tired, so they need more time to recover.
(3) When the load is heavier, the average heart rate is higher, and more and more people feel tired, so they need longer recovery time. 3.8 kg is a significant division, when load is more than 3.8 kg, the heart rate increases more obviously and rapidly, so more and more respondents easily feel very tired.
(4) When stand by bus, the average heart rate is significantly higher than when sit by bus, and more and more respondents were easily to feel tired, so they need more time to recover, even there is considerable proportion of respondents need more than 30 min recover.
(5) In the SP survey, if the respondents encounter the similar subjective fatigue feeling, the results of bus travel decision are that there are 31.67% of the respondents choose to give up bus travel and consider to select other modes of transportation; as well as 68.33% of those continue to choose bus travel.

Therefore, by analyzing the results of survey found that the physical expenditure of the bus travel mainly connect with travel time, load condition and seat availability. When travelers make travel decision, if considered the factors of physical expenditure, they

may abandon bus travel. Next, it is necessary for this research to establish an appropriate model to explore the relationship between physical expenditure and bus travel decision.

4 Bus Travel Decision Research

This study puts the result of bus travel decision as the dependent variables, and puts the factors of bus travel decision as independent variables, so the logistic regression model to quantificational can describe the relationship between the bus decision and factors, especially the factors of physical expenditure. This paper is considered in the case of physical expenditure whether selecting bus travel is a dichotomous variable, with $Y = 1$ said to select bus travel, with $Y = 0$ that does not choose bus. Because of the linear regression analysis of bus travel decision is lack of rationality, and Logistic regression can meet the requirements of such problems [13].

4.1 Logistic Regression Model

The main reason for choosing the logistic regression model is that the model can deal with the classification data effectively, including continuous data, and there is almost no restriction on the explanatory variables. The establishment of the regression model is the same as other traditional models, and they are mainly used to dig the inherent laws of the data and measure the dependent relationship between the explanatory variables and the dependent variables, or provide some advanced information for the decision makers to make more appropriate decision [14].

In practical problems, we often study the relationship between the probability of a random event A occurs and some certain factors. If A occurred, $Y = 1$; if it doesn't occur, $Y = 0$. The number of observed indicators is p, and record them as $X = (X_1, X_2, \ldots, X_p)$. The probability of event A occurring under the P factors can use logistic regression model to express, as shown in the following Formula 1 [15]:

$$P\{Y = 1\} = \frac{exp(a + b_1X_1 + \ldots + b_pX_p)}{1 + exp(a + b_1X_1 + \ldots + b_pX_p)} \tag{1}$$

In Formula 1, the value of X_i is arbitrarily ranged; and the value of P is bound between 0 and 1; $\beta_j (j = 1, 2, \ldots, p)$ is the parameter of the model, and is also called regression coefficient; we can use the maximum likelihood estimation to calculate it. In the Logistic model, $X_1, X_2, \ldots, X_p$ need not be continuous variables, some of them may take a few values, can also be qualitative variables. Therefore, using this model to analyze the relationship between the behavior of bus travel decision and its factors has a certain advantage.

4.2 Establishment of the Model

This study chooses the main factors(include the factors of physical expenditure) of bus travel decision as options, which are trip purpose, start time, the time of arriving at bus

station, the time of waiting for bus, the numbers of transfer, the load condition, the seat status, the time of bus ride and private traffic condition, the specific assignment in Table 1.

Table 1. The options of bus travel decision

Variables	Factors
X_1	Trip purpose
X_2	Start time
X_3	The time of bus ride
X_4	The time of arriving at bus station
X_5	The time of waiting for bus
X_6	The numbers of transfer
X_7	The load condition
X_8	The seat status
X_9	Private traffic condition

Based on the survey data of urban resident bus travel decisions in Jinan City, this research uses software SPSS to test the statistical significance of survey results in the logistic model. It shown that the factors $X_1, X_2, \ldots, X_p$ have a significant effect on the probability of bus choice $P\{Y = 1\}$. As well as the establishment of appropriate Logistic model is meaningful, and further calculate parameters of factors of bus travel decision, such as maximum likelihood estimation, standard deviation and correlation value, etc. as shown in Table 2.

Table 2. The maximum likelihood estimation of parameters

	B	S.E,	Wals	df	Sig.	Exp (B)
X_1	0.182	0.073	6.183	1	.013	1.199
X_2	0.241	0.143	2.849	1	.091	1.272
X_3	−0.470	0.155	9.154	1	.002	0.625
X_4	−0.007	0.121	0.003	1	.957	0.993
X_5	−0.057	0.130	0.189	1	.663	0.945
X_6	−0.238	0.158	2.280	1	.131	0.788
X_7	−0.309	0.130	5.615	1	.018	0.734
X_8	1.215	0.192	39.886	1	.000	3.371
X_9	−0.087	0.086	1.020	1	.312	0.916
Constant	1.516	0.645	5.522	1	0.019	4.556

The results of parameter estimation can be obtained by the followed Formula 2:

$$P\{Y = 1\} = \frac{exp(1.247 + 0.0182X_1 + 0.241X_2 - \ldots - 0.309X_7 + 1.215X_8 - 0.087X_9)}{1 + exp(1.247 + 0.0182X_1 + 0.241X_2 - \ldots - 0.309X_7 + 1.215X_8 - 0.087X_9)} \quad (2)$$

Considered the relevant factors of physical expenditure, this study can calculate the probability of bus choice by above regression model. Such as a traveler who go to work

(no load), and start in morning peak of weekday; the time-consuming of arriving at bus station is 5–10 min; the time-consuming of waiting for bus; the time-consuming of journey is 15 ~ 30 min; sit on the bus and don't need to transfer, and only have a bike, so probability of bus choice is that $p = 0.769$ (Table 3).

Table 3. The probability of bus choice(Include the factors of physical expenditure)

	B	S.E,	Wals	df	Sig.	Exp (B)
Constant	0.769	0.088	76.805	1	0.000	2.158

By analyzing the regression can obtain the following conclusions:

(1) Regression coefficients of the time-consuming of arriving at bus station and the number of transfer are negative, so it indicates that the longer time-consuming of arriving at bus station and the more numbers of transfer may lead to the lower probability of bus choice;
(2) Regression coefficients of the time-consuming of journey and load condition are negative, so it indicates that the longer time-consuming of journey and the heavier load may lead to the lower probability of bus choice;
(3) Regression coefficients of the seat status are positive, it indicates that when the bus is empty and have seats, the probability of bus choice may be larger; and absolute value of regression coefficients of the seat status are significantly larger than other factors', thus the factor of seat status play an important role in the bus decision.

However, without considered the factors of physical expenditure (such as the time-consuming of waiting for bus, load condition and seat status), the specific assignment in Table 4. Then repeatedly calculate parameters of factors, as shown in Table 5 and construct Formula 3.

$$P\{Y=1\} = \frac{exp(1.516 + 0.226X_1 + 0.316X_2 - \ldots - 0.272X_5 - 0.093X_6)}{1 + exp(1.516 + 0.226X_1 + 0.316X_2 - \ldots - 0.272X_5 - 0.093X_6)} \quad (3)$$

Table 4. The options of bus travel decision(Except the factors of physical expenditure)

Variables	Factors
X_1	Trip purpose
X_2	Start time
X_3	The time-consuming of journey
X_4	The time-consuming of arriving at bus station
X_5	The numbers of transfer
X_6	Private transportation

Table 5. The maximum likelihood estimation of parameters (Except the factors of physical expenditure)

	B	S.E,	Wals	df	Sig.	Exp (B)
X_1	0.226	0.070	10.493	1	0.001	1.254
X_2	0.316	0.137	5.307	1	0.021	1.372
X_3	−0.492	0.148	11.135	1	0.001	0.611
X_4	−0.068	0.114	.362	1	0.548	0.934
X_5	−0.272	0.149	3.347	1	0.067	0.762
X_6	−0.093	0.083	1.263	1	0.261	0.911
Constant	1.516	0.645	5.522	1	0.019	4.556

Therefore, such as a traveler who go to work and start in morning peak of weekday; the time-consuming of arriving at bus station is 5 ~ 10 min; the time-consuming of journey is 15 ~ 30 min; don't need to transfer, and only have a bike, so probability of bus choice is that $p = 0.824$ (Table 6).

Table 6. The probability of bus choice(Except the factors of physical expenditure)

	B	S.E,	Wals	df	Sig.	Exp (B)
Constant	0.824	0.079	78.843	1	0.000	3.331

Through the above comparison, we can find that physical expenditure indeed have an impact on bus travel decision. When not consider factors of physical expenditure, the probability of bus choice is significantly greater than when consider the factors of physical expenditure.

5 Conclusion

Firstly, this research investigated the bus travel physical expenditure and acquired the main factors of physical expenditure are that the time-consuming of waiting for bus, load condition and seat status. Secondly, established the logistic model and got coefficient of relevant factors, and found that physical expenditure indeed impacts on the bus travel decision. Finally, according the comparative analysis to find that the relevant factors of physical expenditure can reduce the probability of the bus choice.

Acknowledgement. This work is supported by the Key Laboratory of Road and Traffic Engineering. The authors are grateful for the reviewer of initial drafts for their helpful comments and suggestions.

References

1. Wen X, Yang T, Ling X (2015) Present situation and revelation of bus travel sharing ratio both at home and abroad. Sci Technol Road Traffic(Appl Technol Ed) 02:251–254
2. Yang X, An J, Liu H, Teng J, Zhang D (2010) Evaluation architecture discussion of route—level transit service quality. J Transp Syst Eng Inform Technol 04:13–21
3. Hill MR (1982) Spatial Structure and Decision-Making of Pedestrian Route Selection Through An Urban Environment. University Microfilms International
4. Kulbl R, Helbing D (2003) Energy laws in human travel behavior. New J Phys 5(48):1–12
5. Van Ouwerkerk F (1987) Relationship between Road Transport Working Condition, Fatigue, Health, and Traffic Safety. Transport Research centre, Ri jksuniversiteit Groningen
6. Li C, Zhou Q, Lu M, Zhu T (2014) Non-motorized Accessibility model and application based on energy expenditure. J Chang Univ (Nat Sci Ed) 04:142–146 + 178
7. Guo H (2007) Study on travelers' behavior based on their physiology and psychology in urban passenger transportation. Southwest Jiao tong University
8. An J, Sun M, Guo J (2013) Analysis of travel energy expenditure based on subjective perception and objective measurement. Urban Transp China 02:73–82
9. Jin C (2011) Study on design and management of recreational trail based on human energy expenditure theory. Shan Dong University
10. Jiao C, Dong X, Yang G, Huo X (2002) The methods to assess physical activity and energy expenditure. Foreign Med Sci Biomed Eng 05:196–202
11. Meijer GA, Westerterp KR, Koper H, ten Hoor F (1989) Assessment of energy expenditure by recording heart rate and body acceleration. Med Sci Sports Exerc 21(3):343–347
12. Zheng Z (2011) The testing and evaluation of bus comfort based on Labview. Nanjing University of Information Science & Technology
13. Li D, Chen J (2007) Decision analysis of urban resident public traffic trip with logistic regression model 06:60–62 + 66
14. Meng Y (2012) Using RP/SP survey to analyze travel behaviors under traffic incidents. Southwest Jiao tong University
15. Tan H, Zeng J (2013) Influence analysis for logistic regression model. J Appl Stat. Manage 03:476–485

Research on Optimal Control Strategy of Coupler Force in Urban Rail Transit

Feiyao Jing, Gang Xu(✉), Ying Xu, Jianhao Shen, Cheng Chi, and Yuan Liu

Shenzhen Key Laboratory of Urban Rail Transit, College of Mechatronics and Control Engineering, Shenzhen University, Shenzhen 518060, China
2150160412@email.szu.edu.cn, xugang@szu.edu.cn

Abstract. In this paper the relationship between the coupler force and the traction force is analyzed, based on under two kinds of operating conditions: constant speed motion and constant force start motion, by establishing a multi-particle urban rail transit simulation model in the background of the Shenzhen Metro Line in order to optimize the coupling force between the trains. According to the simulation results of the coupler force, the standard of the evaluation of the coupler force is proposed and the reasonable control strategy of the train is obtained. In the meantime, two models of parallel experiments, rational traction force grouping and mathematical statistics were used to draw the experimental conclusion. Therefore, the validity of the simulation experiment is verified relying on train calculation and comparison of simulation results. Experimental results show that under the precondition of satisfy the standard of metro vehicle running, starting and accelerating the train in the constant force and constant speed operation, the optimal control strategy is not verifiable train traction evenly distributed control strategy. Meanwhile, the train optimal control mode can be obtained.

Keywords: Metro vehicle · Traction calculation · Grouping · Multi-particle model · Coupler force · Simulation calculation

1 Introduction

Urban rail transit occupies an extremely important position in our country. In the process of running, the train and the trailer are connected by a hook-and-tie device, and traction force, running resistance and braking force are formed along the track form an extremely complex multi-particle longitudinal dynamics system. During the constant force start to accelerate and constant-speed operation of the rail transit, different coupler forces appear between the sections of trains. The composition of these couplings is an important measure of the longitudinal impulse evaluation of the train [9]. The train will encounter

Research supported by the National Natural Science Foundation of China under Grant 51577120, Grant 61403259, and Grant 61403258, in part by Science and Technology Research and Development Foundation of Shenzhen under Grant JCYJ20140418182819128.

X. Zeng et al. (eds.), *International Symposium for Intelligent Transportation and Smart City (ITASC) 2017 Proceedings*, Smart Innovation, Systems and Technologies 62, DOI 10.1007/978-981-10-3575-3_17

a complex and changeable environment during operation, and the appearance of these factors will greatly increase the power of the coupler, the more the number of occurrences of larger coupling force, the more likely hook delay device, the end of the body and other train structure lead to failure, If things go on like this, reducing the use of train life, increasing maintenance costs, and greatly decreasing the safety factor. Taking the above factors into account, It's extremely important for the long-term operation of urban rail trains to Study on coupler force in China.

On the one hand, it can provide a reliable data basis for the structural design of the coupler device of urban rail transit. On the other hand, according to the results of the analysis of the coupler force, we can get the different distribution ways of the train power, and then get the optimal control mode of the train based on the train rationalization operation. This paper is in the background of Shenzhen Metro Line 1 (continued construction), through its supplier Siemens made the train performance simulation study. As this is the first by the Chinese enterprises independent bidding, independent research, with independent intellectual property rights of the A-type subway vehicle project, which marks the success of the world's most high-end subway vehicle technology independent production, creating the domestic type A metro vehicle lightweighting records. The overall weight of less than 52t lighter than the same type of vehicle more than 2t, so choosing this train as a research background. Moreover, in view of the globalization of China, it is very important to for designing the rational operation of the urban rail transit to study the urban rail transit.

At present, there are three main types of trains in the form of train formation, including 4 vehicles, 6 vehicles and 8vehicles. In terms of urban rail transit vehicle running status in our country at present, most of them adopt 6 vehicle marshalling, which consists of an electric vehicle with a pantograph, a motor vehicle without a pantograph and a trailer with a driver's cab. When the traffic is large, they use the 8 vehicles formation. Shenzhen Metro Line 1 is composed of 6 vehicles, including 2 trailers (A vehicle) with driver's cab and 4 motor vehicles (B and C). The train is arranged in the following form: —A*B*C = C*B*A— When the train is composed of 8 vehicles, consisting of two trailers (A vehicle) with driver's cab and six motor vehicles (B and C) when the train is composed of eight vehicles. The train is arranged in the following form: —A*B*C*C = C*C*B*A— (Table 1).

Table 1. A model of various types of marshalling typical projects [10]

Project		Initially	Recently	Forward
Shenzhen	Metro Line 1	Six groups	Six groups	Six groups
	Metro Line 4	Four groups	Four groups	Six groups
	Metro Line 5	Six groups	Six groups	Six groups
	Metro Line 11	Eight groups	Eight groups	Eight groups
Shanghai	Urban rail transit Line 1	Six groups	Eight groups	Eight groups
	Urban rail transit Line 4	Six groups	Six groups	Six groups
	Urban rail transit Line 16	Three groups	Three groups	–
Guangzhou	Metro Line 2	Six groups	Six groups	Six groups
Beijing	Metro Line 14	Six groups	Six groups	Six groups

2 Traction Calculation

A. *Subway vehicle input elements*
   (1) the road conditions of train operation, including the curve radius R, slope i and other data;
   (2) the form of subway vehicles, passenger capacity, vehicle type, body mass and other data;
   (3) the basic subway train resistance formula;
   (4) Subway vehicle traction curve, and motor power and other data.

B. *Calculation standard of electric locomotive for urban rail transit*
   (1) *Traction performance of urban rail transit*
   According to the international standard documents [3]: capacity, in the straight dry track, the wheel is semi-wear state, the train from the maximum speed to the parking, If no special requirements, the average acceleration is: the train from 0 to 40 km/h, not less than 0.83 m/s^2; train acceleration from 0 to 80 km/h, not less than 0.5 m/s^2. So the simulation experiments in this article are all made above conclusion to judge the rationality of the simulation experiments. Shenzhen Metro Line 1 in AW_2 load, rated voltage of 1500 V, the average starting acceleration of 1.0 m/s^2(0–40 km/h), 0.6 m/s^2(0–80 km/h average acceleration), the adhesion coefficient 0.17, the maximum operating speed of 80 km/h.
   (2) *Line plane*
      (1) The curvature radius of road surface should be determined according to the comprehensive factors such as vehicle type, terrain condition, running speed and environment requirement. The minimum curve radius should meet the following Table 2:

Table 2. The minimum curve radius of the circular curve (r)

Line	Models			
	A model		B model	
	General lot	Difficult lot	General lot	Difficult lot
Positive line	350	300	300	250
Access line, contact line	250	150	200	150
Yard line	150	–	150	–

      (2) line plane curve radius selection should adapt to the location of the train speed requirements. The relationship between the curve radius and the train speed limit is determined by the following equation by Siemens.

$$v = 3.6\sqrt{R} \tag{1}$$

Where: R-to meet the ultra-high requirements of the minimum curve radius, m; v-design speed, km/h.

C. *Train resistance*

(1) *Basic resistance*

The basic resistance formula of the train is related to the structure of the train, including the following factors: bearing resistance, rolling resistance, sliding resistance, shock, vibration resistance, air resistance. As the factors that affect the basic resistance is extremely complex, so in use, usually calculated by the comprehensive empirical formula derived. Siemens used in Shenzhen Metro Line 1 (continued construction) vehicles and other A-type vehicle project in the conventional Davis formula: F_W - train resistance, N; Mt - train mass and load, kg; v-speed, m/s; n-number of vehicles. $F_W = 516n + Mt(0.006374 + 0.0003291v) + 11.187v^2$ [1] where: In this paper, this formula is used as the expression model of the basic resistance of the train, and the optimization of the control of the coupler force is simulated.

(2) *Additional resistance*

Additional resistance is mainly determined by the line conditions, including ramp resistance and curve resistance. The ramp resistance is:

$$i\% \times m \times g \tag{2}$$

Where: i - slope; m - train mass, t; g - acceleration of gravity, 9.8 N/kg.
Curve resistance formula:

$$m \times g \times 600/(1000 \times R), \text{ kN}. \tag{3}$$

D. *Train characteristics*

(1) In order to meet the requirement of starting average acceleration 1.0 m/s^2 (0 ~ 40 km/h) when the rated voltage 1500 V under AW_2 load, the maximum traction force of the train $F - f \geq Mt \times 1.0$ (Mt is the total train mass and rotating mass). 1TB2010-1GA02, the maximum output traction of a single motor is 25 KN, the maximum traction force of train is 400 KN; the range of constant torque is 0 ~ 40 km/h, the range of constant power is 40 ~ 55 km/h, and the range of natural characteristics is 55 ~ 80 km/h. The traction characteristic curve is shown in the following Fig. 1, and the average acceleration

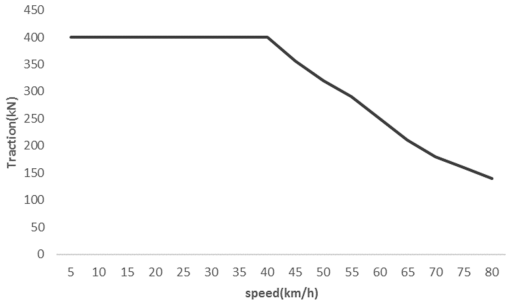

Fig. 1. AW_2–AW_3, 1500 V traction when the curve

a = (400 − f)/Mt = 1.04 m/s^2 is obtained. Furthermore, the train 0 ~ 80 km/h, the average acceleration is 0.61 m/s^2. So in the following simulation experiments, the train in 0 ~ 40 km/h and 0 ~ 80 km/h driving process, must be greater than the above two calculation criteria, to be able to verify the authenticity of the model. Figure 1 for the Shenzhen Metro Line 1 AW_2–AW_3 standard traction when the curve.

(2) the adhesion coefficient of the test as long as the train adhesion and traction and adhesion quality can be substituted into the formula. From $F_\mu = P_\mu \times g \times \mu$, $\mu = F_\mu/(P_\mu \times g)$. F_μ - Calculate the adhesion traction, KN; P_μ - Train the calculation of adhesive quality, t; μ - Calculate the adhesion coefficient. The parameters and traction characteristics of the subway line 1 (sub-construction) of Shenzhen Metro will be 0.169, which satisfies the requirements.

3 Simulation Model Structures

A. *Multi-particle mathematical model*

When the coupling force for the purpose of the analysis, the vehicle lateral force and vertical force as a secondary factor, the longitudinal dynamics generally consider only the vehicle's longitudinal freedom, the vehicle body will be reduced to a particle, so the train constitutes A particle chain, as shown in Fig. 2.

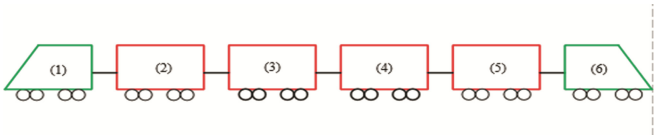

Fig. 2. 6A groups

Figure 3, the train multi-particle model for stress analysis. W_h for the first vehicle on the vehicle after the vehicle hook force, W_z, W_f, Ws, respectively, the basic resistance of the train, the additional Resistance (ramp resistance and additional resistance), braking force. In different driving conditions of the train, these forces will be combined

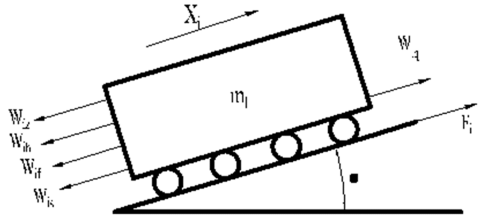

Fig. 3. Stress analysis of single - track train during train operation

in different forms, such as traction in the train process does not exist in the process of Ws (braking force), there is no traction F.

In this simulation for the 4 drag 2 dynamic model, so according to Newton's law force analysis available:

$$m_1 a_1 = -W_{1h} - W_{1z} - W_{1f}; \tag{1}$$

$$m_2 a_2 = F_1 + W_{2q} - W_{2h} - W_{2z} - W_{2f}; \tag{2}$$

$$m_3 a_3 = F_2 + W_{3q} - W_{3h} - W_{3z} - W_{3f}; \tag{3}$$

$$m_4 a_4 = F_3 + W_{4q} - W_{4h} - W_{4z} - W_{4f}; \tag{4}$$

$$m_5 a_5 = F_4 + W_{5q} - W_{5h} - W_{5z} - W_{5f}; \tag{5}$$

$$m_6 a_6 = W_{6q} - W_{6z} - W_{6f}; \tag{6}$$

$$W_{1h} = -W_{2q}, W_{2h} = -W_{3q}, W_{3h} = -W_{4q}, W_{4h} = -W_{5q}, W_{5h} = -W_{6q};$$

If the train is rigid, the translational acceleration of the train as a whole is equal to the translational acceleration of any part of the train, that is,

$$a_1 = a_2 = a_3 = a_4 = a_5 = a_6 = a; \tag{7}$$

$$a = F/((1 + \gamma)M); \tag{8}$$

Among them, the acceleration of the whole train is a, the resultant force of the train is F, the train's rotational mass coefficient is γ, the train's mass is M;

Combining all the equations above, we can get the expression of the vehicle-hook force control target as follows:

$$\begin{aligned}
W_{1h} &= -W_{1z} - W_{1f} - W_{1b} - m_1 a; \\
W_{2h} &= F_1 + W_{1z} - W_{2z} + W_{1f} - W_{2f} + W_{1b} - W_{2b} + (m_1 - m_2)a \\
W_{3h} &= F_2 - F_1 + W_{2z} - W_{1z} - W_{3z} + W_{2f} - W_{1f} - W_{3f} + W_{2b} - W_{1b} - W_{3b} + (-m_1 + m_2 - m_3)a; \\
W_{4h} &= F_1 - F_2 + F_3 + W_{1z} - W_{2z} + W_{3z} - W_{4z} + W_{1f} - W_{2f} + W_{3f} - W_{4f} + W_{1b} \\
&\quad - W_{2b} + W_{3b} - W_{4b} + (m_1 - m_2 + m_3 - m_4)a; \\
W_{5h} &= -F_1 + F_2 - F_3 + F_4 - W_{1z} + W_{2z} - W_{3z} + W_{4z} - W_{5z} - W_{1f} + W_{2f} - W_{3f} \\
&\quad + W_{4f} - W_{5f} - W_{1b} + W_{2b} - W_{3b} + W_{4b} - W_{5b} + (-m_1 + m_2 - m_3 + m_4 - m_5)a.
\end{aligned}$$

Not only can the strength of the train coupler be verified by the multi-particle model, but also the state of single vehicle operation can be analyzed in detail by the multi-particle model.

4 Experimental Simulation

A. *Constant speed process simulation*

Based on the above traction calculation, the multi-particle model of six A-type vehicles was established by using the true mass of the vehicle body of Shenzhen Metro Line 1 as the input condition, and simulation experiments were limited at 80 km/h speed closed loop simulation. In the process of experiment, the method of collocation of train power is constantly adjusted in order to obtain the data of the coupler force between different trains, putting forward to the standard of evaluating the coupler force. Based on the large amount of data analysis, the optimum combination of coupler force is obtained, In the case of optimal coupler force, obtains the railroad transportation the best power match the way, then obtains the optimal control strategy ultimately.

(1) *Model validation*

The train speed and the acceleration curve are obtained under the preconditions of the literature [1] and the literature [2], and then the real reliability of the model is verified by comparing with the traction force calculation, and the following simulation results are obtained under the conditions of AW_2 load, constant speed of 80 km/h and sum of tractive forces of approximately 85.4 KN (Figs. 4 and 5).

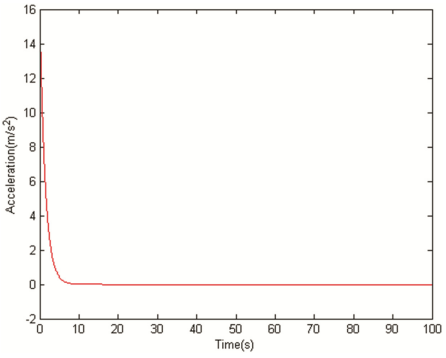

Fig. 4. Acceleration curve

According to the experimental data in the two above figures: Train speed from 0 to 80 km/h in the process, the train after about 14.818 s, the speed eventually stabilized at 80 km/h, According to v = a * t, after a simple calculation, the average acceleration of the train is about 1.50 m/s^2, which is larger than 0.61 m/s^2 calculated by the previous train, and verifying the reliability of the simulation model.

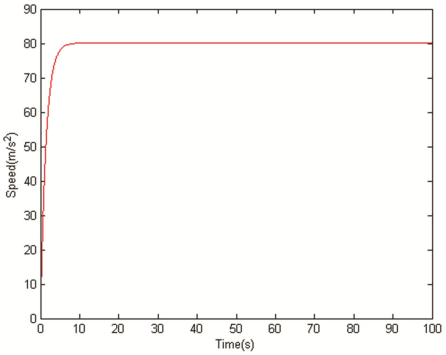

Fig. 5. Speed curve

(2) *Experimental simulation*

The simulation experiment is divided into seven groups. The first four groups of experiments are the simulation of the change of the coupler force with one of the train power F_1 or F_2 or F_3 or F_4, but the total traction is the same as the train. The remaining experiments are the simulation of the change of the coupler force with F_1 or F_2 or F_3 or F_4 any two, but the total traction is the same as the train.

Take the coupler forces with the traction force F_1 or with the traction force F_1 and F_2 changes as an example.

The simulation results of the first group are shown in Figs. 6 and 7. The F_1, F_2, F_3 and F_4 in Fig. 6 are the traction force provided by four motor vehicles, and the abscissa is different traction force combination, the vertical axis traction for the train, KN. In Fig. 7, W_1, W_2, W_3, W_4, W_5 show the interaction force between the trains.

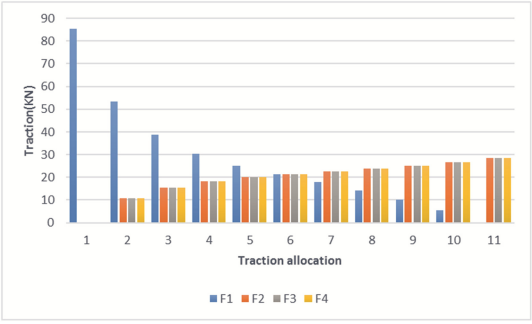

Fig. 6. Changes with traction F_1

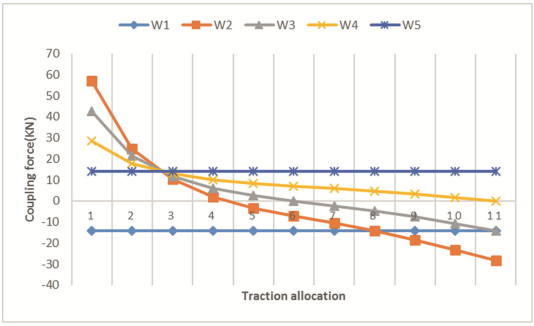

Fig. 7. Constant speed conditions, with the traction force F_1 changes in the size of the distribution of coupler force

Based on the analysis of all experimental charts: Under the condition of meeting the AW_2 load and the constant speed of the train 80 km/h:
Because W_1 and W_5 remained constant throughout the experiment, the following formula is used:

$$J = (W_2 - W_3)^2 + (W_3 - W_4)^2 + (W_4 - W_2)^2$$

As the basis for evaluating the coupler force, the smaller the J is, the better the coupler force is, and the corresponding traction force distribution is the best.

(1) From Fig. 7, in the first set of data, the J is the smallest of the third modes of distribution, and the integrated coupler force is the smallest and close to each other. So this distribution method is optimal.
The second group of experimental simulation results shown in Fig. 8:

(2) From Fig. 8, we can see that the 8th distribution mode J in the second set of data is the smallest and the integrated coupler force is the smallest and close to each other, so this distribution method is optimal.

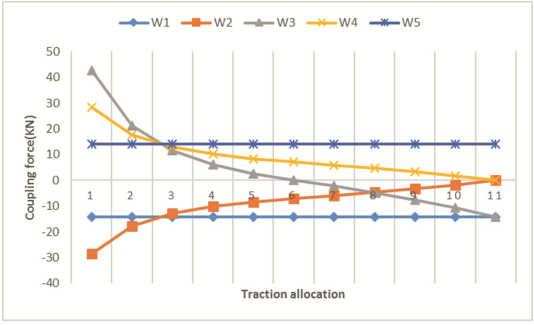

Fig. 8. Constant speed conditions, with the traction force F_2 changes in the size of the distribution of coupler

The third group of experimental simulation results shown in Fig. 9:

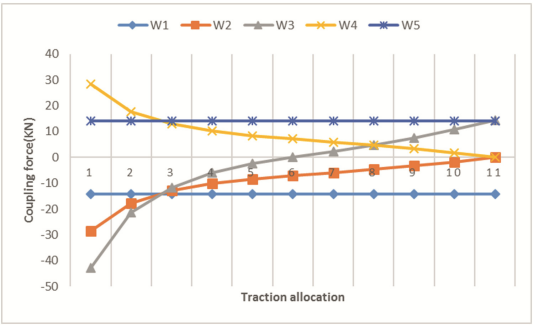

Fig. 9. Constant speed conditions, with the traction force F_3 changes in the size of the distribution of coupler force

(3) From Fig. 9, we can see that the eighth distribution mode J in the third set of data is the smallest, and the integrated coupler force is the smallest and close to each other. This distribution method is optimal.
The fourth group of experimental simulation results shown in Fig. 10:

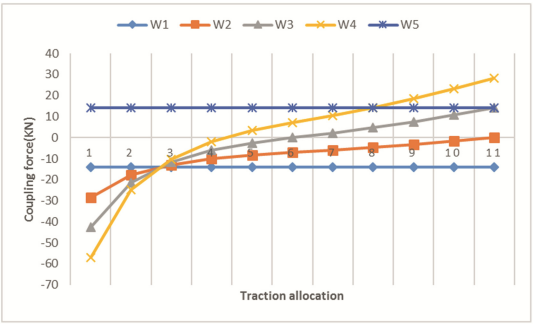

Fig. 10. Constant speed conditions, with the traction force F_4 changes in the size of the distribution of coupler force

(4) From Fig. 10, we can see that in the fourth set of data, the third distribution mode J is the smallest, and the integrated coupler force is the smallest and close to each one, so this distribution method is optimal.
The fifth group of experimental simulation results shown in Figs. 11 and 12:

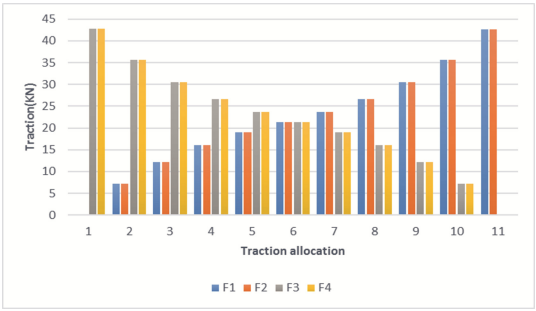

Fig. 11. Changes with traction F_1, F_2

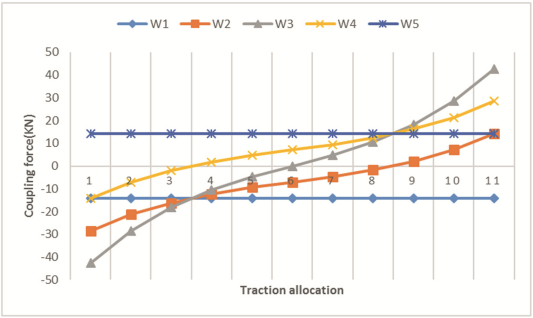

Fig. 12. Constant speed conditions, with the traction force F_1 and F_2 changes in the size of the distribution of coupler force

(5) From Fig. 12, we can see that the 6th distribution mode J in the fifth group is the smallest, and the integrated coupler force is the smallest and close to each other. This distribution method is optimal.
The sixth group of experimental simulation results shown in Fig. 13:

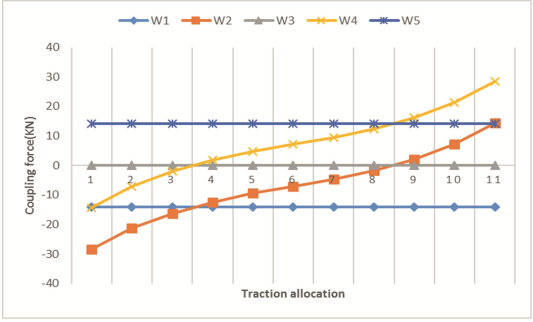

Fig. 13. Constant speed conditions, with the traction force F_1 and F_3 changes in the size of the distribution of coupler force

(6) From Fig. 13, we can see that the 6th distribution mode J in the 6th group is the smallest, and the comprehensive coupler force is the smallest and close to each other. This distribution method is the best.
Seventh group of experimental simulation results shown in Fig. 14:

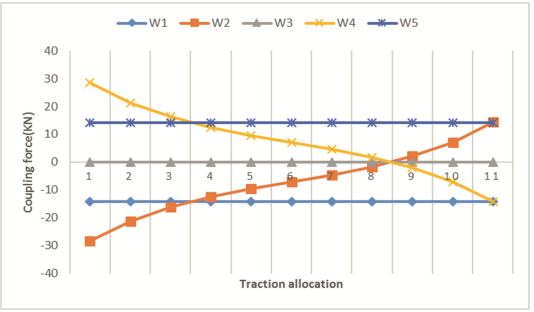

Fig. 14. Constant speed conditions, with the traction force F_1 and F_4 changes in the size of the distribution of coupler force

(7) The comparative analysis of Fig. 14 shows that the seventh set of data in the 8th distribution mode J is the smallest, the overall strength of the smallest and close to each other, this distribution is optimal.

B. *Constant starting process simulation*
In the course of constant force start to acceleration, the trains do the whole acceleration and longitudinal movement. In the simulation process, traction force is directly input into the train simulation model, and the train power simulation is carried out. The same calculation in accordance with the literature [1, 2] standard conditions, the train speed curve of the simulation results, and the traction characteristic curve were compared by calculating the front traction results, to verify the reliability of the model.

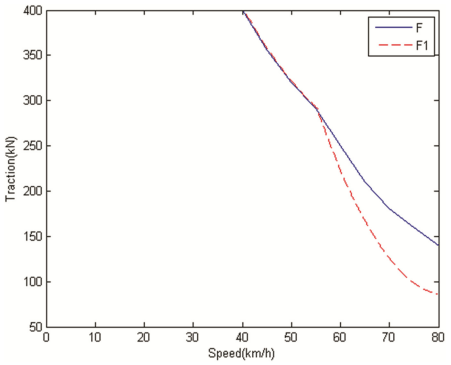

Fig. 15. Traction force characteristic curve simulation and the actual contrast

(1) *Model validation*
In order to verify the real reasonableness of the model, 400 KN is the output traction force provided by the motor of Shenzhen Metro Line 1, and the train stability is 80 km/h and the starting traction is 400 KN. Simulation results see Figs. 15 and 16 below:

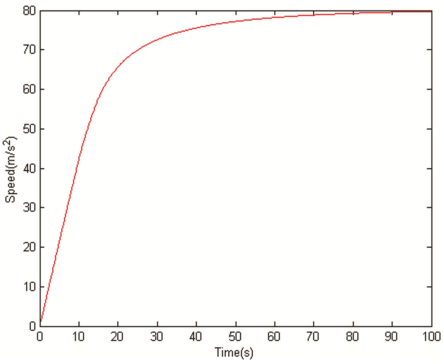

Fig. 16. Speed characteristic curve

Figure 15 shows the comparison between the standard traction force characteristic curve and the traction force curve simulated by the model represented by the broken line F_1. In the constant torque region (0–40 km/h) and the constant power region (40–55 km/h). The two intervals are basically coincident, but slightly different in the natural characteristic interval (55–80 km/h); this is due to the different resistance model.
Figure 16 shows the velocity curve obtained by the simulation. Based on the simple calculation of v = a * t, the average speed of the train (0–40 km/h) is 1.18 m/s^2 when the rail traffic reaches 40 km/h at 9.426 s(0–80 km/h) is 0.63 m/s^2. Compared with the previous traction, it can be seen that the standard of train running is satisfied. The train speed is 0.63 m/s^2, which is about 80 km/h at 35.326 s. So the model can verify the true reliability.

(2) *Experimental Simulation*
The following simulation experiments are divided into seven groups, are in the AW_2 load, train stability at 80 km/h and start the traction and 280 KN under the conditions of the simulation results:
The simulation experiment is divided into seven groups. The first four groups of experiments are the simulation of the change of the coupler force with one of the train power F_1 or F_2 or F_3 or F_4, but the total traction is the same as the train. The remaining experiments are the simulation of the change of the coupler force with F_1 or F_2 or F_3 or F_4 any two, but the total traction is the same as the train (Fig. 17).

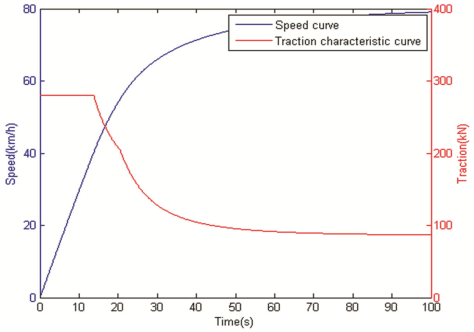

Fig. 17. Speed versus traction comparison curve

Take the coupler forces with the traction force F_1 or with the traction force F_1 and F_2 changes as an example. The first group of experimental simulation results are shown in Figs. 18 and 19:

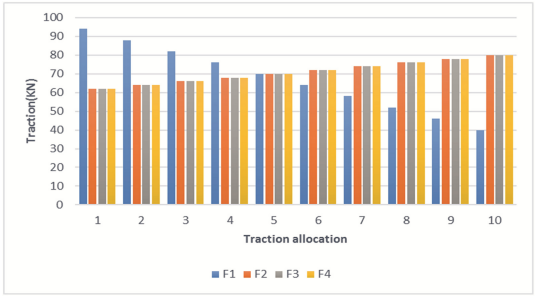

Fig. 18. Changes with traction force F_1

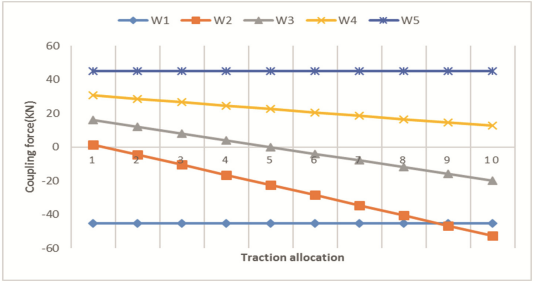

Fig. 19. Constant force start to accelerate the maximum coupler force changes with traction force F_1

Through observation of the experimental data W_1 and W_5 in the constant torque experiment process remains the same, with the constant speed process using the following formula:

$$J = (W_2 - W_3)^2 + (W_3 - W_4)^2 + (W_4 - W_2)^2$$

As the basis for evaluating the coupler force, the smaller the J is, the better the coupler force is, and the corresponding traction force distribution is the best.

(1) From the comparative analysis of Fig. 19, we know that the first distribution mode J is the smallest, and the integrated coupler force is the smallest and close to each other. This distribution method is optimal.
The second group of experimental simulation results shown in Fig. 20:

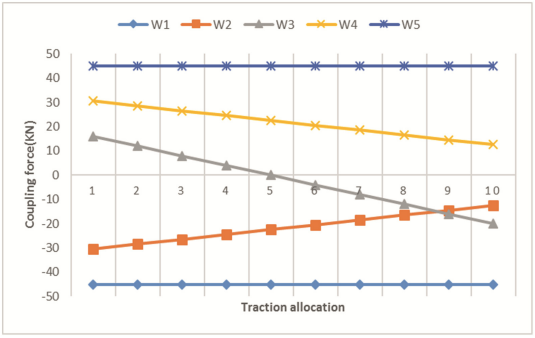

Fig. 20. Constant force start to accelerate the maximum coupler force changes with traction force F_2

(2) From the comparative analysis of Fig. 20, it can be seen that the 10th distribution mode J in the second group is the smallest and the integrated coupler force is the smallest and close to each other. This distribution method is optimal.
The third group of experimental simulation results shown in Fig. 21:

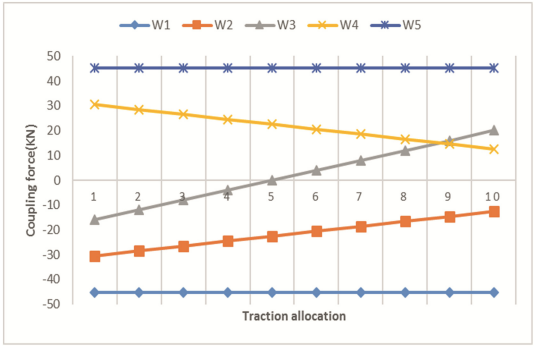

Fig. 21. Constant force start to accelerate the maximum coupler force changes with traction force F_3

(3) From the comparative analysis and calculation of Fig. 24, it can be seen that the tenth distribution mode J in the third set of data is the smallest and the integrated coupler force is the smallest and close to each other. This distribution method is optimal.
The simulation results of the fourth group of experiments are shown in Fig. 22:

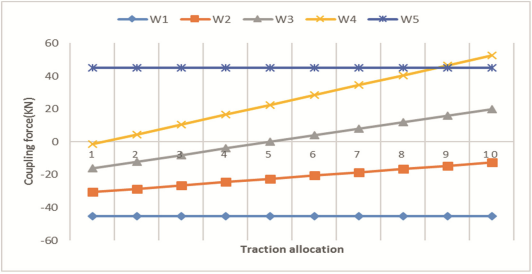

Fig. 22. Constant force start to accelerate the maximum coupler force changes with traction force F_4

(4) From the comparative analysis of Fig. 22, it can be seen that the first distribution mode J in the fourth set of data is the smallest and the integrated coupler force is the smallest and close to each other. This distribution method is optimal.
The simulation results of the fifth group are shown in Fig. 23:

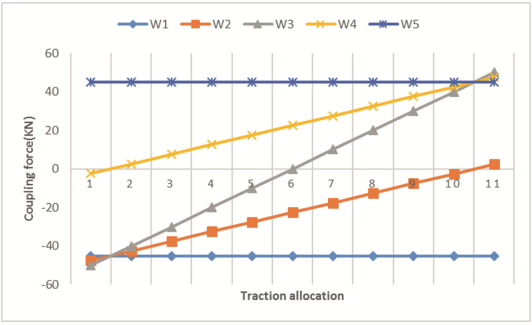

Fig. 23. Constant force start to accelerate the maximum coupler force changes with traction force F_1 and F_2

(5) From the comparative analysis of Fig. 23, it can be seen that the sixth distribution mode J in the fifth group is the smallest, and the integrated coupler force is the smallest and close to each other. This distribution method is optimal.
The simulation results of the sixth group of experiments are shown in Fig. 24:

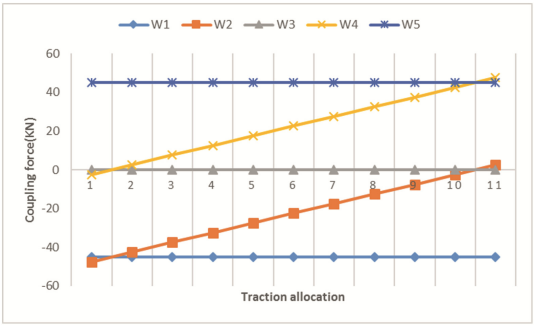

Fig. 24. Constant force start to accelerate the maximum coupler force changes with traction force F_1 and F_3

(6) From Fig. 24, we can see that the sixth distribution mode J in the sixth set of data is the smallest and the integrated coupler force is the smallest and close to each other. This distribution is optimal.
The simulation results of the seventh group of experiments are shown in Fig. 25:

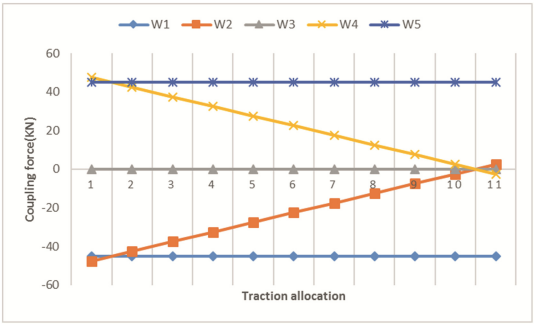

Fig. 25. Constant force start to accelerate the maximum coupler force changes with traction force F_1 and F_4

(7) From Fig. 25, we can see that the 11th distribution mode J in the 7th set of data is the smallest and the integrated coupler force is the smallest and close to each other. This distribution method is optimal.

5 Data Analysis and Comparison

The trajectory of the trains in the constant speed and constant force start-up process corresponding to the best way of traction allocation into the following Figs. 26 and 27.

The abscissa represents the traction pattern and the ordinate represents the traction force. The 6A-1 represents the optimal allocation of the traction force for the first set of experiments in the multi-particle simulation model. 6A-2, 6A-3, 6A-4 are as follows:

In summary, the following conclusions can be drawn:

(1) After compute and comprehend, we can see that the traction force distribution mode J is the smallest and the coupler force is the smallest, and the traction distribution is the best. As shown in Fig. 26, 6A-7, we can see that the rain traction reasonable coordination strategy can make the vehicle between the hook strength to achieve optimal, which can reduce the probability of failure of the hook device, end of the train structure, and other train structure, if things go on like this, extending the use of train life, reducing maintenance costs, and greatly increasing the safety factor.

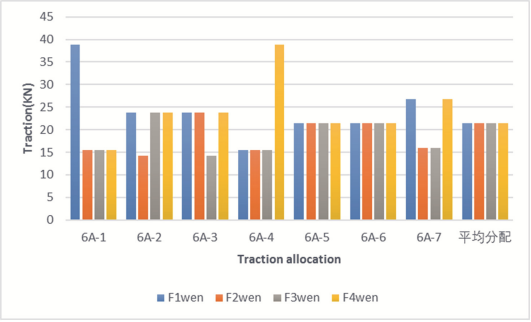

Fig. 26. Comparison of traction force distribution in constant speed process

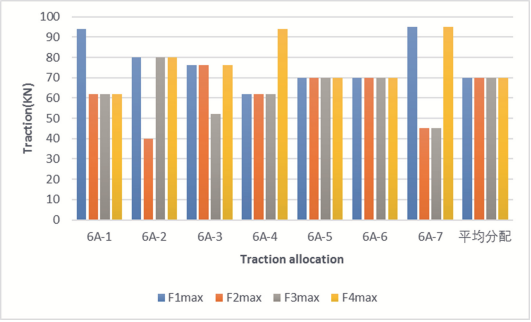

Fig. 27. Comparison of the traction mode of constant force start acceleration

(2) During the constant-force start-up process of the train, the calculation and analysis shows that J of the 11th traction power distribution mode is the smallest and the integrated coupler force is the smallest and the traction force distribution mode is the best. As shown in Fig. 27, 6A-7 shows that the train to meet the AW_2 load, and in line with subway vehicle design standards, the train traction reasonable control strategy can make the train between the hook force to achieve optimal, enhancing Train start-up safety factor; and it can be seen, the rail transit train in the constant force to start the process of acceleration, traction control of the average allocation of traction control strategy is not the best way to control the start.

6 Conclusion

In this paper, the multi-particle simulation model of 6A group formation is established. With the continuous research and experimentation, a lot of data simulations are conducted under the conditions of constant speed and constant speed start-up. The traction control strategy of trains is analyzed and compared. The optimal control strategy of the trains under the two kinds of operating conditions is obtained, and it is proved that the train optimal control starting strategy is not the traction average starting under the condition of avoiding the maximum coupler force. Through this paper, the operation of metro vehicles can provide a rationalized solution. It provides a good reference for reducing the probability of the end of the vehicle, improving the train safety factor, extending the service life of the train, and rationalizing the power. Which has far-reaching significance for the rationalization of subway in China.

References

1. Traction calculation rules for trains (TB/T 1407–1998)
2. Code for Design of Metro. China Plan Publishing House (2003)
3. General specification for metro vehicles (GB-T-7928–2003)
4. Mousavi Zadeh Noughabi SM, Dehghani K, Pouranvari M (2007) Failure analysis of automatic coupler SA3 in railway vehicle carriages. Eng Fail Anal 14(5):903–912
5. Lin W, Liu Z, Fang Y (2012) Readhesion optimization control strategy for metro traction. J Southwest Jiaotong Univ 47(3):465–470
6. Sun Z (2005) Practical train traction calculation course, 2nd edn. China Railway Publishing House, Beijing
7. Tang Z (2005) Analysis on coupler malfunction and research on the procedure. Harbin University of Science and Technology, Harbin. In Chinese
8. Mao B, He T, Yuan Z et al (2000) A general-purposed simulation system on train movement. J China Railway Soc 22(1):1–6. In Chinese
9. Zhuang B, Wang P (2010) Analysis of common troubles in type couplers. Rolling Stock 48(6): 43–46. In Chinese
10. Yang L, Luo S, Fu M (2015) Marshalling scheme of mixed formation freight train based on longitudinal impulse. China Railway Sci 36(4):108–114. In Chinese

Effect of Brake Chamber Pressure Area on Dynamic and Static Braking Performance of Articulated Train

Jin-song Dong[1], Hong-wei Zhang[1], Hai-yan Ji[1,2], Cheng-qiang Zong[1(✉)], and Jia-qi Yang[3]

[1] Key Laboratory of Operation Safety Technology on Transport Vehicles, Research Institute of Highway, Ministry of Transport, Beijing 100088, China
{js.dong,cq.zong}@rioh.cn
[2] School of Transportation Jilin University, Changchun 130025, China
[3] China Automotive Technology and Research Center, Tianjin 300300, China

Abstract. The brake safety of articulated train is the focus of the road freight transport industry. Brake chamber is an important component of the brake system in articulated train, whose performance has a significant impact on the vehicle braking performance. In order to improve vehicle braking performance, the dynamic characteristics of the brake chamber with pressure change were analyzed based on the model of the brake chamber and the brake drum assembly. By changing different specifications of rear axles' brake chamber in tractors, the static and dynamic braking performance were analyzed. The results showed that the larger the bearing area of brake chamber, the better the braking performance of articulated train. Proposed suggestions on how to select the specification of brake chamber in articulated train were made and the research results provided technical reference for the design of the articulated train braking system.

Keywords: Articulated train · Safety operation · Brake chamber · Bearing area

1 Introduction

Road freight transportation play a basic role in aspects of national economic construction and people's living material demand and so on, but traffic accidents caused by brake system occur frequently also brought a lot of casualties and property losses. In 2015, China's road freight volume and freight turnover are 31.5 billion tons and 5.79 trillion ton-kilometers respectively, accounting for 75.5% and 32.7% of the comprehensive transportation system respectively [1]. Articulated trains play a tremendously important role in road freight transportation [2]. Articulated trains are prone to cause accidents such as drift, folding and rollover when braking in emergency, because of the characteristics of articulated vehicle which are large weight, big volume, long length, and so on. So we propose higher requirements on its braking performance [3].

X. Zeng et al. (eds.), *International Symposium for Intelligent Transportation and Smart City (ITASC) 2017 Proceedings*, Smart Innovation, Systems and Technologies 62, DOI 10.1007/978-981-10-3575-3_18

2 Pneumatic Brake System

2.1 Brake Torque Model

As the actuating device of air pressure brake system, the brake chamber transforms the air pressure to mechanical energy which provide braking torque for articulated train [4]. Drum brake device which is composed of dual chamber brake chamber and cam driving device is shown in Fig. 1.

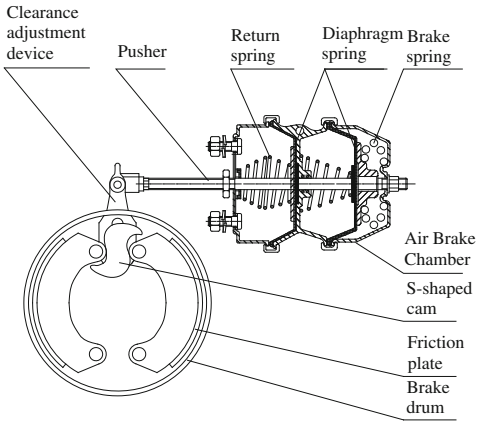

Fig. 1. Schematic diagram of pneumatic braking device

In pneumatic brake system, the braking force generated by each wheel is calculated as [5]

$$M_{\mu} = P_t A_0 \eta_m BF\left(\frac{l_a}{2l_b}\right)R_r \tag{1}$$

The effective area of the brake chamber can be calculated as [6]

$$A_0 = \frac{\pi}{12}\left(D^2 + D \cdot d + d^2\right) \tag{2}$$

2.2 Brake Chamber Pressure Dynamic Characteristic Model

The following assumptions are made in brake chamber pressure characteristic model [7]: Firstly, gas in storage cylinder is ideal gas and its pressure is constant. Secondly, ignore the effect of the volume of air pressure brake system on the change of gas pressure. Thirdly, ignore the effect of the temperature change on the pressure in the air brake system. On the basis of these, the pressure dynamic characteristic model of the brake chamber is consistent with the typical first order ordinary differential equation. According to the formula, the change rate of the brake chamber pressure is proportional to the difference between control pressure and brake chamber pressure.

$$\dot{P}_t = \frac{1}{\tau}(P_c - P_t) \tag{3}$$

As the parameter P_c in the formula (3) is consistent with the characteristic of the first order ordinary differential equation, the form is similar to that of the formula (3).

$$\dot{P}_c = \frac{1}{\tau_t}(P_{ref} - P_c) \tag{4}$$

We can get dynamic characteristic model of air pressure which varies with time of the brake chamber by solving the aforementioned two formulas.

3 Dynamic Characteristics of Brake Chamber Pressure

3.1 Step Input

In actual operation, if the air pressure of the brake chamber wasn't controlled, the control pressure of the brake pedal could be regarded as a step input [8]. Dynamic characteristics of brake chamber were shown in Figs. 2 and 3 when step input control.

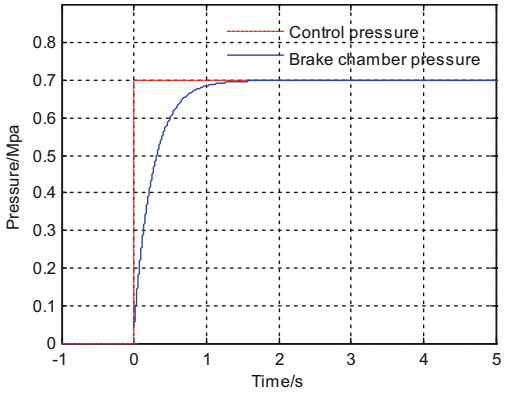

Fig. 2. Brake chamber dynamic characteristics when step input (no braking delay)

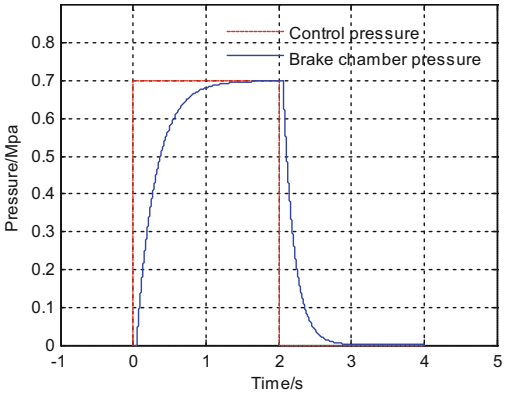

Fig. 3. Brake chamber dynamic characteristics when step input (braking delay 0.06 s)

3.2 Pulse Input

If the outputted air pressure of brake chamber was controlled effectively according to the target, the control air pressure of brake pedal could be regarded as pulse input. The controlled pressure's dynamic characteristics of the brake chamber were shown in Fig. 4 when pulse input.

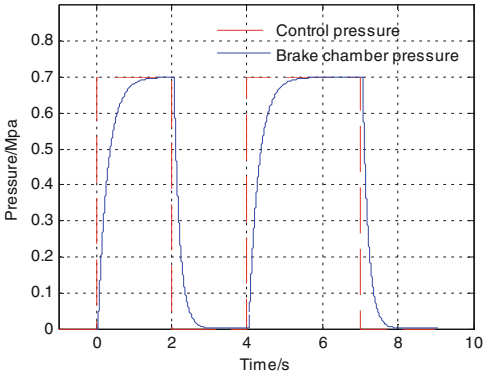

Fig. 4. The dynamic characteristics when pulse input (braking delay 0.06 s)

4 Effect of Air Chamber Bearing Area on Static Braking Performance

Brake chamber bearing area was an important influence factor of the braking force and braking torque. Experimental studies for the static braking performance of the articulated train with different bearing area of the brake chamber had been carried out, according to 'Safety Specifications for Motor Vehicles Operating on Roads' (GB 7258).

4.1 Static Braking Performance Test Method

(1) Test vehicle and test roads. The articulated train constituted of a 6 × 4 tractor and a three-axis semitrailer was chosen as the test vehicle. The test road is a long and straight line performance test road in the highway traffic test field MOT The length of the road was 3330 m, the width was 9 m, and its surface was cement concrete.
(2) Test method of static braking performance. The articulated train was stopped at the test road, and test joints were articulated with the front and rear axle brake chamber of the tractor and brake chamber of the semitrailer. And then, the engine was started for supplying gas to the semitrailer and tractor until the air dryer reached its limited pressure. Start pneumatic and electric tester and turn off the engine as well as releasing the parking brake, tread brake pedal quickly to maximum stroke within 0.2 s. After 5.0 s, release the pedal and the test data would be saved by computer.

4.2 Test Results and Analysis

We adjust air dryer limited pressure of the test vehicle to 850 kPa and change the brake chamber of tractor rear axle in test vehicle. We choose brake chamber with common bearing area, including 24 square feet, 27 square feet and 30 square feet, and they are used to test the static braking performance of the articulated train. Different rear axle brake chamber in tractor and brake chamber pressure of semitrailer are shown in Fig. 5.

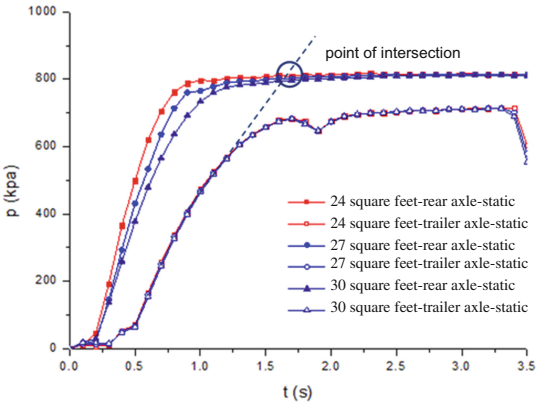

Fig. 5. Brake chamber's pressure of tractor rear axle and semitrailer

In the three static braking performance tests, the brake chamber pressure data were basically the same which showed great effectiveness of the three tests. Air pressure inputted by brake system was same in tests, which extremely eliminated the influence of external factors on test results.

When brake chamber of tractor rear axle was changed into different bearing area, brake chamber inflation rate was changed. With the increasing of bearing area, the inflation rate of brake chamber became slower, which shown that certain relationship of the increase of bearing area leaded to the increase of brake chamber volume.

Under the influence of the dryer limited pressure, the maximum working pressure of brake chamber with different bearing area was the same, and the pressure became stable when it reached the maximum working pressure.

5 Effect of Air Chamber Bearing Area on Dynamic Braking Performance

5.1 Test Method

The VBOX and pneumatic electric tester were adjusted to available state, and the brake trigger of VBOX was fixed with pedal dynamometer, and further they are fixed on the brake pedal of tractor reliably. Start the recording function of VBOX, drive the tractor, and tread brake pedal quickly to maximum stroke within 0.2 s and last about 5.0 s, after putting gear in neutral position when vehicle speed reached target speed, such as 30 km/h or 40 km/h.

5.2 Test Results

Adjust air dryer limited pressure of the test vehicle to 850 kPa, and change the brake chamber of tractor rear axle in test vehicle. The style of brake chamber included 24 square feet, 27 square feet and 30 square feet. The braking performance of the articulated train at 30 km/h, 40 km/h, 50 km/h were done.

(1) 30 km/h emergency brake. The pressure change of brake chamber for articulated train rear axle and articulated train speed were shown in Figs. 6 and 7.

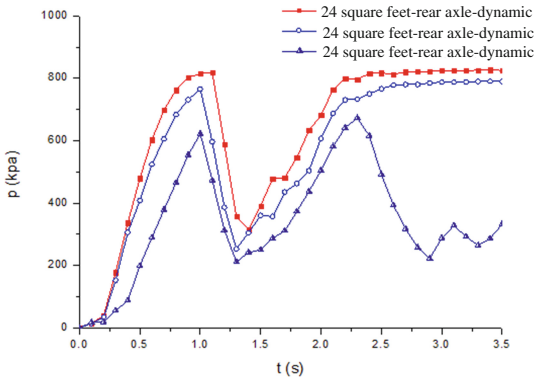

Fig. 6. Brake chamber pressure change at 30 km/h

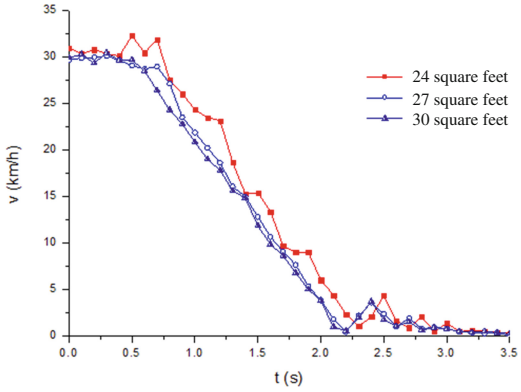

Fig. 7. Articulated train speed change at 30 km/h

(2) 40 km/h emergency brake. The pressure change of brake chamber for articulated train rear axle and articulated train speed were shown in Figs. 8 and 9.

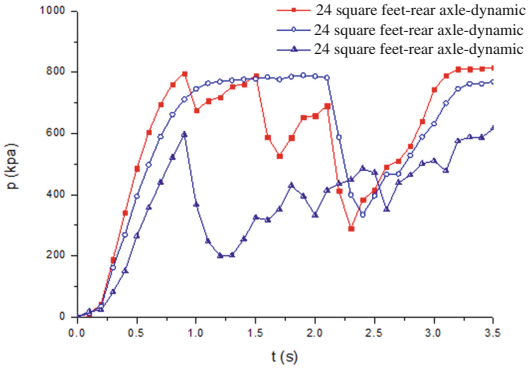

Fig. 8. Brake chamber pressure change at 40 km/h

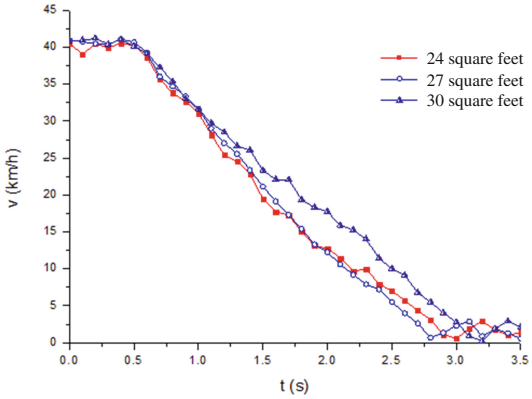

Fig. 9. Articulated train speed change at 40 km/h

(3) 50 km/h emergency brake. The pressure change of brake chamber for articulated train rear axle and articulated train speed were shown in Figs. 10 and 11.

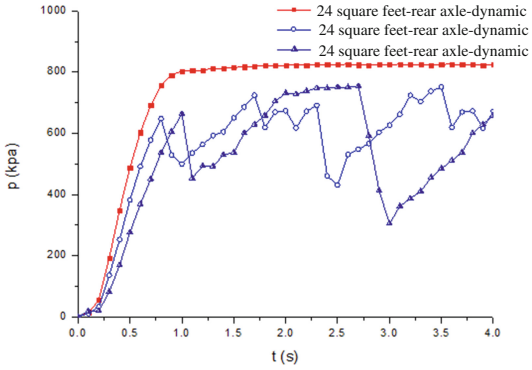

Fig. 10. Brake chamber pressure change at 50 km/h

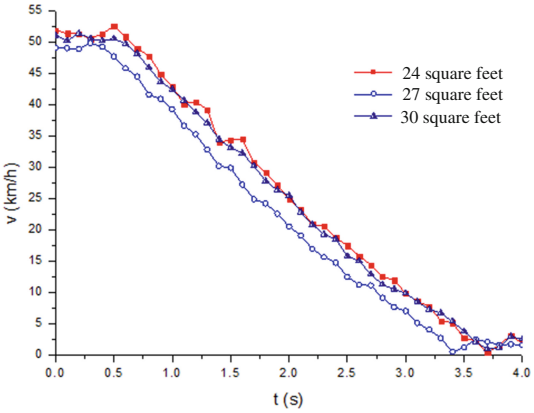

Fig. 11. Articulated train speed change at 50 km/h

5.3 Test Results Analysis

Result curves of the three tests at 30, 40 and 50 km/h were roughly similar. They showed that the influence of different specifications of the braking chamber on dynamic braking performance of the articulated train were same at different speeds.

With the increasing of bearing area of brake chamber, brake chamber inflation rate slowed slightly, and time of brake chamber air pressure rising to the maximum working pressure increased. At the same time. It also leaded to the increase of train's braking distance. The greater bearing area of brake chamber, the faster the speed decrease of articulated train, according to the relations between articulated train speed in emergency braking and different bearing area of brake chamber.

6 Conclusion

The greater the bearing area of brake chamber, the greater the braking force and braking torque of brake chamber outputted. Therefore, the speed of articulated train would decrease faster when the articulated train was equipped with large bearing area of brake chamber.

At the same time, the static braking delay of articulated train should be considered when selecting a large bearing area of brake chamber. The antilock brake system of articulated train should be work when changing different bearing area of brake chamber.

Acknowledgements. This paper is partially supported by the research project funded by the Ministry of transport (2015 312 223 320), the first author would like to thank Pro. Zhang Hongwei for the valuable discussions in improving the quality and presentation of the paper.

References

1. Tong Y (2010) China's Road Transport of Goods and Change of Industrial Organization Research. Fudan university, Shanghai
2. Li X (2015) Articulated with Balanced Suspension Train Ride Comfort Simulation and Analysis. Jilin university, Changchun
3. Zhang Jianguo (2010) Based on the Closed Loop Control of Articulated Train Car Stability Study. Jilin University, Changchun
4. Chen Q (2015) Commercial Vehicle Air Braking System Dynamic Characteristics Simulation Research. Jilin University, Changchun
5. Suh MW, Park YK, Kwon, SJ et al (2000) A Simulation Program for the Braking Characteristics of Tractor-Semitrailer Vehicle 2000-01-3415. SAE Paper
6. Chen J (2000) Tractor Articulated Train Car Brake Static Pressure Increase Process of Research on the Effects of Braking Performance. Wuhan University of automobile industry, Wuhan
7. Dunn AL, Heydinger GJ, Rizzoni G, Guenther DA (2003) Empirical Models for Commercial Vehicle Brake Torque from Experimental Data 2003-01-1325. SAE Paper
8. M En, Jie P (1997) Brake chamber output force experimental research. Tractors Farm Transporter 3:12–18

Standardization and Development of Road Freight Transport Vehicles

Jinsong Dong[1(✉)], Hongwei Zhang[1], Zekai Ren[1,2], and Chengqiang Zong[1]

[1] Key Laboratory of Operation Safety Technology on Transport Vehicles, Research Institute of Highway, Ministry of Transport, Beijing 100088, China
js.dong@rioh.cn
[2] School of Automotive Engineering, Harbin Institute of Technology, Weihai 264209, China

Abstract. The standard "Limits of dimensions, axle load and mass for motor vehicles, trailers and combination vehicles" is one of China's basic technical standard for vehicle management, which regulated the vehicle's dimensions, axle loads and mass limit. It is applicable to all motor vehicles, trailers and combination vehicles. In order to promote the use of new structures and new technologies in vehicle production, China's vehicle management and standardization management departments jointly carried out the technical amendment to GB1589. The revised version of GB 1589 added the type of center axle trailer. It perfected the length, axle load and total mass limit of the vehicle. This standard built China's road freight vehicle modular system and solved the problems of the inadaptability between vehicle width and pallet's size, the mismatching between tractors and semi-trailers, etc.

Keywords: Vehicle dimensions · Freight transport vehicles · International road transport · Vehicle modular system · Standard revision

1 Introduction

Limits of dimensions, axle load and mass for motor vehicles, trailers and combination vehicles (GB 1589), defines the limits of dimensions, axle load and mass. The previous version of the standard in 2004 played an important role in the specification of vehicle design, use and management. But the inadaptability in some aspects such as freight vehicle type standardization, tractor and semitrailer size matching, pallet and box body matching, axle load and total mass matching appears. Technical revision was completed and the new version was published on July 27, 2016. The publishing of GB 1589 has a significant influence on promoting the standardization of China's freight vehicles, improving the integration with the international vehicle standards and regulations and enhancing the healthy development of the domestic and international road freight transport industry.

X. Zeng et al. (eds.), *International Symposium for Intelligent Transportation and Smart City (ITASC) 2017 Proceedings*, Smart Innovation, Systems and Technologies 62, DOI 10.1007/978-981-10-3575-3_19

2 Development Status of Road Freight Transportation in China

Conditions of roads and stations are improving. Firstly, length of road is getting increasing, and road network density is further increased. National highway total mileage reaches 4.58 million kilometers in 2015. National highway density is round 47.7 km/100 km^2. Secondly, structure of road network is becoming better. The length of classified highway reaches 4.046 million kilometers with the increase of 1.46 million kilometers year on year in 2015. Freeway reaches 124 thousand kilometers with the increase rate of 10.7%. Finally, adjustment of freight station is speeded up. The total numbers of station decreased from 3124 to 2928.

Road freight transportation plays a fundamental role in the integrated transportation system. Road freight amount and freight turnover volume increased respectively from 14.66 billion tons and 0.97 trillion tons to 31.50 billion tons and 5.79 trillion tons during 2006~2015. Road freight amount and cargo turnover volume accounted for 75.5% and 32.7% respectively in the integrated transport system in 2015.

The number of employees engaged in road freight transportation is huge and individual transport plays a significant role. The number of employees engaged in road freight transportation reached 7.18 million. The employees belong to enterprises are about 592 thousand and the rest 6.59 million are individual owners, accounted for 8.2% and 91.8% respectively.

Logistics costs are still high. National social logistics was 219.2 trillion yuan in 2015, increased by 5.8%. Total social logistics cost was 10.8 trillion yuan and accounted for 16.0% of GDP.

Phenomenon of illegal modification and overloading is serious. The First one is car transporter with articulated vehicles as main part which with 30 ~ 40-meter-long. The second one is low-plate semi-trailer train with 17.5 m long (Figs. 1, 2, 3 and 4).

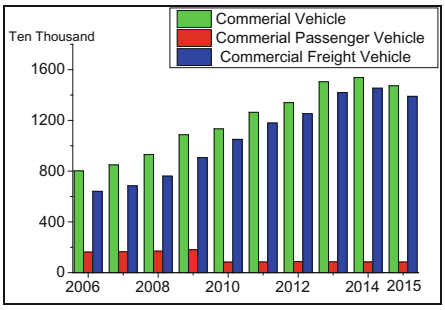

Fig. 1. Statistics of commercial vehicles in recent years

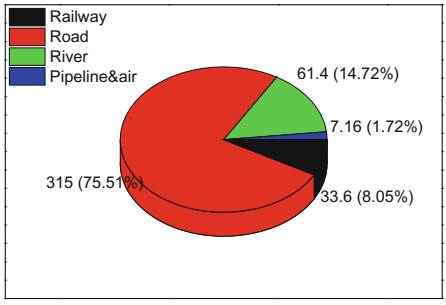

Fig. 2. Percentage of cargo transported in 2015

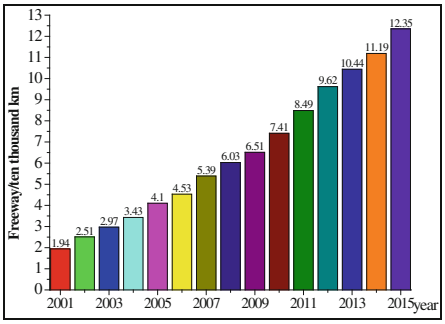

Fig. 3. China's free way mileage in recent years

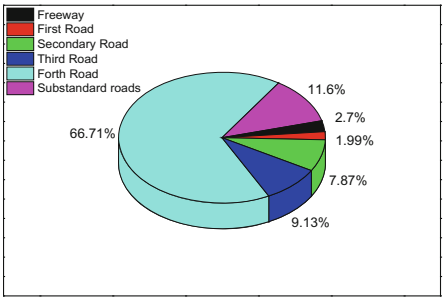

Fig. 4. Percentage of classified roads of China in 2015

3 China Cargo Transport Vehicles Management and Regulatory Standards

A multi-ministries parallel vehicle management system was constructed. China's vehicle management is the implementation of multi-sectoral parallel management system, taking different responsibilities according to the State Council division. Vehicle management departments include the Ministry of Industry and Information Technology, the Product Quality Supervision and Management Departments of State Council, the Ministry of Environmental Protection, the Ministry of Public Security, the Ministry of Transport etc. taking responsibilities for the management of new product announcements, CCC management and recall, vehicle pollutant emission control, motor vehicle registration, vehicle market access. Accumulated experience for many years in vehicle management, a vehicle legal system, vehicle management rules and regulations system and vehicle technology standard system have been constructed gradually, providing a basic guarantee for the development of China's commercial vehicles. The same as China, the EU and Japan adopt also type certification for the vehicles management. But The United States adopt the combination systems of self-certification and recall.

4 Main Adjustments in GB 1589

4.1 Adjust the Length Limits of van Semi-Trailer and Articulated Train

There are two limit requirements on the length of semitrailer in GB1589-2004, 13 m for normal semitrailer and 14.6 m for the enclosed van semitrailer. But the turning clearance circles of 18.1 m long train composed by the14.6 m long semitrailer could not meet the requirements. As a result, the length limit of semitrailer was adjusted to 13.75 m based on a large number of experimental verifications. For the semitrailer carrying 45-foot containers, the length limit is 13.95 m considering the particularity of the vehicle structure. To facilitate the use of standard and simplify the standard structure, the length of

articulated train composed by flat-headed tractor is defined to be 17.1 m. For the long-head tractor, the 18.1 m long-head articulated train can meet the requirements of turning clearance circles under the condition that the dimension of the trailer is not be changed (13.75 m and 12 m).

4.2 Add the Center Axle Trailer Type and Related Requirements

The new standard adds goods center axle trailer type. The length of center axle trailer is 12 m according to the European technical requirements. The length limit of van center axle trailer train is 20 m according the limits of length of fully trailer train in China. Meanwhile, the length of center axle trailer for car transport is added 2 m and reach 22 m.

4.3 Add Articulated Train Size to Match Requirements

The new standard adds the matching technical requirements for semi-trailer and semi-trailer. For semitrailer, it includes two limits requirement - front turning radius and the horizontal distance from the center of the traction pin of the semi-trailer to the end of the semitrailer, thus ensures to satisfy the requirement of length and pass ability after matching the tractor and semitrailer. In order to ensure the combination vehicles could meet the requirement of 4-meter height, the height of semitrailer tractor carrying 2591 mm box should not exceed 1320 mm under the unloading condition, and carrying 2896 mm box, should not exceed 1100 mm.

4.4 Limits of Width and Height

The new standard limit of height is the same with original one which defines the height limit as 4 m in view of the design requirements of highway tunnels, bridges and emergency lanes. The width is adjusted from 2.5 m to 2.55 m to load two pallets (1.2 m × 1.0 m) in the aim to fit for the width. For refrigerating motor vehicle, the width limit is 2.6 m because of the thick box body caused by filling insulation material and to ensure the two pallets could be loaded in the direction of width (Fig. 5).

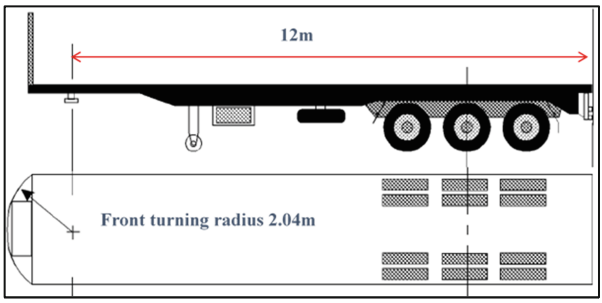

Fig. 5. Match requirements of articulated train

4.5 Limit of Maximum Axle Load

Classification requirements for based on vehicle types is deleted, and the load limit of single axle with single tyre was adjusted form 6 t to 7 t. Axle load limit of dual axle arranged trailer was adjusted from 20 t to 18 t, the same as the limit requirement of gross mass of two-axle trailer, truck and tractor.

4.6 Limits of Maximum Gross Mass

The minimum limits for the maximum design gross mass was canceled. The maximum gross mass for two-axle truck was adjusted from 16 t to 18 t the same as others two-axle vehicle. The gross mass limit requirement of combination vehicle is no longer determined by vehicle composition, mainly based on the number of axes. The gross mass of the four-axle train is adjusted from 35 t to 36 t, which is in accordance with the two-axle truck'. The maximum gross limit of center axle trailer was added which determined by the axle load, 10 t for single axle and 18 t for dual axles and 24t for three axles.

4.7 Vehicle Pass Ability Test Requirements

There is no change in the limit of turning clearance circles, and the inner and outer diameter is 10.6 m and 25 m respectively. The testing method is modified from a half circle passing to the whole circle passing which is the same with the requirement of EU. In addition, the entering direction of test vehicle was also modified from the original diameter tangent direction to the straight line direction.

5 Related Works of Freight Vehicle Management

5.1 Standardization of Freight Vehicles

The State Council clearly calls for the modernization of logistics technology and equipment, and actively develop standardized freight vehicles in the 'long-term logistics industry development planning (2014–2020)'. Standardization system of road vehicles was established basically by the Ministry of Transport. The main characteristic is the two units of 8 m and 13.75 m. The 8-meter short unit consists of swap body C-series, 20-foot container and 8-meter vehicle container and the 13.75-meter long unit consists of swap body A-series, 40-foot container and 45-foot container and 13.75-meter vehicle container. The trailer unit includes the canter axle trailers which carry the short types units mentioned above, the semitrailers and the dollies. The tractor unit includes trucks carrying the short unit and various semitrailers. These three units together constitute the Chinese road freight vehicle standardization system (Figs. 6 and 7).

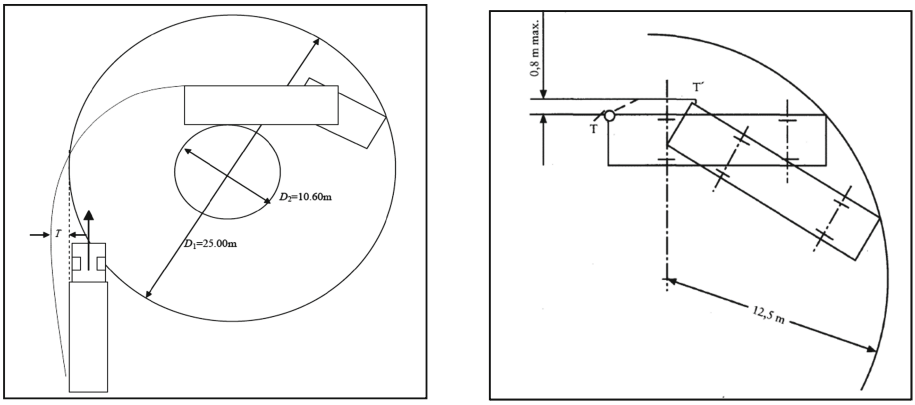

GB1589-2004 GB1589-2016

Fig. 6. Turning clearance circles testing method

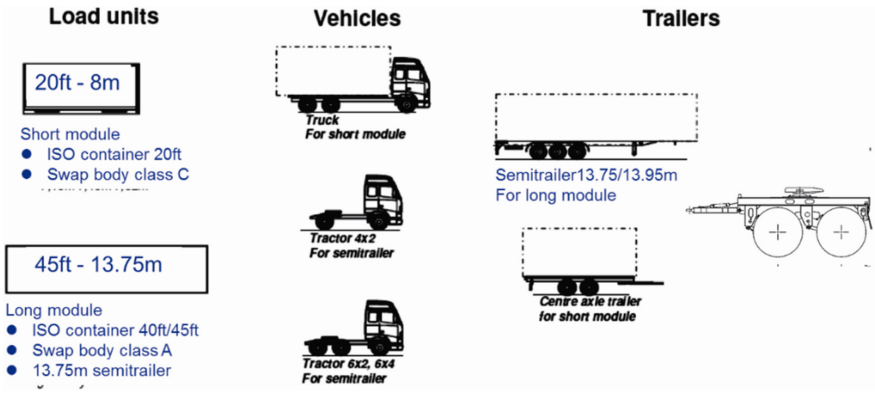

Fig. 7. Chinese road freight vehicle modular system

5.2 Swap Trailer Transport and Multimodal Transport

The relevant functional departments of the state issued 'Circular on promoting the development of transport' and 'hang transport pilot work plan', and the four batches of a total of 209 pilot projects were carried out. Each project could gain no more than 10 million capital allowance as an assistance in some aspects such as vehicle equipment, station building and informatization equipment. Comprehensive transportation Standardization Technical Committee was established by the Ministry of Transport. Integrated transport standard system was announced and the first batch of 16 multimodal transport demonstration projects were established.

5.3 Management on Overload

'Comments on further improving the work of the illegal modification and overloading of trucks' was announced by the Ministry of Transport with the purpose of further strengthening the managements on the illegal modification and overload of goods vehicles. Special actions such as the remediation of road freight vehicles' illegal overload behaviors, the managements on car transporters and the illegal modification of freight vehicles are carried out from August 18, 2016. The Ministry of Transport, the Ministry of Industry and Information Technology and the Ministry of Public Security, unified identification standard, realized the standard unified in the aspects of vehicle design, production, use, and management.

6 Conclusion

The revised version of GB 1589 added the type of center axle trailer. It perfected the length, axle load and total mass limit of the vehicle, and special requirements of special operation automobiles. This standard built China's road freight vehicle modular system and solved the problems of low efficiency cargo loading-unloading, the inadaptability between vehicle width and pallets, the mismatching between tractors and semi-trailers, etc. After this standard published, the Ministry of Transport carried out a series of standards revision and vehicle management, which promote the standardization process of China's freight vehicle effectively and improve the incorporation degree with the international vehicle standards and regulations. This standard will benefit the healthy development of domestic and international road freight transportation industry, and opened up a new market for international cooperation and trade. Of course, there are still some imperfections in the standards, which will be adjusted according to the transport needs.

Acknowledgments. This paper is partially supported by the Soft science research project funded by the Ministry of Transport (2016-3301), the first author would like to thank Pro. Zhang Hongwei for the valuable discussions in improving the quality of the paper.

References

1. GB 1589-2004, Limits of dimensions, axle load and masses for road vehicles
2. GB 1589-2016, Limits of dimensions, axle load and masses for motor vehicle, trailers and combination vehicles
3. Guang-ju W, Juan S, Bing-nan G (2016) Analysis of changes in the new version of GB 1589. AUTO SCI-TECH 4:24–29
4. Hong-wei Z, Wen-long W (2004) Safety analysis of over-size and over-load in road transport. J Highw Transp Res Dev 21(3):132

5. Yahua XU (2011) Considerations of policy for perfecting road freight transport market management. J Highw Transp Res Dev 28(2):154–158
6. Jin-song D, Hong-wei Z, Xue-li Z (2011) Interpretation of freight train (drop and pull transport) recommended model basic requirement-semi-tractor. Criterion Interpretation Appl 23:119–122

Driver's License and Some Personal Factors on the Visual Impact of Hazard Identification

Jian Sun[1(✉)], Jing-Shuai Yang[1], Dong Wang[2], Zhi-Zheng Ma[1], and Peng-Zi Chu[1]

[1] School of Automobile, Chang'an University, Xi'an 710064, China
mrsunjian@outlook.com, jshyang@chd.edu.cn, 1753392743@qq.com, cpz_myhk@163.com
[2] School of Automobile, Jilin University, Changchun 130000, China
351217678@qq.com

Abstract. The ability to identify hazards correctly is essential for safe driving. The purpose of this study is to analyze the driving licenses and personality factors on the impact of hazard identification. Twenty-five participants from Xi'an, China participated in the experiment and finished the simulated driving tasks as well personality factor tests (16PF scale related to personality factors). The Pearson correlation between simulated driving performance (dangerous scene recognition rate, dangerous scene identification time, scanning frequency and scanning angle) and 16PF scale score was calculated to obtain a consistent relationship between simulated driving task performance and 16PF scale scores. In the dangerous scene identification, the drivers with no license, high pressure, low stability and constancy often have low dangerous scene recognition rate and Hysteretic identification time. The results provide the basis of driver's driving licenses and some personality factors effect in hazard identification, and explain the important effects of driving visual training and personality factors on safe driving.

Keywords: Driver · Hazard identification · Personality factor · 16PF scale

1 Introduction

The road traffic safety system composed people-vehicle-road-environment is extremely complex. Many researchers at home and abroad have done a lot of research work in the field of identifying the influencing factors of road traffic safety, quantifying the interaction of various factors and how to prevent traffic accidents. Although the studies of vehicle, road and environmental factors occupies a certain proportion, the research on driver factors is still the mainstream. On the one hand, the driver is a major cause for road traffic accidents; On the other hand, with the gradual application of new technique in the road traffic safety system, the drivers will become the most unreliable factor in the system. The drivers in the proportion of traffic accidents will also be further increased [1].

基金项目:中央高校基金(310822161005).

X. Zeng et al. (eds.), *International Symposium for Intelligent Transportation and Smart City (ITASC) 2017 Proceedings*, Smart Innovation, Systems and Technologies 62, DOI 10.1007/978-981-10-3575-3_20

The driver's behavior research mainly focuses on the driver's perception-judgment-decision information processing model, that is, the driving individual's real-time sensing surrounding traffic situation information and take corresponding driving behavior to maintain the safe state [2, 3]. With the development of driving behavior research, the research on risk perception has been paid more and more attention. Foreign researchers have even pointed out that all the skills related to driving, only the perception of danger is closely related to traffic accidents [4]. Relevant statistics show that the traffic accidents caused by driver's dangerous perception error accounts for 40%–45% of the total number of accidents, and the traffic accidents related to driver's perception errors and judgment errors account for 80%–85% of the total accidents. This statistical result supports this conclusion to a certain extent. Therefore the UK and Australia use the Danger Perception test as a compulsory subject for obtaining a driving license [1]. Danger perception is perceived as the driver's abilities to read, evaluate, and assess dangerous situations, or dangerous situation awareness level of the driver, in the context of road traffic [5–7]. During the driving process, the driver should not only detect possible dangers found in traffic situations timely, but also to determine accurately whether the risk of causing traffic accidents, and thus make the appropriate driving operations. Therefore, the perception of danger is a very complex driving skill.

However, due to limited research on the driver's vision of hazard identification, the driver's different visual search patterns depend on factors such as age, experience and gender [8]. Driverless drivers generally have different visual scanning strategies and risk identification sensitivities, thereby weakening their ability to predict dangerous driving conditions and increasing the likelihood of undetected hazards. In other aspects of the drivers' factors, personality factors, including driver stability, permanence, tension, etc., may have an adverse effect on hazard identification, particularly the driver's visual impact. Among them, stability refers to the ability to resist emotional and environmental factors' influence. Persistence refers to whether or not to deal with specific matters, whether there is a sense of responsibility, whether there is the spirit of the law-abiding. Tension refers to the degree of instability in life and in the mind. The above indicators are closely related to the emotion and attitude of the drivers. The study shows that the negative emotions lead to the weakening of the behavior control ability, which leads to a longer observation time for the individual to observe the reaction conflict. Attitude is an important factor to determine behaviors. Changing the driver's attitude is an effective way to improve their behaviors. More well-known theory is Ahjzen's "Theory of Planned Behavior" (TPB), the driver's behavior is dominated by the purpose. And the purpose is influenced by the behavioral attitude, subjective standard and behavior control [9]. There is a strong correlation between the driver's attitude and the traffic accident and the driver's attitude will influence his behavior and the occurrence of traffic accidents [10, 11]. Therefore, this research is mainly aimed at the visual impact of driving license and personality factors (stability, permanence, tension) on driver's risk identification, and the following hypotheses are proposed: (1) Personality factors (stability, permanence, tension) are related to drivers' identification of dangerous scenes (dangerous scene recognition rate, recognition time). (2) Personality factors (stability, permanence, tension) are related to drivers' visual scan (number of glances, panning angle).

2 Method

Participants.
Twenty-five participants participated in the study. The participants were divided into driver's license group (22.9 ± 1.7 years; 170 ± 11 cm; 69.8 ± 13.7 kg) and no driver's license group (22.6 ± 2.0 years; 168 ± 9 cm; 67.3 ± 9.4 kg). All participants had normal signs or visual responses (equal to or better than 0.7 acuity) and had no known abnormalities in eye movement. The final statistical analysis included 23 participants, 2 of whom were excluded due to a larger error in the calibration of the eye tracker.

Apparatus.
Driving simulation software is able to provide the driver's video with the first view (including 14 dangerous scenes) on the screen and record the scene information according to the driver's mark. The participant's eye movement data were sampled and preliminary data analysis was performed by using a Dikablis head-mounted eye-tracking device (Professional Edition) at a frequency of 60 Hz and weight of 75 g and a D-Lab3.0 authorized software (Fig. 1).

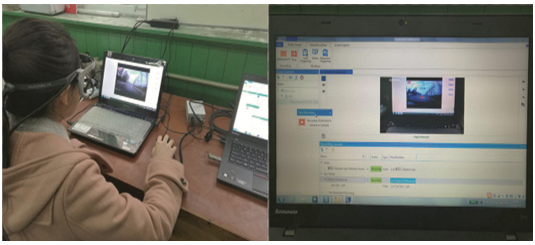

Fig. 1. Head-mounted vision tracking system and simulated driving software

Procedure.
Before the experiment, all participants' basic information and historical driving information were collected and personality factor test (16PF scale related to personality factor) was performed to evaluate the personality characteristics and ensure the integrity of the experimental data.

Participants were introduced to the requirements of the experiment and the use of the equipment (head-mounted visual tracking system and driving simulation software) and complete the calibration of the head-mounted visual tracking system. All participants were required to wear a head-mounted visual tracking system for a 5-min simulation to help them accustomed to the experimental environment.

Following the above steps, after completing the simulated driving operation, the participant was instructed to perform the simulated driving task for 30 min according to the usual driving mode and completed the identification of the risk factors. During simulated driving, participants were required to follow traffic regulations, speed limits and avoid talking. The participants clicked on the screen in the risk factors when the participants thought it is the dangerous scene. The software would also recorded the relevant information. To ensure that all participants were experimenting in the same

driving environment, driving simulation tasks contain the same road conditions and risk factors.

Measures.
Driver's visual measurement with the dangerous scene recognition rate, the dangerous scene identification time, the number of glances and panning angle to estimate: (1) Participants' recognition rate of the dangerous scene(including the sudden merger of 14 typical dangerous scenes) contained in the first-view driving video provided by the driving simulation software. (2) Scene recognition time (represented by the number of frame count corresponding to the video when the driver hits the keyboard), contained in the dangerous scene that the driver clicks on the screen record. The driving simulation software complete the appropriate information collection. (3) The driver's visual scanning range (with the number of saccade times and the saccadic angle), through the head-mounted visual tracking system acquisition and analysis.

Personality factor testing. Before the start of the experiment, the participants were asked to evaluate the stability, persistence and tension by means of a questionnaire (16PF scale related to personality). An example topic: "I often cross the street to avoid people that I do not want to say hello: A. rarely so B. occasionally so C. sometimes so. And according to the option, the answers were converted into standard scores.

Analysis.
In the 16PF scale, a higher conversion to a standard score indicates greater stress, higher persistence (more cautious, responsible), and free from environmental impact. In addition, Pearson correlation analysis between test results and experimental variables was performed in this study. All analyzes were performed in SPSS (IBM SPSS Statistics 19.0).

The Pearson product-moment correlation coefficient (also known as PPMCC or PCCs, R or Pearson's r is often used in paper) was used to correlate the experimental data and measure the correlation (Linear correlation) between some personality factors and participants' simulated driving performance. It was developed by Karl Pearson from a similar but somewhat different idea of Francis Galton in the 1880 s. This correlation coefficient is also called the "Pearson correlation coefficient r", as follows.

$$\rho_{X,Y} = \frac{cov(X,Y)}{\sigma_X \sigma_Y} = \frac{E((X-\mu_X)(Y-\mu_Y))}{\sigma_X \sigma_Y} = \frac{E(XY) - E(X)E(Y)}{\sqrt{E(X^2) - E^2(X)}\sqrt{E(Y^2) - E^2(Y)}}$$

(The X and Y represent the analysis variables)

3 Results

Table 1 lists the Pearson correlation analysis between the 16PF scale score evaluating the personality factors (stability, permanence, tension) and the hazard scene recognition rate. Overall, there was a negative correlation($r = -0.273$, $p < 0.05$) between tension personality factor and hazard scene recognition rate. No significant correlation was observed in the no driver's license group. In the driver's license group, there was a

positive correlation between the stability ($r = 0.273$, $p < 0.05$) personality factor and hazard scene recognition rate. There was a negative correlation between the tension ($r = -0.365$, $p < 0.05$) personality factor and hazard scene recognition rate.

Table 1. Pearson correlation analysis between some personality factors and hazard scene recognition rate

	Stability	Permanence	Tension
Scene recognition rate (overall)	0.168	0.083	−0.273[a]
Scene recognition rate (without license)	0.002	−0.160	−0.053
Scene recognition rate (having driver's license)	0.273[a]	0.158	−0.365[a]

[a]represents $P < 0.05$

Table 2 lists the Pearson correlation analysis between the 16PF scale score evaluating the personality factors (stability, permanence, tension) and the hazard scene recognition time. Overall, there was a negative correlation ($r = -0.527$, $p < 0.05$) between the permanence personality factor and the dangerous scene identification time. There was a negative correlation between the stability ($R = -0.414$, $p < 0.05$), tension ($r = -0.543$, $p < 0.05$) personality factors and dangerous scene identification time in the no driver's license group. There was a negative correlation between the stability ($R = -0.396$, $p < 0.05$), tension ($r = -0.729$, $p < 0.05$) personality factors and the dangerous scene identification time in the driver's license group.

Table 2. Pearson correlation analysis of some personality factors and dangerous scene recognition moments

	Stability	Permanence	Tension
Scene recognition time (total)	−0.181	−0.527[a]	0.041
Scene recognition time (without license)	−0.414[a]	−0.543[a]	0.033
Scene recognition time (having driver's license)	−0.396[a]	−0.729[a]	0.014

[a]represents $P < 0.05$

As to the indicator of driver's license, it has an influence on the correlation of personality factors (stability, permanence, tension) with the saccade times and the saccadic angle. And there is a greater number of saccade times and saccadic angle of drivers compared with those without drivers. Control the variable of driver's license. Table 3 lists the Pearson correlation analysis between the 16PF scale score evaluating the personality factors (stability, permanence, tension) and the driver's visual scan range(the saccade times and the saccadic angle). Overall, there was a positive correlation ($r = 0.392$, $p < 0.05$) between the permanence personality factor and the saccade times. There was a positive correlation ($r = 0.392$, $p < 0.05$) between the stable personality factors and the saccadic angle. In the driver's license group, there is a positive correlation ($R = 0.729$, $p < 0.05$) between the personality factors and the saccade times. There was

a positive correlation ($r = 0.605$, $p < 0.05$) between the permanence personality factors and the saccadic angle. In the driver's license group, there was a positive correlation ($r = 0.306$, $p < 0.05$) between the stable personality factors and the saccadic angle.

Table 3. Pearson correlation analysis between partial personality factors and driver's visual measurement scan range (The saccade times and the saccadia angle)

	Stability	Permanence	Tension
The saccade times (overall)	0.341	0.392[a]	0.141
The saccadic angle (overall)	0.392[a]	0.349	−0.272
No driver's license			
The saccade times	0.545	0.441	0.495
The saccadic angle	0.729[a]	0.605[a]	0.422
Having driver's license			
The saccade times	0.143	0.154	0.292
The saccadic angle	0.306[a]	0.147	0.007

[a]represents $P < 0.05$

4 Discussion

In this study, the dangerous scene recognition rate and the dangerous scene identification time represent the driver's perception of the potential danger. The higher recognition rate and the faster recognition time represent the strong perceptions. The saccade times and the saccadic angle represent the measure of driver' vision which is a situational awareness variable. Because performing a driving task requires frequent scans on both sides of the road in front of the vehicle, such as traffic signs, oncoming vehicles and pedestrians to examine safety-related clues and to predict potential risks [12, 13].

The results show that there is a relationship between the personality factor and the dangerous scene recognition rate in the driver's license group. Compared with those with low stability (21.43%) and permanence (30.95%), the drivers with higher stability (48.21%) and higher permanence (50.00%) had higher risk of scene recognition. Compared to the high tension (41.07%) of the driver, the low tension (57.14%) driver's dangerous scene recognition rate is low, but in no driver's license group has no such conclusion. Moreover, the dangerous scene identification statistics show that the drivers with license (52.38%) found more dangerous scenes than the drivers without license (40.48%), indicating that drivers with license showed a higher risk perception level, which is consistent with previous study [14, 15]. The contents of this experiment can not explain the reasons of the differences in hazard identification capabilities between the driver with license and no license. Further experimental analysis is needed.

In the case of dangerous scene recognition time, the overall analysis showed that the relationship between the persistence and scene recognition time was negatively correlated ($r = -0.527$, $p < 0.05$). There was a negative correlation between the stability ($R = -0.396$, $p < 0.05$), tension ($r = -0.729$, $p < 0.05$) personality factors and the dangerous scene identification time in the driver's license group which meant the driver

could identify the dangerous scene more quickly. Through the recognition time (number of frames) of the three dangerous scenes with high recognition rate (sudden mergence, dangerous scenes caused by truck and tricycle), the first hypothesis is confirmed by the fact that drivers have a higher rate of visual search and are more quickly to see the danger and recognize it (Fig. 2) than drivers without license. This confirms the first hypothesis of the study.

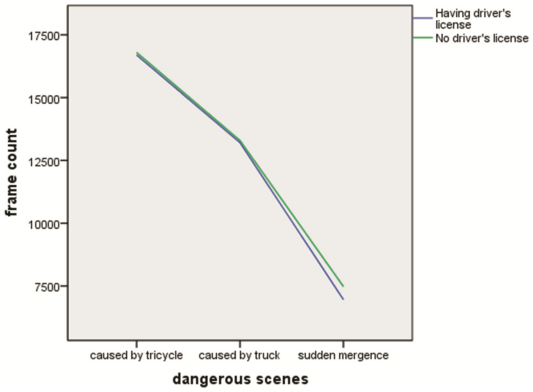

Fig. 2. The driver's dangerous scene identification time (frame count)

Table 3 shows that personality factors have an impact on the driver's visual scanning range (saccade times and saccadic angle), and drivers without driving license are more affected by personality factors, indicating that drivers with license have a relatively fixed visual control strategy and are less affected by personality factors [16], confirming the second hypothesis of the study. And the drivers with license (8.36 times, 36.73°) had more saccade times and wider saccadic angle than the drivers without license (2.57 times, 8.37°). This means that drivers with licenses have a wider range of vision, can effectively deal with more information and make response more rapidly on the dangerous situation. This is consistent with the findings of Hye-In Lee, Seungha Park, Jongil Lim (2015).

5 Limitations

The above conclusion is limited by the participant's identification of the dangerous scene based on the driver's video with the first view provided by the experimental simulation driving software and the driver's video only provide the driver's front the road and the two-side roads, no rearview mirror and dashboard, etc. There is a gap between the visual scene and the reality driving. So, it is a weak alternative to the actual driving situation. In fact, the video has been carried out a certain degree of circumvention on the dangerous scenes. So this study can not provide the relevant measurements about participants take action on dangerous scenes.

The experimental results provide the basis for the influence of driving licenses and personality factors on the identification of dangerous scenes during driving. It can be seen from the experiment that drivers' hazard identification is related to various factors. Due to the limited number of samples and information collection, it is impossible to identify the association with driver-related age, passengers, driving mileage, driving attitude and illegal records. The future studies design should clarify the impact of these factors on the driver's hazard identification.

References

1. 杨京帅, 李秀丽, 任书杭, 王婷, 高扬 (2015) 驾驶人危险感知影响因素建模与试验. 长安大学学报 35:105–110
2. 冯忠祥, 袁华智, 刘静. 驾驶人个人特征对行车速度的影响. 交通运输工程学报 12:89–96. doi:10.3969/j.issn.1674-120X.2012.06.097
3. Elvik R (2010) Why some road safety problems are more difficult to solve than others. Accid Anal Prev 42:1089–1096. doi:10.1016/j.aap.2009.12.020
4. Mcknight AJ, Mcknight AS (2003) Young novice drivers: Careless or clueless? Accid Anal Prev 35:921–925. doi:10.1016/S0001-4575(02)00100-8
5. Borowsky A, Oron-Gilad T, Meir A (2012) Drivers' perception of vulnerable road users: A hazard perception approach. Accid Anal Prev 44:160–166. doi:10.1016/j.aap.2010.11.029
6. Crundall D, Chapman P, Trawley S et al (2012) Some hazards are more attractive than others: Drivers of varying experience respond differently to different types of hazard. Accid Anal Prev 45:600–609. doi:10.1016/j.aap.2011.09.049
7. Scialfa CT, Borkenhagen D, Lyon J (2013) A comparison of static and dynamic hazard perception tests. Accid Anal Prev 51:268–273. doi:10.1016/j.aap.2012.12.006
8. Elvik R (2010) Why some road safety problems are more difficult to solve than others. Accid Anal Prev 42:1089–1096. doi:10.1016/j.aap.2009.12.020
9. Montes SA, Introzzi IM (2015) Selective attention and error proneness while driving: Research using a conjunctive visual search task. Phys Educ 5. doi:10.12804/apl34.2.2016.01
10. 石京, 逍遥 (2014) 驾驶心理对交通安全的影响. 驾驶个体特征与交通安全 5:65–70. doi:10.3963/j.issn1674-4861.2014.05.012
11. Hu TX, Xie X, Li J (2013) Negative or positive? The effect of emotion and mood on risky driving. Transp Res Part F: Traffic Psychol. Behav 16:29–40. doi:10.1016/j.trf.2012.08.009
12. 郭应时, 付锐, 袁伟, 宴国强, 程文冬 (2013) 驾驶人潜在危险预知能力评估系统研究. 中国安全科学学报 23:73–78. doi:10.16265/j.cnki.issn1003-3033.2013.03.009
13. 马勇, 付锐, 孟妮, 郭应时, 袁伟 (2015) 道路环境对驾驶人眼动行为影响的试验研究. 交通运输系统工程与信息 15:83–88. doi:10.16097/j.cnki.1009-6744.2015.03.014
14. Pollatsek A, Narayanaan V, Pradhan A (2006) Using eye movements to evaluate a PC-based risk awareness and perception training program on a driving simulator. Hum Factors 48:447–464. doi:10.1518/001872006778606787
15. Underwood G, Phelps N, Wright C (2005) Eye fixation scanpaths of younger and older drivers in a hazard perception task. Ophthalmic Physiol Opt 25:346–356. doi:10.1111/j.1475-1313.2005.00290.x
16. Lee H-I, Park S, Lim J, Chang SH (2016) Influence of driver's career and secondary cognitive task on visual search behavior in driving: A dual-task paradigm. Psicología Latinoam 34(2):195–203 doi:10.4236/ape.2015.54029

The Research of Design Technology and Application on Permeable Sidewalk: A Technical Summary of Sponge City

Hong Li(✉), Yanfeng Bai, and Ling Zhang

Shanghai Municipal Engineering Design and Research Institute (Group) Co., Ltd., Shanghai, China
279198330@qq.com, baiyanfeng@smedi.com

Abstract. Permeable Sidewalk is an important measure to accelerate the "Sponge City" construction without substantial increase of construction costs. On the basis of existing research results, this paper concluded the classification and design indicators of permeable sidewalks by analyzing traditional sidewalks' problems and their applicability. Then the Shanghai Expo Park and the Bund Channel are taken as examples for introducing the application of permeable sidewalks, which can provide references for promoting the "Sponge City" technology.

Keywords: Sponge City · Permeable paving · Sidewalk

1 Introduction

In some sidewalks of German cities, there are 10 cm square small stones into view. But actually, they are all stone pillars embedded in the ground, with a depth of 30 cm. These sidewalks paved with stone pillars are not only durable but also permeable, which can let rain infiltrate into the ground rapidly, and thus, the earth, rain, and air can form a ecological exchanging system, even profitable for the surrounding plants. Besides, there will not be any water remaining on the ground, so there would be no problem for walking any time. As the planning and investing on urban roads are usually completed without reconstruction in German, although cost relatively higher, it will avoid frequent maintenance and repairing in the future. Such kinds of sidewalks are very good examples for us.

The urban roads construction has been developing almost every day as the urbanization scale is continuously expanding in China. However, some Chinese cities paid much more attention on rapid transportation to achieve a quick success, leaving slow transportation construction relatively weak, especially the sidewalk construction. As a result, loosing and damage usually happen to the paving, and the rain can easily cause water splashing.

In Chinese urban construction, the roads of streets, sidewalks, bicycle ways, parks, courtyards, and public squares are mostly paved with impermeable stones or concrete. It is simple and cheap, but caused many bad effects for urban ecological environment.

X. Zeng et al. (eds.), *International Symposium for Intelligent Transportation and Smart City (ITASC) 2017 Proceedings*, Smart Innovation, Systems and Technologies 62, DOI 10.1007/978-981-10-3575-3_21

Firstly, such impermeable roads caused much less water infiltrating into the earth, and thus most rain can only be drained through urban drainage system, so the groundwater cannot get enough supplement. As the urban water consumption increases, groundwater extraction also increases, which will inevitably cause groundwater lowering. Therefore, the plants growth will be affected and the ecological balance on the earth will be destroyed.

Permeable sidewalk is a new urban paving method. It uses highly porous materials for surface and base layer, and on the premise of ensuring the strength and duration, the water can smoothly enter the inside of paving structure, directly get through the temporary storable earth base or drainage pipes. So it can achieve several functions, such as containing water, improving urban environment, enhancing safety and comforts, etc.

This new kinds of permeable roads are also called the "sponge roads", which means they can rapidly absorb the water like sponge. Also there are some experts call them "the roads which can drink". This paper based on the angle of construction design, illustrates the application of permeable sidewalks in modern urban cities, which may provide reference for the technology application and construction of "sponge city".

2 Problems of Traditional Sidewalks

In urban construction, the roads of streets, sidewalks, bicycle ways, parks, courtyards, and public squares are mostly paved with impermeable stones or concrete. It is simple and cheap, but caused many bad effects for urban ecological environment. Firstly, such impermeable roads caused much less water infiltrating into the earth, and thus most rain can only be drained through urban drainage system, so the groundwater cannot get enough supplement. As the urban water consumption increases, groundwater extraction also increases, which will inevitably cause groundwater lowering. Therefore, the plants growth will be affected and the ecological balance on the earth will be destroyed.

There are many problems of traditional impermeable paving:

(1) The rain water can only be slowly flowed into water wells for draining, so the sidewalks are very easily filled with water, which greatly influenced walking safety and comfort.
(2) As the water is directly drained through drainage pipes, the ground surface lack the ability of adjusting temperature and humidity, which may exacerbate the heat island effect.
(3) The groundwater supplement path is damaged, which is harmful for the surrounding plants.

In some cities like Paris and London, apart from traffic arteries which need high-strength, wear-resistant and noise-reducing pavement, most walking streets, sidewalks, and parking lots are constructed with permeable paving.

In recent years, the new permeable paving has been gradually promoted in China. It can drain the surface water rapidly in rainy days, which can improve the driving safety. Porous permeable paving materials can not only lower the vehicle noise, but also increased the anti-sliding structure depth by their rough surface. Besides, such roads can

also increase the area of porous earth surface, which is helpful for adjusting urban climate and lowering ground surface temperature, so the "heat island effect" will be weakened. As a result, it has positive meaning to promote permeable sidewalks in applicable areas.

3 The Applicability Analysis of Permeable Sidewalks

Based on the international construction requirements for ecological cities, there should be as little concrete cover as possible. Self-drainage system is beneficial to infiltrate the rain, and the ideal index is that 80% of the ground is permeable. Traditional impermeable sidewalks are also highly thermal conductive, whereas the water in the pores of permeable sidewalks can effectively lower the ground temperature.

Permeable sidewalks are applicable for all kinds of new-built and reconstructed rapid urban roads, main roads, secondary roads, branch roads, meanwhile, they can also be used in walking paths in resident area, non-motorized roads, parks, public squares, walking streets, and parking lots.

Earth condition should also be considered when using permeable sidewalks. It is applicable in the foundation with a certain porosity. Firstly, the porosity coefficient should exceeds 1.0×10^{-3} mm/s, and the permeable surface should be at least 1.0 m under the groundwater surface. For the foundation with lower porosity, and permafrost, soft soil, liquefied soil, expansive soil, collapsible loess, saline soil, and water resource protection area, it should take serious consideration.

4 The Classification of Permeable Sidewalks

Based on the permeable principle on the surface, permeable sidewalks can be classified as "gap permeable type" and "multi-pore permeable type". The "gap permeable type" means the surface water can infiltrate through the gap of surface blocks. Consequently,

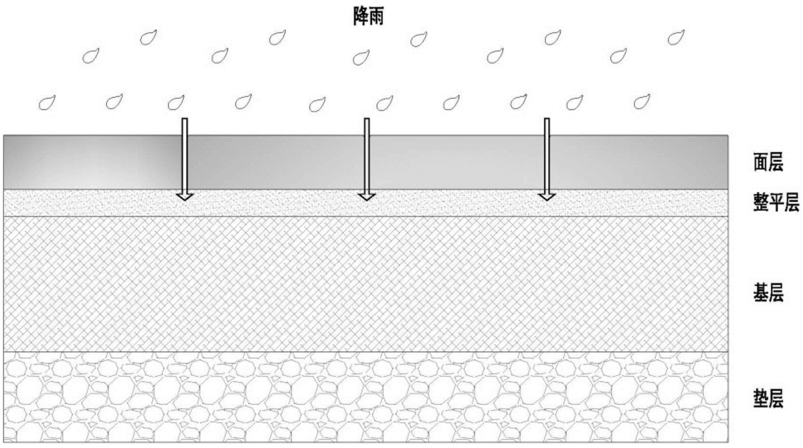

Fig. 1. The schematic diagram of "gap permeable type" sidewalks

such kinds of roads need to leave some gaps on the paving blocks, so the surface water will be able to infiltrate, as shown in Fig. 1. The "multi-pore permeable type" means the surface water can directly infiltrate through the surface layer. Enough porosity is essential to enable the surface water to infiltrate, as shown in Fig. 2.

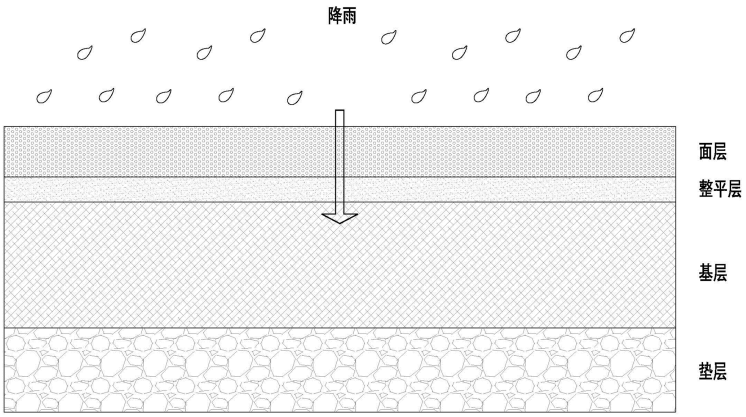

Fig. 2. The schematic diagram of "multi-pore permeable type" sidewalks

Based on the difference of infiltrating paths, the permeable sidewalks can be classified as "Fully permeable" and "Half permeable".

"Half permeable": the surface water will be drained into municipal pipes through road structure layer, as shown in Fig. 3.

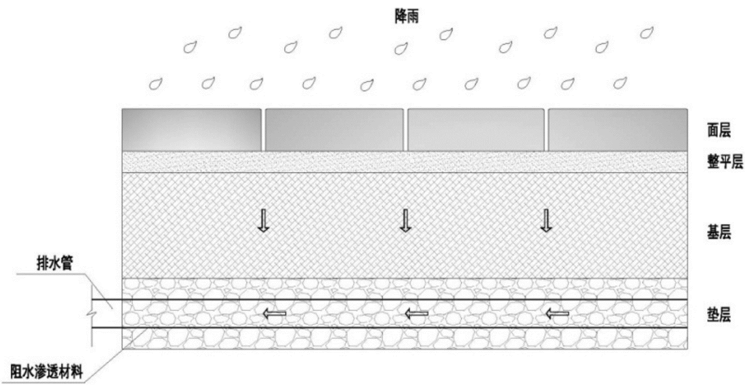

Fig. 3. The schematic diagram of "Half permeable" sidewalks

"Fully permeable": the surface water can be fully or partly infiltrated into the soil, and the rest can be drained into municipal pipes, as shown in Fig. 4.

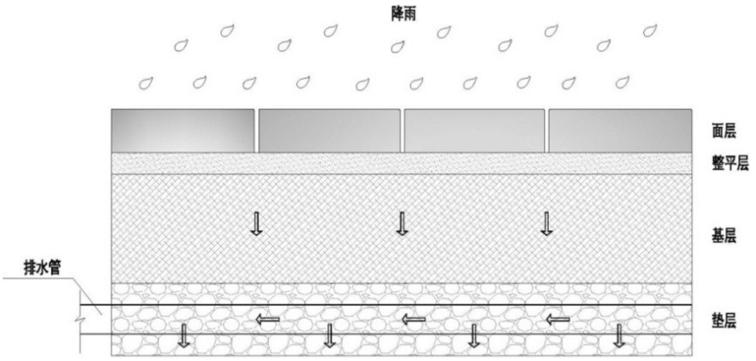

Fig. 4. The schematic diagram of "Fully permeable" sidewalks

5 The Pavement Structure of Permeable Sidewalks

The pavement structure of permeable sidewalks can be determined according to soil bearing capacity, soil uniformity, groundwater distribution and frost heave situation. The basic structure of normal permeable sidewalks can be illustrated as Fig. 5, and the functions of each layer are shown in Tables 1 and 2.

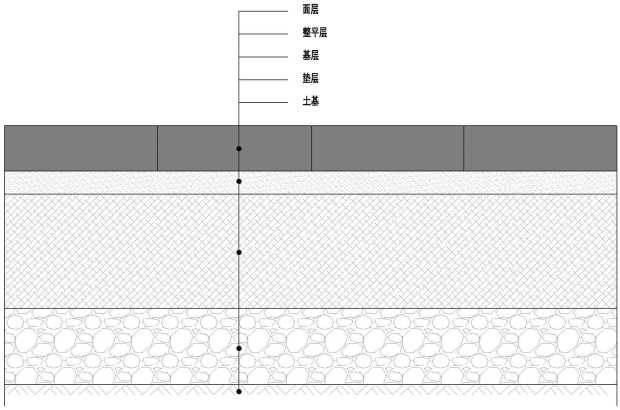

Fig. 5. The basic structure of permeable sidewalks

Table 1. The functions of each part of permeable sidewalk structure

Structure layer	Functions	Materials
Surface	Directly bear the load, permeable, storing water, anti-wear, anti-skid	Permeable brick, permeable concrete
Leveling layer	Permeable, leveling, connect the surface and the base	Medium sand, dry harden cement
Base	Mainly bear the load, permeable, storing water	Permeable concrete, permeable stable gravel, permeable gradation gravel
	Prevent the water into the road bed or rise because of the capillary phenomenon, to ease the frost heave effect of the water-containing soil, which is both bearable and permeable	Permeable gradation gravel
Cushion	Prevent the infiltrated water rise because of the capillary phenomenon, to ease the frost heave effect of the water-containing soil.	Natural gravel
Soil foundation	Storing the infiltrated water	Suitable soil

Table 2. The comparison of three permeable pavements

	Permeable bricks	Permeable concrete	Permeable asphalt concrete
Surface	6 cm permeable bricks	8 cm C30 permeable concrete	4 cm OGFC-10 (modified asphalt with high viscosity)
Leveling layer	3 cm medium or coarse gravel (a kind of acupuncture non-woven geotextile)	–	–
Base	10 ~ 15 cm permeable concrete	15 ~ 18 cm multi-porosity cement stabilized gravel	12 ~ 15 cm permeable concrete
Cushion	10 cm gradation gravel	10 cm gradation gravel	10 cm gradation gravel
Features	Advantages: Construction is simple, low dependence on mechanized construction, low cost, and it can form different patterns by brick shape and color. Disadvantage: Poor integrity, low bear capacity.	Advantage: Construction is simple, well structure integrity, high bearing capacity, low cost, construction speed is fast by mechanized construction Disadvantage: landscape effect is not good because of the grey color of permeable concrete, and if mixed with pigments, it is restricted by material itself, color, and cost.	Advantage: well structure integrity, high flatness, high bearing capacity, construction speed is fast by mechanized construction. Disadvantage: paving and rolling must be done under high temperature, so the machine is indispensable, the high-cost modified asphalt with high viscosity is necessary, and if mixed with other pigments, it may cost higher. The asphalt concrete is usually black, which has no good landscape effect, and even mixed with asphalt mixture, it is still monochrome.
Scope of application	It is suitable for sidewalks where need not much bearing capacity, and the construction area is not too large, or somewhere cannot be constructed with machine because of complex underground situation	It is suitable for the place with large area, which can be constructed with machines, and the places where need enough bearing capacity and not much landscape requirements, such as squares, car parking lots.	It is suitable for the places with large area for mechanized construction, and those with high bearing capacity requirements, such as squares, non-motorized lanes, car parking lots.

6 Main Technology Requirements for Permeable Sidewalks Structure

The permeable sidewalks are formed with road structure and drainage facilities. The road structure includes surface, leveling layer, base, cushion, soil foundation, and the drainage facilities include the blind ditch and water collection wells. The road structure material structure requirements are concluded according to the related codes and engineering experiences, as shown in Table 3.

(1) Permeable bricks

The surface materials are mainly precast concrete permeable bricks. The compressive strength and permeability coefficient are the most important two indexes. The compressive strength ensures the bearing capacity, which needs dense material with little porosity. On the other hand, the permeability coefficient reflects the infiltration capacity, which needs the material to have some connectivity porosity. The two indexes are both contradictory and interdependent. It requires the design to consider the balance of both indexes instead of partially emphasizing only strength or permeability.

According to the permeable brick standard, the compressive strength should be Cc30 ~ Cc60, and the permeability coefficient should be no less than 0.1 mm. According to engineering experience, the strength of the permeable bricks for just walking can use Cc30, and the permeability coefficient should be no less than 0.03 cm/s. While for some small cars or parking, the strength of bricks can be Cc40, and the permeability coefficient should be more than 0.1 mm/s.

Leveling layer: the material of leveling layer is usually medium and coarse gravel. The first function of this layer is to level the surface of base, which will be available for paving, and the second function is to provide a little deformation to promote preliminary embedded lock and certain permeability. There should be acupuncture non-woven geotextile at the bottom of this layer, which could prevent the gravel to block the pores.

Base: the base can be constructed together with cushion layer with gradation gravel in order to meet the bearing capacity requirements; it can also choose porous stable gravel or permeable concrete.

When the bearing capacity requirement is not too high, the base and the cushion can also be constructed together with gradation gravel, and the aggregate gradation should follow the related specifications. The crushing value should be no more than 35%, and the needle sheet content should be no more than 20%. When the bearing capacity requirements is relatively high, it can be done with porous stable gravel or permeable concrete.

Cushion: When the base is gradation gravel, the cushion is usually merged with base with the same gradation gravel, while the base is constructed with porous stable gravel or permeable concrete, the cushion can be paved with gravels of 15 cm ~ 25 cm, with 3 ~ 5 mm stone chips on the surface.

Table 3. The requirements of permeable sidewalk structure materials

Structure	Material	Strength requirements	Permeable requirements	Thickness requirements	Remarks
Surface	Permeable bricks	≥6kN ≥C40, ≥ 6kN	Effective porosity ≥ 15%, Permeability coefficient k ≥ 0.1 mm/s	6 ~ 8 cm	Anti-sliding index BPN ≥ 80
	Permeable concrete	≥3.5 MPa	Effective porosity ≥ 15%, Permeability coefficient k ≥ 0.1 mm/s	5 ~ 8 cm	BPN ≥ 80 Anti-sliding index BPN ≥ 80
	Permeable asphalt	OGFC-10	Effective porosity ≥ 15%, Permeability coefficient k ≥ 0.1 mm/s	3 cm	–
Leveling layer	Stone chips	–	Effective porosity 10% ~ 5%, Permeability coefficient k ≥ 0.1 mm/s	2 ~ 3 cm	No need to set acupuncture non-woven geotextile
	dry harden cement	≥M15	Effective porosity 10% ~ 5%, Permeability coefficient k ≥ 0.1 mm/s	2 ~ 3 cm	No need to set acupuncture non-woven geotextile
Base	Permeable concrete	≥3.5 MPa	Effective porosity ≥ 15%, Permeability coefficient k ≥ 0.05 mm/s	10 ~ 15 cm	–
	Permeable cement, stable gravel	2.5 ~ 3.5 MPa	Effective porosity ≥ 15%, Permeability coefficient k ≥ 0.1 mm/s	15 ~ 18 cm	
	Gradation gravel	Crushing value ≤ 30% Compactness ≥ 95%	Effective porosity ≥ 15%, Permeability coefficient k ≥ 0.1 mm/s	15 ~ 18 cm	
Cushion	Gradation gravel	Crushing value ≤ 35% Compactness ≥ 93%	Effective porosity ≥ 15%, Permeability coefficient k ≥ 0.1 mm/s	8 ~ 10 cm	
	Nature gravel	Crushing value ≤ 35% Compactness ≥ 93%	Effective porosity ≥ 15%, Permeability coefficient k ≥ 0.1 mm/s	8 ~ 10 cm	
Soil foundation	The soil which is suitable for sidewalks construction	Modulus of elasticity ≥ 15 MPa, Compactness is between 90% to 93%		–	

(2) Permeable concrete

The strength of permeable concrete is usually C30. Pigments and color stones can be used to make colorful concrete if there is landscape requirement. The base and the cushion material can be gradation gravel or porous stable gravel according to the bearing capacity. The cushion is usually gradation gravel. The soil foundation should be consolidated and leveled. The technical requirements of permeable concrete, porous stable concrete and gradation gravel are basically the same as the permeable bricks.

(3) Permeable asphalt concrete

The material of permeable asphalt paving is a kind of drainage asphalt mixture, and the gradation type is usually OGFC-10. Considering the difficulties of paving and consolidation when used on the sidewalks, the porosity can be designed as no less than 15% for enough durability. Colorless asphalt can be used together with pigments and colorful stones to make colorful mixture if there is landscape requirements. The base of asphalt paving can be constructed with porous stable gravel or permeable concrete, and the cushion is usually constructed with gradation gravel.

7 Project Example

(1) Permeable sidewalks in Shanghai Expo

All the sidewalks of Shanghai Expo are constructed in fully permeable structure. The permeable sidewalks not only ensured the supplement of underwater from rain, which reduced the ground settlement, and also prevented the erosion and damage on the paving itself. Besides, the rain can be infiltrated into ground through permeable sidewalks, which both saved the water for green space and eased the drainage pressure, ensured the walking safety and comfort, and meanwhile, it also preserved the overall landscape, which can produce tremendous social economic benefits both directly and indirectly. Therefore, the sidewalks can be treated as an important measure to improve environment quality, reduce heat and preserve water resource to use permeable sidewalks in Expo area.

There are three paving materials in Shanghai Expo area, which are permeable asphalt, permeable concrete and permeable bricks.

The permeable asphalt paving is mixed with color elements, which changed the monochrome traditional asphalt roads. The colors are perfectly merged with the surrounding landscape, which brought wonderful visual enjoyments for people. The colorful asphalt paving can also be used to help to induce traffic, improve environment and enhance urban view, etc.

The structure of permeable concrete is divided as half permeable and fully permeable. It consists of coarse aggregate and water or mortar, which can drain the water rapidly through the inside pores.

The permeable brick is relatively simple because its type and color. It can be implemented by manpower, which is adopted in many sidewalks in Expo area (Fig. 6).

(2) Permeable sidewalks in Shanghai Bund aisle

Fig. 6. The roads in Shanghai Expo area

The Shanghai Bund aisle is a key project in Shanghai, there is about 940 m from Xinkaihe Rd. to Laotaiping Rd. linked to the Bund waterfront landscape renovation project, which should have very high landscape requirements, so the design of these sidewalks adopted asphalt paving. The final scheme was the combination of Homogeneous cement concrete bricks and permeable asphalt paving. The bricks were used in the area by the side stone and street trees, and the rest were paved by permeable asphalt.

8 Conclusion

Permeable sidewalk is a kind of the sponge city technology, which has better performance than traditional walking road in many ways, such as conserving water, improving city environment and improving traffic comfort, etc. On the basis of analyzing the suitability of permeable sidewalks, this paper concludes the classification, typical structure and technical requirements, and introduces its application by the example of Shanghai Expo and Shanghai Bund aisle. It can provide some reference for the application and promotion of permeable sidewalk technology in the sponge city construction.

References

1. Guiding Opinions of the State Council on Promoting the Construction of Sponge City
2. Song ZB, Zhao HR, Bai JL (2006) Promoting the application of permeable paving and urban ecological benign development. J Hebei Eng Tech Coll 3:16–18
3. Wang QX, Shen MX, She GH (2006) Experimental study on porous concrete without sand. Urban Roads Bridges Flood Control 6:154–157
4. Wang B, Wang Y, Gao JM (2004) Permeable system of permeable pavement. Architect Technol 7:531–532
5. Technical Guide for Sponge City Construction, Ministry of Housing and Urban - Rural Development (2014)
6. Zhang WJ, Ding YY, Zhang SH (2006) Study on the persistence of permeable concrete brick. New Building Materials 6:22–24

Digitalization and Application Research of BIM-Based Power Plants Lifecycle Information

Ling Su(✉)

CRRC Information Technology Co., LTD, Beijing, China
108359286@qq.com

Abstract. With the current Internet, cloud computing, big data, such as technology continues to progress, intelligent power plant construction is the future trend. As a base of intelligent power plant, the digitization and informatization construction are achieving good results on the application of part and point. But on the aspect of full life-cycle management, there are lack of depth research and practice on integration application to existing information, management of power plant construction, production, operations, etc. From the management angle of plant life cycle, the thesis brings the idea that establish panoramic, digital and smart power plant to realize controlling establishing investment, schedule, quality and establishing process data of power plant. Visualized operation and maintenance system of power plant would be realized with the base of three-dimension models of digital power plant in panoramic power plant, including equipment intelligent communication during operation and maintenance, Intelligent sense of equipment information collection, intelligent assessment and analysis of equipment status and so on, which can increase continuity and analytical of plant life cycle and realize digital and intelligent power plant. Meanwhile, the thesis suggests informationized master plan of power plant life cycle, which is to realize perceived reliability, virtual reconstruction, response instantly and business collaboration and management decision by uniformly planned and realized step by step with three levels of "panoramic power plant, digital power plant and intelligent power plant".

Keywords: Life cycle · BIM technology · Visible operation and maintenance · Digital power plant · Intelligent power plant

1 Introduction

Safety, efficiency and cleaning have become an inevitable trend of power plants development. In order to guarantee power plants' production safety and management quality, and meanwhile lower down the energy consumption, digitalization and informatization techniques must be adopted to promote their own development. By adjusting the manufacturing methods and management modes, an integration of lifecycle management and control can be realized, and thus guaranteeing the safety production, to maximize the lifecycle running benefits.

X. Zeng et al. (eds.), *International Symposium for Intelligent Transportation and Smart City (ITASC) 2017 Proceedings*, Smart Innovation, Systems and Technologies 62, DOI 10.1007/978-981-10-3575-3_22

Innovation policies in the industry techniques have been gradually carried out and implemented, such as Energy Internet and smart energy. Thanks to the requirements of energy saving and emission reduction, the construction of digital power plants, smart power plants, intelligent power plants have already been researched and promoted. It is definitely an inevitable trend to build new digital power plants and smart power plants.

The cognition of digital power plant by power design institutes, power group companies and power plants is more or less different, but basically they have a common sense. It can be concluded that, digital power plants should include three conditions: panorama visible, process standardized, and management sensible and controllable [1]. As there is a rapid development in Chinese power industry these years, the cognition of digital power plant has already been far beyond the original knowledge abroad. Now, the digital surveying, digital control and digital presentation have also been concluded into the application of power plant construction, which greatly enriched the content of digital power plant [2]. Consequently, this has also become a character of digital power plant's concept development, and meanwhile, the concept integration is also consistent with the lifecycle management.

The lifecycle information management of power plant by BIM can largely improve the informatization level of power plant design, construction and maintenance, and as a result, it can improve the efficiency and benefits of all kinds of work, which provides a powerful method and technical support for market competition.

Engineering and financial management are the main contents of lifecycle management. Engineering management mainly includes equipment duration analysis, equipment reliability analysis, equipment maintenance, failure analysis and diagnosis, system analysis and diagnosis, substitute components' impact and system maintenance. Financial management mainly includes comparison analysis upon system or equipment, preliminary and maintenance costs analysis, equipment reformation and technique innovation costs control, etc. [4]. All these cost calculation, high-efficient maintenance are based on sophisticated digital and information analysis. Besides, there is also the research of BIM standards. Standards are very essential for synchronized work in such large systems, and the range and depth of the standards can lead to design an available project process plan.

There are many requirements in power plants lifecycle management, especially in the maintenance visualization, such as:

(1) The requirement of improving assets management level
(2) The requirement of information construction
(3) The requirement of concealed engineering construction
(4) The requirement of new staff training

According to these requirements and the success of BIM in building, the application of BIM concept and techniques in digital power plant lifecycle information management is mainly researched in this paper. The application should be able to largely reduce the construction and maintenance costs. Besides, if the power plants design, construction, adjustment and installation, and maintenance are implemented in a single platform, all work efficiency will be highly improved, which can greatly promote the development of lifecycle management in digital power plants' construction.

2 Main Research Content and Key Problems

(1) The research of power plant's lifecycle information management based on BIM. It includes the integration and application of building and equipment model, which covers both the design stage and the maintenance stage, in detail, there are the equipment research and production, raw material procurement, logistic, equipment testing, maintenance management, and lifecycle information management. The collaboration OA model based on Cloud-BIM is very helpful for the research and application of lifecycle information management.
(2) The research of power plant's maintenance model. The digitalized power plants' lifecycle information management based on BIM can bring great changes to their maintenance model, which will cause power plants' maintenance reformation. As a result, the maintenance model should be seriously discussed.

3 The Digitalization of Power Plants' Information

The digital power plant is a comprehensive data analysis model for all kinds of spatial objects, such as buildings, pipe network, Electromechanical system, and working objects as well, such as equipments, materials. By information method, the data of construction and operation can be easily collected and analyzed, which can help to control the power plant's operation and decision management, and thus, the economy and social profits can be improved. Consequently, several energy problems could be alleviated, such as contaminants discharge, equipments repairing and improving. During the implementation of digital power plants, the most difference from traditional informational power plants is its systematic information management. The integration of traditional management model, application and overall analysis can maximize the advantage of digitalization in the whole lifecycle of the plant implementation, including its design, construction and operation, so the working efficiency can be significantly improved.

The main idea of digitalized power plant is to make both construction and operation data and information digitalized, and then put these data into the control platform for intelligent analysis to get accurate results. It can provide precise strategies on operation optimization, units repairing plan, and equipment maintenance, so as to improve the working efficiency, cut down the power generation costs, and maximize the existing resources. The implementation of power plants can be divided into three stages.

(1) Design stage

Based on all kinds of the construction drawings, build the power plants 3D model by software (such as 3DMAX) according to real architecture and equipments parameters. The facilities and devices which could not be accurately presented on traditional drawings, such as those with complex structure and implementation process, can be presented more visually, three-dimensionally, and precisely.

(2) Construction stage

The 3D model of the power plant serves as a carrier in the construction stage. And then the lifecycle control and management system based on BIM technology can be set up, which can synchronously implement the design, construction, operation and management. The participants of power plants can cooperate more smoothly through the BIM platform. They can do the construction schedule control, quality control, and safety management on this visualized platform, and meanwhile, the project management can also be realized by integrating outer professional system, such as video surveillance, in order to strengthen the process management timely by monitoring the construction quality comprehensively. In another hand, this visualized model can be the original material carrier, including all kinds of files, which can be transferred to the operational stage for further use.

(3) Operational stage

Based on the panoramic power plant model integrated by BIM technology, as the 3D digitalized power plant is built, main working principals can be presented in many ways, such as 3D graphics or 2D pictures, videos, texts. etc. For example, the main parts of the power plants, such as boiler, motor, thermal controlling part, can be presented with scenes, colors, transparency, and flashes, and thus, their structure and working principal can be directly explained, which can be used in the employees' training. Actually, it can comprehensively support the power plants management and applications, e.g., it can provide data inquiring and viewing, modifying management, online training, inspection and monitoring, strategy support, and technology assistance, etc.

4 The Implementation and Application of the Power Plant's Lifecycle Data Model

The BIM-based lifecycle information management system can provide pretty good solution for all stages of the project, and meanwhile, it can promote the information transferring, storing, management and sharing for all construction participants. The main values are illustrated as following:

(1) Synchronous design and efficient examination during design stage

BIM technology has made synchronous design possible. During the design stage, engineers with different specialties can design their parts respectively, and examine the collision and mistakes in the same model by BIM technology. So they can simply find the problems and make adjustments programs accordingly. And besides, the model components' modifying is overall in the whole system, different designers need not to do this respectively, which can significantly reduce design mistakes. As a result, new problems can be greatly avoided.

In conclusion, BIM technology can provide a method to ensure collaboration among different specialties, multiple measures such as collision examination can be used for design adjustments timely, which can make sure the design results are correct.

(2) Improve the information reusability

The BIM model integrates all the project information of all construction participants, which also reduces data losses and mistakes caused by human errors. By accurate connection of the model and information, it can provide related information timely according to the real-time model. It can be treated as a very well solution to improve information reusability for all the project participants in all stages.

(3) Information cooperation for all project participants in the construction stage

Through BIM lifecycle information management, it is possible to provide a cooperation platform for all construction participants. Based on this BIM platform, together with the help of the internet of things, mobile internet, 3D-visualization, it can realize the digitalization, internet-based data transferring of structure construction, equipments installation, and moreover, the installation can be standardized, all the site equipments can be virtualized on the platform. In sum, the single platform with all information can unify the construction standards, making the management rules ahead of the construction, and the working schedule can also be easily planned, as a result, many management functions can be set on this platform, such as further installation visualization, fast data collection and efficient professional management strategy.

Unified standards: build a construction management database for construction and installation, and set the controlling aspects and management templates for the construction and installation. this can provide standardized controlling methods for construction, working flows, technical index, and greatly reduce the management difficulty of the construction and installation process.

Pre-set rules: the management nodes, standards, templates and requirements should be implemented according to the pre-set rules, which is seriously made based on the construction processes. Meanwhile, the site equipments should be perfectly jointed with the virtualized equipments in the system, which can realize the unity of real elements and virtualized model, and paper material and digital information as well.

Pre-control: the digital project of construction and equipment installation can make deduction and data analysis based on virtualized models, so as to intuitively present the status of construction and installation quality, which can efficiently help the construction simulation and dynamic management. It can provide working platform for all the participants by comprehensively monitoring and recording the site construction work, and thus, it can efficiently support the multiple-specialty communication and cooperation during the construction and equipment installation, ensuring the synchronous and cross construction work implement smoothly. And consequently, the construction conflicts, slacks, and reworks can be significantly reduced, and unnecessary wastes could be avoided as well, therefore, the construction duration and quality can be satisfying. It can be concluded that the pre-control function can realize the digitalization, standardization and visualization management.

The construction process management by BIM based on the internet of things and digitalized power plant construction information, which includes several management features, such as full participation, full perception, full control, full improvement. It can realize the digitalization, standardization, visualized management of the whole installation process, and also the management of contracts, schedule, quality, safety and files

during the construction, supervision, transportation, installation, and acceptance of the structure construction and equipment installation.

(4) Provide tremendous management value for operation

Traditional power plants' information system pay their attention only on the data itself or 2D drawings through the construction and operation, so it cannot intuitively and vividly present the whole view or equipment details of the power plant. There are no similar virtual platforms to store these information, so the digital assets could not be built, which caused plenty of construction data lost after the power plants were built. However, the BIM-based power plants' construction model completely saved all the previous data when they are finished, including all the stages of the early files, project bidding, design and construction, and by data representation and analysis, the deliverable data assets will be produced. During operation, combined with 3D power plants technology, the equipments management can be extended both in time dimension and space dimension, and the concealed engineering construction, remotely inspection and repairing, employee training can also be use this platform, which may greatly improve the system availability and reliability. So as a result, the assets lifecycle management and application can be markedly improved, and perfect information management can also reduce the assets maintenance costs.

For example, in a large nuclear power plants overhaul project, the nuclear island equipment 3D model and spatial location are built with the digitalized power plant technology, and together with the schedule, plenty of work was seriously arranged synchronously, and by the simulation of equipment dismantling, entering, moving and paths, the detailed scheme was optimized, which ensured the whole project to be implemented reasonably. Especially, the construction plan included specific location of the equipments and tools, so the construction duration was successfully controlled, which enabled the whole project completed 92.5 h ahead of the preliminary plan.

5 Conclusion and Prospect

This paper mainly analyzed the BIM technology, the idea of digitalized power plant, and lifecycle information management. The digitalized power plant can be divided into panoramic power plant, digitalized power plant and smart power plant. BIM technology provides a measure to realize the power plants' lifecycle information management. for a digitalized power plant project, it plays a significant role in the power plants construction and operation to use BIM technology for information digitalization and lifecycle data management.

References

1. 魏思源.建筑给排水工程施工组织优化研究[D].郑州:郑州大学 (2010)
2. 张丽.基于 RFID 技术的图书馆智能书架系统的研究与设计[D].南昌:南昌航空大学 (2013)
3. Zaijun W (2013) Application of BIM in operation and maintenance management of the building. Constr Econ 09:94–97

4. 何力.数字化电厂关键技术分析与探讨[J].科技创新与应用 (2013),(15):165
5. Jianhua C, Hui W (2012) Application and popularization of BIM technology in project management. Constr Technol 41(37):19–41
6. ANCOLD (Australian national committee on large dams), Guidelines on risk assessment (2003)

Review on the Legal System of Unban Underground Space in China

Yingjuan Qiao(✉)

Shanghai Municipal Engineering Design and Research Institute (Group) Co., LTD, Shanghai, China
qiaoyingjuan@smedi.com

Abstract. This paper summarizes and analyzes the current situation of urban underground space development and utilization, underground space right research, underground space registration system, and the characteristics of underground space utilization and the composition of rights system, and puts forward the legal system of underground space utilization in China, Spatial resources of the rational, orderly, efficient, coordinated development and utilization, which can be a reference for relevant works.

Keywords: Urban underground space · Development and utilization · Legal system proposal

1 Introduction

With the rapidly increasing urban population and shortage of land resource, it has become a trend to use the land three-dimensionally. The three-dimensional land use has brought changes of land rights concept and legislation, which has already been established in several western countries, more still, the land legislation has also become three-dimensionally. However, China has a long way to catch up both in the practice and legislation of 3D land use [1].

In the recent 30 years, China's rapid urbanization made the urban land more and more precious, especially in big cities and mega-cities. According to the prediction, there will be no new land to explore in Shanghai in 2040, therefore, it has become a consensus to use the land intensively. The use of underground space is an important solution for many urban problems, such as land shortage, traffic congestion, air contamination, rain flood and water logging, etc. [2, 3].

The scale and speed of underground space development are significant in China. However, the existing related laws and regulations are not able to cover those areas, and there are even conflicts among the laws and regulations themselves, which caused difficulties for using and managing the underground space recourses [4].

Based on the present utilization conditions of underground space in China, this paper did research on the underground space rights, registration system and space utilization rights, and proposed a conception of legislation system, which may provide references

X. Zeng et al. (eds.), *International Symposium for Intelligent Transportation and Smart City (ITASC) 2017 Proceedings*, Smart Innovation, Systems and Technologies 62, DOI 10.1007/978-981-10-3575-3_23

for the utilization of Chinese underground space in a reasonable, orderly and high-efficient way.

2 Research of Space Rights

The ownership management mainly includes the land right and space rights during the underground space development. The research and laws for the land rights have been relatively mature in China, instead, the study of the space rights is still in the preliminary stage. According to various theories and examples, the space rights can be generally classified as shown in Fig. 1.

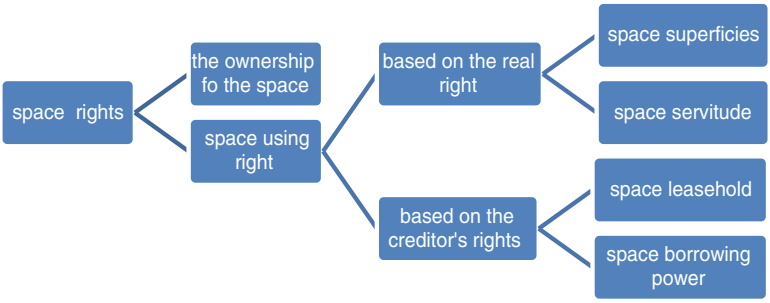

Fig. 1. The classify of space rights

According to the property laws, the space using right with the nature of creditor's rights can be classified as a kind of debt law. From the perspective of usher property rights, only the space using rights with the nature of property belongs to the rights with property legislative meanings [5]. Based on this, the development of the space rights is mostly promoted around those with property characters.

The Anglo-American countries have specifically enacted the space rights, such as America. According to law, the space belongs to the real estate, which can be possessed, transferred, leased, guaranteed and inherited. Civil law countries treated the space rights as a special form of normal ground rights, which has no essential differences from other ground rights, and there are rules specially made for the space ground rights. In Taiwan, the space rights system is configured with "law package", which not only depends on the "Mass transit law", but also revises the laws with connections with ground rights, such as civil law, land law, land tax law, etc. Meanwhile, the land registration and repetition regulations are proposed as well [5]. The space right in Taiwan is actually the extension and expansion of traditional ground rights.

China has also enacted laws and regulations for urban underground space, such as the Law on Urban Planning, the Land Management, the Urban Real Estate Management, the People's Air Defense, the Mineral Resources, etc. But none of these laws is directly enacted for the development and utilization of urban underground space [6]. Article 136 of the Property Law of the People's Republic of China stipulates that "the right to use land for construction may be established on the surface, ground or underground of the

land, and the newly established right of construction land shall not harm the established usufructual rights". Therefore, on the same land, depending on the scope of their respective rights, there may be a number of independent construction land use rights and construction land users. This requires that the scope of their rights must be defined to avoid the disputes. Where the right to use land is established on the ground, on the ground or under the ground, all directions and the related contents of the rights shall be defined specifically. The ownership of the land in China only belongs to the state or the group, people only have the rights to use the land on or under the ground.

3 Underground Space Registration System

3.1 Underground Space Registration in China

Article 5 of Chap. 2 of the Land Registration Act, which was formally implemented in February 2008, stipulates that the land shall be registered in the form of parcels, and the parcel refers to the land or space where the land tenure boundary is closed. The definition of the concept of parcel is the corresponding "property law" in the construction of land use rights registration. Some cities made rules by local laws and regulations for the registration of underground space, which varies significantly in different places (Table 1).

Table 1. Provisions for the registration of the underground in different cities

Document	Article	Content
Interim measures for the use and registration of the right to use land in the underground (ground) space of Suzhou City	Article 15	Legally registered underground, land use space construction rights and other rights protected by law. Set the underground and space on the use of land use rights registration type and procedures, in accordance with the relevant provisions of the state, provincial and municipal implementation, and indicate the "underground space construction land use rights", "ground floor construction land use rights"
Interim measures for the development and utilization of underground space in Shenzhen City	Article 5	The city land and real estate management department is responsible for the use of underground space transfer and property rights registration management
Regulations on the planning and construction of underground space in Shanghai	Article 28	Underground construction should be registered for land use together with the upground construction. Single underground construction should be registered for its underground space using rights and housing ownership

3.2 Establish and Improve Space Rights Registration System

The registration system is closely related to the construction land use rights. As a real right, the construction land use rights' acquisition generally needs to be registered. But our current legislation in this regard is still lagging behind.

The land registration system stipulates that the land registration book should specify the relevant contents, although the registration system can refer to the relevant provisions of the ordinary construction land use rights, such as the name of the parties, the purpose of the establishment and the use terms of registration. Space ground has its own characteristics, it is established within a certain space away from the ground surface, which is neither specified nor guided by the original registration system. In the real estate registration system, we should first clear the principle of registration, the real estate registration law must add the necessary provisions of the "space range"; Secondly, to clear the scope of the specific measurement of space, both the plane and depth scale should be specified according to the underground structure.

The purpose of registration is to clarify the rights of various spaces, protect people's legitimate rights and interests. The space right to confirm, change or destroy can be regulated according to the legal provisions of the existing real estate registration. After the establishment of the space right registration system, we can ensure the transfer, rent, lease and mortgage of space rights.

4 The Characteristics of Underground Space Utilization and the Constitution of Right System

As a real estate, underground building's ownership is often vague. Most high-rise buildings include underground structure, which normally takes a large proportion, and it is causing more and more disputes. In China, the ownership and use rights are separated, Therefore, in order to protect the lawful rights and interests of the investors who acquire the land use right according to law, it is still necessary to clarify the subject's rights, responsibilities and obligations, etc. [7].

The characteristics of urban underground space utilization are mainly due to the relationship between itself and the upground part, and the difference between the relationship will affect the type of underground space rights, which will impact on the establishment of the rights system, The types of rights are:

(1) the using right of the construction land: the right to use state-owned land for buildings or other crops;
(2) Building ownership: Owners have ownership for those residential and operating buildings, and share the common or co-managed rights of the common part of the exclusive buildings;
(3) easements: the rights to use other people's real estate according to contracts in order to improve their efficiency and agreed by the contract to use rights;
(4) Space ground right: the right to use the space above or under other people's land for some certain purpose;
(5) space service: the right of cheaply using other people's certain space.

(6) space lease right: a specific space for the purpose of the establishment of the right to lease.
(7) space lending rights: a specific space for the purpose of the establishment of the right to borrow.

On the basis of underground using situations, the space rights above and under the ground surface can be classified as shown in Table 2.

Table 2. Rights types for different building forms

The earth, the earth's surface and underground	The right type	building forms
Overground building Underground building	①②③⑥⑦	Combined with construction project; Consistent subject for the ground or underground property rights.
Space or road Underground building	④②⑤⑥⑦	The single Underground building; The underground space that can be transfered
Overground building A B C D Underground building/E	①②③④ ⑤⑥⑦	Incongruity subject for the ground or underground property rights. Get the granted underground space for the subject of land use right; transfer the underground space use rights all alone
Overground building/A Underground building/B Deep underground space/C	①②③④ ⑤⑥⑦	Deep underground space applications; The connection part between the in and exit of underground space or the ground property rights subject; transfer the underground space use rights alone or government free transfer underground space

In the process of establishing the legal system of underground space, by comprehensive consideration of different rights types, it is helpful to consider the establishment of laws and regulations in detail and to clarify the scope of underground space rights, so as to reduce disputes, and as a consequence, there will be a clear right for possession, use, income and disposition.

5 Conception of Underground Space Legal System

5.1 Form a Special Space Law System and Clarify the Law Status for Underground Space Development and Utilization

At present, China has no specific laws for urban underground space. With the large-scale development of urban underground space, the establishment of space law becomes urgent. On the basis of the introduction of basic laws, the state government departments and the provinces, municipalities and autonomous regions of the People's Congress and the government can enact corresponding administrative regulations, local regulations and departmental rules and regulations, and refine and specify the basic laws and regulations, In order to better implement in reality [6].

Space law includes:

(1) Basic regulations for underground space utilization: basic policies and policies such as the right to use underground space (space right, space service, etc.), compensation standard for underground space construction, and occupation permit of public underground facilities.

Table 3. Laws for different stages of underground space development

Phase	Classification	Content
Design and construction	The implementation laws of underground space construction	Underground complex, the subway, underground road, comprehensive utility tunnel, underground parking garage, underground electric power facilities, underground water resources, underground mineral resources, deep underground space use of facilities
Implementation of operating	Safety regulations in underground space	Structure safety equipment, construction safety assurance, disaster prevention safety rules and regulations
Maintenance and management	Maintenance and management regulations of underground space	Underground building environmental regulations on hygienic standards; electrical, heating management laws and regulations, oil storage management laws and regulations, the protection of the common ditch management rules, and the provisions of the noise, vibration, etc.

(2) The laws and regulations for underground space development and utilization, including the design of underground space, construction, cost management and maintenance aspects of [6], as shown in Table 3.

The spatial resources of multiple functions related to so many departments of space management. Therefore, in the process of underground space legislation, the coordination between the departments should be also paid attention to.

5.2 Establish and Improve the Underground Space Planning and Regulatory System

Underground space development and utilization is irreversible, so it is necessary to make laws to guarantee reasonable and orderly development and utilization, to avoid damage and waste. Adhere to the planning first, pay attention to the underground space planning system, basic, overall and forward-looking, we must improve the planning and regulatory system, so as to use the plan to achieve full and effective use of underground space purposes.

The Law of China Urban Underground Space Use Planning and the local urban planning regulations do not have the relevant provisions for the planning and management of underground space utilization. However, urban underground space planning should be included in the entire city design planning to avoid development blindness.

5.3 Establish the Space Registration System, Including the Orderly Development, Use and Transfer of Underground Space

The underground space of the city is fixed and immovable. It shall be recognized as real property, and its ownership shall be confirmed, changed and eliminated In accordance with the relevant provisions of the real estate laws and regulations. The registration shall be the legal way of confirming and publicizing the public based on the agreement.

The core content of urban underground space registration is the registration of using rights for underground space [8]. Land owners, land users, space users can coexist in the same land of the upper and lower layers of space, resulting in the rights of the main plane or three-dimensional relationship between the three. But the right person to use the space must be specific, which cannot be extended to others' territory. Therefore, the legislation should stipulate that the right to use space must be legally registered. It not only protects the rights of people, but also protects the interests of other land owners, so the social and economic life stability could be maintained. The urban underground space registration authority should choose the land management department; the procedure for the registration of urban underground space should be guided by legitimate process theory and connected with the existing land registration system.

Access to the using rights of urban underground space, can be either through the free transfer, or be paid through the rental. Underground space holders can obtain a certain amount of underground space right by paying a certain amount of the transfer fee, and then register to get an underground space certification. In order to reduce disputes and clarify their respective rights, the legislation should stipulate that the space using right

certification should clearly record the spatial scope of the using rights. Due to the particularity of the object of underground space use, the scope of underground space should be clearly documented in the registration, and the underground space should be specified in the upper, lower, left, right, front and rear places.

5.4 Establish the High-Efficient Management System

The current situation of China's space management is inconsistent. Several departments are involved, such as the Ministry of Construction, the Ministry of Civil Affairs, the department of housing management, and other relevant departments involved in the development of underground space. There is no legislation to implement unified department management [9].

The unified management of underground space needs to be strengthened, and the "comprehensive coordination, professional management" framework is proposed, which is led by the government coordination, and the professional joint management mechanism. Legislation and implementation are unified by single management department to make decisions, and at the same time, actively guide industry associations and non-governmental organizations, so that they can not only provide information and advice, but also coordinate the government affairs. To establish an efficient organization and management system, the formation of information sharing mechanism, security mechanisms, decision-making mechanism, the implementation mechanism, and supervision mechanism, give full play to the organization and management in the underground space development and utilization of the core organizational role.

6 Conclusions

The acceleration of urbanization has caused the city congestion, pollution, serious waterlogging and other disasters, the use of urban underground space has become an inevitable trend of sustainable urban development. China's urban underground space has entered a rapid, large-scale development stage, the legislation on the right to space has been increasingly urgent.

Based on the research status of space right, the registration system of space right and the establishment of underground space right system, this paper analyzed the related problems in the establishment of underground space legal system. It is necessary to establish the basic law system of underground space, improve the underground space planning regulations and the registration system. It is essential to construct efficient management organization to ensure the rational, orderly, efficient and coordinated development and utilization of underground space resources.

References

1. Jingui L (2007) Research on use right of space and analyzing design of use right of space in real right law, Master's degree thesis. Fujian normal university, Fuzhou, pp 3–5
2. Qihu Q (2015) The fundamental solution for Urban traffic congestion, air pollution, and the rainfall flood and waterlogging. J Sci Technol Rev 12:1–2
3. Qihu Q (1998) Sustainable development of the cities and the development and utilization of underground space. J Undergr Space 19(2):69–75
4. Xu S, Zhu X (2012) Legislation on the urban underground space in China. J China Land Sci 26(9):54–59
5. Liu Q (2007) Research on the space rights, Master degree thesis. Southwest university of political science and law, Chongqing, pp 32–47
6. Ni B, Liu X (2005) Legislation system of urban underground space in China. J Undergr Space Eng 1(1):19–24
7. Liu A (2008) Research on the city underground space registration, Master degree thesis. Nanjing agricultural university, Nanjing, pp 35–55
8. Zhang H (2008) Research on underground space rights, Master degree thesis. Nanjing university of aeronautics and astronautics, Nanjing, pp 31–37
9. Feng Z (2008) The establishment and perfection of legal system of underground space right in China. J New Heights 27(1):118–120

Multi-Field Depth Vehicle Headlight Detection by Model Construction and Long Trajectory Extraction in Nighttime City Traffic

Chunming Tang(✉), Yancheng Dong, Xiangqing Lin, and Wenna Xiao

School of Electronics and Information Engineering, Tianjin Polytechnic University, Tianjin 300387, China
tangchunminga@hotmail.com, dong_yancheng@foxmail.com

Abstract. Due to the limitation of headlights detection algorithm, obtained vehicles' tracking trajectories are rather short in existing traffic surveillance systems. A novel vehicle tracking system is proposed in this paper to deal with nighttime traffic surveillance videos. It consists of three parts. An effective headlight detection model is firstly constructed based on the optical imaging principle, noises are then filtered out according to the field depth among the far, middle and near regions by different evaluations. Parallel perspective principle is secondly applied to remove the LED lights disturbance. The headlights are tracked and then paired according to vehicles' type. Vehicles' tracking is realized finally via trajectory feedback correction. Experiments are presented to show the proposed system's superiority over several state-of-the-art methods in headlight detection, pairing and tracking.

Keywords: Multi-field depth · Model construction · Optical imaging principle · Parallel perspective principle

1 Introduction

Video surveillance is important for road safety, Accident statistics show that 48% of fatalities occur during night [1]. Therefore, the research on intelligent surveillance algorithm of nighttime traffic video has been paid more attention.

Because of the limited light of nighttime, the contour and color of the vehicle cannot be extracted accurately, the headlight in the running process have the relatively stable characteristics, so it is the main target of the vehicle detection at night. Because of the challenge of the cluster of the headlights with their on-road reflections in the far region of the video scene, the algorithms of headlight detection and tracking so far are only focus on the ROI (region of interest) regions in the middle and near views [2–8], which leads to the obtained trajectory relatively short. Furthermore, the disturbance of environment light and on-road reflection lead to the current algorithms with relatively low detection rate, such as Zou et al. [4] presented a tracking system including off-line training and on-line detection and tracking, which requires a lot of samples for training and is also time consuming. The shape of the headlight is changed after morphology

X. Zeng et al. (eds.), *International Symposium for Intelligent Transportation and Smart City (ITASC) 2017 Proceedings*, Smart Innovation, Systems and Technologies 62, DOI 10.1007/978-981-10-3575-3_24

operations are processed, which affects the subsequent steps. Tang et al. [5] presented a model based on the atmospheric reflection-scattering theory to detect the headlight, the diffuse reflection lights from the road surface are firstly suppressed according to the diffuse reflection principle, then the headlight was recovered by improved atmospheric scattering model, but when the headlight has high power or their reflection is clustered, these headlights may be missed in detection. In addition, some frames cannot be recovered from the model in a video occasionally.

Pairing the headlights followed detection is vital for obtaining the valid trajectory. Geometric symmetry paring is based on the area, roundness, distance and other geometric features [6–10]. Tang et al. [11] introduced the minimum feature matching cost and correct the trajectory by feedback correction. Zou et al. [4] proposed the maximum weight independent set framework to the headlight pairing. But they did not consider the various types of headlights in one video.

Addressing to the above problems, we propose a system including headlight detection, pairing, and tracking in the far, middle and near regions, shown in Fig. 1.

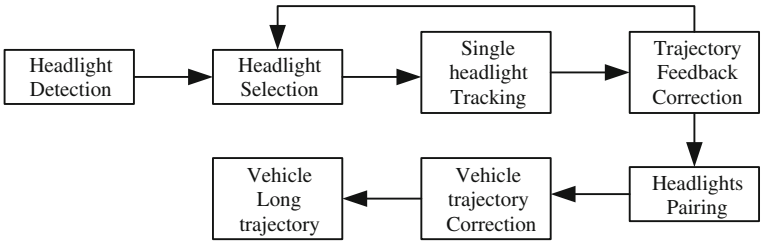

Fig. 1. System diagram

2 Vehicle Headlight Detection

A. Model building. In the nighttime scene, the brightness of the atmospheric light is negligible compared to the brightness of the other light sources. The lights captured by the camera mainly include the headlights, reflected lights and ambient lights, as shown in Fig. 2.

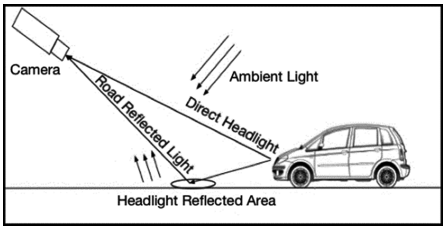

Fig. 2. Decomposition of nighttime light sources

Equation (1) is the atmospheric scattering model [12], and it is divided into two parts: the direct attenuation part in (2) and the ambient light part in (3).

$$E(x) = E_{dt}(x) + E_a(x) \tag{1}$$

$$E_{dt}(x) = \frac{I_0(x)t(x)}{d^2(x)} \tag{2}$$

$$E_a(x) = A_b(x)(1 - t(x)) \tag{3}$$

Here, $E(x)$ represents the image captured by the camera; $d(x)$ represents the depth of field; $I_0(x)$ represents the restored image; $t(x) = e^{-\beta(\lambda)d(x)}$ represents the transmission; $A_b(x)$ represents the ambient lights.

When the headlight power is high, the brightness of its on-road reflection, $E_{reflection}(x)$, is very close to the headlight, which makes it similar to the light source, to emphasis it, (1) is decomposed into (4). As it is also affected by the smoothness of the road surface, $E_{reflection}(x)$ can not be calculated directly.

$$E(x) = E_{dt}(x) + E_a(x) + E_{reflection}(x) \tag{4}$$

So the $I_0(x)$ in (2) is decomposed into the headlight $I_0(x)$ and the strong reflection $I_r(x)$, as in (5).

$$E_{dt}(x) = \frac{(I_0(x) + I_r(x))t(x)}{d^2(x)} \tag{5}$$

$E_a(x)$ in (1) can be decomposed into background ambient light $A_b(x)$ and headlight $A_l(x)$, with two weights ω_1 and ω_2, as in (6).

$$E_a(x) = (\omega_1 A_b(x) + \omega_2 A_l(x))(1 - t(x)) \tag{6}$$

Here, $\omega_1 A_b(x) + \omega_2 A_l(x)$ is all ambient light in the nighttime scene, as the dominant light source that affects the imaging is $A_l(x)$, ω_1 and ω_2 are set 0.4 and 0.6. The finally headlight restoration model is in (7).

$$E(x) = \frac{(I_0(x) + I_r(x))t(x)}{d^2(x)} + (\omega_1 A_b(x) + \omega_2 A_l(x))(1 - t(x)) \tag{7}$$

B. Parameter Estimation. The light sources in the nighttime scene are point light sources, and the particles suspend in the air are mainly single scattering to the point light sources [13], $I_0(x)$ can be deduced as:

$$I(x) = \frac{d^2(x)(E(x) - (\omega_1 A_b(x) + \omega_2 A_l(x))(1 - t(x)))}{\max(t(x), t_0)} \tag{8}$$

Here, $I(x) = I_0(x) + I_r(x)$, $t_0 = 0.01$. We have to estimate the unknown parameter $t(x)$, $A(x)$ and $d(x)$ to restore $I(x)$.

Dong et al. [15] proposed a method to estimate the transmission of the gray scale inversion map of the haze image after median filtering, $A_b(x)$ is set to 122 empirically. To estimate $A_l(x)$, we firstly confirm ROI, then via (9) to remove the influence of the headlights and strong headlight reflections, which are shown in Figs. 3(a) and (b), respectively.

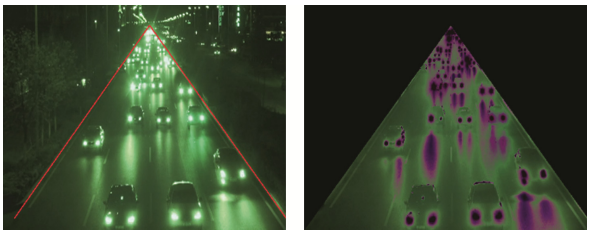

Fig. 3. (a) Pavement area; (b) Removal of headlights and strong reflections

$$E^C_{road}(x) = \min(E^C(x), 255 - E^C(x)) \tag{9}$$

$E^C_{road}(x)$ is the image after the removal of the headlights and strong reflections. $A_l(x)$ is estimated via [14]. The different light sources with different depth have different contribution on imaging [15], according to $t(x) = e^{-\beta(\lambda)d(x)}$, $d(x)$ can be calculated in (10):

$$d(x) = -\frac{\ln(t(x), t_0)}{\beta(\lambda)} \tag{10}$$

Here, β is the total scattering coefficient which was set (10) empirically, λ is the wavelength of the visible light.

Narasimhan [16] thought the particles in the atmosphere are uniformly distribute, and it is a fixed value in a given scene. Therefore, (10) can be rewritten as in (11).

$$d(x) = -\frac{\ln(t(x), t_0)}{\beta} \tag{11}$$

After these three parameters are estimated reasonably, the recovery image $I_0(x)$ can be obtained, which is shown in Fig. 4.

Fig. 4. (a) Original image; (b) recovery image

3 Vehicle Headlight Selection

A. Headlight Preliminary Selection. The recovered headlights need to be further processed to remove LED lights and other noises. We divide the video scene into three parts: near, middle and far regions, shown in Fig. 5. The corresponding headlight selection methods are adopted according to the noises characteristics, as shown in Table 1.

Fig. 5. Video scene

Table 1. Headlight preliminary selection

Scene	Method			
	Area method	Improved watershed algorithm [17]	Ratio of length to width	RGB variation method [2]
Far	Remove large, small noise	Remove the headlights on adhesion	–	–
Middle	Remove small noise	Remove the cluster of the headlights with their on-road reflections	Delete the long and narrow reflections	–
Near	Remove small noise	–	–	Remove the headlight reflections that like headlights

B. LED Removal. The LED lights and other noises still make the paring confused, that means one vehicle with one trajectory is still challenging. We convert the 2D scene to 3D firstly, the height from the headlight to the ground can then be calculated. Figure 6(a) is a gray level image. The horizontal red line in it is a forbidden line under the traffic monitor and the two red crossed lines are the borders of the road. The line connecting the two centroids of a car's headlights is labeled as a blue line, and their corresponding reflections on road labeled as a yellow line. Figure 6(b) is Fig. 6(a) being processed after headlight restoration and before headlight selection. We can get a red narrow rectangular marked in Fig. 6(b), according to the parallel perspective principle, the green solid and dashed lines in the far and middle region are obtained in the same way.

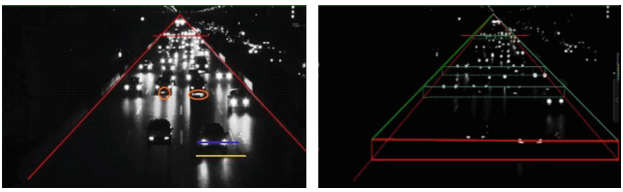

(a) (b)

Fig. 6. 2D to 3D; (a) Gray-level image; (b) Parallel perspective image (Color figure online)

We add a coordinate system to Fig. 6(b), as shown in Fig. 7. The crossed point of the two border lines is called vanishing point (x_0,y_0). W_{light} is the distance between the two headlights of a car closest to the camera, H_{light} is the height from the headlights to their reflections.

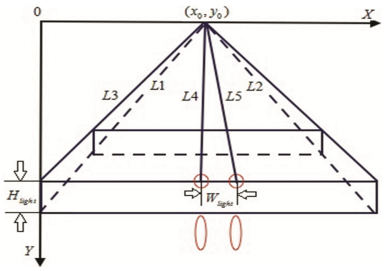

Fig. 7. Perspective principle diagram

The equations of lines *L1* ~ *L5* can be obtained as:

$$y = k_i x + b_i \tag{12}$$

k_i and b_i are the slopes and intercepts, $i = 1,2,3,4,5$, according to (13) and (14), W^j_{light} and H^j_{light} can be obtained.

$$W^{j}_{light} = |k_i(Y_j - b_i)/k_3 + b_3| \tag{13}$$

$$H^{j}_{light} = |(Y_j - b_4)/k_4 - (Y_j - b_5)/k_5| \tag{14}$$

Here, j is the number of bright spots. Each bright spot is framed in a rectangle which is defined by the statistical prior knowledge as follows: (a) the rectangle's center is the centroid of the bright spot; (b) the rectangle's height is H^{j}_{light}; (c) the rectangle's width is $0.7 \times W^{j}_{light}$. Along x axis of the centroid with the biggest area of all the bright spots in this rectangle., if there is another bright spot in the range: $[-W^{j}_{light}, W^{j}_{light}]$, these two bright spots are a pair of headlights. All other bright spots in this rectangle are then deleted. If there is no other bright spot in the range: $[-W^{j}_{light}, W^{j}_{light}]$, we will repeat this process on the second biggest bright spot. The rest can be done in the same method. In this way, the LED lights and other noises can be removed and the goal that one vehicle with one trajectory can be reached. The results are shown in Fig. 8:

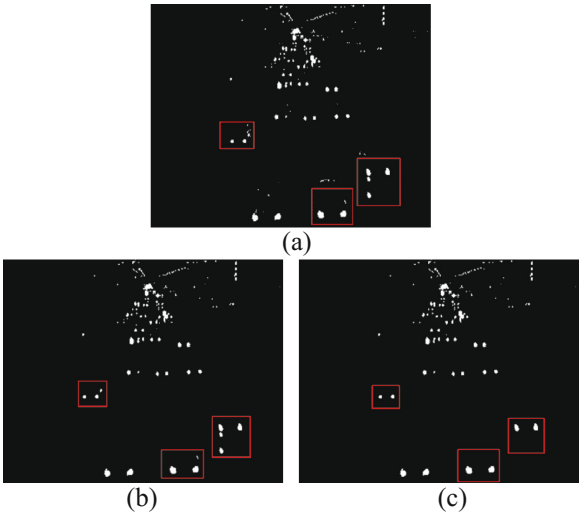

Fig. 8. Detection result; (a) Restoration image (b) After selection; (c) After LED lights and other noises removal

4 Headlights Pairing and Tracking

A. Coordinate Transformation. Apply homography matrix between the plane $\Gamma 1$ of the video scene and the plane $\Gamma 2$ of the real world [18] to establish a relationship between them, the position of the headlight, the real width and the velocity of vehicle in the world system can then be calculated.

B. Single Headlight Tracking. According to the spatial continuity of the moving object, the same headlight has some overlap in the adjacent two frames as the frame interval is 0.04 s. The initial trajectory of every headlight with a unique ID can be obtained. Due to the interference in pairing, such as adhesion, occlusion, the average speed of vehicle and a trajectory feedback correction are also added to correct the error pairing, which is shown in Fig. 9.

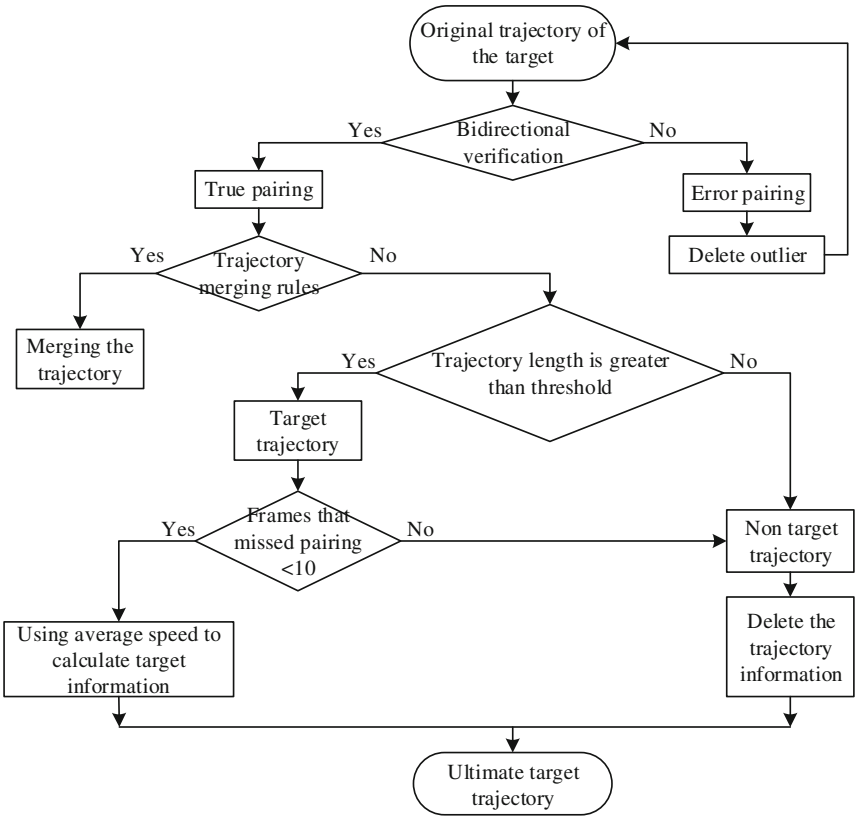

Fig. 9. Flow chart of trajectory feedback correction

We firstly use the bidirectional position verification [4] to ensure the data association of the headlight is correct. When the vehicle speed is very fast or occlusion appears for a long time, it is apt to cause the data association fail. The broken trajectory will be linked according to the similarity of the movement direction. The stable headlight has motion continuity and shape stability which can be used to eliminate the non headlight.

C. Headlight Pairing and Vehicles' tracking. The pairing of the headlights is realized based on the space-time similarity. We select the line slope θ of a pair of headlights, Euclidean distance d of the corresponding centroids, velocity difference ΔV and the width w of the vehicle as the pairing features to complete the ordinary headlight pairing.

The one trajectory of each vehicle can be obtained after linking the midpoints of the paired headlights. Another trajectory correction is finally used to improve the tracking accuracy, the results are shown in the next section. The flow chart is shown in Fig. 10.

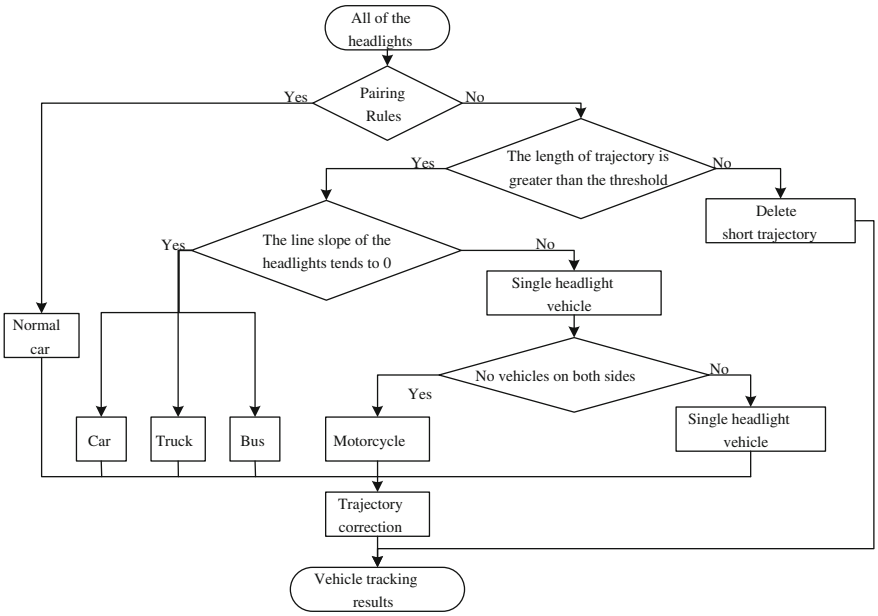

Fig. 10. Tracking flow chart

5 Experimental Results

Our proposed system has tested on 12 videos, captured by a Sony camera setting on an overpass in Tianjin City. The lens' angle is 30 degrees to the horizon. Frame rate is 25f/s and the size of the image is 720×576 pixels.

To evaluate the performance of the headlight detection model, the Jaccard coefficient is used, TPR (True Positive Ratio), FNR (False Negative Ratio), FPR (False Positive Ratio) are computed: $TPR = TP/(FP + TP + FN)$, $FPR = FP/(FP + TP + FN)$, $FNR = FN/(FP + TP + FN)$. TP is the number of correctly detected vehicles, FP is the number of falsely detected vehicles; FN is the number of missed vehicles. Figure 11 shows some detection results of various vehicles, such as the normal vehicle, bus, trucks and the motorcycle. The original images, the detection results and LED removal results are shown in the first, second and third rows, respectively. The detection performance is quit good except that in the far region because of the reflection, the cluster of the headlights and the noises.

Fig. 11. Headlight detection of various vehicles

The proposed headlight detection model is compared with reference [5], shown in Fig. 12, which appears higher performance than [5], especially in the far region. Table 2 shows the comparative detection results tested via 8 videos.

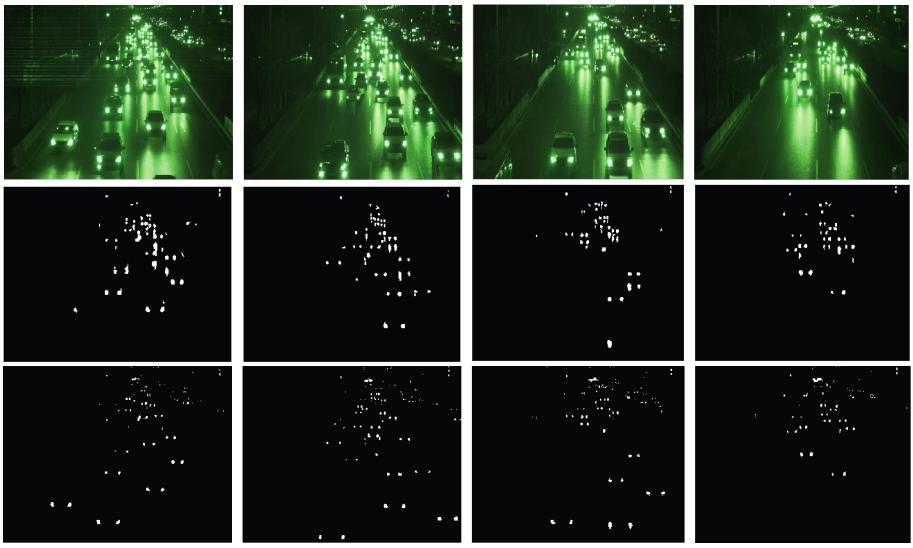

Fig. 12. Comparative results of vehicle detection of the proposed model and atmospheric reflection-scattering model [5] for video sequences

Table 2. Comparative results of vehicle detection performance

Video sequence	Parameter	Seq 1	Seq 2	Seq 3	Seq 4	Seq 5	Seq 6	Seq 7	Seq 8
[4]	E	59.28%	58.74%	68.98%	50.01%	67.56%	57.03%	58.34%	64.25%
	FNR	26.35%	29.56%	24.15%	19.58%	19.23%	18.25%	16.12%	15.78%
	FPR	19.88%	16.78%	9.13%	22.23%	19.36%	17.27%	16.23%	10.69%
Proposed	E	90.47%	91.32%	96.21%	91.65%	95.98%	93.52%	94.67%	95.59%
	FNR	1.25%	1.13%	0.78%	0.33%	1.84%	1.23%	0.64%	0.14%
	FPR	5.17%	7.31%	4.34%	7.33%	4.45%	6.28%	4.34%	3.08%

The biggest tracking frames of Zhang [6] and Zou [4] are 126 and 200, whereas ours can reach up to 626. The rather long trajectory of each vehicle is obtained from far to near. Tracking of the single headlight and vehicles after pairing are shown in Figs. 13 and 14. The one trajectory of each vehicle can be obtained also, the results are shown in Fig. 15.

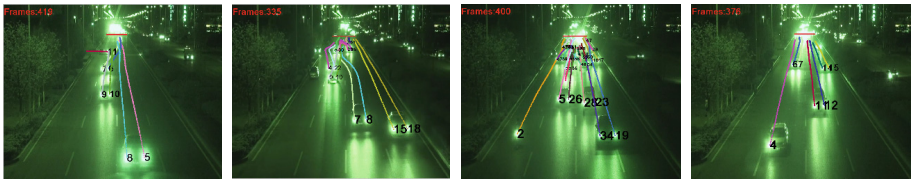

(a) (b) (c) (d)

Fig. 13. Single headlight trajectory in special situations. (a) Vehicle appears from the side; (b) Vehicle changes lane; (c) Motorbike; (d) One headlight broken

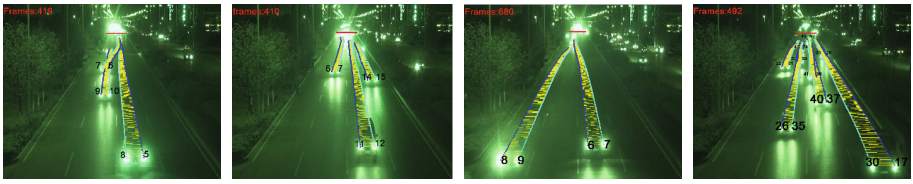

Fig. 14. The headlight pairing and tracking results.

Fig. 15. The one trajectory of each vehicle.

6 Conclusion

This paper has proposed a vehicle tracking system in nighttime city traffic. Headlights are detected via a model based on optical imaging principle. We have divided the field depth into the far, middle and near regions which are filtered out the noises by different approaches. The filtered result is then applied the parallel perspective principle to remove the LED lights. The headlights are tracked, feedback corrected and paired according to vehicles' type, vehicle trajectory can be obtained after headlights pairing and another trajectory correction finally. The experimental results have revealed that proposed system can accurately detect the headlights and extract the long trajectories of various vehicles in nighttime urban traffic. It is worth noting that, we didn't test the proposed system in curved road, the future work may concentrate on testing and improving the system to apply to more conditions.

References

1. Traffic safety facts (2012) Motor vehicle crashes: Overview. U.S. National Highway Traffic Safety Administration (2013), Washington, DC, USA
2. Guo JM, Hsia CH, Wong K, Wu JY, Wu YT, Wang NJ (2016) Nighttime vehicle lamp detection and tracking with adaptive mask training. IEEE Trans Veh Technol 65(6):4023–4032
3. Yongjie M, Pengfei L, Bin W (2015) A new method of traffic flow detection at night. J Northwest Norm Univ (Nat Sci) 51(3)
4. Zou Q, Ling HB, Luo SW, Huang YP, Mei T (2015) Robust night-time vehicle detection by tracking and grouping headlights. IEEE Trans Intell Transp Syst 16(5):2838–2849
5. Chunming T, Zhisheng C, Xiangqing L et al (2016) Headlights detection in traffic videos based on atmospheric reflection-scattering model via reconstructing restoration images. Acta Autom Sin 42(4):605–616
6. Zhang W, Wu QMJ, Wang GH, You XG (2012) Tracking and pairing vehicle headlight in night scenes. IEEE Trans Intell Transp Syst 13(1):140–153
7. Chen Y-L, Wu B-F, Huang H-Y, Fan C-J (2011) A real-time vision system for nighttime vehicle detection and traffic surveillance. IEEE Trans Industr Electron 58(5):2030–2044
8. Tang C-M, Hussain A (2015) Robust vehicle surveillance in night traffic videos using an Azimuthal-Blur technique. IEEE Trans Veh Technol 64(10):4432–4440
9. Wu H, Huo H, Fang T, Zheng C (2007) Nighttime video detection in complex environment. Appl Res Comput 24(12):386–389
10. Salvi G (2014) An automated nighttime vehicle counting and detection system for traffic surveillance. In: International conference on computational science and computational intelligence. IEEE, Naples, pp 131–136
11. Chunming T, Meiling N, Tengfei D, Huanfei H, Xu H (2015) Nighttime vehicle detection and tracking based on minimum feature matching cost. Comput Appl Softw 32(4): 292–296
12. McCartney EJ (1976). Optics of atmosphere: Scattering by molecules and particles. Wiley, New York, pp 23–32
13. Qi B-J (2013) The Application of Atmospheric Scattering Model in Image Contrast Enhancement and Surface of the Small Target Detection [Ph. D. dissertation], National University of Defense Technology, China

14. He K (2011) Single image haze removal using dark channel prior. The Chinese University of Hong Kong, Hong Kong
15. Linna D, Yan X (2015) A novel method for image haze removal based on dark channel prior. Electronics
16. Narasimhan SG, Nayar SK (2002) Vision and the atmosphere. Int. J. Comput. Vis. 48(3):233–254
17. Cheng Y, Hai T, Hongzhou T, Danliang W, Zheng Z, Zhibing Z (2015) Detection and analysis of bubble size distribution in liquid phase. J Nanjing Univ (Nat Sci) 51(2):304–309
18. Hartley R, Zisserman A (2004) Multiple view geometry in computer vision, 2nd edn. Cambridge University Press, Cambridge

A Game Theoretical Based QoS-Aware Routing Mechanism with IEEE802.16 Mesh Networks in ITS

Jun Yu(✉) and Wei Zhang

Jiangsu Province Communications Planning and Design Institute Limited Company, Nanjing 210009, China
yj_njut@163.com

Abstract. Traffic informationization is the embodiment of traffic modernization, networked and intelligentization. To speed up the development of ITS, developing public Travel Information Service system with Mobile Internet technique is a practical application. As the latest development trend, WMN containing a lot of research hotspots. The routing mechanism is one of the key technology to be considered in IEEE802.16 mesh networks. This paper proposed a game theoretical based QoS-aware routing mechanism (GTQR). The main idea of GTQR is to periodically record node's congestion state and forecast mainstream type next period. Then GTQR directional send MSH-DSCH message to make path selection. GTQR sets a repeated game model to assess the advantage and disadvantage of path selection to optimize relaying strategy. Our simulation results demonstrate that GTQR performs better than other routing algorithms.

Keywords: ITS · IEEE802.16 · Mesh networks · Game theoretical · QoS-aware · Routing mechanism

1 Introduction

The interline and sharing of traffic information is the precondition to implement ITS. Public Travel Information Service system technique has becoming a hot spot in domain of the research transportation information gradually. The announcement on that Mobile Internet-based traffic state and communication technologies are applied to the Travel Information Service is one of the important means to promote traffic information and will also greatly facilitate public travel. As the emerging technology of Mobile Internet, the WMN based on IEEE802.16 protocol has many researching space. The routing protocol of WMN hasn't been finalized as a standard. The present ideas of routing algorithm mainly develop basing on the routing protocols of Ad Hoc network. Like Ad Hoc network, according to path generating sequence, the WMN routing protocols are divided into two types: proactive routing protocols and posterior routing protocols. The WMN routing protocols are also divided into source routing protocols and hop-by-hop routing protocols according to the way of transmission. It is necessary to design an appropriate routing protocol suiting for WMN. The relative representative work is OLSR (Optimized Link State Routing) proposed by Yang etc. in document [5]. The document [6] pointed out the network nodes with low mobility bear low delay requirement transmitting

X. Zeng et al. (eds.), *International Symposium for Intelligent Transportation and Smart City (ITASC) 2017 Proceedings*, Smart Innovation, Systems and Technologies 62, DOI 10.1007/978-981-10-3575-3_25

message. The document [7] proposed to set SINR being the routing metric. The document [8] designed routing protocol with the consideration of node's reputation. The document [9] mainly take path quality into account. The algorithms mentioned above being free of traditional protocol's designing ideas, while it lacked consideration in both nodes' processing capacity and different type businesses' QoS demands. Also in the relaying strategy based on IEEE802.16 distributed scheduling, nodes negotiate the allocation of channel resources in a collision-free style. It needs more consideration of cooperation-oriented to design protocol algorithm.

We made corresponding improvements. We proposed a game theoretical based QoS-aware routing mechanism (QTQR). It mainly included QoS comprehensive evaluation of nodes participating in game, cooperation-oriented repeated game model. It measured the advantages and disadvantages for setting up a link and optimized path selection strategy.

The structure of the article is: in Chap. 1, introducing the three handshakes procedure in IEEE802.16 Mesh networks; proposing a game theoretical based QoS-aware routing mechanism (QTQR) in Chap. 2, discussing its details; demonstrating its performance by simulation experiments in Chap. 3; making a conclusion in Chap. 4.

2 Distributed Coordinate Scheduling

2.1 The Frame Structure in Mesh Network

In TDMA mode, time is partitioned into frames of fixed duration. Each frame consists of a control sub-frame and a data sub-frame, as illustrated in Fig. 1. The control sub-frame is divided into network control sub-frame and scheduling control sub-frame. It makes a three handshakes procedure to negotiate bandwidth by broadcasting MSH-DSCH messages among neighbor nodes, during the scheduling control sub-frame. MSH-DSCH message contains a list of information elements (IEs): RequestIE, GrantIE (direction = 0), GrantIE (direction = 1). The data sub-frame consists of a fixed number of data min-slot up to 256 (hereafter slots), which is an opportunity to transmit data. The slots are viewed as the link bandwidth resources in the scheduling mode.

2.2 Coordinate Scheduling

Nodes negotiates the allocation of channel resources in a collision-free style by distributed exchanging the scheduling message hop-by-hop. To be specific, as illustrated in Fig. 2, the requesting node A (wanting some slots to transmit data) first asks one of its neighbor nodes (B, C, D, E) to allocate bandwidth by broadcast MSH-DSCH with RequestIE to make a reservation of some slots. Then one of its neighbor nodes (B, C, D, E) return MSH-DSCH with GrantIE (direction = 1), based on its slots occupation situation. At last node A feeds back authorization message GrantIE (direction = 0) to achieve the slots reservation. So, in the distributed coordinate scheduling mode, there is not specific selection method of next hop, while current way is just restricted to promote three handshakes procedure by broadcasting MSH-DSCH. When received RequestIE, node return GrantIE if it will be vacant on that slot, without consideration on its own benefit.

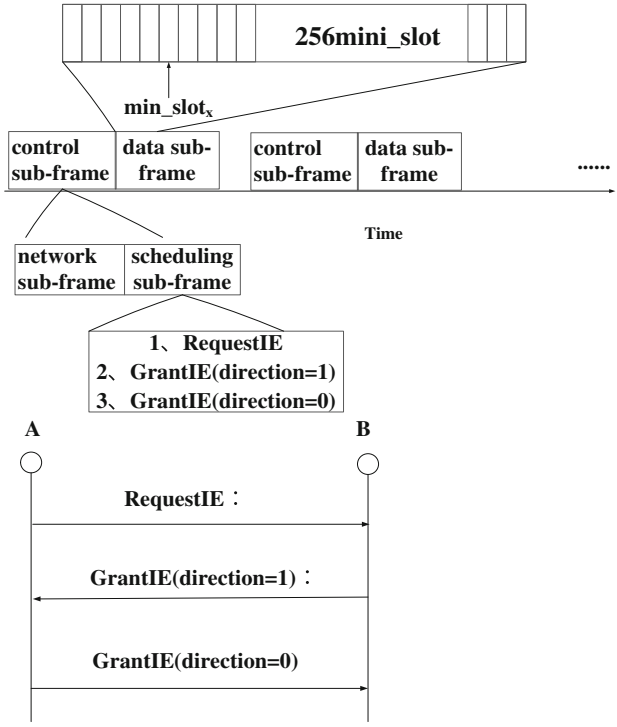

Fig. 1. Frame structure in mesh

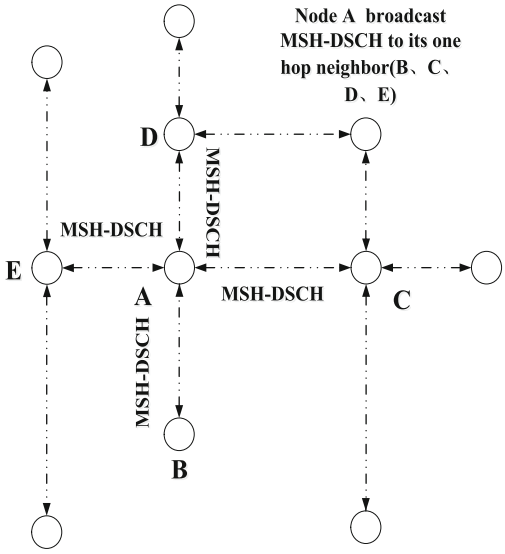

Fig. 2. The broadcast of MSH-DSCH

3 Game Theoretical Based QoS-Aware Routing Mechanism (QTQR)

We proposed a game theoretical based QoS-aware routing mechanism (QTQR) in Chap. 2. GTQR consists of two parts. (1) QoS comprehensive evaluation of nodes participating in game; (2) cooperation-oriented repeated game model.

3.1 QoS Comprehensive Evaluation

We view node's buffer queue as queuing model with single sever, the rule being FCFS. We assume the businesses arrive the queue with characteristics:

(1) Non-aftereffect: some business arrive the queue in a mutual independence way during overlap time interval.
(2) Stability: for minimal Δt, there to be no correlation between a business's arriving and value of t, during time interval $[t,t+\Delta t]$.
(3) Generalization: for minimal Δt,the probability of two or more businesses arriving is infinitesimal, to be negligible.

Also we assume to view the mean value of time scale span of business arriving the queue as a constant approximatively. So the stochastic process with arriving of some businesses can be viewed as a Poisson process with λ density during time interval. We can make research with Poisson process 's property.

Node make statistics of Real-Time (hereafter RT) and non-Real-Time (hereafter nRT) businesses every T and we can calculate some kind of business's arrival rate:

$$r(k)_x = (1-d_r)\times\frac{Num\_x}{T} + d_r \times r(k-1) \tag{1}$$

Where, $d_r = e^{-\frac{T}{\mu}}$, μ is control parameter; k represents statistics time. Num_x means arrival numbers of some kind of business.

Via Formulas (2), (3), we can make prediction of probability of some kind of business in next period:

$$P_{Num\_RTs} = \frac{r(k)_{RT}^{Num\_RT}}{Num\_RT!}e^{-r(k)_{RT}} \tag{2}$$

$$P_{Num\_nRTs} = \frac{r(k)_{nRT}^{Num\_nRT}}{Num\_nRT!}e^{-r(k)_{nRT}} \tag{3}$$

To prevent data bursting, we bring in weighted smoothing disposal:

$$P_{Num\_RTi} = \zeta \times P_{Num\_RT(i-1)} + (1-\zeta)\times P_{Num\_RTs} \tag{4}$$

$$P_{Num\_nRTi} = \zeta \times P_{Num\_nRT(i-1)} + (1-\zeta)\times P_{Num\_nRTs} \tag{5}$$

Where ζ is set 0.3, based on historical experience, to weigh more on the current sampled value, producing the most accurate estimations on node's current statement.

Definition 1. RT_{er}: when $P_{NUM\_RT\,i} > P_{NUM\_nRTi}$ the mainstream type of arriving business of node is RT, in the next period.

Definition 2. nRT_{er}:when $P_{NUM\_RT\,i} > P_{NUM\_nRTi}$ the mainstream type of arriving business of node is nRT, in the next period.

The source node should choose relative vacant node to be next hop as soon as possible. As the document [4] introducing of node's vacant degree, GTQR proposes a concept of SC_i to reflect the node n_i's vacant degree:

Definition 3.

$$SC_i: \quad SC_i = \frac{r(k)_i}{RcvR_i^2} \tag{6}$$

Where $r(k)_i$ represents business's sending speed of node. $RcvR_i$ represents business's receiving speed of node. The sampling period is T as same as the sampling value before, which is set to be 6 s in the simulation experiment. Receiving is the premise of sending, for this dominance, $RcvR_i$ has a higher order than $r(k)_i$ [4]. The node with a large value of SC_i will be more vacant and more reliability. It will get more transportation QoS guarantee when these nodes chosen to be next hop.

Every node broadcasts its identity $\{Identity|Identity = RT_{er}, nRt_{er}\}$, probability of mainstream type of arriving business$\{P_w|P_w = P_{RT},P_{nRT}\}$, vacant degree SC_i to its neighbor. GTQR requires nodes to choose nRT_{ers} from its neighbor nodes $\{nRT_{er1},nRT_{er2},..,nRT_{erq}\}$, then sends MSH-DCSH to node (from $\{nRT_{er1},nRT_{er2},..,nRT_{erq}\}$) with a biggest SC_i. If two nodes accomplish the three handshakes procedure, the data will be transmitted during the slots they reserved in the three handshakes.

If there is only RT_{er} in node's neighbor nodes$\{RT_{er1},RT_{er2},..,RT_{erq}\}$, then it sends MSH-DCSH to node (from $\{RT_{er1},RT_{er2},..,RT_{erq}\}$) with lowest probability of mainstream type of arriving business to guarantee RT businesses'QoS.

Nodes make path election independently by exchanging scheduling information, the next hop selection strategy showed as Fig. 3.

3.2 Cooperation-Oriented Repeated Game Model

As showed in Chap. 2.1, when source node send MSH-DSCH with RequestIE to one of its neighbor node (hereafter chosen node), whether the three handshakes procedure will be promoted depending on the chosen node feeding back MSH-DSCH with GrantIE (direction = 0) or not. While the wireless channel resource is constrained and if the chosen node choose to feed back GrantIE, it will unavoidable waste energy, slots resources, and the possible delay and congestion would degrade the chosen node's status in "Mesh election"—costing more slots resources to be relay node rather than resource node to transmit data itself. So we view the behavior that the node weights the advantages

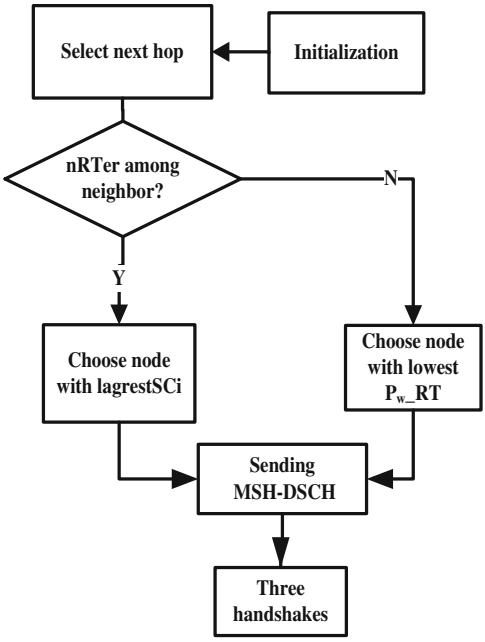

Fig. 3. Next hop selection strategy

and disadvantages before making choice whether return GrantIE (direction = 0), when it receives the RequestIE to be a game action.

GTQR proposed a cooperation-oriented repeated game model $G(n,S,U)$.

(1) There to be n($i = 1,2,\ldots,n$) node participating in single game.
(2) For every gamer node, there to be two strategies ($s_i = \{\text{ZF, IG}\}$) and the strategy sets to be $S_i = s_i(s_1,s_2,\ldots,s_n)$. Where the ZF meaning the gamer node choosing feedback behavior with probability s_{ZF}, and the IG meaning the gamer node choosing to ignore the RequestIE with probability $1-s_{ZF}$.
(3) For each strategy, every gamer node would get benefit $u_{i,}U_i = u_i(u_1,u_2,\ldots,u_n)$ for each game.

Nodes exchange QoS characteristic information and distributed scheduling results, so we can view gamer node knowing each other's strategy space, profit function. Each game, every gamer node participates in game in a asynchronously way. So we define every game to be complete information dynamic game model and the routing process could be viewed as complete information dynamic repeat game model.

We define PR_i to value some node's competitiveness:

Definition 4.

$$PR_i: \quad PR_i = \frac{S_{dn} + S_{db}}{fF_{dur}} \tag{7}$$

Where fF_{dur} means the average maximum continuous time slot length. The S_{dn} means numbers of slots in $fF_{dur,}$ value the ability to respond different nodes' RequestIE and fulfill the three handshakes. The S_{db} means numbers of slots in $fF_{dur,}$ value the ability to respond one node's RequestIE for different business and the ability to transmit the data itself. It represents the capacity to eliminate neighbor node' burst data within the shortest possible slot and the interaction capability when transmitting data itself.

The node with higher PR_i would win in the "Mesh election", so it could save more slots to transmit data itself. GTQR proposed a mechanism that increase PR_i to stimulate gamer node participating in relay data actively:

$$u_{ci} = \lceil b_{PR} \times 256 \rceil \tag{8}$$

Where, u_c presents node's benefit choosing to cooperate. The b_{PRv} means corresponding PR reward income. The 256 presents slot amounts.

For node denying cooperation, GTQR adjusts the value of exp (Transmission collision avoidance index) to punish them, in consideration of document [11]'s demonstration about the influence of exp on efficiency of three handshakes.

$$u_{rfi} = \alpha w \times |\exp^*| \tag{9}$$

Where, u_{rfi} presents node's benefit deny to cooperate. The $|exp^*|$ means jitter of exp. The aw (less than 1) presents jitter value of exp mapping to data sub-frame.

Node's exception profit function u_i:

$$u_i = (u_{ci} - u_{wt}) \times s_{ZF} - u_{rfi} \times (1 - s_{ZF}) \tag{10}$$

Where u_{wt} presents node's QoS wastage choosing to cooperate. We draw on document [15] to solve the profit function's "Nash Equilibrium":

$$s_i(t+1) = s_i(t) + \theta_i \times s_i(t) \times \frac{\partial u_i(s)}{\partial s_i(t)} \tag{11}$$

Where s_i(t) means node i's strategy at no.t game. The θ_i presents convergence parameter of speed. The adaptive dynamic distributed algorithm would save more resources than the centralized algorithm of "Nash equilibrium", automatic updating node's game strategy by historical information.

So the set of s_i(t):

$$U_i(s_1^*, s_2^*, \ldots, s_i^*) \tag{12}$$

GTQR requires nodes maintain a grade chart where recorded every neighbor node's mainstream type and probability of arriving business、 QoS features. Where node choosing its next hop, it send the MSH-DSCH with RequestIE only to the most suitable node meeting the QoS requirements rather than broadcasting MSH-DSCH with RequestIE. So GTQR could sharply save scheduling resource:

$$\eta = \frac{1}{k} \tag{13}$$

Where k means the amount number of chosen nodes and η means level for saving scheduling resource.

GTQR will bring extra wastage, while in wireless mesh networks, the routing node tending to be static state equipments. These nodes do not be subject to power dissipation, so the extra wastage would be acceptable.

4 Performance Analysis and Evaluation

We demonstrate GTQR's performance by simulation experiments in Chap. 3.

4.1 Experimental Designing

We adopt document [12]'s simulation model and parameter setting situation. On this basis, we design two grouping experiments to inspect GTQR's performance. The first experiment is to compare the performance of GTQR, OLSR, IEEE802.16 under environment of different type mainstream arriving businesses in the network. The evaluation index is average throughput. The second experiment is to compare the performance of GTQR, OLSR, IEEE802.16 under network environment with different node density. The evaluation index is influence on cooperation among nodes. We make statics of wastage of scheduling resource at last. It assumes the channel to be ideological. The parameter setting situation is showed in Table 1, nodes random distributes in area (1000 m × 1000 m).

Table 1. Experimental parameters

Parameter	Value
Modulation codes	QPSK-1/2
Bandwidth	20 Mbps
Coverage	1000 m × 1000 m
MAC	IEEE802.16
Arrival time interval	15
MSH-CTRL-LEN	10
MSH-DSCH-NUM	6
Number of node	Two scenes :25, 35 (experiment 1 adopted scenes 1)

4.2 Result Analysis

The Fig. 4 shows the improvement of GTQR on average throughput. The three groups of curve respectively represent the throughput changing of GTQR, OLSR, IEEE802.16 under network environment with different mainstream type of businesses. V means voice businesses and H means Web browsing businesses. The curve from top to bottom is performance of GTQR (under V, H), OLSR(under V, H), IEEE802.16 (under V, H).

With the increase of data rate (kb/s), the average throughput (Mb/s) gradually increase sharply until leveled off. When the mainstream type of businesses changed, three protocol can all adaptive made adjustment to improve throughput. While under the same networks load, GTQR performed much better than OLSR, IEEE802.16, and the difference tends to be obvious, with the increase of data rate. Watch the groups of curve of GTQR, we can find the average throughput of V tends to be higher than that of H. It proves that GTQR not only directed adopted different routing strategy to improve the average throughput for different type businesses and also performed better than OLSR and IEEE802.16.

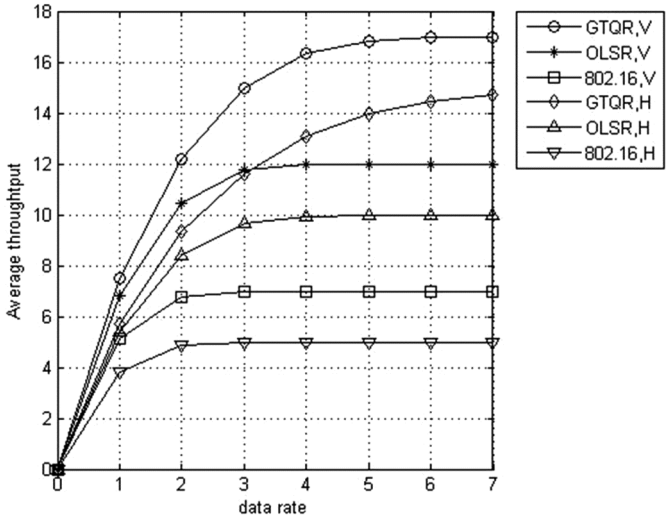

Fig. 4. GTQR's influence on average throughput

According to the document [11]'s demonstration, the cooperation degree among nodes have effect on routing efficiency, so we propose Fcop to value cooperation degree:

$$F_{cop} = \frac{Ns}{Nz} \tag{14}$$

Where Ns means the effective number of MSH-DSCH among adjacent node. The Nz means the amount number of MSH-DSCH among adjacent node.,

According to the M. Cao[13]'s works and document [11]'s demonstration, there is intimate relationship between node density and congestion. So, we adopt two experiment scenes to measure the influence of GTQR on Fcop with different node density environment. As Fig. 5, the three groups of curve respectively represent the Fcop' changing of GTQR, OLSR, IEEE802.16. The two curve of every group of curve represents the Fcop' changing under different network environment. We can find that GTQR improved Fcop better than OLSR、IEEE802.16 did. GTQR also could adaptive affect Fcop under different node density environment to promote the three handshakes process.

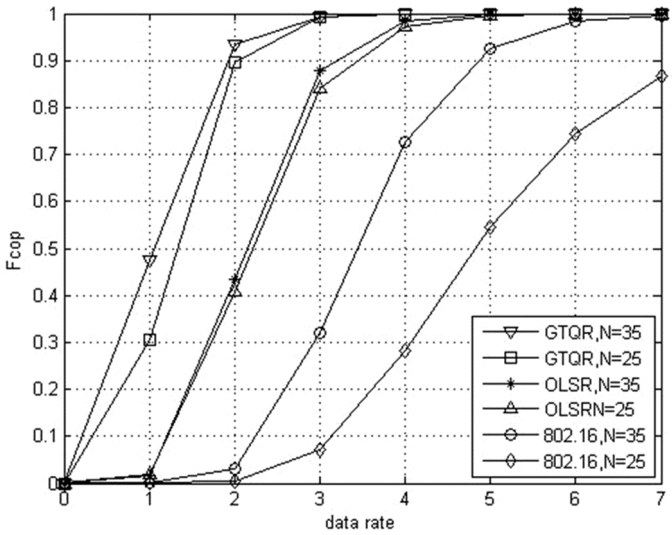

Fig. 5. GTQR's influence on Fcop

5 Conclusion

Researching the characteristics of distributed coordinate scheduling, we proposed a game theoretical based QoS-aware routing mechanism (QTQR). It designed routing path based on the probability of arriving mainstream businesses. We set up repeated game model to measure the advantages and disadvantages for setting up a link and optimized path selection strategy. The simulation experiment showed GTQR performed well.

References

1. Akyildiz IF, Wang X, Wang W (2005) Wireless mesh networks: a survey. Comput Netw 47:445–487
2. He J, Yang K, Guild K (2007) Application of IEEE802.16 mesh networks as the backhaul of multihop cellular networks. IEEE Commun Mag 45(9):82–91
3. Akyild IF, Wang X, Wang W (2005) A survey on wireless mesh networks. Commun Mag 43:23–30
4. 沈呈,陆一飞,夏天勤 (2010) 基于综合判据的无线 Mesh 网路由协议. 计算机学报 33(12): 2300–2311
5. Jacquet P, Muhlethaler P, Clausen T et al (2001) Optimized link state routing protocol for ad hoc networks. In: Proceedings of the IEEE international multi topic conference, Pakistan, pp 62–68
6. Yang Y, Wang J (2008) Design guidelines for routing metrics in multihop wireless networks. In: Proceedings of the 27th IEEE communication society conference on computer communications, Phoenix, pp 2288–2296

7. Elshaikh M, Kamel N, Awang A (2009) High throughput routing algorithm metric for OLSR routing protocol in wireless mesh networks. In: Proceedings of the 5th international colloquium on signal processing & its applications, Kuala Lumpurm, pp 445–448
8. Ding Q, Jiang M, Li X, Zhou X (2009) RePro: a reputation-based proactive routing protocol for the wireless mesh backbone. In: Proceedings of the 5th international joint conference on INC, IMS and IDC, Seoul, pp 516–521
9. De C Paschoalino R, Madeira ERM (2007) A scalable link quality routing protocol for multi-radio wireless mesh networks. In: Proceedings of the 16th International Conference on Communications and Networks, Honolulu, HI, pp 1053–1058
10. QoS 技术介绍. [EB/OL] (2008–05) (2013). http://www.h3c.com.cn/Products___Technology/Technology/QoS/Other_technology/Technology_recommend/200805/605881_30003_0.htm
11. 康晓筠 (2007) IEEE802.16 Mesh 网络节点合作及分布式调度研究. 湖北省武汉市:华中科技大学通信与信息系统系
12. 冯陈伟 (2011) WiMAX Mesh 网络路由与调度算法研究. 计算机工程 37(4): 93–95
13. Cao M, MA W, Zhang Q et al (2005) Modeling and performance analysis of the distributed scheduler in IEEE802.16 mesh mode. In: Proceeding of the 6th ACM international symposium on mobile ad hoc networking and computing, MobiHoc 2005, NY, USA. ACM Press, pp 78–89
14. 由磊,王一凡,张勇,毛安峰,蔡杰,宋俊德 (2008) 基于 NS2 的 IEEE802.16 Mesh 模式的功能模型与仿真.计算机应用研究 8(25):2505–2508
15. 丛犁 (2011) 基于博弈论的无线网络资源分配策略研究[D]西安:西安电子科技大学

Study on Durability of Railway Subgrade Structure Based on Indoor Sand-Blown Model Experiment

Hongdi Zhang(✉)

Cangxi County Transportation Department, 588 Red' Army Road West, Cangxi County, Guangyuan, Sichuan, China
742216734@qq.com

Abstract. Sandstorm erosion plays an important role in destroying the durability of structure of railway subgrade, so this research studies the mechanism and factors that sandstorm erosion erodes the railway subgrade structure in Northwest Loess Area through indoor sand-blow model experiment. The experiment uses the sand-blasting machine to produce the sand flow to erode the railway subgrade model which components is the improved loess, and simulates the sand erosion by controlling the velocity and time of sand flow. After completing the test, the research elaborates the impact of sand erosion on the durability of railway subgrade structure which provides certain theoretical guidance for the sandstorm prevention design and the control of the existed sandstorm disaster of railway in Loess Windy Area, according to measure the density, moisture content, quality and unconfined compression strength of the experimental models.

Keywords: Railway subgrade · Durability · Sandstorm erosion · Indoor model experiment

1 Introduction

Sandstorm erosion refers to a cyclic process that the loose soil grain on the surface of subgrade under the effect of sandstorm for a long term is taken away by the wind, then the grain of sand loosens the subgrade surface soil grain and the loose soil grain is taken away by the wind again. Under the effect of sandstorm erosion all the year round, railway subgrade in windy and sandy area [1] may suffer from erosion at different levels and produces subgrade settlement, subgrade stability decrease and even side slope collapse, etc., which have seriously affected the driving security [2]. A long mileage of railway in Northwest Loess Area of our country suffers from suffering from the sandstorm disaster. Hereinto, the newly built Lanxin High-Speed Rail crosses the area which suffers from sandstorm most seriously, including Anxi Windy area within the territory of Gansu and Qinghai, Yandun Windy Area, Baili Windy Area [3], Sanshili Windy Area, and Dabancheng Windy area within the territory of Xinjiang, easily suffer from sandstorm erosion and produce subgrade damage. Therefore, the research on the sandstorm erosion in Northwest Loess Area has a significant meaning on the railway maintenance, sand prevention and disaster prevention. So far, foreign and domestic researches on wind

X. Zeng et al. (eds.), *International Symposium for Intelligent Transportation and Smart City (ITASC) 2017 Proceedings*, Smart Innovation, Systems and Technologies 62, DOI 10.1007/978-981-10-3575-3_26

erosion theory [4] mainly focus on the land desertification, wind prevention and sand control, etc. There are fewer researches concerning the effect of sandstorm erosion on the durability of railway subgrade in Northwest Loess Area. In order to reduce the subgrade damage of railway in Loess Area and study the erosion mechanism and the factors influencing the subgrade structure, the paper made a qualitative study on the relationship among velocity, time of sand flow and the durability of loess railway subgrade structure and further provides certain theoretical guidance to the sandstorm prevention design of railway and the existed sandstorm disaster control in windy area [5, 6].

2 Experimental Design

By utilizing the sand blasting machine to produce sand flow and acting on the subgrade model, the experiment adopts indoor model test to study the impact of sandstorm erosion on the durability of subgrade structure on the experimental conditions of different velocities and time of sand flow.

The experimental equipments mainly include sand blasting machine, air compressor and air tank, etc. Sand blasting machine is able to cause different intensities of airflow filed in the indoor environment and simulate airflow with sand included. And, Air compressor is able to load and unload intelligently.

The research object of the experiment is high-speed railway subgrade. The experiment selects normalized ballastless track single track railway embankment as the experimental subgrade model [7]. According to the similarity theory of model experiment [8], as well as considering the experimental condition of sand blasting machine model casing, the proportion between experimental subgrade model and prototype is 30:1 and the experimental subgrade is semi-range section subgrade. The side slope grade is 1:1.5, the height is 20 cm and the longitudinal length is 20 cm. Heavy-duty compaction test for the modified loess with C32.5 ordinary Portland cement of 4%, 5%, 6% and 7% is conducted against the experimental subgrade filling. According to the experimental result of compaction test curve, the experiment selects 0.95% of compaction and 6% of mixed cement modified loess as the filling.

According to the research of Dong Guangrong et al. [9], soil erosion is mainly caused by gale. According to the experiment, he gets the linear relation between wind scale and wind speed. See Table 1.

Table 1. Linear relationship between wind level and wind speed

Wind level	4	5	6	7	8	9	10	11	12
wind speed (m/s)	6.7	9.4	12.3	15.5	19.0	22.6	26.5	30.5	32.6

The sand blasting machine in the experiment is 20 cm from subgrade model. When the outlet pressure of spray gun is 0.2, 0.3 and 0.35 MPa, the wind speed measured by anemograph is 25.32, 30.14 and 33.07 m/s respectively. By utilizing the linear interpolation, the corresponding wind scale can be calculated according to Table 1 to be Grade 9.7, 10.9 and 12. According to the wind scale and the effect time of sandstorm, the

experiment is divided into 12 groups, as seen in Table 2. Each experimental group evaluates the impact of sandstorm erosion on the durability of subgrade structure by determining the effect time of sandstorm on the subgrade model, and determining the density, moisture content, quality and unconfined compression strength of subgrade model.

Table 2. The grouped table of sand-blown model experiment

Wind speed (m/s)	Windstorm action time/h			
	15	25	35	45
25.32 (9.7 level)	Group 1	Group 2	Group 3	Group 4
30.14 (10.9 level)	Group 5	Group 6	Group 7	Group 8
33.07 (12 level)	Group 9	Group 10	Group 11	Group 12

3 Experimental Analysis

After the end of each group of sandstorm experiment, take out the subgrade model from the toolbox, determine the quality, density, moisture content and unconfined compression strength of subgrade model. The experimental process is seen Figs. 1, 2, 3, 4, 5 and 6 and experimental result is seen Figs 7, 8, 9, 10, 11, 12, 13, 14 and 15.

Fig. 1. Subgrade model is fed into sand blaster

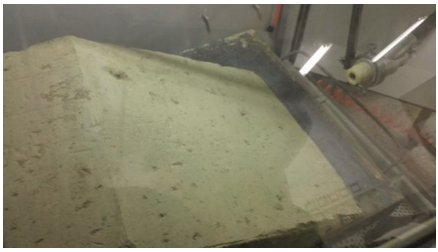

Fig. 2. Sandstorm experiment simulation by using sand blaster

Fig. 3. Subgrade model after sandstorm erosion

Fig. 4. Water content measured

Fig. 5. Mass measured

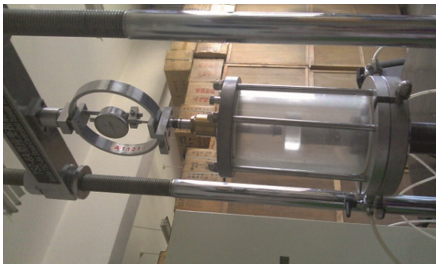

Fig. 6. Unconfined compressive strength measured

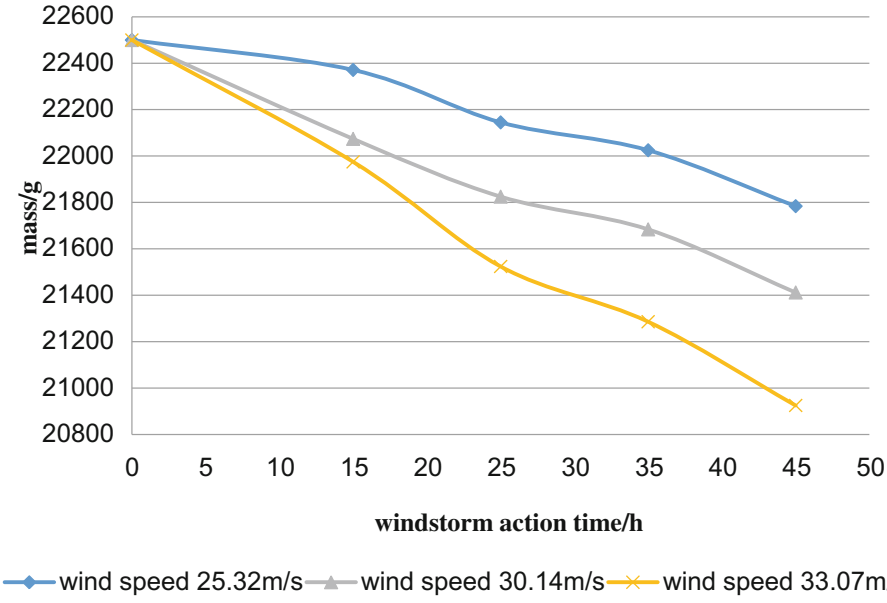

Fig. 7. The mass change of subgrade model with the change of windstorm action time after sandstorm erosion at different wind speeds

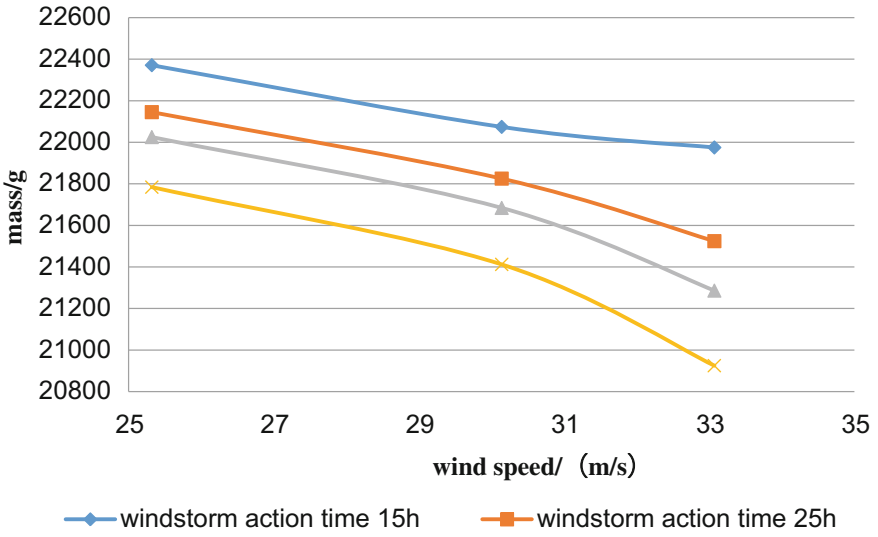

Fig. 8. The mass change of subgrade with the change of wind speed on the condition of the same windstorm action time

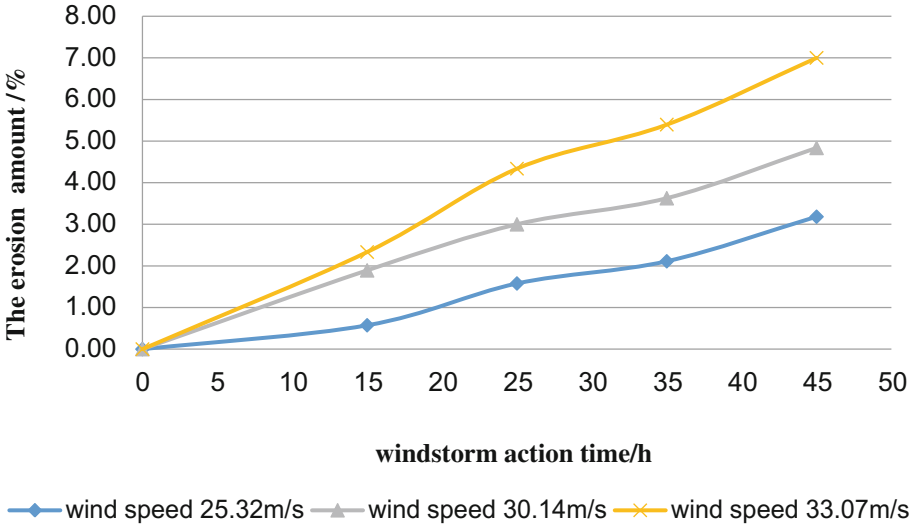

Fig. 9. The erosion amount change of subgrade model with the change of sandstorm action time

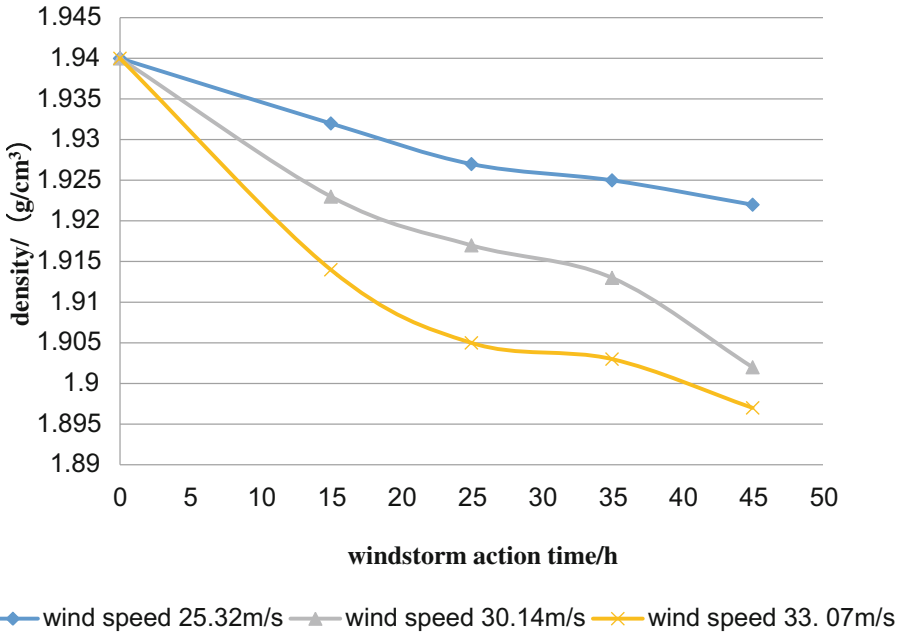

Fig. 10. The density change of subgrade model with the change of windstorm action time after sandstorm erosion at different wind speeds

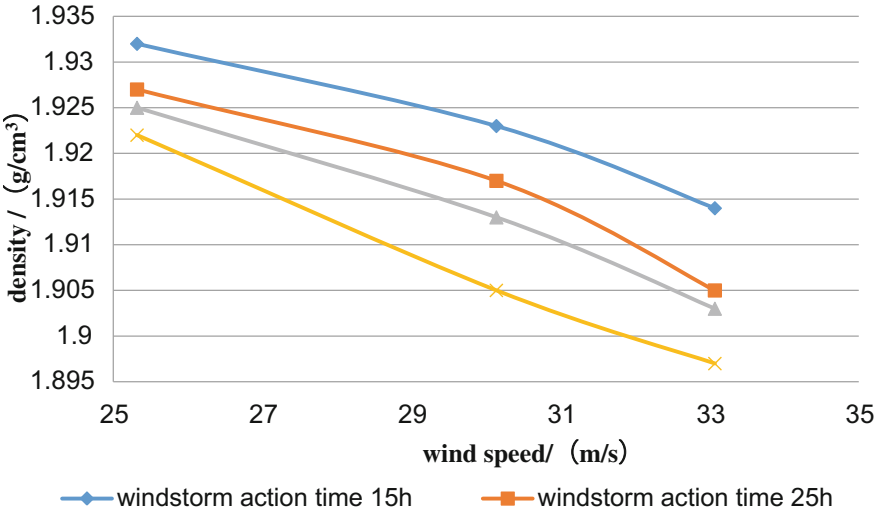

Fig. 11. The density change of subgrade with the change of wind speed on the condition of the same windstorm action time

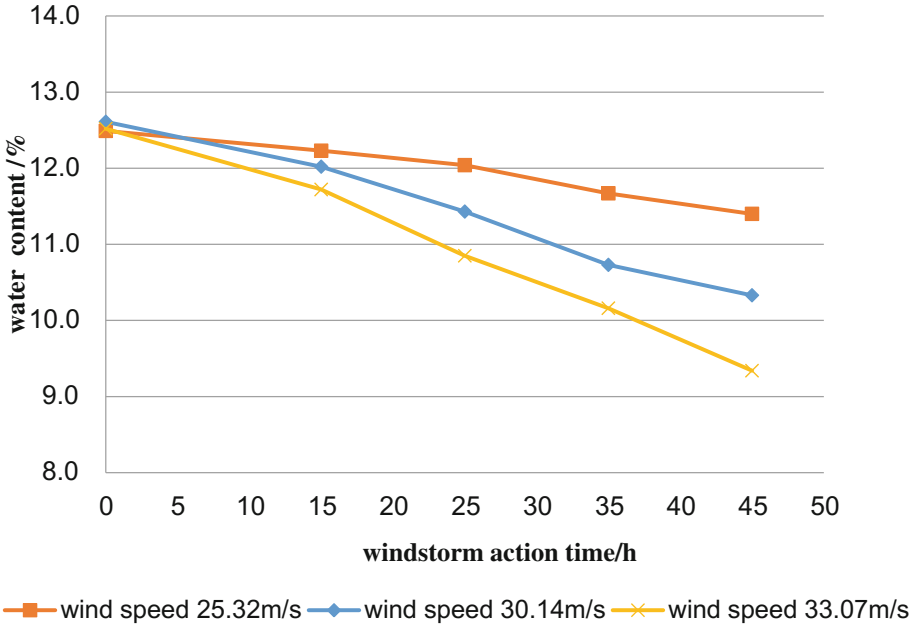

Fig. 12. The water content change of subgrade model with the change of windstorm action time after sandstorm erosion at different wind speeds

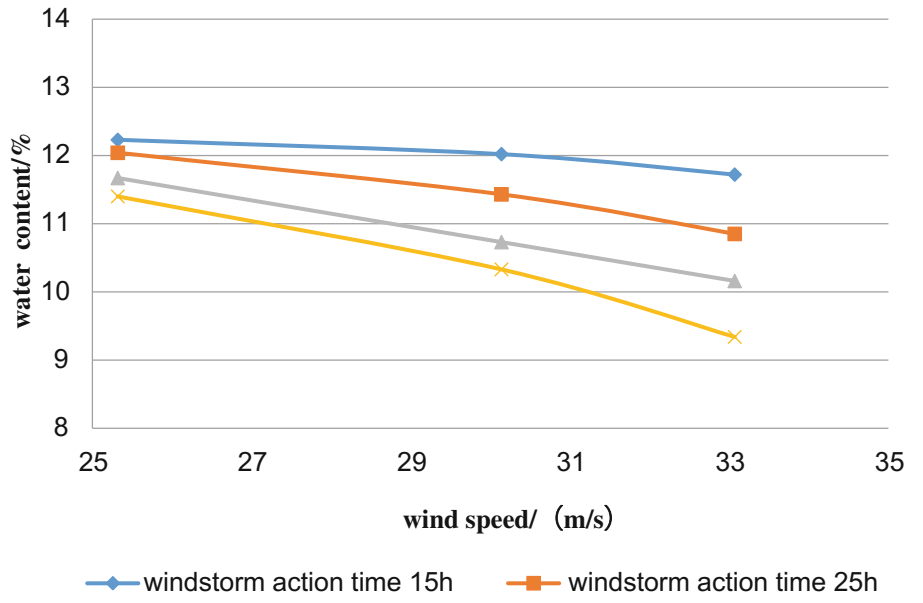

Fig. 13. The water content change of subgrade with the change of wind speed on the condition of the same windstorm action time

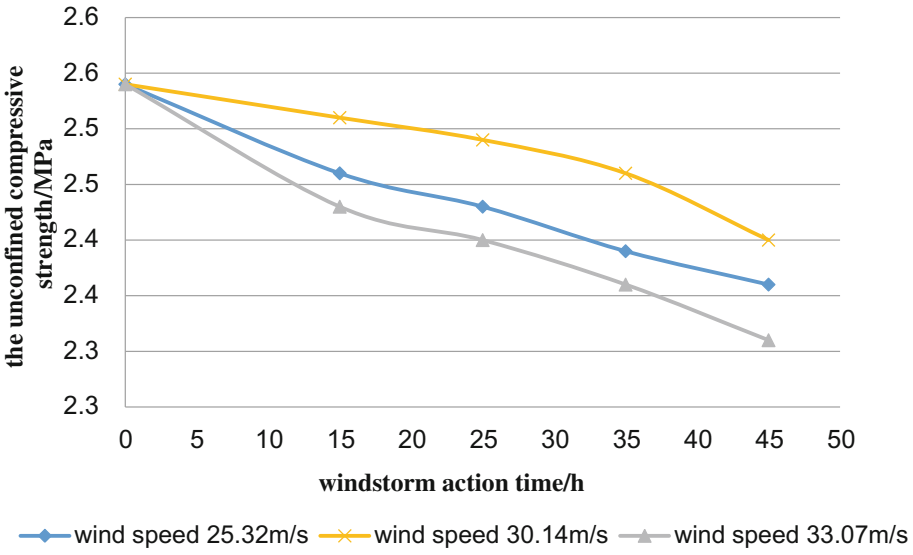

Fig. 14. The unconfined compressive strength change of subgrade model with the change of windstorm action time after sandstorm erosion at different wind speeds

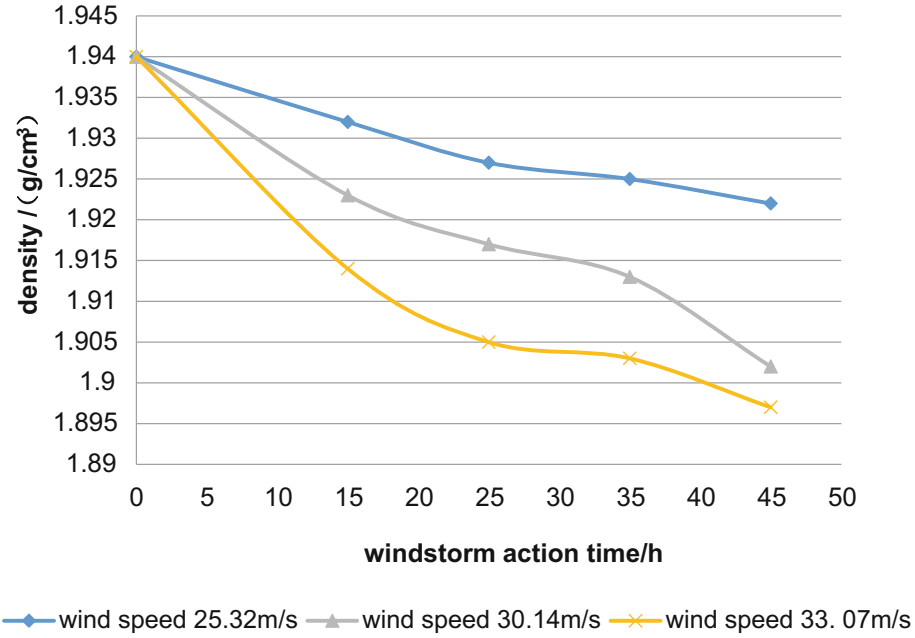

Fig. 15. The unconfined compressive strength change of subgrade with the change of wind speed on the condition of the same windstorm action time

According to Fig. 7, on the condition of invariable wind speed, with the time increasing of sandstorm erosion, the quality of subgrade model appears the law of linear decrease. The higher the wind speed is, the slope of quality decrease curve of subgrade model is greater. According to Fig. 8, on the condition of the same time of sandstorm erosion, with the increasing of the wind speed, the quality decrease rule of subgrade model shows: when the wind speed is low, the quality decrease rate of subgrade model is slow; when the wind speed is high, the quality decrease rate of subgrade model is fast. It indicates that on the condition of high wind speed, the quality of subgrade model is easily lost and subgrade model is easily eroded. Fig. 9 is the erosion amount change curve of subgrade model with the effect time change of sandstorm.

As shown in Fig. 10, on the condition of invariable wind speed, the density of subgrade model is inversely proportional to the sandstorm erosion time and the density decrease range appears fast followed by slow. It may be because the moisture content of subgrade model in the early stage of sandstorm erosion is relatively high, and soil grain has good cohesiveness. Consequently, the soil grain is not easy to be lost. And, with the increasing of the sandstorm erosion time, the moisture content of subgrade model diminishes gradually, the cohesiveness among soil grains is weakened and the acceleration of soil grain loss rate causes the density decrease rate of subgrade model speed up. According to Fig. 11, on the experimental condition of the same sandstorm erosion time, the relation between the density of subgrade model and wind speed is: when the wind speed is low, the density decrease speed of subgrade model is slow; when the wind speed is high, the density decrease rate of subgrade model is fast.

According to Fig. 12, on the condition of the invariable wind speed, the moisture content of subgrade model decreases gradually with the increasing of sandstorm erosion time. The higher the wind speed is, the diminishing range of moisture content is greater. According to Fig. 13, it can be known that through controlling the sandstorm erosion time as the invariant and under the effect of the wind speed rule, the moisture content of subgrade model shows: when the wind speed is low, the decrease speed of moisture content in the subgrade model is slow; when the wind speed is high, the decrease speed of moisture content in the subgrade model is rapid. It indicates that the moisture of subgrade model is easy to be lost in the case of high wind speed.

According to Fig. 14, it can be known that on the condition of invariable wind speed, with the increasing of sandstorm erosion time, the unconfined compression strength decreases gradually and the decrease range is small, no more than 0.5 MPa. According to Fig. 15, it can be known that on the condition of the same sandstorm erosion time, with the sudden increasing of wind speed, the decrease speed of unconfined compression strength is very slow. It indicates that the change of unconfined compression strength in subgrade model is moderately affected by the wind speed change. However, sandstorm erosion may cause pit and groove on the subgrade side slope. The pit and groove may further form voids on the subgrade, which makes the bearing capacity of subgrade reduce greatly and produce subgrade settlement, etc.

4 Experimental Conclusion

By utilizing the sand blasting machine to manufacture sand flow and acting on the subgrade model, the experiment determines the density, moisture content, quality and unconfined compression strength of subgrade model affected by the sandstorm erosion and studies the impact of sandstorm erosion on the durability of subgrade structure by controlling the velocity and time of sand flow. The research result indicates that:

(1) Under the effect of sandstorm erosion, the quality of subgrade model decreases gradually and the quality loss of subgrade model appears linear positive relation with the wind speed. The higher the wind speed is, the quality loss is greater. The sand flow rate of the experiment is 25.32, 30.14 and 33.07 m/s. After acting on it for consecutive 45 h, the erosion amount is 3.18%, 4.84% and 7% respectively.
(2) The density of subgrade model decreases with the increasing of sandstorm erosion time. Besides, the density decrease is rapid in early period of sandstorm erosion. However, with the increasing of sandstorm erosion time, the density decrease speed of subgrade model becomes slow increasingly. In addition, the increasing of wind speed will accelerate the density decrease speed of subgrade model. The sand flow rate of the experiment is 25.32, 30.14 and 33.07 m/s. After acting on it for consecutive 45 h, the density decrease is 0.93%, 1.96% and 2.22% respectively.
(3) The moisture content of subgrade model decreases with the increasing of sandstorm erosion time and the moisture content loss of subgrade model appears linear positive relation with the wind speed. The higher the wind speed is, the moisture content loss speed is higher. The sand flow rate of the experiment is 25.32, 30.14 and 33.07 m/s. After acting on it for consecutive 45 h, the moisture content decrease amount is 8.73%, 18.08% and 25.40% respectively.
(4) Unconfined compression strength of subgrade model decreases gradually with the increasing of wind speed and the increasing of sandstorm erosion time. The loss speed of unconfined compression strength has no direct relationship with the wind speed and the increasing of wind speed will not accelerate the decrease speed of unconfined compression strength. The sand flow rate of the experiment is 25.32, 30.14 and 33.07 m/s. After acting on it for consecutive 45 h, the unconfined compression strength decrease amount is 5.51%, 7.09% and 9.06% respectively.

According to the experimental result, on the condition of invariable sand flow rate, the quality, density, moisture content and unconfined compression strength of loess subgrade structure decrease gradually with the increasing of sand flow effect time. When the sand flow rate increases, the quality, density, moisture content and unconfined compression strength loss of subgrade structure is fast. Thus, it can be seen that wind speed is the main factor of affecting the speed of sandstorm erosion. Wind speed has significance on the durability of subgrade structure. In the sandstorm prevention design and existed sandstorm disaster control of railway in loess area, people usually take effective measures like wind speed control to reduce the damage of sandstorm erosion to the subgrade structure.

References

1. Weifeng X (2013) Research on Wind Erosion Rule and Prediction in Railway Engineering. Southwest Jiaotong University
2. Yaqi W (2010) Research on Wind Erosion Rule in Railway Engineering of North of Shaanxi Windy and Sandy Area-Take Zhunshuo Railway for an Example. Beijing Jiaotong University
3. Shisheng T, Yongge S, Xiaoyong Z (2011) Gale characteristic statistic analysis of baili windy area of xinjiang railway. Railway Tech Supervision 01:36–40
4. Zhenshan L, Jinren N (1998) History, current situation and trend of wind sand flow research. Resour Environ Arid Reg 03:90–98
5. Huijiuan B, Zhenshan L (2004) Experimental research on longitudinal pulse of wind speed in wind sand flow. Chin Desert 02:132–135
6. Shenghu L (2012) The Experiment and Numeric Study on Wind Sand Flow Structure. Lanzhou University
7. TB10621-2009, Design Code for High-Speed Railway
8. Meili Z (1998) Similar Engineering. China Machine Press, Beijing
9. Guangrong D, Changzhi L, Jiong J, Shangyu G, Dan W (1987) Some results on soil wind erosion and wind tunnel experiment. Chin Sci Bull 04:297–301

"Four-A-Services" Oriented Evaluated System of Intelligent City

Zhijie Li(✉) and Wei Zhang

China Design Group Co., Ltd, Nanjing 210014, Jiangsu, China
503170693@qq.com

Abstract. With the development of information technology, intelligent city has attracted extensive attention worldwide. Currently, there are various standards of intelligent city estimation. Since the construction of intelligent city is a complex program which contains many different science and technology areas, such as information technology, communication technology, control technology, sensor technology, and computer technology et al. These existing estimation systems set a great number of estimation factors to cover the areas as much as possible. In order to reduce the estimation factors, as well as estimate the developed status of intelligent city objectively and comprehensively, a "Four-A-Services" oriented evaluated system for intelligent city has been designed. This system estimates the Intelligent City based on Four factors which are "Anyone", "Anytime", "Anywhere", and "Any Device" as well as tests the operation status of intelligent city in real-time so that the problems could be identified and solved in time.

Keywords: Intelligent transport system · Intelligent city · Four-A-Services · Estimate system · Influence factors

1 Introduction

With the development of information technology, Intelligent City becomes a new trend after Industrialization, Electrification and Informatization. Intelligent city, the perfect fusion of human society and the physical world by using IOT, connects virtual world and real world which will bring great convenience to people's lives, as well as change the operation mode of human society [1].

The assessment of intelligent city, an effective method to guide the sustainable development of smart city, should run through all steps of its planning, construction, and operation. Since the concept of "intelligent city" has been proposed, it becomes a very popular method which has been treated as national strategy in many countries and regions all over the world. Lots of countries made national planning documents, such as "REALISING THE iN2015 VISION" of Singapore, Economic Recovery Plan of USA, i-Japan Strategy 2015 of Japan, "EUROPE 2020" and "Smart Cities and Communities European Innovation Partnership" of the European Commission et al. [2].

Currently there is no unified cognitive and no widely recognized definition of intelligent city. IBM, Intelligent Community Forum (ICF), Chinese Academy of Sciences,

X. Zeng et al. (eds.), *International Symposium for Intelligent Transportation and Smart City (ITASC) 2017 Proceedings*, Smart Innovation, Systems and Technologies 62, DOI 10.1007/978-981-10-3575-3_27

Cisco et al. proposed the concepts and strategies of intelligent city. In order to accurately measure the progress and development level of intelligent city, it is necessary to make a clear, scientific, reasonable, comprehensive, and maneuverable intelligent city estimated system [3]. The construction of intelligent city in our country also needs an estimated system, which is suitable for it develops in China, so that to evaluate the development level of intelligent city, take scientific and rational decision- making, assess the effectiveness correctly, detect and correct the deficiencies in time, as well as ensure the construction of intelligent city rapidly and healthily [4].

Intelligent city is a comprehensive method related to multidisciplinary and multifield which has wildly extension and related work. Although the focuses of intelligent city construction are different in different research fields, information, intermingle, coordination and sustainability are the common concepts of intelligent city [5]. Intelligent service is one of the most important concepts of intelligent city development [3]. The vision of intelligent city is to realize anyone could enjoy the service of intelligent city in anywhere and anytime by any device. Based on this principle, this paper proposes a "Four-A-Services" Oriented Estimate System of intelligent city to improve the development of intelligent city healthily and rapidly.

2 Related Work

It is necessary to build an estimate system to assess the development of intelligent city. The intelligent city estimated standard of Europe contains many indexes including intelligent economy/innovative economy, intelligent mobile (including intelligent transportation, intelligent education, intelligent purchasing et al.), intelligent environment (focusing on ecological environment of city), intelligent management (adjusting and improving the management mode of government), which focuses on the people's livelihood and service, the innovation and development, the public participation and interaction and so on [6].

IBM proposed that intelligent city should based on 6 core system, including human (such as public security, medical and education, and the quality of live et al.), business (such as business plan, opening to the outside world, investment, labor legislation, and product market legislation et al.), transportation (such as public transportation network, ocean carriage, and air freight et al.), communication (such as telephone system, network, and wireless network et al.), water (such as circulation of water supply and cleaning), and energy (such as production, transportation system and waste disposal et al.). These 6 core systems provide useful reference for the estimate system of intelligent city [7].

ICF, long-term interests in the development of intelligent city, studies intelligent city based on wisdom community and makes best practice to improve the sustainable development of city. ICF estimate the level of intelligent city through 5 index including network connection, knowledge based labor, innovation, digital integration, community marketing and publicity et al.

In China, the researchers, scientific institutions, government also focus and set the estimate index system of intelligent city recently. Nanjing Information Center published

"the research of smart city evaluation index system" in 2010, which analyzes the index of city informatization and summarizes the evaluation index system based on the connotations and development characteristics of city.

In 2013, National intelligent building and residential digital standards committee published "the research on the standard system of China's smart city" [9], which studies 5 standards of intelligent city construction including infrastructure, construction and livable, management and services, industry and economy, security and operation and maintenance. Currently, It is the latest and most authoritative document on intelligent city in national level.

In December of 2014, Chinese intelligent city forum and "China International Smart City Blue Book (2014)" conference held in Beijing. This conference focuses on typical case, latest technology, development mode and operation of intelligent city, as well as publish the development index of it.

Currently the study on evaluation system of intelligent city in China at the exploratory stage. There is no unique and clear evaluation system in national level. There are many issues of current estimate system, such as limited usage scope, high proportion of subjective indicators, high quantity of index, less evaluation objects et al. In order to solve these problems, this paper designed an objective and accurate estimate system of intelligent city based on its service target.

3 "Four-A-Services" Oriented Intelligent City

This paper sets "Four-A-Services" standard model of intelligent city, which estimates intelligent city based on citizen access to intelligent services in any place at any time as standard, to evaluate its situation objectively. "Four-A-Services" contains four factors which are anyone owned authorization, anywhere, anytime, and any device. In order to

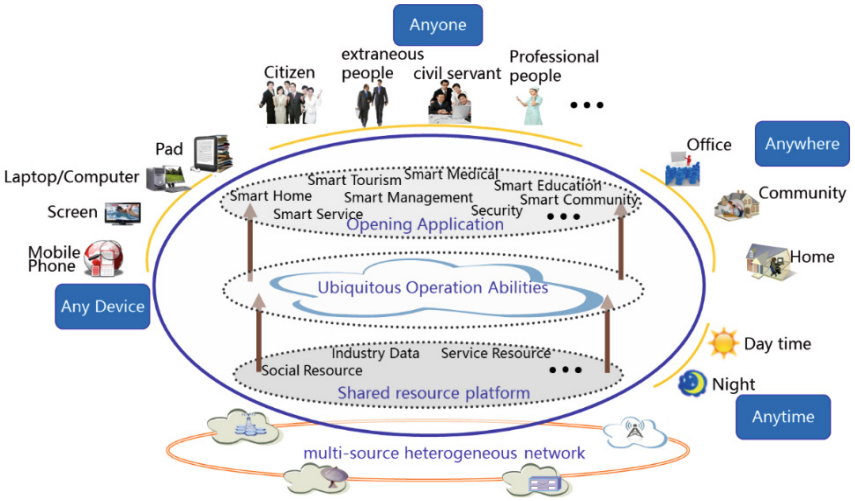

Fig. 1. Architecture of Four-A-Services

reach this target, intelligent city have to be supported by many technologies, including multi-source heterogeneous network which are fusion and exchanged, resource platform which can share and provide data, cloud computing service which can provide high quality operation processing, opening application which can provide different types of services. The architecture of "Four-A-Services" is shown as Fig. 1.

The development of intelligent city, based on advanced technologies such as information technology, intelligent technique, network and so on, includes intelligent technology, intelligent industry, intelligent service, intelligent management, intelligent culture, intelligent life et al. There are many supported technologies such as cloud computing, virtualization, big data mining, IOT, wireless network and so on. Its service includes public service, government service, transportation service, medical service, education service et al. There are many challenges of intelligent city development, such as wide range of services and technology, lots of contents, complex standards. Current technique or industry standards cannot evaluate the situation of intelligent city comprehensively and objectively.

This paper summarizes the key words related to intelligent city and classifies them as the method of "Four-A-Service":

1. Anyone oriented technologies: the techniques and service to identify user, distribute accounts et al.
2. Any device oriented technologies: the techniques and service to realize cross platform, cross network, and cross terminal et al.
3. Anywhere oriented technologies: the techniques and service to break the limitation of space so that users could get services at anywhere.
4. Anytime oriented technologies: the techniques and service to break the limitation of time so that users could get services at anytime.

The classification of technologies and services of intelligent city is shown as Fig. 2:

1. The realization of "Anyone-Oriented" service based on major technologies and services such as identification, social network, resource-shared platform, information service, public service and so on.
2. The realization of "Anytime-Oriented" service based on major technologies and services such as big data mining, real-time information distribution, safeguard, ecological city and so on.
3. The realization of "Anywhere-Oriented" service based on major technologies and services such as network, wireless city, 3G, WIFI, WLAN, cloud computing, digital globe et al.
4. The realization of "Any device-Oriented" service based on major technologies and services such as digital city, GIS, IOT, Data center et al.

The core technologies of intelligent city include information technologies, intelligent technologies, and network technologies, consist of cloud computing, big data mining, IOT, wireless city, digital city and so on. The development of intelligent city is related to multi-faceted, innovative urban development model, such as space, economy, society, institution, and management and so on. This paper designed a comprehensive and objective evaluation model based on the service objects of intelligent city.

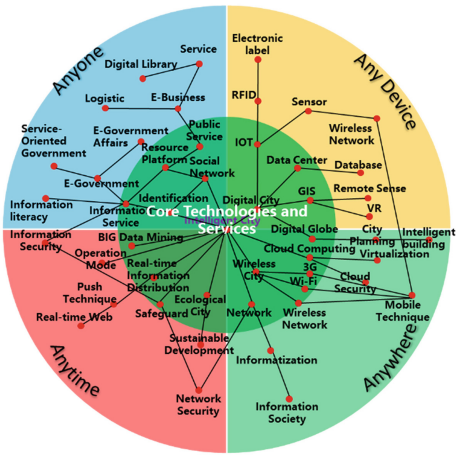

Fig. 2. Key words analysis of Four-A-Services

4 Evaluated System of "Four-A-Service"

There are four factors of evaluated system which are human, temporal, geographyical and device. As Fig. 3 shows that, four factors could evaluate the developed situation of intelligent city objectively. Every two factors composite a pair of impact factors. Based on people oriented principle, this paper group the impact factors as "human-temporal", "human-device", "human-geographyy". These three impact factors could illustrate user i access the service of intelligent city at time t in location l through device A.

Since the users of intelligent city are different. The impacts of service are different as well. For example, doctors and patients are care more about medical services, teachers and students are care more about education services. Thus, it is necessary to arrange different weight to different service based on different users. Through the concept of

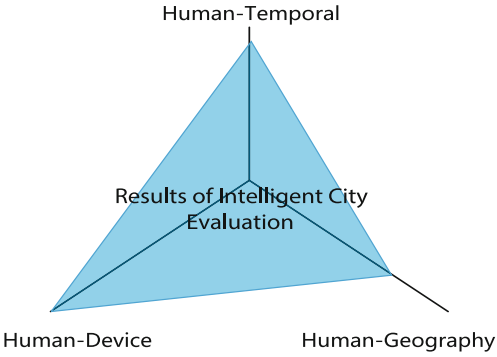

Fig. 3. The relationship between four factors and intelligent city estimation

social network [10], the weight between user and service at time t could be shown as Function 1:

$$w_t^{ij} = \frac{w_{t-1}^{ij} * \alpha + tally_{t-1}}{\alpha + 1} \tag{1}$$

$tally_t$ is the length of time that user i access to the service at time t. α is time-effect factor. The influence power of intelligent city service according to time is marked as $S_{T,}$ which is:

$$S_T = \sum_1^n s_j \tag{2}$$

n is the total quantity of the services of intelligent city, the impact of service is s_i. With the change of time, the impacts of service of intelligent city also be changed. For example, the impacts of government service and public service will be higher in daytime. The impacts entertainment service will be higher at night. If the service cannot be provided at high impact time, it will cause great negative impacts. Assuming the relationship between service impact and time is follow Gaussian distribution, the service impact could be shown as Function 3 and Fig. 4:

$$s_j = f_j(t) = Ae^{-\frac{(t-\mu_j)^2}{2*\sigma_j^2}} \tag{3}$$

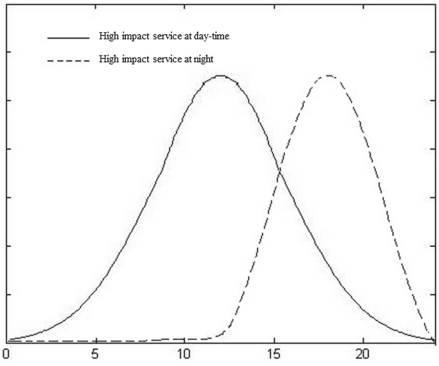

Fig. 4. Temporal influence on the services of intelligent city

The impact power of service j to user i at time t is:

$$s_{ij} = w_t^{ij} * f_j(t) = \frac{w_{t-1}^{ij} * \alpha + tally_{t-1}}{\alpha + 1} * Ae^{-\frac{(t-\mu_j)^2}{2*\sigma_j^2}} \tag{4}$$

The impact power of intelligent city considered "people-time" factor is:

$$S_t = \sum_1^m \sum_1^n s_{ij} \tag{5}$$

Besides the impact of time, geography is another important factors which has to been considered. Based on social network and power law probability distributions, the location with large flow of people is stable. This paper located the geography by using Access Point (AP), including wireless access points, routers, base stations et al. The probability of user *i* appeared in location *l* could be indicated as:

$$P(i, l) = \frac{\sum_{z=1}^{z_i} \eta(l, L_z(i))}{z_i} \tag{6}$$

Where z_i represents the number of APs user i visited and $L_m(i)$ is a vector to store all location information of user i. Function $\eta(x, y)$ is:

$$\eta(x, y) = \begin{cases} 1 \text{ if } x = y \\ 0 \text{ if } x \neq y \end{cases} \tag{7}$$

We utilize APs (Access Points) to locate the location of each node in different time. The probability for user *i* appeared in AP_m is changed with time *t*. Assuming during time period $[t_{start}, t_{end}]$, AP_m detects user *i* in its range. If a user *i* stay over a time period ΔT, it can be treated that this node appears in location *l*. Thus the probability of node I appear at location *l* in time $t \in [t_{start}, t_{end}]$ is:

$$P(i, l, t) = \frac{\sum_{z=1}^{z_i} \eta\left(l, L_z(i)\right) H(\Delta T - (t_{end} - t_{start}))}{z_i} \tag{8}$$

Where H(x) is the Heaviside Step Function [11] defined as:

$$H(x) = \begin{cases} 0 \ x < 0 \\ 1 \ x \geq 0 \end{cases} \tag{9}$$

The probabilities of every user appeared in every location could be indicated as Table 1:

Table 1. The probabilities of user i visits AP_k

	AP_1	AP_2	…	AP *l*	…	AP_z
1	P(1, 1, t)	P(1, 2, t)	…	P(1, *l*, t)	…	P(1, z, t)
2	P(2, 1, t)	P(2, 2, t)	…	P(2, *l*, t)	…	P(2, z, t)
…	…	…	…	…	…	…
i	P(i, 1, t)	P(i, 2, t)	…	P(i, *l*, t)	…	P(i, z, t)
…	…	…	…	…	…	…
n	P(N, 1, t)	P(N, 2, t)	…	P(N, *l*, t)	…	P(N, z, t)

Based on Function (4) and (8), the service impact of intelligent city to user i a time t in location l is:

$$S_{ijl} = w_t^{ij} * f_j(t) = \frac{w_{t-1}^{ij} * \alpha + tally_{t-1}}{\alpha + 1} * Ae^{-\frac{(t-\mu_j)^2}{2*\sigma_j^2}} * P(i, l, t) \tag{10}$$

Thus, the service impact considered "human-temporal" and "human-geography" is:

$$S_t = \sum_1^m \sum_1^n \sum_1^z s_{ijl} \tag{11}$$

With the development of information technology, mobile terminal become more and more popular. People could get the service of intelligent city through many different way, such as computers, laptops, self-service terminal, smart phone, tablet and so on. Also the service of intelligent city is provided by account through uniform identity platform. It is too difficult to know which device that everyone used to get the service. This paper cares about whether people could get the intelligent service successfully rather than the specific device that people use. This paper introduces parameters r_{ij} to record whether user i can get server j successfully:

$$r_{ij} = \begin{cases} 0 & \text{It is faiure that user i access to service j} \\ 1 & \text{It is successful that user i access to service j} \end{cases} \tag{12}$$

In total, the service impact of intelligent city based on human, temporal, geography, and device could be indicated as:

$$S_t = \sum_1^m \sum_1^n \sum_1^z r_{ij} s_{ijl} \tag{13}$$

Since the population of different level of city is different, population M of a city has to be considered:

$$S_T = \frac{\sum_1^m \sum_1^n \sum_1^z r_{ij} s_{ijl}}{M} \tag{14}$$

5 Application Scenes of Function

There are three different application scenes of this function:

(1) Evaluate the service of intelligent city macroscopically. Function (14) could evaluate an intelligent city based on time change. In order to get a comprehensive result, we could select X different durations of time Δt to calculate the service impact $S_{\Delta tk}$:

$$S = \frac{\sum_{k=1}^{k=X} S_{\Delta tk}}{X} \tag{15}$$

Function (15) could divided different levels of intelligent city by three preselect threshold A, B, and C:

$$\begin{cases} \text{First level of intelligent city} & S > A \\ \text{Second level of intelligent city} & B < S < A \\ \text{Third level of intelligent city} & \text{C} < S < B \\ \text{Fourth level of intelligent city} & \text{S} < C \end{cases} \tag{16}$$

The results could be re-evaluated in period.

(2) Search the status of intelligent city service in-time. Function (14) could get the service impacts of intelligent city in time. Compare the current result with history records, it is easy to find and fix the problems of intelligent service.

(3) Search the status of individual service in-time. If the service impact of Function (14) is changed into individual or particular service, such as intelligent transportation, intelligent medical, intelligent education, the public service of smart expressway and so on, manager could get the result of particular service.

6 Conclusion

Intelligent city is a program including multidisciplinary and multifield. In order to evaluate the development of intelligent city, this paper introduced "Four-A-Service" method and designed an evaluation model. Based on this model and system, we could estimate the level of intelligent city objectively, as well as manager and control all services of intelligent city in-time.

References

1. Zhou J (2013) Study on the Smart City Assessment System. Huazhong University of Science and Technology, Wuhan
2. Luo W, Intelligent City: Planning, Construction, Evaluation. Posts & Telecom Press, 2020:420–435
3. Feng L, Zhao JY, Guo LS (2014) The Construction of Service System of Intelligent City, Beijing. J Beijing City Univ 1:65–70
4. Chen M, Wang QC, Zhang XH et al (2011) Research of the evaluation system of wisdom city—smart nanjing for example. Urban Stud 8(5):84–89
5. Dan K (2014) Explore the evaluation system of wisdom city. Urbanism Architect 2:335
6. Giffinger R, Christian F, Hans K, Robert K et al (2007) Smart cities: ranking of European medium-sized cities. Vienna University of Technology, Centre of Regional Science, 11
7. Robinson R, The six steps to a smarter city; and the philosophical imperative for taking them. http://theurbantechnologist.com/2013/01/08/the-six-steps-to-a-smarter-city-and-the-philosophical-imperative-for-taking-them-updated-2/
8. Joseph NP, Indu S (2008) Future cities designing better, smarter, more sustainable and secure cities, The Intelligent Community Forum
9. Guo LQ (2013) The Research Report on Standards System of China Smart City. China Architecture & Building Press, Beijing, pp 150–250

10. Chan Shu-Yan, Hui Pan, Xu Kuang (2009) Community detection of time-varying mobile social networks. In: Zhou Jie (ed) Complex 2009, vol 4., LNICSSITE. Springer, Heidelberg, pp 1154–1159. doi:10.1007/978-3-642-02466-5_115
11. Lange RJ (2012) Potential theory, path integrals and the laplacian of the indicator. J High Energy Phys 11:1–46

Overview of Non-contact Pantograph-Catenary Arc Detection Based on Image Processing

Shize Huang[1(✉)], Fan Zhang[1], Liangliang Yu[2], and Meiyu Pan[1]

[1] Key Laboratory of Road and Traffic Engineering of Ministry of Education, Tongji University, Caoan Road, Shanghai 4800, People's Republic of China
hsz@tongji.edu.cn, zhangfandyq@163.com, pan-meiyu@163.com
[2] College of Electronics and Information Engineering, Tongji University, Caoan Road, Shanghai 4800, People's Republic of China
1076884038@qq.com

Abstract. The pantograph-catenary system of high-speed EMU is the only way to get the power of high-speed trains. Pantograph-catenary arc fault is a kind of common fault of pantograph-catenary system, which brings fatal harm for train and becomes an important factor to hinder the stable operation of the train. The pantograph-catenary arc detection based on image processing can detect the state of pantograph-catenary system quickly, which can judge whether there is an arc in system and maintain the safety of train. Compared with the traditional detection method, it will be divided into infrared, ultraviolet and visible light accordance with the detection of the use of image information, which on the basis of summarizing all kinds of non-contact arc detection methods in recent years. The edge detection, threshold segmentation and other algorithms are summarized and the characteristics of pantograph-catenary arc are highlighted by using image enhancement technology. In view of the shortcomings of the existing non-contact pantograph-catenary arc detection, the future development is prospected.

Keywords: Pantograph-catenary system · Arc detection · Image processing

1 Introduction

Pantograph-catenary system is an important part of the power supply system of electrified railway. It bears the responsibility of transmitting the traction power to the electric locomotive. The close contact between pantograph and contact wire is a must for the stable and safe operation of train. As a result of the complex interaction between mechanics and electric, pantograph arc is a serious threat to the safe operation of the electrified railway. Pantograph-catenary arc may cause the interference to the communication system which aggravates the friction between the pantograph slide and contact

Submitted to 2017 International Symposium on Intelligent Transportation and Smart City - Green Transportation Urban Utility.

X. Zeng et al. (eds.), *International Symposium for Intelligent Transportation and Smart City (ITASC) 2017 Proceedings*, Smart Innovation, Systems and Technologies 62, DOI 10.1007/978-981-10-3575-3_28

wire, or even cuts the electric supply to the electric locomotive. Therefore, fault detection of the pantograph-catenary is of great significance to the normal operation of the electric railway and construction and development of the railway system [1].

2 Cuase and Feature of Pantograph-Catenary Arc

In the course of high-speed sliding between the pantograph slide and contact wire, the short separation occurs because of irregularity of railway and vibration of contact wire and catenary. At the moment of separation, voltage difference increases dramatically, creating an electric field in the air gap of the pantograph [2–5]. The breakdown phenomenon occurs and the gas radiates energy in the form of arc light which causes the pantograph-catenary arc. There are some features of the arc because of disconnection. It distorts the sinusoidal waveform and generates the transients during the current zero crossings. The contact force also decreases. Furthermore, the traction current will generate heat thus an increase in the contact resistance. And the arc also gives out infrared, ultraviolet and visible light during its occurrence [6–8].

3 Traditional Way of Pantograph-Catenary Detection

3.1 Manual Detection

The original way of detection cannot detect pantograph- catenary fault in real time. Basically, the detection is a manual task, which requires operating personnel inspecting along the railway to understand the operating state. However, the overall situation of the contact wire is unlikely to be detected, so there are many problems need to be solved [9].

The advantage of manual detection is flexibility which means that different kinds of faults can be detected respectively. The disadvantage is low inefficiency, insecurity and human disturbance to train operation. The result of detection may be largely influenced by the environment and staff's experience.

3.2 Contact Pantograph-Catenary Arc Detection

Contact pantograph-catenary arc detection emerged with the development of the electrified railway. Foreign countries have developed detection equipment serving as multiple purposes, focusing on their own need. For example, Germany focuses on contact force detection. Basically, force and acceleration telemetry equipment mounted on the pantograph are used for detection [10]. Too much metallurgy powder being used on the pantograph slipper in Japan leads to severe wear of contact wire. Therefore, much attention has been paid to detecting the friction between pantograph-catenary and contact wire. Optical fiber interferometer sensors are used to sense the contact force between pantograph and catenary [11]. Our country begins the study of pantograph-catenary detection system in the 1960s, which emphasizes on the parameters detected by pantograph-catenary mobile monitor. Other approaches have also been applied to

monitor the current such as embedded optical fiber, transducers in the pantograph slipper and current circuit [12].

Compared to manual detection, these approaches are more accurate and efficient. However, different testing programs require different equipment and some transform the pantograph. In this way, the dynamic behavior will be interfered resulting inaccuracy. Others occupy the railway while using the mobile monitor which disturbs operation [13–16].

4 Arc Detection Based on Image Processing

The main features of the pantograph-catenary are optical, thermal and electromagnetic characteristic. The most obvious one is optical character. By processing images involving infrared, ultraviolet and visible light, related features can be extracted. Then pantograph-catenary arc will be detected.

4.1 Arc Detection Based on Infrared Light

Infrared image reflects the thermal state and temperature distributions under operation. Whether they are normal or not it is a critical feature to estimate whether there is a discontinuity between pantograph and catenary. Therefore, infrared thermography can monitor the state and fault of the equipment by analyzing infrared images. Hough

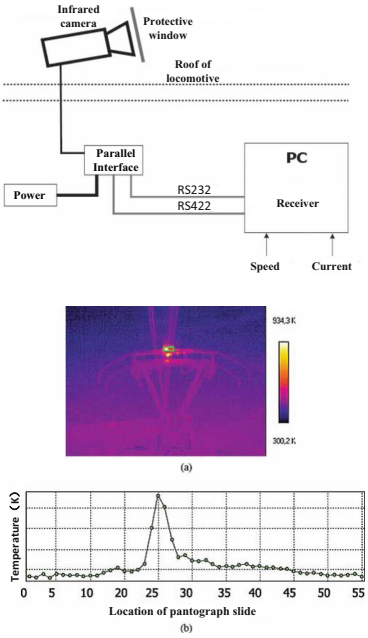

Fig. 1. Infrared measurement based on Hough transform

transform is used to track the position where temperature is abnormal in the infrared images. An infrared camera is installed on the train to record the running state of pantograph and catenary. After Hough transform, much information can be drawn from the image such as temperature distributions of pantograph slide, location of pantograph-catenary arc and irregular orientation of contact wire [17]. Figure 1 shows the detection process.

Online infrared imager installed on the electric locomotive is used to monitor temperature of critical parts of contact wire and pantograph continuously. This system records real-time data and then analyzes current temperature. After getting a data report, we will know the location where the temperature is abnormal indicating that a failure may happen. Figure 2 shows the system diagram.

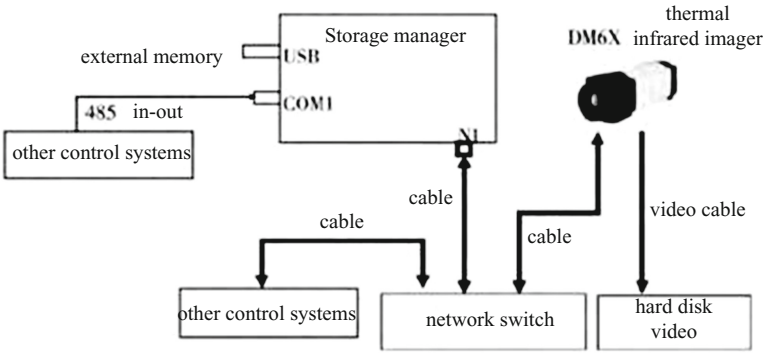

Fig. 2. Infrared image acquisition and storage system

Focusing on the characteristics of the railway system, different products are developed to detect temperature specifically. Infrared imaging device is mounted on the train roof to detect the temperature of joint between pantograph and contact wire. Arc temperature and fault location are recorded for timely repair [18].

The technology of temperature measurement without the need of additional equipment or inspections can be a substitute for traditional method which makes electric temperature measurement possible. Therefore, it would be more and more common to use infrared image to detect pantograph arc. It is a good way to monitor temperature in real time and locate where the arc occurs. However, the results are likely to be affected by environment. Moreover, if the sun is also recorded, there would be a bright spot in the image leading to a wrong conclusion. Furthermore, a vehicle-mounted infrared imager is likely to be affected by the electrical equipment along the railway and pantograph arc is hard to be detected.

4.2 Arc Detection Based on Ultraviolet Light

Spectral characteristic curve of sunlight and pantograph-catenary arc is drawn from optical spectrum analyzer. The wavelength of sunlight is wide ranging from 300 nm to 1100 nm, while the spectrum of pantograph-catenary arc distributes from 240 nm to

260 nm, 300 nm to 330 nm, 390 nm to 400 nm in the form of ultraviolet. As sunlight cannot radiate light whose wavelength ranging from 240 nm to 260 nm and there is little on the earth either, it can be used as a characteristic value to detect pantograph-catenary arc. This detection system is developed including optical image measurement system, ultraviolet sensor system and data analyzing-and-processing system. Photoelectric sensor can detect ultraviolet light given out by pantograph arc and transform light signal to measurable electric signal. After analyzing the electric signal we can get the related data about pantograph-catenary arc [19].

Ultraviolet light transducer will send response signals when detecting ultraviolet. It would be transformed into response pulse after amplification, filtering and analog digital conversion (A/D). Response pulse becomes denser and amplitude higher when ultraviolet accumulates. Spectral features of pantograph arc are extracted based on the principle above to design a detection system. It combines ultraviolet sensor and technology of digital signal processing (DSP) which helps to get a clear view of the discontinuity. Figure 3 shows the block diagram.

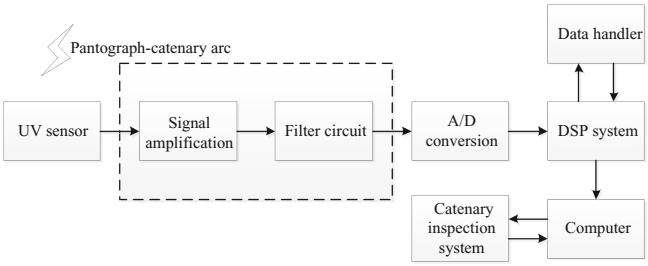

Fig. 3. Diagram of catenary off-line arc detection

4.3 Pantograph-Catenary Arc Detection Based on Visible Light

Arc occurred in a video frame is detected by using image processing techniques based on model. Light image is transformed into binary one. Then features are extracted to serve as input signal. Voltage signals are detected by modeling the arc. These signals are analyzed to detect the condition of the pantograph-catenary system [20]. Another way applies a threshold value to each video frame. The rate of sudden glares is converted to time series. The phase space of the obtained time series is constructed and the arc event is found by using particle swarm optimization. Peak value is detected in an area of pantograph arc [21]. Figure 4 shows the system diagram.

Rectangle $m \times n$ areas of binary image are set, in which every pixel is detected and accumulated. Maximum value is used as pixel value of arcing area in a frame, which will be analyzed later in target identification. As the operation environment is complex and illumination always changes, gray scale histogram is used for image segmentation. Visual features are obvious when arc occurs. This pixel has maximum gray value compared with others around. By selecting a proper threshold value can these features be extracted to detect pantograph arc [22].

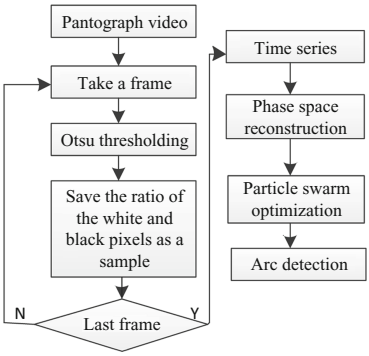

Fig. 4. Arc detection of pantograph-catenary system process

A new way is detection without the need of additional equipment. Each video frame is used as an independent image. The location of pantograph and contact line is obtained by edge detection. The contact force is also monitored to diagnose irregular positioning of the contact line and whether pantograph arc occurs. Figure 5 shows the detection process [23].

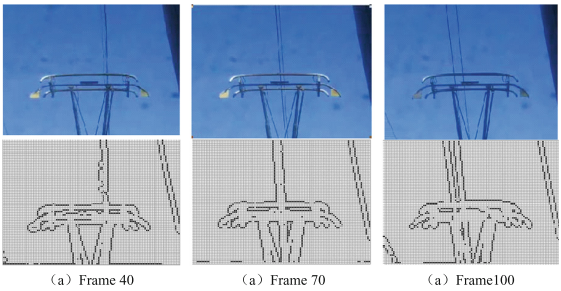

Fig. 5. Images processed by edge detection

5 Algorithm of Arc Detection

5.1 Edge Detection Algorithm

Edge detection is an important factor which decides the quality of the detection. Compared with canny edge detection, morphological edge detection and wavelet edge detection, canny edge detection is of higher accuracy. While morphological edge detection positions precisely, it is less accurate [24]. Therefore, edge processing based on canny operator can better detect pantograph arc online. CCD cameras are used to acquire images of pantograph slide. These images will then be read into computer for edge detection [25].

5.2 Threshold Segmentation Algorithm

Otsu algorithm is used to decide threshold value of the pantograph arc image. Distributed domain solver is used for gray scale image segmentation to eliminate the interfering targets which helps to increase the accuracy in processing image later [26]. Based on the simplified Mumfoud-Shah Level Set image dispose model, a new segmentation method on discharge area for UV images is proposed. By segmenting UV images using this method, the area and contour of the corona discharge are obtained, and it is useful for further pattern recognition study. In this way, Poisson noise and Gaussian noise were effectively reduced without filtering precondition which is adaptable to UV images [27].

5.3 Algorithm Based on Image Enhancement Technology

Fuzzy enhancement technology of infrared image is able to enhance the visual effect of infrared image of electric power equipment, highlight the thermal anomaly area and help engineers analyze the faults. First, the wavelet transform of the infrared image, homomorphic filtering enhancement and fuzzy enhancement were processed. Then the dynamic adaptive genetic algorithm was used to optimize the parameters of fuzzy method. Finally, the images were reconstructed. The image contrast, resolution, and clarity can be improved by using this method, which is favorable in thermal anomaly location and fault diagnosis. Figure 6 shows the system diagram.

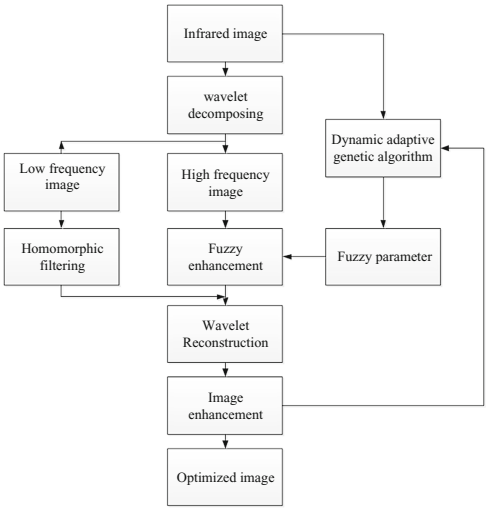

Fig. 6. Fuzzy enhancement technology of infrared image

An image enhancement and segmentation algorithm is put forward for the object recognition and diagnosis of electric equipment infrared images based on CA(Cellular Automata) and OTSU method. The top hat transformation and low cap transformation are combined to enhance the infrared images of electric equipment and CA is then applied to detect the edges of the enhanced images, which are transformed into binary

variables and merged into images segmented by OTSU. Experimental results show that after algorithm processing, the objects of infrared image become clearer and more suitable for observation by naked eyes. Figures 7 and 8 shows the system diagram.

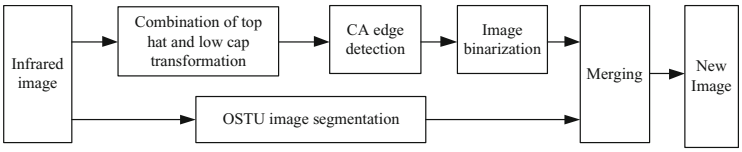

Fig. 7. Image enhancement based on CA and Otsu method

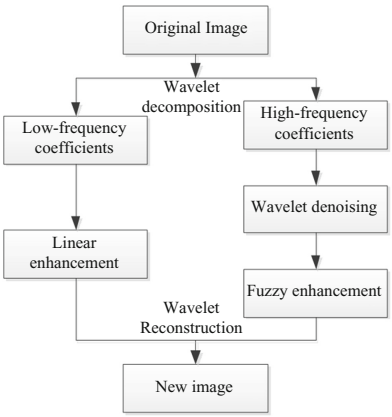

Fig. 8. Image enhancement based on wavelet transform and improved fuzzy set theory

Focused on the problem that noise is enhanced with image enhancement in the traditional image enhancement methods, an image enhancement algorithm based on wavelet transform and improved fuzzy set theory was presented. Firstly, the multi—scale wavelet transform was adopted to decompose the input image. Secondly, the low frequency coefficients were enhanced by the linear piecewise function and wavelet threshold was used for the high frequency coefficients de-noising,then a new membership function of fuzzy was defined and the high frequency coefficients of different directions of each scale were enhanced by fuzzy enhancement transformation. Finally, the inverse wavelet transform was applied to synthesis image. This algorithm demonstrates that the disadvantages of traditional enhancement methods are avoided. And the presented algorithm can enhance the key characteristic of the image and restrain noise effectively [28]. The system diagram is as follows:

6 Propects and Suggestions

6.1 Improved Image Recognition

The existing equipment used for collecting visible, infrared and ultraviolet light given out by pantograph arc is susceptible to the environment, weather and so on. Therefore, the quality of the image is always unsatisfactory. Dedicated devices can be developed to detect pantograph arc to improve the quality of the image in the future. On the other hand, the existing image detection algorithm should be optimized. Even when there are frequent environmental changes, we could get clear pictures.

6.2 Information Integration

Different detection systems, so incorrect results are likely to be ignored through the process. However, the advantage of detection based on image is that different kinds of information can be integrated and analyzed. If features of infrared, ultraviolet and visible light are combined, detection system will be much more accurate.

Former ministry of railways has issued documents to ensure a safe operation of high-speed railway and power supply system. Among them, 'technical specifications of safety of high-speed railway power supply' is most technically demanding. Instrument for checking pantograph-catenary, pantograph and catenary alone help us get much information. However, different kinds of information are not connected. If we combine them together, the cause of pantograph arc can be further explored.

6.3 Arc Detection Based on 3D

With the development of three-dimension technique(3D), it has been applied to more and more areas. Technology of 3D can give the precise location of fault. Traditional image collected is always two-dimensional viewed from a single angle. A 3D camera may solve the problem. We are able to know the exact location of pantograph-catenary arc through 3D image.

6.4 Real-Time Information Processing

Most existing technology of pantograph-catenary detection is like remedy after event. Large amount of information, complicated image processing and difficult positioning make the real-time detection almost impossible. However, real-time detection is a better way to detect pantograph arc and promote the technology of contactless detection.

7 Conclusions

Most existing technology of pantograph-catenary detection is like remedy after event. Large amount of information, complicated image processing and difficult positioning

make the real-time detection almost impossible. However, real-time detection is a better way to detect pantograph arc and promote the technology of contactless detection.

Acknowledgements. This work is supported by the 13th Five-Year National Key Research and Development Plan (2016YFB1200402). The authors are grateful for the reviewer of initial drafts for their helpful comments and suggestions.

References

1. Qingquan Q, Shibin G, Zhengyou H, Qizhi C, Jiqin W (2015) Study of China high-speed railway traction power supply key technology. Eng Sci 4:9–20
2. Zongbao G, Guangning W, Wei L, Changhong H, Zhou L (2009) Research review of arc phenomenon between pantograph and catenary in high-speed electrified railway. High Volt. Appar. 03:104–108+127
3. Ying W, Zhigang L, Fuqiang F, Shibin G (2013) Review of research development of pantograph-catenary arc model and electrical characteristics. J China Railway Soc 08:35–43
4. Zhu G, Wu G, Han W, Gao G, Liu X (2016) Simulation and analysis of pantograph-catenary arc steady-state characteristics during static lifting and lowering of high-speed railway pantograph. J China Railway Soc 02:42–47
5. Yan C (2015) Application of the pantograph dynamic detection system in chengdu metro line 2. Electric Drive Locomot. 05:91–94
6. Wang Y, Liu Z, Mu X, Huang K, Wang H, Gao S (2016) An extended Habedank's equation-based EMTP model of pantograph arcing considering pantograph-catenary interactions and train speeds. IEEE Trans Power Deliv **31**(3), 1186–1194
7. Wang Z, Guo F, Wang X, Zhang Y, Wang B, Yan H (2015) Experimental research on radiated electromagnetic noise of pantograph arc. In 2015 IEEE 61st Holm Conference on Electrical Contacts (Holm), San Diego, CA, pp 256–261
8. Ge X, Liu W, Yang Z, Wang Y (2014) The study on electrical temperature characteristics of high speed pantograph. In: 2014 IEEE Conference and Expo Transportation Electrification Asia-Pacific (ITEC Asia-Pacific), Beijing, pp 1–4
9. Han Z, Liu Z, Zhang G, Yang H (2013) Overview of non-contact image detection technology for pantograph-catenary monitoring. J China Railway Soc 06:40–47
10. O'Donnell C, Palacin R, Rosinski J (2006) Pantograph damage and wear monitoring. Railway Condition Monitoring
11. Boffi P, Cattaneo G, Amoriello L et al (2009) Optical fiber sensors to measure collector performance in the pantograph-catenary interaction. Sens J IEEE 9(6):635–640
12. Liu F, Wang L, Gao X, Wang ZY, Zhao QK (2006) Study of measuring the contact force between pantograph and catenary. Electr Locomot Mass Transit Veh 06:19–21+54
13. Barmada S, Raugi M, Tucci M, Romano F (2014) Arc detection in pantograph-catenary systems by the use of support vector machines-based classification. IET Electr Syst Transp 4(2):45–52
14. Taran MF, Rodriguez-Ayerbe P, Olaru S, Ticlea A (2013) Moving horizon control and estimation of a pantograph-catenary system. In: 2013 17th International Conference System Theory, Control and Computing (ICSTCC), Sinaia, pp 527–532
15. Zhiwei H, Zhigang L, Xiaoxiao Z, Yucheng L (2013) Pantograph-catenary contact force data anlysis based on data correlation decomposed by EEMD. J China Railway Soc 09:25–30

16. Kuo M-T, Lo W-Y (2013) Magnetic components used in the train pantograph to reduce the arcing phenomena. In: Industry Applications Society Annual Meeting. IEEE, Lake Buena Vista, FL, pp 1–8
17. Landi A, Menconi L, Sani L (2006) Hough transform and thermo-vision for monitoring pantograph-catenary system. Proc Inst Mech Eng Part F J Rail Rapid Transit 220:43–47
18. Weiqun L (2014) Application of infrared thermography technology. Chin Railways 10:70–72
19. Pu W, Chen T, Liu B, Yu L (2014) Study of pantograph and catenary arc detection system based on ultraviolet light. Inst Tech Sens 07:64–67
20. Yaman O, Karakose M, Aydin I, Akin E (2014) Image processing and model based arc detection in pantograph catenary systems. In: 2014 22nd Signal Processing and Communications Applications Conference (SIU), Trabzon, pp 1934–1937
21. Aydin I, Yaman O, Karakose M, Celebi SB (2014) Particle swarm based arc detection on time series in pantograph-catenary system. In: Proceedings of 2014 IEEE International Symposium on Innovations in Intelligent Systems and Applications (INISTA), Alberobello, pp 344–349
22. Mingjie Z (2013) Status detection of railway catenary based on image processing, Southwest Jiaotong University
23. Aydin I, Karaköse M, Akin E (2012) A new contactless fault diagnosis approach for pantograph-catenary system. In: 2012 15th International Symposium on MECHATRONIKA, Prague, pp 1–6
24. Zhu X (2011) Study of image detection algorithm for the typical malfunction of pantograph slide
25. Ma L, Wang ZY, Gao XR, Wang L, Yang K (2009) Edge detection on pantograph slide image. In: 2nd International Congress on Image and Signal Processing, CISP 2009, Tianjin, pp 1–3
26. Cai X (2008) Study on high-speed OCS dynamic inspection system based on image processing, Southwest Jiaotong University
27. Fangcheng L, Ma G, Liu Y, Yang X (2008) Discharge area segmenting of power equipment in UV image based on level set technology. High Volt Eng 19:20–24
28. Liu X, Wang S, Zhao J (2010) Image enhancement algorithm based on wavelet transform and fuzzy set theory. J Proj Rocket Missiles Guid 04:183–186

Research on the Arc Image Recognition Based on the Pantograph Videos of High-Speed Electric Multiple Unit (EMU)

Liangliang Yu[1], Shize Huang[2(✉)], Fan Zhang[2], and Guanhua Li[1]

[1] College of Electronics and Information Engineering, Tongji University, 4800 Caoan Road, Shanghai, People's Republic of China
Jayce_yu@163.com, hughieli@126.com

[2] Key Laboratory of Road and Traffic Engineering of Ministry of Education, Tongji University, 4800 Caoan Road, Shanghai, People's Republic of China
hsz@tongji.edu.cn, zhangfandyq@163.com

Abstract. Pantograph-catenary system is a key component for transmitting the electric energy to the high-speed Electric Multiple Unit (EMU), and the arc on the pantograph-catenary affects directly the power supply quality and the train operation. Pantograph-catenary condition can be monitored by 6C-system, and extracting the information of arc image from vast videos automatically is difficult. In this study, a new approach has been proposed to get the image and occurrence time of the pantograph-catenary arc. The pantograph-catenary video is separated into continuous frame images, and converted into a discrete time series to analyze, by extracting the optical characters of the arc through image processing technique, and defining the ratio between the number of white and black pixels as arc coefficient. Due to the interference from weather, surroundings and operation routes, the arc parameter is fluctuated overtly. To eliminate this interference, a band-pass filter is used to process the spectrograms transformed by FFT in this paper, and the time domain graphs with the clear arc characters are acquired by IFFT, so that the pantograph-catenary arc can be accurately recognized. In the end the proposed method is demonstrated by a pantograph-catenary video of CRH380D as a case, and the pantograph-catenary arc image and arc occurrence time are correctly obtained.

Keywords: Electric Multiple Unit (EMU) · Pantograph-catenary arc · Image processing · FFT · Time series

Submitted to 2017 International Symposium on Intelligent Transportation and Smart City - Green Transportation Urban Utility

X. Zeng et al. (eds.), *International Symposium for Intelligent Transportation and Smart City (ITASC) 2017 Proceedings*, Smart Innovation, Systems and Technologies 62, DOI 10.1007/978-981-10-3575-3_29

1 Introduction

Pantograph-catenary system is used to transmitting the electric energy to the trains in the high-speed Electric Multiple Unit (EMU), pantograph-catenary system is showed in Fig. 1. Because of the complex impacts between the pantograph-catenary systems in mechanics and electric, arcs occur on the pantograph-catenary frequently, which influences the safe operation of electrified railway critically [1, 2]. In order to monitor the pantograph-catenary system, 6C-system is equipped to shoot the videos of the pantograph-catenary in real time and record the operation conditions, the camera for recording pantograph-catenary system is showed in Fig. 2. It is an important sector that how to extract the image when the arc happens from vast videos correctly and efficiently, which is also the basic element in pantograph-catenary condition analysis. Therefore, the arc recognition and image processing based on videos are critical to the electrified trains maintaining, and both the construction and development of railway system [3, 4].

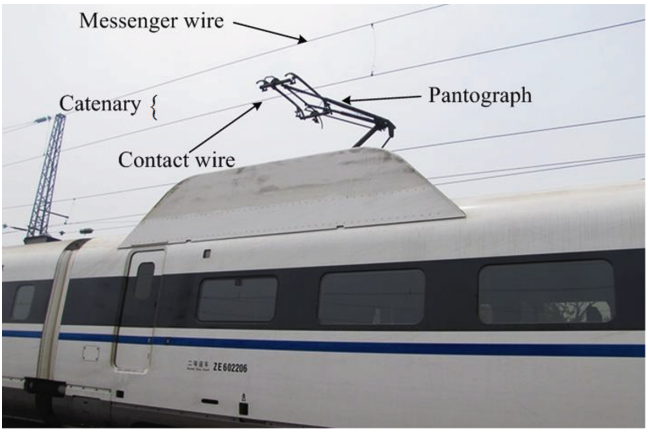

Fig. 1. Pantograph-catenary system

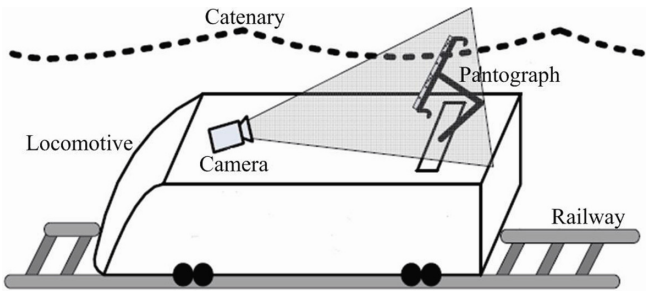

Fig. 2. Camera for recording pantograph-catenary system

The analysis of pantograph video based on image recognition is an active research area and breakdown of this system causes huge economic losses [5]. The researchers

has been tended to automatic approaches based on computer vision and signal processing methods [6]. The edge detection based method was applied to pantograph videos and the position of contact wire was determined in each frame [7]. M. Li and W. Zeyong et al. [8] combined Hough transform and wavelet analysis to obtain the edges in the image. The obtained results are used to get the image of the pantograph strip. The wear of the pantograph strip was detected by extracting the edges of the pantograph image and photoelectric sensors [9]. A computer vision based control system was proposed to adjust the pantograph height in active pantograph system [10]. Phototube or photodiode sensors used to detect the arcing condition by using ultraviolet emissions [11]. Image processing and image recognition also have many applications in other fields. Based on the theory of binocular stereo vision technique, Wang and Liu [12] propose a method, which can acquire deep information from switching arc of low voltage apparatus and acquire useful information of arc image and make the image edge more clear. In order to investigate the mechanism of discharge on insulator, Fang and Zhou et al. [13] use high speed camera to catch the process of the occurrence and development of the partial arc on the porcelain insulator surface and the image were stored.

These methods mentioned in the theses above are lack of the consideration of the interference to the image, such as the weather, the surroundings and the change of operation routes. Some of the methods require additional device installed on the roof of the train to recognize the arc, which increases the cost in some way. Aiming at the optical character of the arc, in this paper an arc coefficient is defined to measure the size of the arc in the image, by converting the pantograph videos into the time series relating to the arc coefficient through image processing. Therefore, FFT, a band pass filter and IFFT are introduced to reconstruct the time series, and obtain the arc occurrence image clearly apart from non-arc interference. By contrast, this method is simpler and more accurate to abstract the arc image.

2 The Proposed Method for Image Recognition of Arc

The method proposed in this paper is separating the pantograph video into frame images, so that continuous video is converted into discrete images to process. In each frame image, Otsu threshold is also used to eliminate the interference and clarify the pantograph-catenary area. Then the place where arc can happen on the pantograph-catenary is located by edge detection, and the pantograph-catenary area is sheared for each image as the arc recognition objective. Since the difference of white pixels whether there is an arc or not, an arc coefficient is defined that the ratio between the number of white and black pixels is utilized to decide if the arc exists. In this way, the images are transformed into the time series. To eliminate this interference, a band-pass filter is used to process the spectrograms transformed by FFT, and the time domain graphs with the clear arc characters are acquired by IFFT, so that the pantograph-catenary arc can be accurately recognized. Pantograph video and frame images are corresponding, so the sequence numbers of the frame images indicate the arc images and the time when it occurs. The whole image recognition flow diagram is showed in Fig. 3.

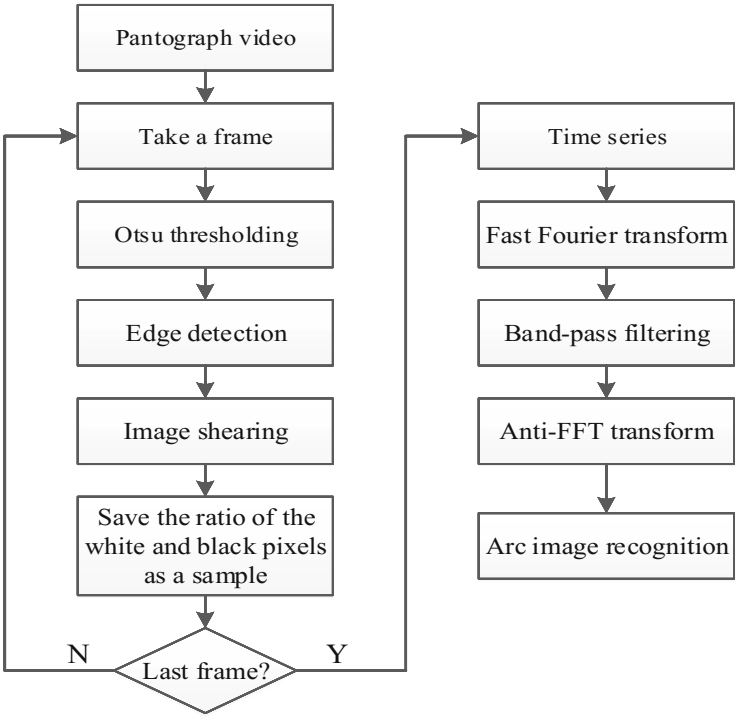

Fig. 3. The proposed Algorithm for arc image recognition

2.1 Otsu Threshold Segmentation for Frame Images

Otsu threshold is a common method that has been used in many image processing applications, and how to choose the proper threshold to separate the images is very significant. This method is based on the gray level histogram and deduced by the principle of least square method, which is an optimal threshold in statistics [14]. The fundamental is to separate the gray value of the image into two different parts with the maximum variance, that is, the largest separability, according to the optical threshold.

If $f(x, y)$ is the gray value of position (x, y) in the image $I_{M\times N}$, and its gray level is L, then $f(x, y) \in [0, L-1]$. And if the number of the whole pixels is f_i in gray level i, then the probability of i gray level occurrence is

$$p(i) = \frac{f_i}{M \times N} \tag{1}$$

Where $i = 0, 1, \cdots L-1$, and $\sum_{i=0}^{L-1} p(i) = 1$.

The pixels are divided into two different part according to the gray level by threshold t, which are the background C_0 and the objective C_1. The gray levels of the background C_0

is from 0 to t–1, and the objective from t to L–1. Therefore the pixels of C_0 and C_1 are $\{f(x, y) < t\}$ and $\{f(x, y) \geq t\}$ respectively.

The probability of C_0 occurrence is

$$\omega_0 = \sum_{i=0}^{t-1} p(i) \tag{2}$$

The probability of C_1 occurrence is

$$\omega_1 = \sum_{i=t}^{L-1} p(i) \tag{3}$$

Where $\omega_0 + \omega_1 = 1$, and the average gray value of C_0 is

$$\mu_0(t) = \sum_{i=0}^{t-1} i * \frac{p(i)}{\omega_0} \tag{4}$$

The average gray value of C_1 is

$$\mu_t(t) = \sum_{i=t}^{L-1} i * \frac{p(i)}{\omega_1} \tag{5}$$

The average gray value of the whole image is

$$\mu = \sum_{i=0}^{L-1} ip(i) \tag{6}$$

The variance between the background and the objective is

$$\delta^2(k) = \varpi_0(\mu - \mu_0)^2 + \varpi_1(\mu - \mu_1)^2 \tag{7}$$

Let k varies from 0 to L–1, and calculate the between-class variance $\delta^2(k)$. Then choose the maximum variance and its k is the optical threshold. In this way the interference irrelevant can be eliminated.

2.2 Edge Detection and Image Shearing

The basic idea of edge detection is to find the pixel with the maximum gradient in the image. That has to meet two conditions, one is that it is able to restrain the noises effectively, and the other is to locate the edge as precisely as possible. Canny operator detection uses the derivative of the Gauss filter to find the maximum gradient [15]. Tow thresholds are applied to detect the strong and the weak edges, only when the two edges are connected will the weak one contained in the output. Therefore, using this approach

is not likely to be interrupted by noises, and is able to obtain the true weak edge. Its detection flow diagram is shown in Fig. 4.

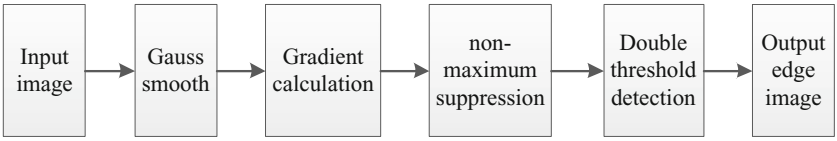

Fig. 4. The flow diagram of canny operator detection

The purpose of shearing the image is to acquire the key elements required for the arc image recognition in the images, including the whole pantograph and the partial contact wire. Since the camera is fixed on the roof of the train and the shooting angle is constant, the shearing area at different time also does not change. After the procedures processing the images above, the key binary image is acquired, in which the white pixels are saved as 1 and black as 0.

2.3 Arc Image Recognition in Time Series Based on Fast Fourier Transform

As already mentioned in Sect. 2.2, if the number of white pixels is defined as w, and the black as b, then the arc coefficient is indicated as

$$C = w/b \tag{8}$$

Then calculate the coefficient of each different frame image and all the result constitutes the discrete time series. The value of the coefficient at different time demonstrates the possibility of whether the arc happens, for the value is larger when the arc occurs than it does not. Moreover, with the change of surroundings and routes while the train operating, there are some fluctuations in the series after image processing, so it is necessary to eliminate the interference by means of FFT and a band-pass filter.

FFT is a simple kind of DFT, which is able to convert a discrete time domain signal into frequency domain [16]. The DFT of a finite-duration discrete signal $x(n), n = 0, 1 \cdots N-1$ is defined as

$$X(k) = \sum_{n=0}^{N-1} x(n) W_N^{kn} \tag{9}$$

$$\begin{bmatrix} X(0) \\ X(1) \\ \vdots \\ X(N-1) \end{bmatrix} = \begin{bmatrix} W_N^0 & W_N^0 & \cdots & W_N^0 \\ W_N^0 & W_N^{1\times 1} & \cdots & W_N^{(N-1)\times 1} \\ \vdots & \vdots & \cdots & \vdots \\ W_N^0 & W_N^{1\times(N-1)} & \cdots & W_N^{(N-1)\times(N-1)} \end{bmatrix} \cdot \begin{bmatrix} x(0) \\ x(1) \\ \vdots \\ x(N-1) \end{bmatrix} \tag{10}$$

$$k = 0, 1 \cdots N-1, W_N = e^{-j\frac{2\pi}{N}}$$

As indicated in (10), about N^2 times multiplications and N^2 times additions are required by using DFT, which is too enormous. Nevertheless, due to the symmetry and periodicity of W_N, the signal with N elements can be divided into two signals with N/2 elements, which means the amount of computation is halved. By that analogy, the signal with N/2 elements is divided into two with N/4 elements, and so on.

The signal then $x(n)$ is divided into two sequences, that is

$$x(n) = x_1(n) + x_2(n) \tag{11}$$

Where $x_1(n)$ is the even sequence and $x_2(n)$ is odd, and the lengths of $x_1(n)$ and $x_2(n)$ are both $N/2$.

$$X(k) = \sum_{n=0}^{\frac{N}{2}-1} x_1(n) W_N^{2kn} + \sum_{n=0}^{\frac{N}{2}} x_2(n) W_N^{(2n+1)k} \tag{12}$$

$$X(k) = \sum_{n=0}^{\frac{N}{2}-1} x_1(n) W_N^{2kn} + W_N^k \sum_{n=0}^{\frac{N}{2}-1} x_2(n) W_N^{2kn} \tag{13}$$

Since $W_N^{2kn} = e^{-j\frac{2\pi}{N}2kn} = e^{-j\frac{2\pi}{N/2}kn} = W_{N/2}^{kn}$,

$$X(k) = \sum_{n=0}^{\frac{N}{2}-1} x_1(n) W_{N/2}^{kn} + W_N^k \sum_{n=0}^{\frac{N}{2}-1} x_2(n) W_{N/2}^{kn} = X_1(k) + W_N^k X_2(k) \tag{14}$$

Where $x_1(k)$ and $x_2(k)$ are the DFT results of $x_1(n)$ and $x_2(n)$ with $N/2$ elements. Since the periods of $x_1(k)$ and $x_2(k)$ are both $N/2$, and $W_k^N + N/2 = -W_k^N$, $X(k)$ can be indicated as

$$X(k) = X_1(k) + W_N^k X_2(k) \tag{15}$$

And by this analogy, one DFT with N elements is divided into $N/2$ DFT with two elements after m−1 times computations. FFT converts a large scale transform into smaller scales and simpler transforms, which reduces the calculation requirement but improves the calculation speed.

After FFT the time series, the corresponding spectrogram is obtained, in which the amplitudes of different frequencies is observed. Non-arc interference is eliminated by a proper band-pass filter and the reconstructed time series is acquired by IFFT. In the reconstructed series it can be apparently observed when the arc happens, and realize the recognition of the arc image.

3 Experimental Results

3.1 The Research Object of Experiment

A pantograph-catenary video of CRH380D is demonstrated as a case to recognize the arc through the proposed method in this paper. Select a part of the video containing the arc and divide it into 200 frame images. The images of normal operation and the time when arc happens are shown in Fig. 5.

(a) Image of normal operation (b) Image with arc

Fig. 5. The images of normal operation and the arc

3.2 Verification of Arc Image Recognition

According to the image processing method in Sects. 2.1 and 2.2, process the frame images in the order of Otsu threshold, edge detection, and image shearing, then the binary images are obtained. The original and processed binary images at frame 50, 62 and 100 are indicated in Fig. 6. and the process of calculating arc coefficients are shown in Table 1.

Table 1. The arc coefficient of different frame images

Image	White pixels	Black pixels	Arc coefficient
Frame 30	13304	9196	1.4467
Frame 62	14663	7837	1.8710
Frame 100	13670	8830	1.5481

Owing to the differences between white and black pixels in the binary images, we can get the time series about the arc coefficients from 200 frame images and it's shown in Fig. 7. It can be observed that the coefficient varies at different time, and when the arc happens it changes dramatically. Also the interference from the weather, the surroundings and the operation route to the coefficient is obviously, which brings some fluctuations in the time domain discrete figure and makes it hard to distinct arc image between normal one.

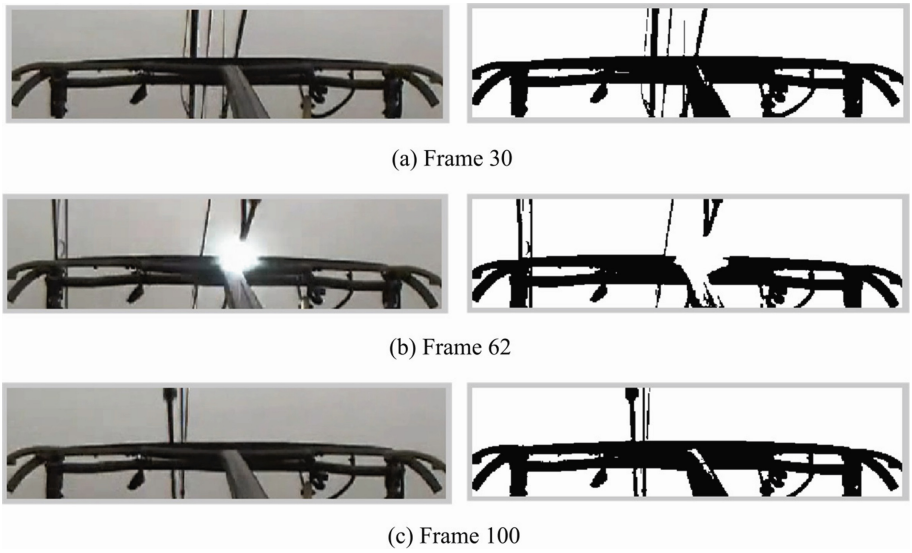

Fig. 6. The original and processed binary images

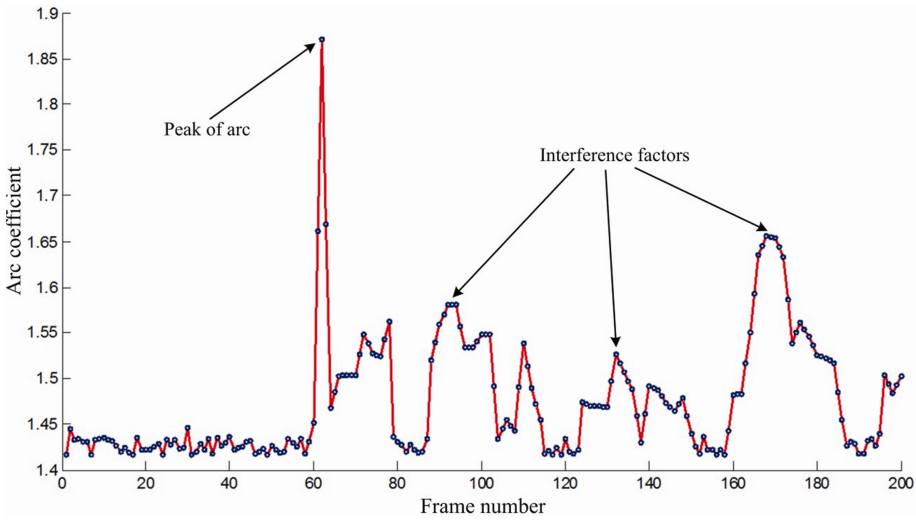

Fig. 7. The time series

According to the method of 2.3, FFT is used to transform the time series and the sample frequency is 50 Hz. Then a band-pass filter is to eliminate the interference in the spectrogram previously acquired, with the order is 6, and the pass band is set from 8.3 Hz to 24.6 Hz. The spectrograms of the time series before and after the filtering are shown in Fig. 8.

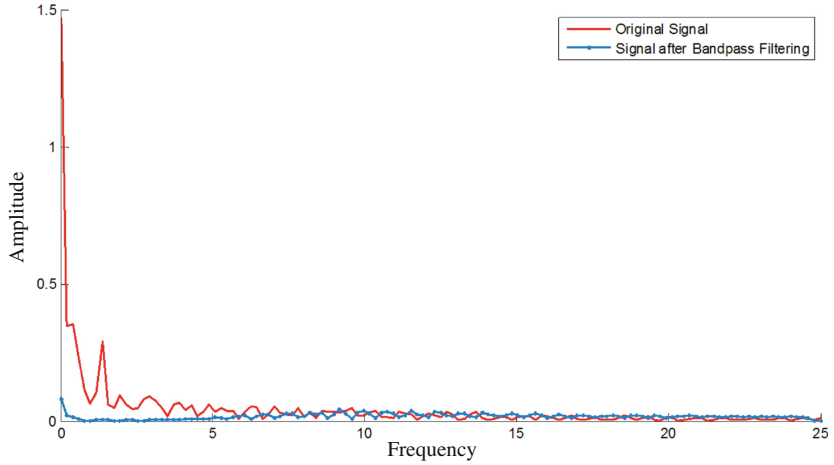

Fig. 8. The original and filtered spectrograms

The filtered spectrogram is transformed through IFFT to get the time series after eliminating the interference. For convenience, the reconstructed time series is normalized and the comparison with the original one is shown in Fig. 9. It can be noticed that the band-pass filter can eliminate the large interference and the characteristic of the arc happens is apparent with a sawtooth wave. The arc occurs at frame 62 and lasts for about 4 frames from the figure, and this result accords with the arc images of the video, which verifies the proposed algorithm.

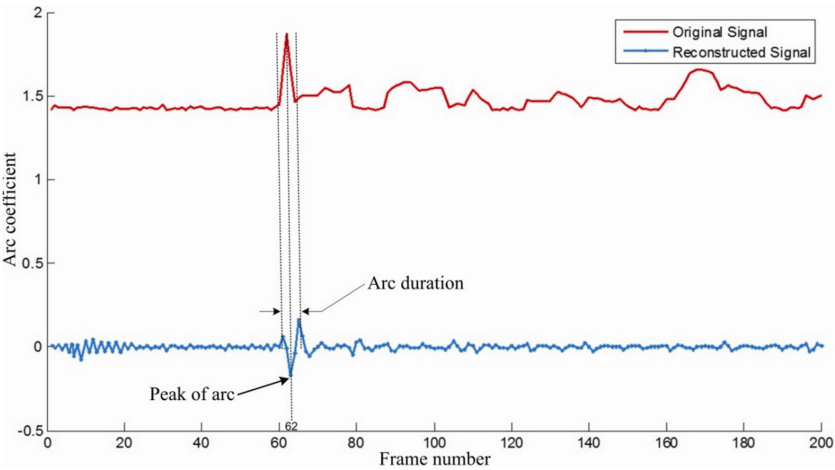

Fig. 9. The original and the reconstructed time series

This CRH380D pantograph video is provided by the Chongqing motor train station, which operates in good condition. If the pantograph video contains more than one arc,

the proposed method also can be used to get the arc image of pantograph-catenary system effectively with setting the range of band pass filtering reasonably.

4 Conclusions

The arc on the pantograph-catenary is one of the commonest faults in pantograph-catenary system, and affects the operation of trains badly. An arc image recognition algorithm based on the pantograph video is proposed to abstract the arc image efficiently, which is contributed to the train supervision system. By analyzing the optical characters of the arc through image processing technique, and defining the arc coefficient, the video is converted into a discrete time series so that FFT can be used. To eliminate the interference from the weather, the surroundings and the operation routes, a band-pass filter is used to process the spectrograms, which improves the accuracy to recognize the arc image. Compared with other theses, this method proposed is used to process the true pantograph video and the arc image is effectively recognized, which proves the correctness and the reliability of this method.

For the next study, we would consider the recognition of different types of arc by the proposed method. At the same time, optimizing the characteristics of the arc is important to make the arc more obvious and improve accuracy. At last, we would try other algorithms to improve the speed of arc image recognition and achieve real-time results.

Acknowledgements. This work is supported by the 13th Five-Year National Key Research and Development Plan (2016YFB1200402). The authors are grateful for the reviewer of initial drafts for their helpful comments and suggestions.

References

1. Zong-bao GAO, Guang-ning WU, Wei LU et al (2009) Research review of arc phenomenon between pantograph and catenary in high-speed electrified railway. High Voltage Apparatus 03:104–108, 127
2. Guangya ZHU, Guangning WU, Weifeng HAN et al (2016) Simulation and analysis of pantograph-catenary arc steady-state characteristics during static lifting and lowering of high-speed railway pantograph. J China Railway Soc 02:42–47
3. Barmada S, Raugi M, Tucci M, Romano F (2014) Arc detection in pantograph-catenary systems by the use of support vector machines-based classification. IET Electr Syst Transp 4(2):45–52
4. Yaman O, Karakose M, Aydin I, Akin E (2014) Image processing and model based arc detection in pantograph catenary systems. In: 22nd Signal processing and communications applications conference (SIU), Trabzon, pp 1934–1937
5. Zhiwei H, Zhigang L, Guinan Z et al (2013) Overview of non-contact image detection technology for pantograph-catenary monitoring. J China Railway Soc 06:40–47
6. Aydin I, Yaman O, Karakose M, Celebi SB (2014) Particle swarm based arc detection on time series in pantograph-catenary system. In: Proceedings of 2014 IEEE international symposium on innovations in intelligent systems and applications (INISTA), Alberobello, pp 344–349

7. Aydin I, Karakose M, Akin E (2012) A new contactless fault diagnosis approach for pantograph-catenary system. In: 15th IEEE international conference on mechatronika, pp 1–6
8. Li M, Zeyong W, Xiaorong G, Li W, Kai Y (2009) Edge detection on pantograph slide image. In: International congress on image and signal processing, pp 1–3
9. Xiao-heng Z, Xiao-rong G, Ze-yong W, Li W, Kai Y (2010) Study on the edge detection and extraction algorithm in the Pantographslipper's Abrasion. In: International conference on computational and information sciences, pp 474–477
10. Aydin I, Karakose E, Karakose M, Gencoglu MT, Akin E (2013) A new computer vision approach for active pantograph control. In: IEEE international symposium on innovations in intelligent systems and applications, pp 1–5
11. Barmada S, Landi A, Papi M, Sani L (2003) Wavelet multi-resolution analysis for monitoring the occurrence of arcing on overhead electrified railways. Proc Inst Mech Eng Part F, J Rail Rapid Transit, pp 177–187
12. Jinhong W, Jiaoming L (2011) Switching arc image processing based on binocular stereo vision. Trans China Electr 01:86–91
13. Chunhua F, Yi Z, Jianguo W et al (2016) Extraction of insulator discharge arc area based on the theory of image processing techniques. Insulators Surge Arresters 02:35–39
14. Zhiyong H, Weiguo SLH et al (2012) Thresholding segmentation algorithm based on Otsu criterion and line intercept histogram. Opt Precis Eng 10:2315–2323
15. Fei P, Weirong C, Bobo M et al (2012) Rail-framework abstraction based on canny edge detection and poly-connection. J China Railway Soc 02:52–57
16. Bo W, Qiheng Z, Jianlin Z et al (2011) Real-time processing method of 2D-FFT/IFFT for high-resolution image and hardware implementation. Appl Res Comput 11:4376–4379